Electrically Enhanced Ultrafiltration of Industrial Enzyme Solutions

Enevoldsen, Ann Dorrit

Publication date:
2007

Document Version
Publisher's PDF, also known as Version of record

Electrically enhanced ultrafiltration of industrial enzyme solutions

Ann Dorrit Enevoldsen

PhD Thesis

November 2007

Technical University of Denmark

Department of Chemical Engineering

Supervisors: Gunnar Jonsson and Ernst Hansen

ISBN 978-91435-64-1
Printed by Frydenberg a/s, Copenhagen, Denmark

Preface

This industrial PhD thesis is the outcome of $3\frac{1}{2}$ years' study. The project was done in collaboration with the Department of Chemical engineering at the Technical University of Denmark and the Recovery Pilot Plant at Novozymes A/S under the supervision of Associated Professor Gunnar Jonsson and Ernst Hansen.

I would like to take the opportunity to thank the people who have contributed to this thesis.

First of all I like to thank my main supervisor Gunnar Jonsson, for his kindness, helpfulness and great patience. I'm grateful for the opportunity to carry out my project under his competent supervision. I would also like to thank Ernst Hansen for his comprehensive and competent guidance and for being a continuous source for relevant discussion.

I also owe thanks to the people at the Recovery Pilot Plant at Novozymes A/S who has been a great help throughout my project. A special thanks to Sune Jakobsen for always being helpful and for taking the time to answer my questions. I would also like to thank Jesper Haugaard for his help and motivation, especially with the economical aspects of my project.

I'm also grateful to my mother, who has always supported me. Finally, I would also like to thank Peter for his help and patience.

English Abstract

Fouling and concentration polarization are well known problems in crossflow ultrafiltration of proteins. Application of an external dc (direct current) electric force field across the membrane is a promising method to reduce fouling and concentration polarization. The electric field imposes an electrophoretic force on the charged proteins, which drags them away from the membrane surface. The concentration polarization layer is thereby reduced and the flux increases. The solvent flow through the membrane might also be enhanced by the electroosmotic effect; but this effect is considered secondary.

In this Industrial PhD project, crossflow electro-ultrafiltration (EUF) is carried out with enzyme solutions from Novozymes A/S, Denmark. The aim is to investigate the use of EUF in industrial application.

Five different enzymes have been tested including two amylase solutions where the application of an electric field across the membrane resulted in a significant flux enhancement. The other three solutions, which consisted of a lipase and two proteases, did not show any flux improvements during EUF, mainly due to a low surface charge of the enzymes and impurities in the solutions.

The relative flux improvement increases as the enzyme concentration increases. The flux increases around 6-7 times at a concentration of around 100 g/L. EUF is therefore applicable as a final concentration step during enzyme production. The effect of a pulsed electric field has also been tested, but showed no improvement compared to a constant electric field due to the quick formation of the concentration polarization layer.

The effect of the trans membrane pressure (TMP) and crossflow velocity has also been studied. An increased TMP and crossflow velocity did not improve the flux considerably -since the process is controlled by the strength of the electric field. A study of the conductivity of the enzyme solutions showed that the flux in EUF is not affected by conductivities up to around 3 mS/cm.

Energy calculations show that EUF is economically profitable when filtering solutions of high enzyme concentration if the conductivity of the solution is low. In case the enzyme concentration is low UF is more cost-efficient. The conductivity is however a key factor for the economical feasibility of the EUF process; since the energy requirements increases proportional to the conductivity of the enzyme solution. If the conductivity becomes too high, the advantage of using EUF disappears.

Dansk resume

Fouling og koncentrationspolarisation er velkendte problemer i crossflow ultrafiltrering af proteiner. Påtrykning af et eksternt elektrisk felt hen over membranen er en lovende metode til reduktion af fouling og koncentrationspolarisation. Det elektriske felt introducerer en elektroforetisk kraft på de ladede proteiner, som derved bliver trukket væk fra membranoverfladen. Koncentrationspolarisationslaget bliver derved reduceret og fluxen stiger. Solvent flowet igennem membranen kan også stige pga. den elektroosmotiske effekt, men denne effekt bliver betragtet som sekundær.

I dette ErhvervsPhD-projekt er der udført crossflow elektro-ultrafiltrering (EUF) med enzymopløsninger fra Novozymes A/S, Danmark. Formålet er at undersøge industriel anvendelse af elektro-ultrafiltrering.

Fem forskellige enzymer er blevet testet herunder to amylaseopløsninger, hvor påtrykning af et elektrisk felt hen over membranen resulterede i en signifikant flux forbedring. De andre tre opløsninger, som bestod af en lipase og to proteaser, viste ikke nogen flux stigning ved EUF, hovedsageligt fordi enzymerne har en lille overfladeladning og pga. urenheder i opløsningerne.

Den relative flux forbedring stiger med stigende enzymkoncentration. Fluxen stiger ca. 6-7 gange ved en koncentration på omkring 100 g/L. EUF er derfor anvendelig som et sidste koncentrationstrin i en enzymproduktion. Effekten af et pulserende elektrisk felt er også blevet testet, men viste ingen forbedring sammenlignet med et konstant elektrisk felt, da koncentrationspolarisationslaget hurtigt bliver gendannet.

Effekten af det transmembrane tryk (TMP) og crossflow hastigheden er også blevet undersøgt. Øgning af TMP og crossflow hastigheden forbedrede ikke fluxen betragteligt -da processen er kontrolleret af det elektriske felts styrke. Et studie af enzymopløsningernes ledningsevnen viste at fluxen i EUF ikke er påvirket af en ledningsevne op til omkring 3 mS/cm.

Energiberegninger viser at EUF er en økonomisk fordel når opløsninger med en høj enzymkoncentration og lav ledningsevne bliver filtreret. Hvis enzymkoncentrationen er lav er omkostningerne ved UF lavere. Ledningsevnen er en væsentlig parameter for den økonomiske gennemførlighed af EUF processen, da energibehovet stiger proportionalt med ledningsevnen af enzymopløsningen. Hvis ledningsevnen bliver for høj forsvinder fordelene ved at bruge EUF.

Contents

List of Figures

List of Tables

List of Symbols

A_e	Electrode area [m^2]
A_T	Total membrane area [m^2]
B	Constant
D	Diffusion coefficient [m^2/s]
E	Electric field strength [V/m]
EMF	Electro-microfiltration
EUF	Electro-ultrafiltration
E_c	Critical electric field strength [V/m]
E_{feed}	Electric field strength across the feed chamber [V/m]
I	Current [A]
J	Flux [L/(m^2h)]
J_0	Flux at 0 V [L/(m^2h)]
J_∞	Limiting flux [L/(m^2/h)] [m/s]
J_{0g}	Flux through the gel layer at 0 V [L/(m^2h]
J_{0m}	Flux through the membrane at 0 V [L/(m^2h]
J_{av}	Average flux [L/(m^2h)]
J_{max}	Flux at the critical electric field strength [L/(m^2h)] [m/s]
J_m	Flux through the membrane in presence of an electric field [L/(m^2h]
M	Molecular weight [Da]
MF	Microfiltration

N_i	The number of ions per unit volume
P_E	Power consumed by the electric field [kW]
$P_{booster}$	Power consumed by the booster pump [kW]
P_{feed}	Power consumed by the feed pump [kW]
P_{in}	Inlet pressure [Bar] [Pa]
$Q_{booster}$	Flow in booster pump [m^3/h]
Q_{feed}	Feed flow [m^3/h]
Q_p	Permeate flow [m^3/h]
Q_r	Retentate flow [m^3/h]
R_T	Total resistance [m^{-1}]
R_a	Adsorption resistance [m^{-1}]
R_g	Gel layer resistance [m^{-1}]
R_m	Membrane resistance [m^{-1}]
R_p	Pore-blocking resistance [m^{-1}]
R_{0cp}	Resistance of the concentration polarization layer at 0 V [m^{-1}]
R_{0g}	Resistance of the gel layer at 0 V [m^{-1}]
R_{0m}	Resistance of the membrane at 0 V [m^{-1}]
R_{cp}	Resistance of the concentration polarization layer [m^{-1}]
Re	Reynolds number
Sc	Schmidt's number
Sh	Sherwood number
T	Temperatur [K]
TMP	Trans membrane pressure [Bar] [Pa]
U	Voltage [V]
UF	Ultrafiltration
U^*	Voltage across the other items [V]

U_a	Applied voltage [V]
U_e	Voltage across the electrolyte chamber [V]
U_{feed}	Voltage across the feed chamber [V]
U_p	Voltage across the permeate chamber [V]
W	Total energy consumption [kWh/m^3]
W_E	Energy consumed by the electric field [kWh/m^3]
$W_{booster}$	Energy consumed by the booster pump [kWh/m^3]
W_{feed}	Energy consumed by the feed pump [kWh/m^3]
W_{pump}	Energy consumed by the pumps [kWh/m^3]
Δl	Distance between turbulence promoters [m]
Δp	Pressure-drop across the feed channel [Bar] [Pa]
α	Cross-section [m^2]
δ	Thickness of the concentration polarization layer [m]
η	Viscosity [Ns/m^2]
η_E	Efficiency of the power supply
η_{pump}	Pump efficiency
κ_{dia}	Conductivity of the enzyme solution after diafiltration [mS/cm]
κ_{feed}	Conductivity of the feed solution [mS/cm]
$\kappa_{initial}$	Conductivity of the enzyme solution before diafiltration [mS/cm]
μ_e	Electrophoretic mobility of the molecule [m^2/Vs]
μ_{eg}	Electroosmotic mobility of the gel layer [m^2/(Vs)]
μ_{em}	Membrane electroosmotic mobility [m^2/(Vs)]
π	Osmotic pressure [Pa]
ρ	Density [kg/m^3]
σ	Charge density [C/m^2]
ε	Dielectric constant

ε_0	Permittivity [F/m]
ζ	Zeta potential [V]
a	Constant
$a^\dagger$	Constant [m/V]
b	Constant
c	Concentration [g/L]
c	Constant
c_b	Bulk concentration [g/L]
c_g	Gel layer concentration [g/L]
c_m	Concentration at the membrane surface [g/L]
c_p	Permeate concentration [g/L]
c_{feed}	Feed Concentration [g/L]
c_r	Concentration of the retentate [g/L]
d	Constant
d	The effective thickness of the diffuse double layer [m]
d_h	Hydraulic diameter [m]
e	Elementary charge [C]
f	Friction factor
h	Height of the feed channel [m]
k_0	Mass transport coefficient [L/(m^{2}h)] [m/s]
k_B	Boltzmann constant [J/K]
l	Length of the filtration module [m]
n	Exponential factor
n	Number of cells
pI	Isoelectric point
r^*	Specific resistance of the other items [m^2/S]

r_e	Specific resistance of the electrolyte chamber [m^2/S]
r_{feed}	Specific resistance of the feed chamber [m^2/S]
r_p	Specific resistance of the permeate chamber [m^2/S]
w	Width of the filtration module [m]
x	Distance from membrane surface [m]
z_i	Valence of the ions of the i'th type
v	Crossflow velocity [m/s]
v_e	Electrophoretic velocity [m/s]

Chapter 1

Introduction

Membrane processes are widely used in the Biotech industry for separation and concentration of proteins due to the relatively low operating costs. However, the build up of a secondary membrane together with concentration polarization and fouling results in a low throughput (flux) and a long process time. The problem expands the higher the concentration of the product becomes. Large membrane areas are therefore required to ensure a reasonable production time.

A method to increase the throughput is by applying an electric field across the membrane. The electric field imposes an electrophoretic force on the charged molecules, which are dragged away from the membrane surface. An increased flux is thereby obtained. Electrofiltration has been used to enhance the flux and selectivity in many model systems, and a flux improvement of a factor 2-10 is not unusual [1]. A flux enhancement in that range makes it possible to expand the capacity, since the membrane area needed to filter a certain amount of product is reduced.

Novozymes A/S is the world leading producer of industrial enzymes and microorganisms and develops 8-12 new products each year. Compared to pharmaceutical companies the development time and the price of enzymes are relatively low. Since the competition is tough, the cost of manufacturing the enzymes must be low. Novozymes is therefore constantly optimizing their recovery process to reduce the production costs. The aim with this Industrial PhD project is to investigate whether crossflow electro-ultrafiltration can be used to enhance the filtration performance of enzymes during concentration. An important part is to compare the production costs of conventional crossflow ultrafiltration with crossflow electro-ultrafiltration, and most important to identify the cost drivers

in the electro-ultrafiltration process.

This thesis is outlined as follows: The theory of crossflow ultrafiltration and crossflow electro-ultrafiltration is given in chapter 2. Chapter 3 gives a general description of protein fouling, and some common ways to enhance the filtration process. A literature review of crossflow electrofiltration can be found in chapter 4. Chapter 3 and 4 also describes microfiltration and electro-microfiltration, since the main part of these chapters have been composed in the beginning of the PhD project. At that time it had not been decided whether the experimental work was going to be based on a microfiltration or an ultrafiltration process. Chapter 5 describes the experimental procedures and methods, while the results are placed in chapter 6. The economy of the electro-ultrafiltration process is considered in chapter 7.

The busy reader and readers familiar with ultrafiltration and electro-ultrafiltration can skip chapter 2-4 and go directly to the experimental part in chapter 5.

Chapter 2

Theory

In this section the theory concerning ultrafiltration (UF) and electro-ultrafiltration (EUF) is discussed. In the ultrafiltration section the emphasis is on the gel layer model and the calculation of the mass transport coefficient. A detailed description of the mechanisms of membrane fouling and methods to enhance the filtration process is given in chapter 3. The electro-ultrafiltration section presents the mechanisms in the process, origin of charge, electroosmosis and the models used for describing the flux in EUF.

2.1 Ultrafiltration

Crossflow ultrafiltration is a pressure driven membrane process where the feed flows parallel to the membrane surface, and the solvent goes through the membrane due to the trans membrane pressure (TMP). The flux J can be described by Darcy's law [2]:

$$J = \frac{TMP}{\eta R_T} \tag{2.1}$$

where η is the viscosity of the solution and R_T the total membrane resistance. The major problems with UF is related to concentration polarization and fouling of the membrane, which may cause a flux decline of an order of magnitude from its initial value. This means that the total resistance of the membrane increases throughout the filtration process [2] [3]. Concentration polarization is characterized as the accumulation of retained molecules near the membrane surface, while fouling is characterized as adsorption and deposition of particles on the membrane. Depending of the ratio between the size of the molecules and the

membrane pore size, fouling can be caused by pore blocking or constriction, as illustrated in figure 2.1 [3].

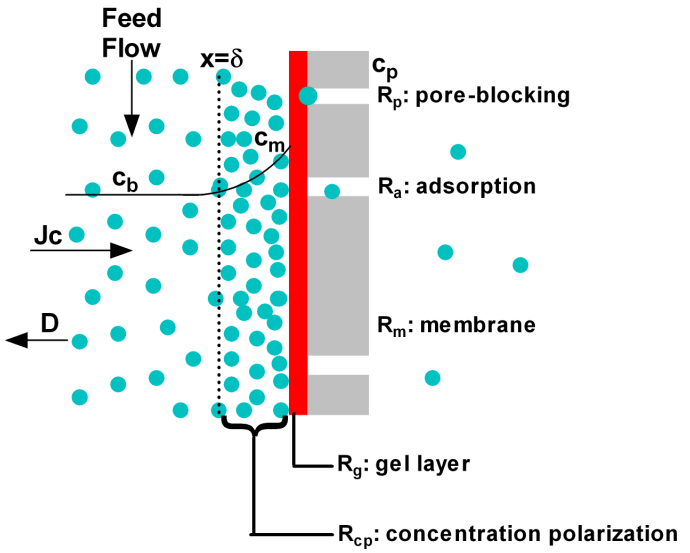

Figure 2.1: Concentration polarization and fouling resistances in UF.

where c_b is the bulk concentration, c_m the concentration at the membrane surface and c_p the permeate concentration. δ is the thickness of the concentration polarization layer and D the diffusion coefficient of the molecules. The total resistance is considered as sum of the various resistances given in figure 2.1.

In UF the flux can be controlled by the crossflow velocity (v) and TMP as shown in the schematic drawing in figure 2.2 [3].

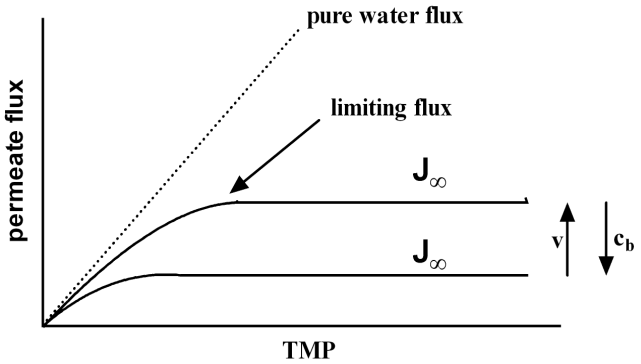

Figure 2.2: Schematic drawing of the flux versus TMP for increasing crossflow velocity and bulk concentration in UF.

The flux increases when TMP increases, but only until the limiting flux (J_∞) is reached after which it becomes independent of TMP. A higher crossflow velocity

is therefore necessary if a higher flux is required, since it increases the shear rate at the membrane surface, and thereby decreases the concentration polarization layer. Figure 2.2 also shows that the flux level decreases when c_b increases due to a thicker concentration polarization layer. The gel layer model or the osmotic pressure model is often used in UF to described the flux. Both models will be presented below.

2.1.1 Gel layer model

The gel layer model is based on a mass balance of the solute under the assumption that the osmotic pressure is negligible. At steady state the convective transport of solutes towards the membrane surface is equal Jc, while the diffusive back transport from the boundary layer to the bulk solution is $D\frac{dc}{dx}$ as illustrated in figure 2.1. If the retention, defined as $\left(1-\frac{c_p}{c_b}\right)$, is not 100%, the transport of solute through the membrane is Jc_p. Hence the mass balance may be written as [3]:

$$Jc + D\frac{dc}{dx} = Jc_p \tag{2.2}$$

Integrating equation 2.2 with the boundary conditions:

$$\begin{aligned} x = 0 \;&\Rightarrow\; c = c_m \\ x = \delta \;&\Rightarrow\; c = c_b \end{aligned} \tag{2.3}$$

where x is the distance from the membrane surface, gives the following equation:

$$J = k_0 \ln \frac{c_m - c_p}{c_b - c_p} \tag{2.4}$$

where the mass transport coefficient k_0 is equal to [3]:

$$k_0 = \frac{D}{\delta} \tag{2.5}$$

In UF of proteins concentration polarization is often severe due to a low diffusivity of the proteins and a high retention. In that case the protein concentration at the membrane surface is high, and may reach a maximum concentration called the gel layer concentration (c_g) [3]. Assuming that $c_p = 0$, equation 2.4 becomes equal to:

$$J = k_0 \ln \frac{c_g}{c_b} \tag{2.6}$$

To test if the gel layer model can be used to describe the flux, J_∞ is plotted as a function of $\ln(c_b)$, which, if the gel layer model is valid, results in a straight line. The slope is then equal to $-k_0$ and the intercept with the ordinate equal $\ln(c_g)$. The coefficients in the gel layer model assumes that the flux is independent of TMP, which means that the limiting flux is required. The model also assumes that the gel layer concentration is independent of the bulk concentration and the crossflow velocity, which may not always be case.

Calculation of the mass transport coefficient

k_0 is expressed by the Sherwood number (Sh), the hydraulic diameter d_h and the diffusion coefficient D by [3]:

$$Sh = \frac{k_0 d_h}{D} \tag{2.7}$$

where the Sherwood number can be calculated by [3]:

$$Sh = a\,\mathrm{Re}^b\,Sc^c\left(\frac{d_h}{l}\right)^d \tag{2.8}$$

where a, b, c, d are constants depending on the hydrodynamic conditions in the module. l is the length of the membrane, and d_h the hydraulic diameter, which for a rectangular slit is defined as [3]:

$$d_h = \frac{2wh}{w+h} \tag{2.9}$$

where w is the width and h the height of the slit. The width of the filtration module is normally several magnitudes greater than the height of the module, which means that d_h is approximately equal $2h$. The Reynolds and Schmidt's number are defined as [3]:

$$\mathrm{Re} = \frac{\rho \mathrm{v} d_h}{\eta} \tag{2.10}$$

$$Sc = \frac{\eta}{\rho D} \tag{2.11}$$

where ρ is the density of the feed solution. The diffusion coefficient D can be calculated from an empirical expression given by Young *et al.* [4]:

$$D\left(m^2/s\right) = \frac{8.34 \cdot 10^{-12} \times T}{\eta\ M^{1/3}} \tag{2.12}$$

where M is the molecular weight of the protein and T the temperature of the solution. Equation 2.8 has some general approximations, which is given in table 2.1 for a rectangular channel [3]:

Flow conditions	Sherwood approximation
Laminar flow	$Sh = 1.85 \left(\mathrm{Re}\, Sc \frac{d_h}{l}\right)^{0.33}$
Turbulent flow	$Sh = 0.04\, \mathrm{Re}^{0.75}\, Sc^{0.33}$
Gröber [5]	$Sh = 0.664 \left(\mathrm{Re}\, \frac{d_h}{l}\right)^{0.5} Sc^{0.33}$
Turbulence promoters (fig 3.11)	$Sh = 1.94\, \mathrm{Re}^{0.5}\, Sc^{0.33} \left(\frac{h}{\Delta l}\right)^{0.5}$
Feed spacer (fig 3.11)	$Sh = 0.0096\, \mathrm{Re}^{0.5}\, Sc^{0.6}$

Table 2.1: Sherwood correlations for rectangular channel.

The first two equations are valid for empty channels under either laminar or turbulent conditions. The third equation is also valid for an empty, but short channel, where the velocity and concentration profiles are not fully developed [5]. Hence, the length of the module must be less that $0.029\, \mathrm{Re}\, d_h$. The fourth and fifth equation represents channels filled with either turbulence promoters or spacers, as seen on figure 3.11 (see next chapter).

2.1.2 The osmotic pressure model

Usually the osmotic pressure is low during UF of macromolecules, since the major contribution to the osmotic pressure is caused by low molecular weight compounds, which are able to pass the UF membrane; hence there is no concentration gradient of small compounds across the membrane. However, under certain conditions where concentration polarization is severe, the osmotic pressure cannot be neglected, and equation 2.1 becomes equal to [3]:

$$J = \frac{TMP - \Delta\pi}{\eta R_m} \tag{2.13}$$

where π is the osmotic pressure given by:

$$\pi = a c_m^n \tag{2.14}$$

where a is a constant and n an exponential factor greater than 1. By combining equation 2.13 with 2.14 and using equation 2.4 as an expression for c_m, the flux

under osmotic pressure conditions is given by [3]:

$$J = \frac{TMP - ac_b^n \exp(\frac{nJ}{k_0})}{\eta R_m} \tag{2.15}$$

assuming that $c_p = 0$. Figure 2.3 shows the reduced osmotic pressure of BSA as a function of the concentration at different pH [6].

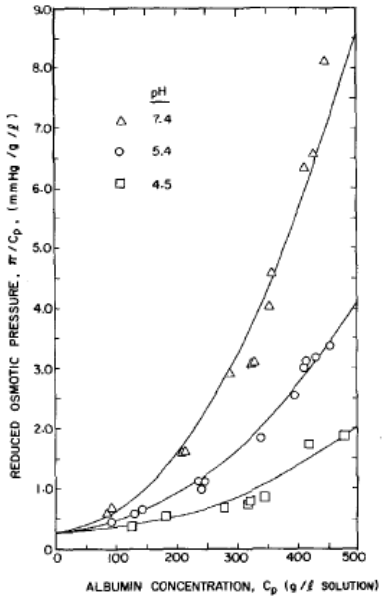

Figure 2.3: Reduced osmotic pressure (osmotic pressure divided by the concentration) of BSA at different pH in 0.15 M NaCl [6].

The osmotic pressure is lowest at pH 4.5, due to the lack of repulsing electrostatic forces at pH values close to the isoelectric point (pI) of BSA [6].

2.2 Electro-ultrafiltration

Application of an external dc (direct current) electric force field across the membrane is a promising method to reduce fouling and concentration polarization. A schematic drawing of a crossflow EUF module is shown in figure 2.4.

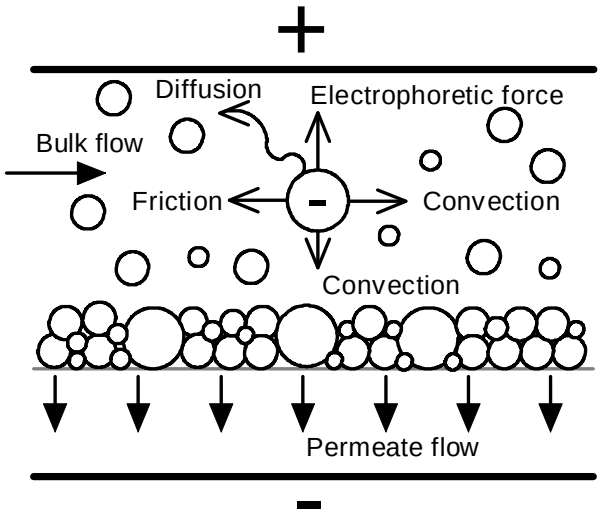

Figure 2.4: Principle of crossflow EUF. Inspired by Weigert et al. [7].

The electric field imposes an electrophoretic force on the charged molecules dragging them away from the membrane surface. The concentration polarization layer is thereby reduced and the flux increases. The solvent flow through the membrane might also be enhanced by the electroosmotic effect; but this effect is considered secondary [1]. The effect depends on the electrophoretic mobility of the molecules (μ_e) and the electric field strength across the membrane (E). The electrophoretic mobility is proportional to the surface charge of the particles, which is given by the ζ-potential [8]. Figure 2.5 shows the definition of the ζ-potential.

When charged molecules are dissolved, a diffuse double layer is formed around it. It consists of an inner layer of counter-ions, which are strongly attached, called the Stern layer. Outside the Stern plane there is a diffuse double layer, which mainly consists of counter-ions and a few co-ions. When an electric force is acting on the charged molecules, liquid will move along in a certain distance from the molecules. The moving layer is called the hydrodynamic stagnant layer, and defines the slipping plane beyond which no liquid will move along.

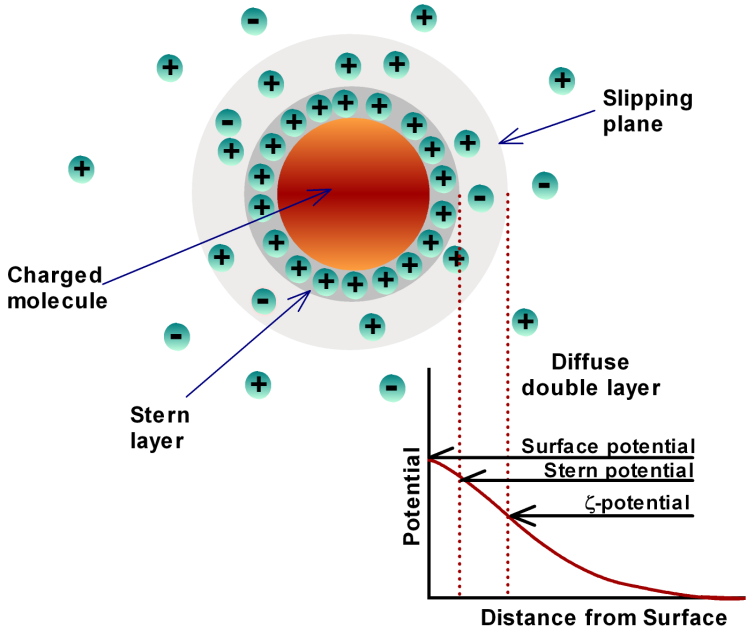

Figure 2.5: Illustration of the ζ-potential and the diffuse double layer. Inspired from ref. [9].

The slipping plane is placed outside the Stern plan and defines the ζ-potential. The ζ-potential represents the surface charge of the particles, and is influenced by the pH and the ionic strength of the solution. At a pH equal the isoelectric point of the molecule the net surface charge is zero, and the particles will not migrate in an electric field. The ζ-potential is given by [8]:

$$\zeta = \frac{\sigma d}{\varepsilon_0 \varepsilon} \tag{2.16}$$

where σ is the charge density, d the effective thickness of the diffuse double layer, ε_0 the permittivity in vacuum and ε the dielectric constant of the solvent [8]. d can be calculated from the Debye-Hückel theory by the following equation:

$$d = \left(\frac{\varepsilon_0 \varepsilon k_B T}{e^2 \sum N_i z_i^2} \right)^{1/2} \tag{2.17}$$

where e is the elementary charge, T the temperature, N_i the number of ions per unit volume and z_i the valence of the ith ion. From equation 2.16 and 2.17 it can be seen that the ζ-potential is proportional to d, which decreases with the square root of the ionic strength $\left(= \frac{1}{2} \sum N_i z_i^2\right)$ of the solution. It is therefore important to have a low salt concentration in the solution to achieve a high ζ-potential, and thereby a high effect of the electric field.

The electrophoretic mobility μ_e of the molecules is given by the ζ-potential as [8]:

$$\mu_e = \frac{\varepsilon_0 \varepsilon \zeta}{\eta} \tag{2.18}$$

and is proportional to the electric field strength. The flux improvement depends on the electrophoretic velocity of the molecule v_e by [8]:

$$v_e = \mu_e E \tag{2.19}$$

and is proportional to the electric field strength.

A critical electric field strength E_c is defined in EUF as:

$$E_c = \frac{J_{\max}}{\mu_e} \tag{2.20}$$

where $J_{\max}$ is the maximum solvent flux at a given TMP, under the assumption that no concentration polarization or cake formation takes place. Hence E_c increases when operating at a higher TMP. In theory $J_{\max}$ is equal the pure water flux through the membrane, in practice it will be lower due to irreversible fouling of the membrane.

Electroosmosis is the motion of a liquid through an immobilized set of particles like a porous plug, a capillary, or a membrane, when an electric field is applied. Figure 2.6 shows the mechanism of electroosmosis.

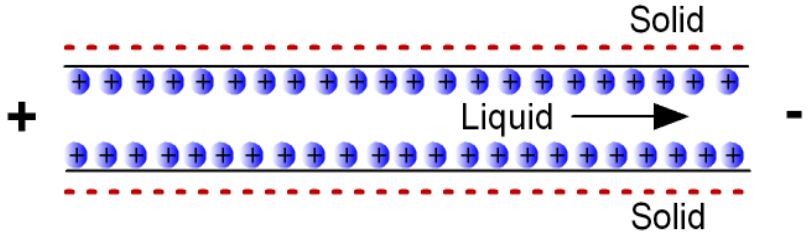

Figure 2.6: Mechanism of electroosmosis [10].

The electroosmotic effect is due to the force acting on the counter-charge in the liquid inside the charged pores [11]. When the electric field is applied the moving ions drag the liquid in which they are dissolved in along [10] [11].

2.3 Models

There exists no general model to predict the influence of an electric field in crossflow membrane filtration. Different authors have developed different models [1]. Most of the models are modified expressions of the resistance-in-series model [12] [13] [14] or the gel layer model [15] [16] [17].

The simplest model to adapt is the gel layer model. By adding an electrophoretic term on the left hand side of the mass balance given in equation 2.2, the mass balance for EUF can be written as:

$$Jc + D\frac{dc}{dx} - \mathrm{v}_e\,(c - c_p) = Jc_p \tag{2.21}$$

which can be integrated with the same boundary conditions as given is equation 2.3 as:

$$\int_0^\delta dx = \frac{D}{(J - \mathrm{v}_e)} \int_{c_m}^{c_b} \frac{1}{c - c_p} dc$$

The following equation is hereby obtained [15]:

$$J = k_0 \ln \frac{c_m - c_p}{c_b - c_p} + \mu_e E \tag{2.22}$$

where $\mu_e E$ represents the flux enhancement during EUF. Introducing $c_m = c_g$ and $c_p = 0$, the modified gel layer model becomes equal to:

$$J = k_0 \ln \frac{c_g}{c_b} + \mu_e E \tag{2.23}$$

Equation 2.23 predicts a linear relationship between the flux and the electric field strength [1].

Radovich *et al.* [16] found a linear dependency during crossflow EUF of BSA for concentrations in the range of 1-4 %w and electric field strengths between 0-1000 V/m. However, equation 2.23 could not be used directly, since k_0 and c_g did not remain constant, but depended on E. By introducing an exponential decay of the gel layer concentration as a function of the electric field strength, they expressed the concentration at the membrane surface by [16]:

$$c_m = c_g e^{-BE} \tag{2.24}$$

where B is a constant, and found the following linear equation:

$$J = J_0 + \left(\mu_e - \frac{J_0}{E_c}\right) E \tag{2.25}$$

where J_0 is the flux at 0 V. With this equation they were able to describe the EUF data [16].

The total membrane resistance during EUF is given by a sum of the resistance of the concentration polarization layer, the gel layer, and the membrane [18]:

$$R_T = [R_{cp} + R_g + R_m] \tag{2.26}$$

The membrane resistance may be defined as the resistance of the membrane in absence of the electric field R_{0m}, and the resistance in presence of the electric field R_m as [18]:

$$R_{0m} = \frac{TMP}{\eta J_{0m}} \tag{2.27}$$

$$R_m = \frac{TMP}{\eta J_m} \tag{2.28}$$

where J_{0m} is flux through the membrane in the absence of an electric field, and J_m is the flux through the membrane in presence of an electric field. If the flux due to permeability and electroosmosis through the membrane is assumed to be additive J_m can be expressed as:

$$J_m = J_{0m} + \mu_{em} E \tag{2.29}$$

where μ_{em} is the membrane electroosmotic mobility. Combining equation 2.27-2.29, R_m can be expressed as [18]:

$$R_m = \frac{R_{0m}}{1 + \frac{\mu_{em} E}{J_{0m}}} \tag{2.30}$$

A similar reasoning can be made for R_g, which can be expressed as [18]:

$$R_g = \frac{R_{0g}}{1 + \frac{\mu_{eg} E}{J_{0g}}} \tag{2.31}$$

where R_{0g} is the cake resistance in absence of an electric field, μ_{eg} the cake electroosmotic mobility and J_{0g} the flux though the gel in absence of an electric field. R_{cp} can be expressed by the flux though the concentration polarization layer, which is given by equation 2.1 and 2.23 as [18]:

$$R_{cp} = \frac{TMP}{\eta \left(J_0 + \mu_e E \right)} \tag{2.32}$$

and can be written as:

$$R_{cp} = \frac{R_{0cp}}{\left(1 + \left(\frac{\eta E}{J_0}\right)\right)} \tag{2.33}$$

where R_{0cp} is the resistance of the concentration polarization layer in absence of an electric field. The total membrane resistance can therefore be expressed as [1]:

$$R_T = \left[\frac{R_{0cp}}{\left(1 + \left(\frac{\eta E}{J_0}\right)\right)}\right] + \left[\frac{R_{0g}}{1 + \frac{\mu_{eg} E}{J_{0g}}}\right] + \left[\frac{R_{0m}}{1 + \frac{\mu_{em} E}{J_{0m}}}\right] \tag{2.34}$$

Radovich and Chao [12] found a nonlinear flux dependency of the electric field strength during EUF of cationic electrodeposit paint. They divided the flux into four steps as shown in figure 2.7.

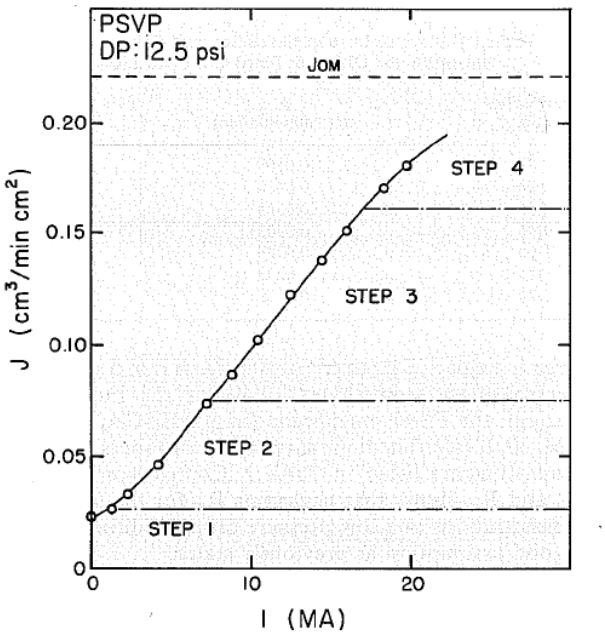

Figure 2.7: EUF of 0.24 %w cationic electrodeposit paint [12].

The authors described that the flux is controlled by different resistances in the four steps. The first step is dominated by the resistance of the gel layer and a linear relationship can describe the flux as seen in equation 2.29. In the second step the electric field strength becomes sufficiently high to disrupt the gel layer, and the flux is controlled by diffusion in the concentration polarization layer given by equation 2.23. This step has a non-linear flux versus electric field strength development, since the thickness of the concentration polarization layer continues

to decrease as the electric field increases, hence the mass transport coefficient is not constant. In the third step the flux is controlled by electrophoretic migration given by the second term in equation 2.23 ($J = \mu_e E$), and the flux increase linearly until the total resistance is close to the membrane resistance. In the fourth step the flux levels off since the electric field strength is close to the critical value. The flux is controlled by the membrane resistance, which means that the flux is equal the solvent flux [12].

2.4 Summary

- The UF process can be described by the gel layer model if the molecules form a gel at the membrane surface. The mass transport coefficient can be calculated from the Sherwood, Reynolds and Smith's number.
- The EUF process is controlled by electrophoretic and electroosmotic forces. The ζ-potential of the molecules and the membrane determines the effect of these forces. A high ζ-potential is obtained at a high charge density of the molecules and a low ionic strength of the solution.
- There exist no general model to describe the flux enhancement in EUF, but a modified expression of the gel layer model or the resistance in series model may be used.

Chapter 3

Description of protein fouling

This chapter will outline the main reasons concerning protein fouling of ultrafiltration (UF)[1] and microfiltration (MF)[2] membranes, and describe some general ways to reduce the problems. The emphasis will be on crossflow modules, but results reported from stirred cell experiments are also considered, since they to some extent give a picture of the fouling mechanisms occurring under crossflow conditions.

MF and UF are used for many types of industrial purposes. MF is mainly used for separation and can be employed for bacterial cell harvesting, recovery of proteins from the fermentation broth, cleaning of wastewater and clarification of wine, juice and beer [2] [19] [20]. UF can be used for fractionation and concentration of macromolecules like proteins, and is used e.g. in the dairy and Biotech industries [3] [21] [22] [23].

Flux decline due to fouling and concentration polarization is however still a major problem in MF and UF. During the first stage of filtration the flux declines drastically, and the steady state flux is usually only a fraction of the initial flux. Figure 3.1 shows a typical development of the permeate flux in a filtration experiment with different protein solutions [24]. The flux drops to under one tenth of the initial value within the first minutes of filtration, and continues to decline until a steady state level is reached after approximately one hour. As mentioned in the previous chapter the flux decline is caused by concentration polarization and fouling. Concentration polarization is characterized as the accumulation of retained particles near the membrane surface. It depends on the hydrodynamic

[1] Membrane pore size 0.002 - 0.1 μm

[2] Membrane pore size 0.1 - 10 μm

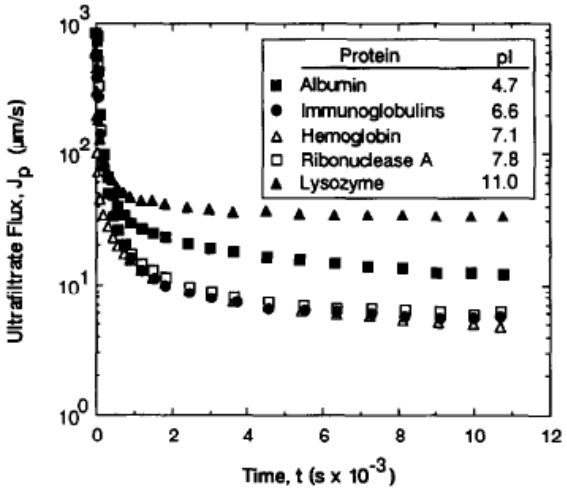

Figure 3.1: Flux decline during filtration of 5 g/L protein solutions at pH 7.4. The isoelectric points of the proteins are given in the legend text [24]

conditions in the filtration module, but is independent of the physical properties of the membrane [25]. Fouling is characterized as adsorption and deposition of particles on the membrane surface or inside its pores, which leads to a change in the properties of the membrane. Depending on the ratio between the size of the particles and the membrane pore size, fouling can be caused by pore blocking or constriction, together with gel or cake layer formation on the membrane surface [2] [3]. Figure 3.2 illustrates the different fouling mechanisms [2].

While concentration polarization is a reversible process, fouling is often irreversible and chemical cleaning is required to restore the properties of the membrane. The two phenomena can not be considered completely independent of each other, since the concentration polarization layer may transform into a gel or cake layer under certain operating conditions [26] [27]. The presence of other components in solution besides the proteins like e.g. lipids, polysaccharides and fatty acids may also foul the membrane [28]. Priyananda and Chen [28] showed that the extent of fouling is affected, if fatty acid is present in BSA solutions. At low pH the fouling increased while a reduction was observed at high pH. This was ascribe to the solubility of the fatty acids. At high pH they can dissociate and act as anionic surfactants, which may reduce the positive charges on the BSA protein, essentially making it more negatively charged [28].

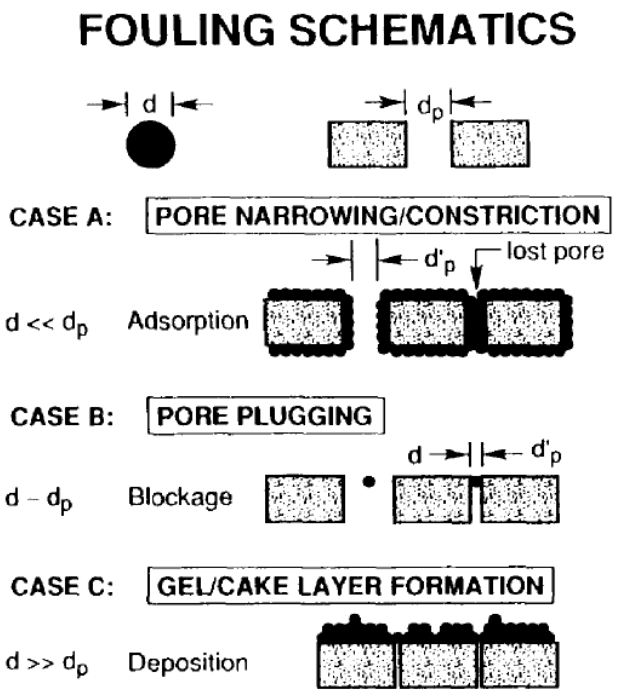

Figure 3.2: Illustration of different fouling mechanisms [2].

3.1 Protein fouling of MF and UF membranes

Due to the complex nature of protein fouling characterization of fouled membranes is a difficult task. Different methods are therefore used by different authors and have been reviewed by Chan and Chen [29]. UF membranes are mainly fouled at the membrane surface, while fouling of MF membranes are dominated by internal fouling like pore plugging and constriction. In the initial stage of filtration, concentration polarization and adsorption of proteins to the membrane cause a rapid flux decline. Pore constriction also contributes to the initial flux decline, especially in MF where the steady state flux usually is several magnitudes lower than its initial value. After the initial decline the flux continues to decrease gradually due to pore plugging and further deposition of proteins to the initially adsorbed layer; and a gel or cake layer may be formed at the membrane surface [25] [30] [31]. The protein-protein interactions are therefore mostly important in the final stage of filtration, while hydrophobic membrane-protein interactions are the dominating factor in the initial stage [30]. In general, the amount of proteins retained by the membrane increases with time due to an

increased membrane resistance represented by the flux decline. This is an advantage during UF where the purpose of the process often is concentration, but a disadvantage in MF where the purpose of the process usually is recovery of proteins from a feed stream containing other macromolecules and microbial cells; hence a high transmission is required [25].

Li *et al.* [32] studied fouling of BSA on polysulfone (PS) membranes (35 kDa) by an ultrasonic technique. They found that the thickness of the gel layer grew fast in the initial stage of filtration followed by a slow increase. The flux decline was mainly controlled by the density of the gel layer, which depends of the pH. Deposits of BSA were also found inside the pore structure and the fouling resistance was related to pore plugging or constriction due to BSA adsorption and deposition. Using multiphoton microscopy Hughes *et al.* [33] showed that internal fouling dominated during the first stages in MF of ovalbumin and BSA. After a short period of time external fouling became the dominating factor.

Several factors like the pH and ionic strength of the feed solution, ζ-potential of the proteins and membrane, and the stability of the proteins have a major influence on the filtration performance. The effect of these parameters is discussed in the next sections.

3.1.1 Effect of feed properties

Effect of pH

The pH and ionic strength are important and can have a major effect on the filtration performance. Generally, the flux is lowest, and the amount of protein adsorbed to the membrane surface greatest when the pH of the solution is equal to the isoelectric point (pI) of the protein, as the electrostatic membrane-protein and protein-protein interactions are at a minimum [25] [34]. The effect of pH can be seen in figure 3.1 where the steady state fluxes of immunoglobulin, hemoglobin and ribonuclease are lower than the fluxes obtained for albumin and lysozyme, since their pI-values are close to the pH of the solution.

Protein aggregates are also formed more easily at pI due to the lack of repulsive forces, and contributes to the fouling of the membrane. Stirred cell MF experiments have also shown that the quasi-steady flux increases linearly with the surface charge density squared (σ^2) of the proteins, see figure 3.3 [24]. The quasi-steady flux depends only on the surface charge and not on the mole-

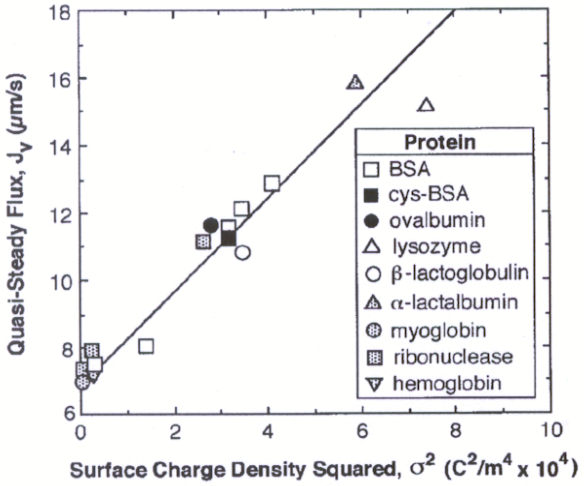

Figure 3.3: Quasi-steady flux obtained during protein MF over a range of pH values as a function of the protein surface charge density squared [35].

cular weight or the physical properties of the proteins.

The amount of adsorbed protein also depends on the charge of the membrane. Proteins with opposite surface charge compared to the membrane are more likely to be adsorbed than proteins with the same surface charge as the membrane [36] [37] [38]. Persson *et al.* [39] tested the influence of the pH in crossflow MF of BSA using two different membranes with different charge characteristics. When the charge of the membrane and the protein had identical signs, the proteins repelled from the membrane surface and caused a decrease in transmission. However, if the charge of the membrane and the protein had opposite signs the proteins could adsorb onto the membrane.

The pH may also affect the structure of the fouling layer. At pI the fouling layer of BSA is densest due to the lack of electrostatic repulsing, which allows the proteins to arrange closer together [30] [32]. This was observed by Li *et al.* [32] who also found that the thickness of a BSA gel layer on a 35 kDa PS membrane was smallest at pI due to the larger density of the layer. The location of BSA fouling on ceramic MF membranes was investigated by small angle neutron scattering by Su *et al.* [40]. The nature of fouling changed with pH. At pH 3 fouling was caused by blockage on the membrane surface, while at pH 5 and 7 fouling was located inside the membrane pores. The structure of BSA is stated as a possible explanation, since the protein becomes longer and the formation of aggregates occur when pH is below 4.

Huisman *et al.* [30] showed in crossflow UF experiments of BSA (pI $\simeq$ 4.9), using PS membranes with cut-off values in the range of 30 to 300 kDa, that both the flux and the transmission in most cases were lowest at pH equal pI. The transmission was however affected by the membrane pore size. Using a membrane with a pore size close to the particle size of BSA resulted in maximum transmission when pH was equal pI. This was due to the smaller size of the protein at pI, which made the transport through the membrane easier.

Effect of ionic strength

Changing the ionic strength may affect the filtration rate in different ways depending on the pH of the solution. An increased ionic strength decreases the thickness of the diffuse double layer around the protein, and the electrostatic protein-protein and membrane-protein interactions decreases (see the theory chapter section 2.2). If the surface charge of the membrane is of opposite sign of the proteins, a higher ion strength will in general decrease the adsorption of proteins to the membrane due to weaker electrostatic membrane-protein interactions. A higher adsorption may on the other hand be achieved by increasing the ionic strength in a solution where the surface charge of the membrane has the same sign as the proteins, since the repelling forces are reduced [34] [36] [37].

Addition of salt to a solution can also cause molecular contraction and thereby decrease the permeability of the gel layer [41] [42]. Palecek *et al.* [42] showed in UF of BSA that the permeability of the deposit layer decreased at increasing ionic strength both at pH above and below the isoelectric point due to a denser layer. The valence of the ions also had an effect. At neutral pH, where BSA is negatively charged, the permeability was reduced relatively more when divalent cations was present in the solution compared to monovalent cations. The valence of the anion did not affect the permeability. Marshall *et al.* [43] also reported an increase in the fouling resistance during constant flux experiments when calcium was present in a β-lactoglobulin solution, especially at a high flux rate. This was explained by molecular unfolding caused by shear, and intermolecular calcium bridges formed by cross-links between adjacent carboxyl groups on different peptide chains.

A higher ionic strength can however increase the transmission in MF [39] [43]. The transmission was increased by adding NaCl in crossflow MF experiments of BSA by Persson *et al.* [39]; although a decrease in the permeate flux was observed. The salt ions decreased the repulsing protein-cake and protein-

membrane forces, thereby making transport through the cake and membrane easier.

Feed concentration

An increased concentration will in general result in an enhanced flux decline and a lower steady state flux due to a thicker concentration polarization layer [3]. The amount of irreversible fouling is usually not affected by an increased concentration [25].

Effect of stability

The stability and conformation of the proteins can also affect the degree of fouling, since degraded proteins tend to foul more than stable proteins [44]. Fourier-transform infrared spectroscopy carried out by Maruyama *et al.* [45] has shown that the secondary structure of BSA in a gel layer changes to a structure containing less α-helix and more β-sheet conformations compared to the BSA protein in the bulk solution. The tertiary structure of BSA also changes with pH. At neutral pH, the BSA molecule is heart shaped, whereas the protein is unfolded and has a ribbon shape at pH 3 [28].

Stirred cell experiments have shown that protein aggregates play an important role in the fouling process. Aggregates bind to the membrane in the initial stage of filtration, which causes a flux decline due to pore blocking. Further decline in the flux is caused by additional deposition of proteins to the first adsorbed layer [35] [46] [47] [48] [49] [50]. Kelly and Zydney [35] investigated fouling of MF membranes in stirred cell experiments using proteins with different structural characteristics. It was concluded that the flux decline was due to protein aggregates. The formation of aggregates was linked to the presence of free thiol-disulfide groups in the protein. Proteins containing one or more free thio-disulfide groups such as BSA, ovalbumin and β-lactoglobulin resulted in significantly flux reductions in the initial stage of filtration. Proteins not containing any free thio-disulfide groups like lysozyme only caused a small gradually flux decline. If the aggregates were removed by prefiltration, the extensive initial flux decline was almost eliminated. For the proteins containing free thio-disulfide groups a slow flux decline was however still observed due to continuously formation of new aggregates. It has also been shown that the filtration rate is strongly

correlated to the presence of BSA dimers, which favors the formation of aggregates [46]. Stirred cell experiments of binary and tertiary mixtures of lysozyme, BSA and ovalbumin showed that fouling was most severe when ovalbumin was present, which was related to its four free thiol-disulfide groups [48].

3.1.2 Membrane properties

The membrane material and structure also have an effect on the degree of fouling. Generally proteins adsorb less to hydrophilic membranes than to hydrophobic membranes due to their large hydrophobic regions. If the membrane is produced for high transmission a high porosity is important, since it is easier for foulants to block the membrane pores if the surface porosity is low [48] [39]. The surface roughness are also a factor to consider, since proteins adhere less to smooth surfaces, or surfaces where fouling only can occur at the peaks [39] [51]. The membrane material is not always crucial, its influence depends on the filtration system. The advantage of hydrophilic membranes is more pronounced in rotary systems where the effect of concentration polarization is low compared to crossflow systems [25]. However there are other considerations to take into account when choosing a proper membrane for an industrial filtration process. The selectivity, life time and cleaning needs are also important parameters, since they are important for the product quality and economy in the process. Ho and Zydney [52] showed that pore morphology and structure have an effect on membrane fouling in stirred cell UF. Membranes with straight-through pores were more sensitive to fouling than isotropic membranes, where the pores made up a network structure, because the fluid could pass the blocked pores. Asymmetric and composite MF membranes consisting of a top layer of straight-through pores with an underlying layer of highly interconnected pores showed similar results [53].

Increasing the hydrophilicity of the membrane by surface modification can also reduce fouling [54] [55] [56] [57] [58]. The more hydrophobic polysulfone (PS) and polyethersulfone (PES) membranes have been shown to cause severe fouling compared to the hydrophilic surface modified poly(vinylidene fluoride) ETNA membrane during filtration of BSA [59] [60]. Wei *et al.*[61], found that the water permeability was easily restored just by water rinsing after filtration with BSA for the ETNA membrane, in contrary to a PES membrane that needed chemical cleaning. The filtration rate was on the other hand higher using the PS

membrane compared to the ETNA membrane, probably due to a higher water permeability. Beier *et al.* [60] found that the adsorption of an amylase enzyme under static conditions (TMP equal zero) was significantly higher for a PES membrane compared to the ETNA membrane. The skin layer of the membrane was in this case in contact with the amylase solutions at different concentrations for 144 h, and the adsorption measured as the difference in permeability for a clean and fouled membrane. See figure 3.4.

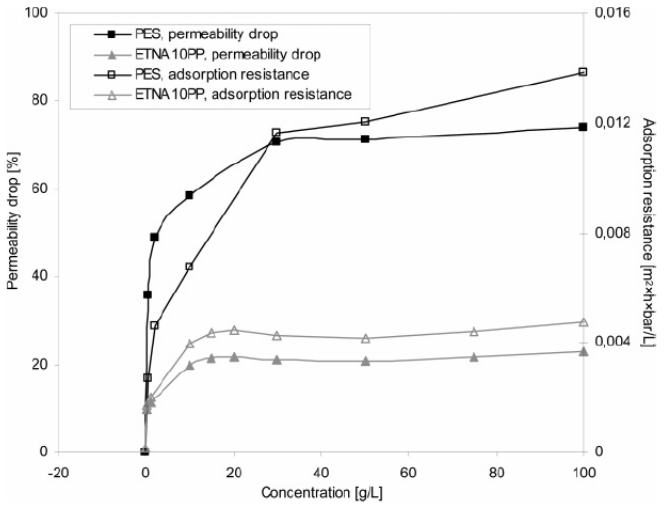

Figure 3.4: Adsorption isotherms. Permeability drop and adsorption resistance vs. enzyme concentration for static adsorption experiments on the two membrane types at constant temperature (5°C) [60].

The adsorption followed a Langmuir isotherm for both membranes. The maximum adsorption was reached at concentrations of around 30 g/L and 10 g/L, for the PES and the ETNA membranes corresponding to a decrease in the permeability of 75% and 23%, respectively [60]. Further information about this study can be found in appendix G.

The transmission and the permeate flux can be increased by the presence of a secondary membrane composed of for example yeast, see figure 3.5. The secondary membrane reduces fouling during the initial stage of filtration by preventing protein aggregates to bind to the membrane surface [62] [63].

Kuberkar and Davis [62] reported that crossflow MF carried out with a mixture of BSA and yeast doubled the long-term transmission compared to experiments with pure BSA solutions. The long-term flux was on the other hand lower for the mixture, due to additional fouling resistance caused by the yeast

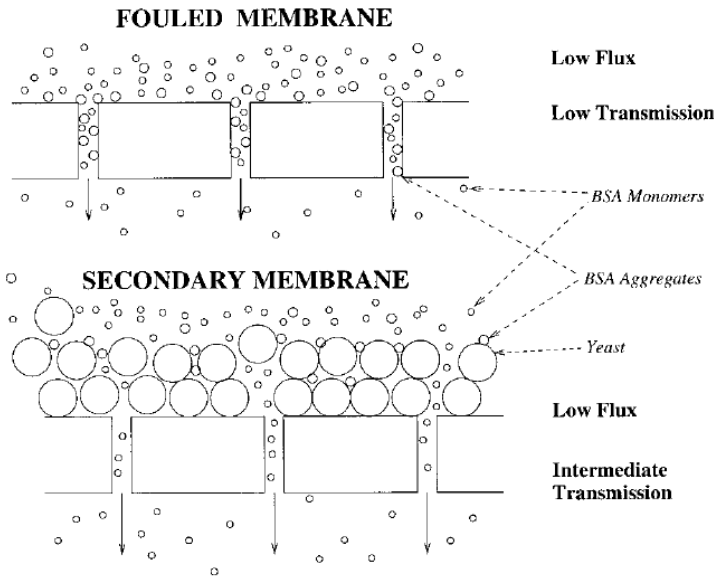

Figure 3.5: Schematic drawing of the effect of a secondary membrane to prevent fouling [62].

layer. Increasing the yeast concentration, and at the same time keeping the BSA concentration constant, was beneficial up to a certain point, above which the thickness of the yeast layer would result in a high hydraulic resistance.

Nemade and Davis [63] investigated the effect of a secondary yeast membrane in crossflow MF of BSA, and UF of a cellulase enzyme. The yeast layer was here added before the filtration of BSA and cellulase was carried out. MF of BSA showed an improvement in both flux and recovery, which was further improved when operating with backflushing (described in section 3.2). Using secondary membranes in UF also increased the flux, but not as pronounced as in MF. Individual proteins caused fouling in the UF system, where in MF the primary cause of fouling was protein aggregates, which was efficiently removed by the second membrane compared to individual proteins.

3.1.3 Operating conditions

The flux can be controlled by the operating conditions as described in the theory chapter section 2.1 for UF. A typical effect of the crossflow velocity and the TMP is shown in figure 3.6 for UF of skimmilk in a hollow fiber module 3.6 [64]. The flux increases when the crossflow velocity increases due to a higher shear rate at the membrane surface, which reduces concentration polarization. Increasing

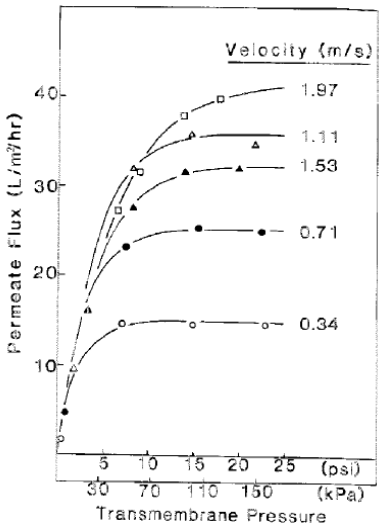

Figure 3.6: Flux as a function of TMP at various crossflow velocities during UF of skimmilk [64].

TMP up to 7-15 kPa depending on the crossflow velocity also enhances the flux until a limiting flux is reach, beyond which the flux becomes independent of TMP.

In MF the term "critical flux" is often used as a value above which fouling is no longer negligible. When operating below the critical flux, the flux increases linearly with TMP and is independent of time; if the flux exceeds the critical value the TMP increases rapidly and becomes dependent of time [65]. An example is shown in figure 3.7 where BSA (pH 9.0) is filtered through a 0.2 μm polycarbonate track-etched membrane.

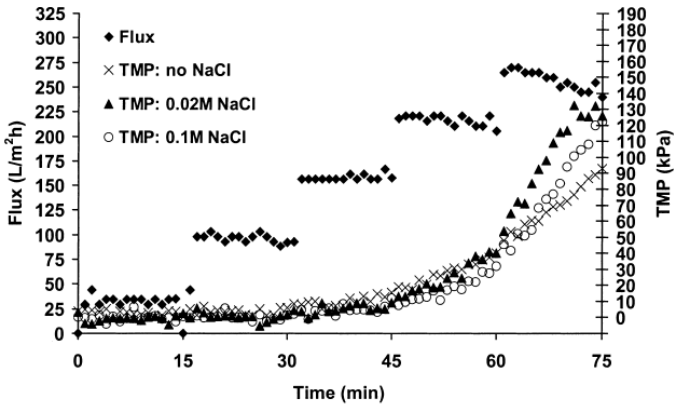

Figure 3.7: Flux as a function of TMP in MF of 1.0 g/L BSA at pH 9.0 using a 0.2 mm track-etched membrane. The conductivity was increased by adding NaCl [65].

The critical flux was here determined to 220 L/(m^2h), since the TMP increases quickly when this value was exceeded [65]. Chen *et al.* [27] showed in a crossflow UF and MF study of colloidal silica that the concentration polarization layer transformed into a cake when the critical flux was exceeded. Electron microscopy showed that the membrane only contained small deposits on the surface when operated below the critical flux; whereas large deposits was observed, when it had been exposed to a flux higher than the critical.

The transmission is also affected by the operating conditions. This is shown in crossflow MF experiments of β-lactoglobulin by Marshall *et al.* [66]. The experiments were carried out in constant flux mode by adjusting the TMP. The degree of fouling was strongly related to the filtration rate. When the flux increased, the level of fouling increased and the protein transmission decreased. It was concluded that the fouling mechanism was caused by internal fouling. This was the result of protein unfolding at the pore entrance due to shear stress near the pore wall. The author stressed that the solution did not contain any aggregates that could participate in pore blocking, as often observed in many stirred cell experiments [66].

Although mostly used in MF, a critical flux can also be determined in UF [26] [67]. Metsämuuronen *et al.* [67] showed that the TMP at which the critical flux was obtained during UF of skimmed milk increased when the pore size of the membrane decreased. However, a critical flux could only be determined when the protein concentration was below 0.3 w%. Given the low concentration it is difficult to see the usefulness of a critical flux in UF, since the concentration will often be much higher, if the purpose is concentration of e.g. proteins.

3.2 Methods to prevent fouling

There are several ways to reduce fouling in MF and UF. The preferred method depends on the filtration system. Pretreatment of the feed solution by adjusting the pH, prefiltration or operating below the critical flux can reduce fouling as described previously. This section describes methods to prevent fouling by flow manipulation and cleaning of fouled membranes.

3.2.1 Flow manipulation

Backflushing, backpulsing, crossflushing and flow reversal are all methods to reduce concentration polarization and cake formation by periodically reversing the permeate flow or feed stream. The principle of backflushing is shown in figure 3.8.

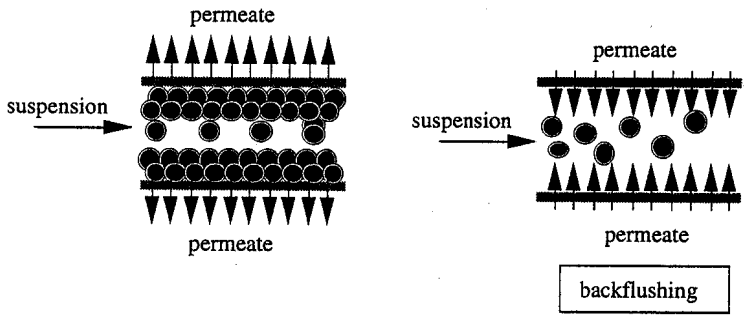

Figure 3.8: The principle of backflushing [3].

The permeate is periodically send back through the membrane pores, thereby releasing the filter cake from the membrane surface, which then is carried away by the crossflow stream. This is usually done 1-10 times per minute for a period of 1-5 seconds. The pressure on the permeate side must be higher than the operating pressure on the feed side, normally 1-10 bar.

A schematic drawing of the flux versus time for a filtration experiment using the backflushing technique is shown in figure 3.9.

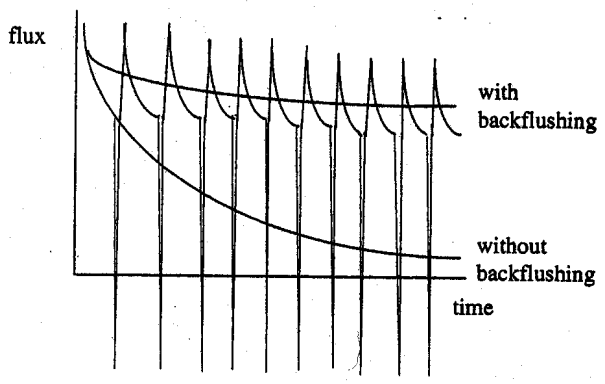

Figure 3.9: Illustration of the flux versus time with and without backflushing [3].

The backflushing ensures that a higher average flux is obtained and the initial flux decline is reduced. The effect of backflushing depends on the nature of the

deposit; sticky deposits are for example hard to remove. Backpulsing is based on the same principles as backflushing but with a higher frequency and a shorter duration of the pulses. A less effective way to reverse the permeate flow is by crossflushing (or lumen flush). This technique reverses the permeate flux by turning of the permeate flow for a few seconds. The disadvantage is that only the part of the membrane close to the permeate outlet will be affected [68]. Backflushing and backpulsing are mostly used in MF, since it can be difficult to reverse the permeate flow through an UF membrane due to its low porosity. The membrane most also be made of non-fragile material like e.g. ceramic or hollow fiber membranes, which can handle pressure from both the permeate and feed side without breaking. It is also more efficient for big molecules due to their relatively small diffusion coefficients. In UF, techniques like flow reversal [69] and TMP pulsing [70] [71] [72] can be used to enhance the flux by disturbing the concentration polarization layer.

Kuberkar *et al.* [73] showed that backflushing had a positive effect in MF of yeast. However, when BSA or a mixture of BSA and yeast was used, backflushing only had a small effect, due to different fouling mechanisms. Yeast cells formed a cake on the membrane surface which was easily removed with backflushing. BSA can, due to its small size, foul the membrane internally, which decreases the effect of backflushing. The crossflushing technique was also tested. The flux was improved when yeast was filtered with crossflushing compared to conventional crossflow filtration; but not as much as with backflushing. Crossflushing had no effect when BSA or a BSA-yeast solution was filtered [73]. Mores and Davis [74] obtained a flux of 71 % of the pure water flux after 2 hours of filtration when using backpulsing in crossflow MF of yeast.

In a study by Hargrove *et al.* [69] a substantial flux enhancement was reported in crossflow UF of BSA when the flow reversal technique was used, since a stable concentration polarization layer could not be formed under these conditions. By periodically reversing the feed stream a flux of 200 $\frac{\text{ml}}{\text{min m}^2}$ was reported, compared to only 10 $\frac{\text{ml}}{\text{min m}^2}$ after 1h of filtration for a 3.0 w% BSA solution, which is shown in figure 3.10.

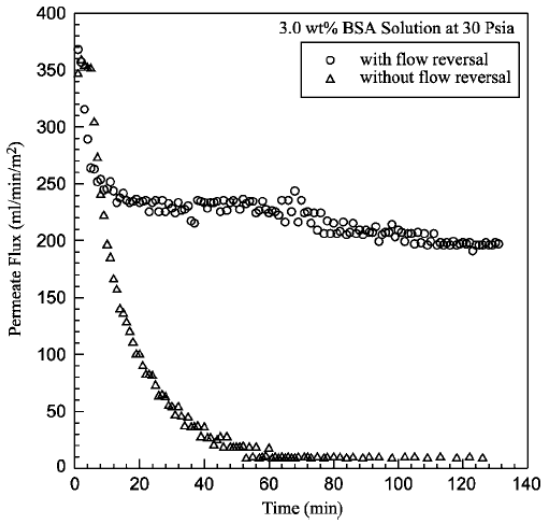

Figure 3.10: Permeate flux data with and without flow reversal for a 3.0 w% BSA solution [69].

The effect of flow reversal increased with increasing BSA concentration and TMP [69].

It is also possible to use a system where the membrane is moving instead of been fixed. Beier *et al.* [75] [76] showed that it was possible to filter yeast, and to separate yeast and enzymes in a vibrational hollow fiber module, where the module is vibrating along the feed flow direction. The flux could be kept at a high constant value at a low TMP. Rotational membrane disks can also be used to prevent fouling by introducing additional shear [77].

3.2.2 Turbulence promoters

Spacers, inserts or objects placed onto the membrane surface increases the turbulence of the feed stream, which enhances the flux [78] - [83]. A review and analysis of the performance of spiral wound modules and spacers is given by Schwinge *et al.* [84]. Examples of turbulence promoters can be seen in figure 3.11. These objects can have many different forms and shapes [68]. They prevent concentration polarization and cake formation due to increased velocities and wall shear stress at the membrane surface. A flux enhancement must be compared with the additional power consumption caused by an increased pressure loss in the filtration module. Spacers can also in some cases destroy the particles in the feed solution [68]. A 700 % increase in the permeate flux and

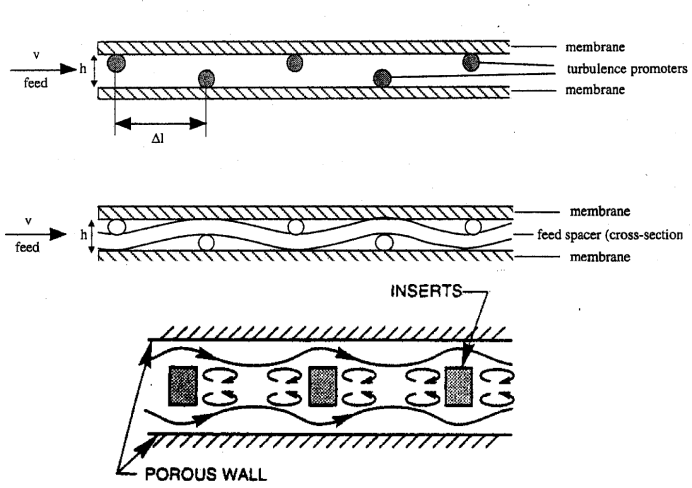

Figure 3.11: Schematic drawing of flow channels with turbulence promoters, feed spacers [3] and inserts [2].

a 25 % decrease in specific energy consumption were observed by Krstić *et al.* [81], when static turbulence promoters were used in MF of skim milk.

Spiral wound modules are commonly used in industrial processes due to their high membrane area to volume ratio [84]. Figure 3.12 show the principle behind spiral would modules.

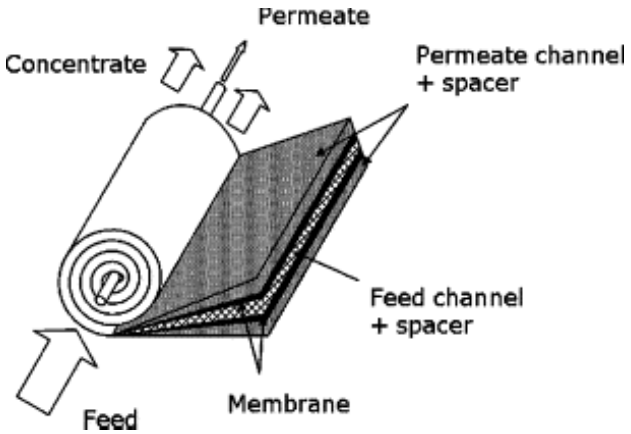

Figure 3.12: Illustration of a spiral wound module [84].

The feed solution flows parallel through the module along the central pipeline, while the permeate flows perpendicular to the center of the module [3]. The feed channel contains spacers, which depending on their shape have different impact on the flux. Lipnizki *et al.* [78] showed e.g. that spiral wound modules

containing a diamond shaped spacer resulted in a higher flux than an asymmetric spacer when filtering whey proteins.

3.2.3 Cleaning

Periodically cleaning of the membrane helps reduce the fouling problem. Time spend cleaning the membrane often pays of, instead of continuing the filtration process with a low flux. In industrial application cleaning is necessary since the equipment often is used for several different products, and to keep the filtration unit free of contamination like bacterial growth. The cleaning procedure can for most chemicals be accomplished within 30-60 min [3] [68]. The membrane can be considered clean when the pure water flux for a virgin membrane is obtained. In practice, it is however difficult or maybe even impossible to clean the membrane entirely. It is the physical and chemical properties of the foulant that decides, which cleaning agent that should be used; since it is the interactions between the foulant and the cleaning agent that controls the cleaning process. However, the cleaner should of course not harm the membrane [3] [68].

The temperature during the cleaning process is important, since it increases the rate of the chemical reactions, and should be as high as possible without destroying the membrane. A high crossflow velocity is also important. Cleaning should take place both on the permeate and feed side, and if possible, backflushing with the cleaning agent can be useful with colloidal and particulate fouling [68].

The TMP should on the other hand be low to prevent foulants to be forced further into the membrane. The water used in the cleaning procedure is also important. Soft water should be used; especially concentrations of iron, manganese, alumina, calcium and silica should be low [68].

Water rinsing is usually the first step in the cleaning procedure. Rinsing with water was shown to restore the membrane efficiency by 90% in a study of ceramic ultrafiltration membranes fouled with whey proteins [85].

Biofilms are particular difficult to clean, they consist of polysaccharides and micro-organisms; and have a gel or slimy nature that sticks to the membrane. In some cases it can therefore be necessary to use a cleaner with a high pH ($\approx$ 13) to get a successful cleaning, which normally is above the recommended value from the membrane manufactures [86].

Proteins can be removed using alkaline cleaners containing NaOH or KOH.

They break down the bonds between the membrane and the fouling layer, and can solubilize the proteins by peptization [68] [87]. Inorganic salt fouling can be removed by an acid cleaner. Blanpain-Avet *et al.* [87] used NaOH followed by HNO_3 to clean ceramic MF membranes fouled with whey protein, however full recovery was not accomplished. The cleaning efficiency also depends on the membrane type. Wei *et al.* [61] showed that the water flux of low fouling membranes could be around 98 % restored after water rinsing, while the water flux of PES membranes could only be restored around 50 % after BSA fouling. A full 100 % recovery could be accomplished for all membranes by cleaning with the commercial cleaning agent ultrasil 10.

Enzymes can also be used to clean membranes fouled with proteins. A 100% flux recovery was almost reached when inorganic UF membranes fouled with whey proteins were cleaned with enzymes. The cleaning time was very short, only 20 min, and the enzyme solution could be reused, although a 30% loss in activity was observed after each cleaning cycle [88]. Lipnizki *et al.* [78] showed that membranes fouled with whey protein can be cleaned completely with enzymes followed by a caustic cleaning cycle. Some of the drawbacks using enzyme cleaners are that they can act as a foulant themselves and cause contamination of the product. Enzymes are also typically expensive.

It is also possible to clean membranes using external force fields such as ultrasonic and electric fields, this is described in the next chapter.

3.3 Summary

- Flux decline in membrane filtration is caused by fouling and concentration polarization. UF membranes are mainly fouled at the membrane surface while MF membranes are fouled internally. In the initial stage of filtration, the proteins adsorb to the membrane and a huge decline in the flux occurs. After the initial stage the flux continues to decline due to further deposition to the initial adsorbed layer.

- The pH, ionic strength and stability of the solutions are important. Generally filtration of proteins should be carried out at a pH different from pI, since the electrostatic interactions are at a minimum at pI, which favours fouling due to a denser deposit layer. Aggregates are also formed more easily due to the lack of repulsive forces at pI. The ionic strength decreases

the electrostatic forces and a decrease in the filtration rate is generally observed at high ionic strengths.

- Proteins generally adsorb less to hydrophilic membranes compared to hydrophobic due to their large hydrophobic regions. The membrane surface can be modified to become more hydrophilic.
- Flow manipulation like backflushing, backpulsing or flow reversal can be used to maintain a high average flux in crossflow filtration.
- Turbulence promoters can reduce concentration polarization and cake formation by increasing the velocity and wall shear stress at the membrane surface.
- Membranes fouled with proteins can be cleaned with alkaline cleaners like NaOH or KOH. A high temperature and low TMP are important in the cleaning procedure to ensure a reasonable cleaning time, and preventing fouling material from entering deeper into the membrane pores.

Chapter 4

Literature review: Crossflow electrofiltration

In this chapter a review of electrically enhanced microfiltration (EMF) and ultrafiltration (EUF) (generally referred to as electrofiltration) is given. The emphasis is on crossflow modules, and the influence of the process design, electric field and feed properties is explained. Further, a short introduction to dead-end electrofiltration is given, together with ultrasonic assisted filtration. Both biological and mineral solutions are discussed in order to provide an elaborated explanation of the phenomena occurring in electrofiltration.

As described in section 2.2, electrofiltration utilizes that charged molecules migrate in an electric field. Application of an electric field across an UF or MF membrane enhances the flux by dragging the molecules from the concentration polarization layer at the membrane surface into the bulk solution. Hence the flux increases. Electrofiltration has been used to enhance the flux in many systems, and an significant improvement of a factor of 2-10 is common when applying an electric field during filtration of solutions containing biomolecules or minerals. Many authors have investigated the flux enhancement during filtration of anatase (TiO_2) [89] - [92], BSA [93] - [97] and gelatin [15] [98].

A 70% flux enhancement was e.g. reported by Oussedik *et al.* [96] when filtering a 10 g/L BSA solution at an electric field strength of 700 V/m using a 25 kDa flat sheet fluoride polyvinylidene membrane. The TMP was 1 bar and the crossflow velocity 0.4 m/s. Weigert *et al.* [7] obtained a 6-fold increase in the filtration rate for bakers yeast at an electric field strength of 125 V/m; and a 10-fold increase for a 0.2 vol% cristobalit solution when 150 V/cm was applied.

The TMP was 0.1 MPa and the crossflow velocity 0.6 m/s. The membrane had a pore size of 0.2 μm.

It is also possible to improve the filtration rate and purity of wastewater [99] [100]. Usually a direct current is applied; however, Zumbusch *et al.* [101] showed that it is also possible to use an alternating current (ac) to improve the flux during filtration of BSA. Lazarova and Serro [13] applied an electric field during MF of silicon oxide solutions. Here the relative flux improvement increased in the range of 2-3.5 times depending on the feed concentration.

Chemical reactions at the electrodes are one of the side effects in electrofiltration. A typical electrode reaction is electrolysis of water [1]:

$$2H_2O + 2e^- \longrightarrow H_2\,(g) + 2OH^- \;\; (cathode, -0.83\ V) \tag{4.1}$$

$$2H_2O \longrightarrow O_2\,(g) + 4H^+ + 4e^- \;\; (anode, +0.40\ V) \tag{4.2}$$

where hydrogen and hydroxide are developed at the cathode; and oxygen and hydrogen-ions are developed at the anode. These electrode reactions may cause a change in pH.

4.1 Process design

The electrofiltration module can be either tubular [15] [17] [99] [102] or flat sheet [7] [13] [90] [93] [103] [104]. In the tubular module an electrode consisting of a tube is placed inside the module. The anode is often covered with an inert material such as platinum, and the cathode is usually made of stainless steel. The simplest construction of a flat sheet electrofiltration module is made by placing the electrodes directly into the feed and permeate solutions on each side of the membrane as shown in figure 2.4. The electrode can also function as a support layer for the membrane [91]. There have also been some examples of the membrane been used as an electrode itself -usually the cathode [1] [98] [102]. In this case the electroosmotic force will be zero, since there is no electric field across the membrane. There are some disadvantages with this configuration. If the feed solution contains any fragile components they can be damaged by direct contact with the electrodes or by any pH changes caused by electrolysis of water. Fouling of the electrodes can also occur. Protein degradation has been observed by Wakeman [93] when solutions of BSA, ovalbumin and lactalbumin are in direct contact with the anode. Here the membrane was completely blocked by

degraded BSA when the concentration was higher than 15 g/L, which decreased the permeate flux to zero. The evolution of gas bubbles due to electrolysis of water can also affect the electrofiltration process. Huotari *et al.* [99] reported that formation of foam on the membrane surface due to gas bubbles had a negative influence on the permeate flux during electrofiltration of oily waste water. The membrane was in this case used as a cathode. The bubbles caused a decrease in the current efficiency, which especially was a problem when the conductivity of the feed solution was high. On the other hand Bowen *et al.* [91] reported that the bubbles prevented fouling by releasing the fouling layer on the membrane surface during pulsed electrical cleaning.

To avoid degradation of feed components the electrodes can be shielded by e.g. ion-exchange membranes [7] [105] [106] or dialysis membranes [107]. This will however increase the complexity of the EUF module and increase the distance between the electrodes, which increases the resistance, and thereby the energy consumption of the module. Like in electrodialysis, a limiting current effect can also be a problem in such a module. The limiting current effect occurs when the transport of ions through the ion-exchange membrane is faster than the transport of ions to the surface of the ion-exchange membrane [108].

4.2 Electric field

In electrofiltration a direct current (dc) is generally applied across the membrane; the current can be either constant or pulsed with different time intervals between the pulses. It is also possible to apply an alternating current (ac), but this is not common [101].

The effect of the electric field depends primarily on the size and surface charge of the solute and the electric field strength. Small particles with a high surface charge results in the greatest flux enhancements [109] [110].

As described in section 2.2 there exists a critical electric field strength at which the concentration polarization layer has been removed and a further increase in the electric field strength do not result in a higher flux. The appearance of the concentration polarization layer at the membrane surface is illustrated in figure 4.1 when the electric field is below, equal or above E_c. If the electric field is less than E_c there is a net migration of particles towards the membrane surface, and a gel or cake layer is formed, see figure 4.1a. A further increase in

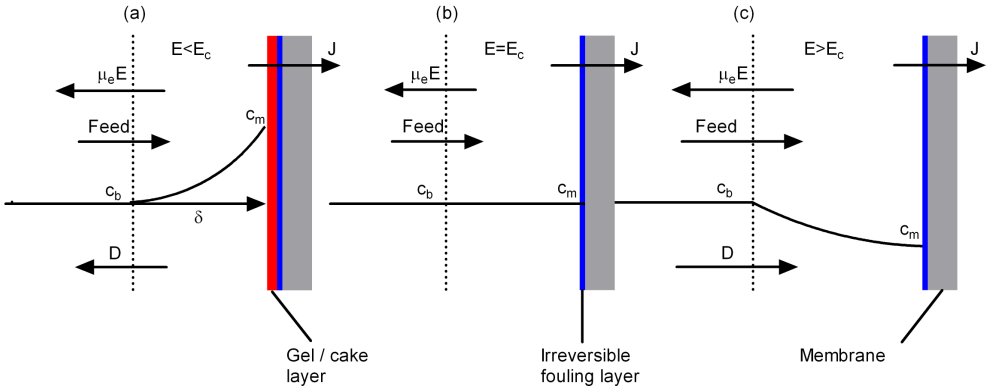

Figure 4.1: Illustration of the effect of the electric field strength on the particle concentration at the membrane surface. (a) shows the situation when the electric field strength is less than the critical electric field strength. In (b) the critical electric field strength is obtained and in (c) it is exceeded. Inspired from Henry et al. [14].

the permeate flux can then be achieved by increasing the electric field strength. When the electric field strength is equal E_c there is no migration of charged particles towards the membrane surface, and a further increase in the flux cannot be achieved by increasing the electric field strength any further, as illustrated in figure 4.1b. Above E_c, the concentration of particles at the membrane surface is less than in the bulk solution, and there is a diffusion of particles towards the membrane surface as shown on figure 4.1c.

An example is given in figure 4.2 where EMF was used in treatment of waste water containing minerals [104].

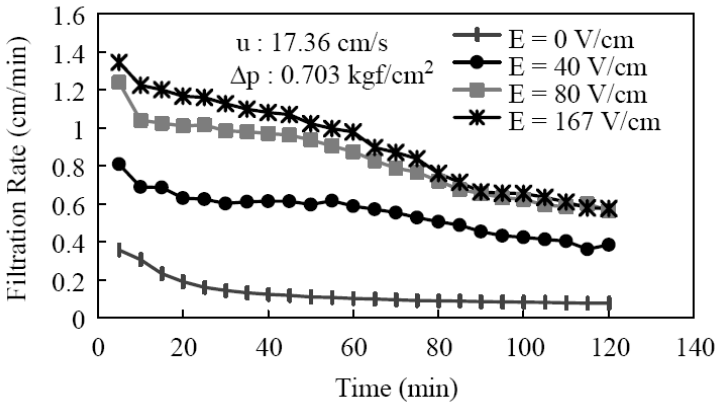

Figure 4.2: Electrofiltration of waste water [104].

As observed from figure 4.2 the filtration rate increases significantly when an electric field strength of 40 V/cm is applied and even more when 80 V/cm is used. The application of 167 V/cm gives a flux in the same range as 80 V/cm. This means that the critical electric field strength is reached around 80 V/m for this system [104].

4.2.1 Pulsed electric field

The use of a pulsed electric field can reduce the energy costs, and in some cases result in a higher flux compared to a constant electric field. Weigert *et al.* [7] used electrofiltration to filter cristobalit and bakers' yeast (saccharomyces cerevisiae). Experiments with both constant and pulsed electric fields were carried out. For the cristobalit solution, a significant decrease in the flux was observed when a pulsed electric field was used instead of a constant. In the case of bakers' yeast the opposite effect was observed. The author concluded that in biological systems it is an advantage to use a pulsed electric field compared to a constant field; and the opposite if the solution is a mineral slurry. The reason was suggested to be due to the different particle sizes and charge conditions [7]. Some parallels can be made between the pulsed electric field and backpulsing, which has been described in section 3.2. The effect of backpulsing is also more efficient during filtration of particles like yeast cells, compared to smaller molecules like proteins. Yeast cells have due to their large size a smaller diffusion coefficient compared to BSA, and will therefore bounce slowly back to the membrane surface, hence the effect of an electric pulse will last longer.

These observations are consistent with other examples found in the literature. A significant decrease in the filtration rate was observed when a pulsed electric field was applied to the system shown in figure 4.2 [104]. Filtration of titania solutions also showed a decrease in the flux when a pulsed electric field was used instead of a constant field [90]. Robinson *et al.* [97] showed that the solute related resistance decrease when using a constant electric field compared to a pulsed electric field in EUF of BSA. The effect of the pulse duration is shown in figure 4.3.

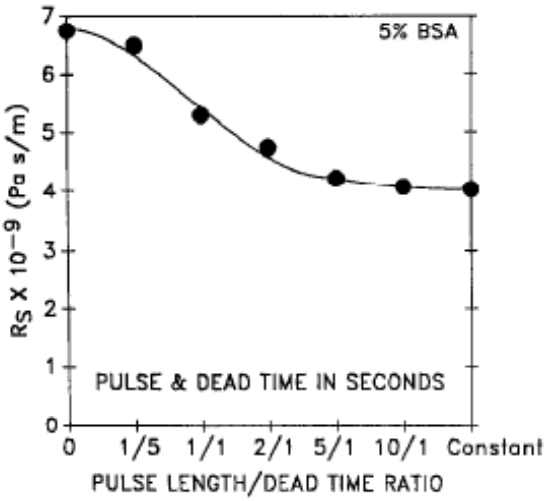

Figure 4.3: Effect of pulse length on the solute related resistance during EUF of BSA [97]. E=1600 V/m, TMP=60 kPa and f=0.03-1 Hz.

The solute related resistance decreases as the ratio, between the time the electric field is switched on with respect to the time it is turned off, decreases. The pulse length must in this case be 10 times longer than the dead time before the resistance is close to the constant field value. The frequency of which the electric field was turned on and off did not have an effect, only the ratio [97]. However, contradicting results have been reported for BSA. Oussedik *et al.* [96] reported a significant flux enhancement when a pulsed electric field was applied instead of a constant field in EUF of BSA. However the flux improvement was in this case low at a constant electric field. The reason for this contradiction is complex, but might be due to the different membranes and operating conditions [96].

4.3 Effect of feed properties

4.3.1 Feed concentration

In electrofiltration as in conventional crossflow filtration, the flux generally decreases when the concentration increases. However, an increased efficiency of the electric field at higher concentrations have been reported in several cases [13] [96] [97] [111]. When the concentration increases the thickness of the concentration polarization layer increases, which makes the impact of the electric field greater [106]. An example can be seen in figure 4.4 where a mineral slurry of silicium

oxide particles is filtered.

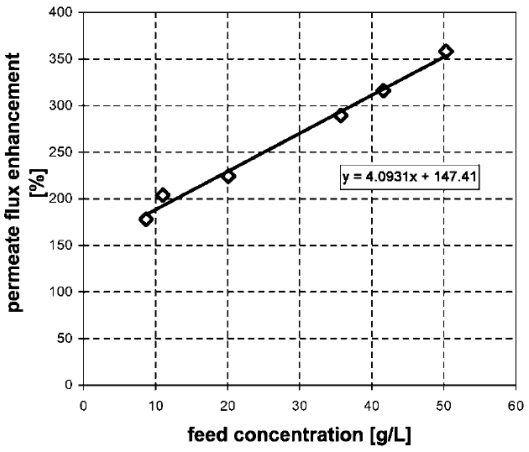

Figure 4.4: Permeate flux enhancement as a function of the concentration of silicium oxide particles at E =133 V/cm, ΔP = 2.15 bar and v = 0.23 m/sec [13].

The flux enhancement increases from an improvement of around 200% to around 350% when the feed concentration increases from 10 to 50 g/L. Similar trends have been reported for water soluble polymers [111] and BSA [96] [97].

4.3.2 ζ-potential and conductivity

Generally the greatest flux enhancement is achieved when the ζ-potential of the solute is high [92]. The ζ-potential of e.g. proteins can be changed by changing the pH of the solution. Proteins are positively charged at a pH below the isoelectric point and negativity charged above the isoelectric point due to ionization of the carboxyl and amino groups [1]. Figure 4.5 shows the ζ-potential as a function of pH for BSA [9].

The ζ-potential is zero around pH 5, which is the isoelectric point of BSA. The net protein charge due to hydrogen ion dissociation of BSA is also shown in figure 4.5. The isoionic point pII is defined as the pH where the net H^+ charge of the BSA protein is zero [9]. However, only the ζ-potential is considered in electrofiltration since it is directly related to the electrophoretic mobility.

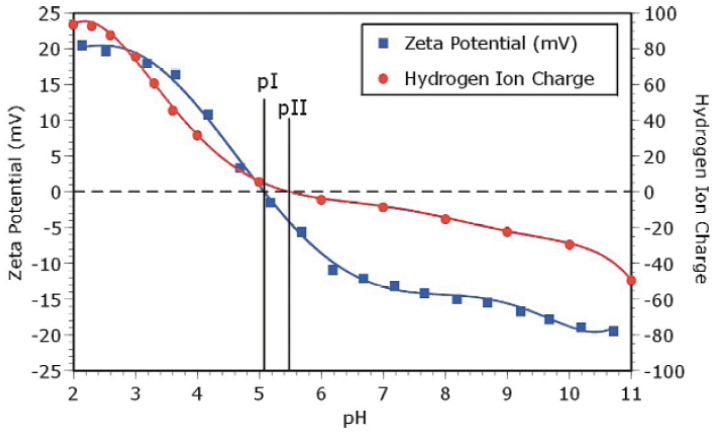

Figure 4.5: ζ-potential vs. pH obtained by titration of BSA in 100 mM NaCl. pII represents the pH-dependent hydrogen ion charge [9].

The conductivity of the solution also affects the ζ-potential, since the presence of ions decreases the thickness of the diffuse double layer as described in section 2.2. The effect of pH and conductivity on the electrophoretic mobility can be seen in figure 4.6 for solutions of cristobalit TiO_2 and yeast [7].

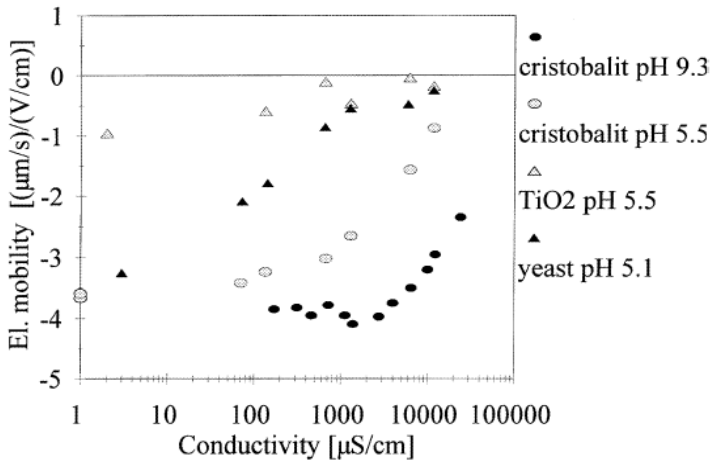

Figure 4.6: Electrophoretic mobility of different solutions as a function of the conductivity [7].

The conductivity was increased by adding KCl to the solutions. Figure 4.6 clearly shows that the electrophoretic mobility decreases when the conductivity increases. The ζ-potential and conductivity are also decisive parameters when considering the economy of the EUF process, which will be described later in this chapter.

4.4 Effect of crossflow velocity and TMP

The effect of TMP and crossflow velocity is more complex in electrofiltration compared to conventional UF and MF, as the influence of these parameters depend on the electric field strength and the ζ-potential of the solute. The magnitude of the crossflow velocity and the electric field strength both influence the thickness of the concentration polarization layer. Usually a higher flux can be achieved by increasing the crossflow velocity if $E < E_c$, since a concentration polarization layer is present at the membrane surface [1]. If $E = E_c$, a higher crossflow velocity will have no effect, since the concentration polarization layer already has been removed [1]. An increased crossflow velocity might even lead to a decrease in the flux if $E > E_c$ due to increased back diffusion towards the membrane surface. An example of this is given by Lazarova and Serro [13] in figure 4.7, where silicium oxide particles are filtered at different crossflow velocities and electric field strengths.

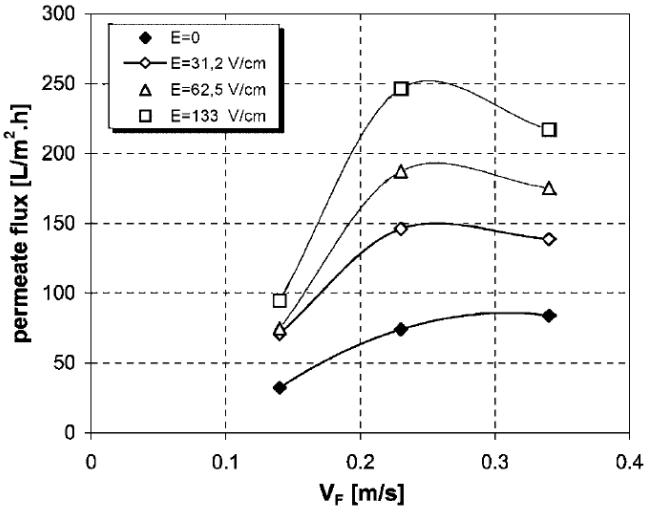

Figure 4.7: Influence of crossflow velocity during filtration of 10 g/L silicium oxide particles at different electric field strengths [13].

The flux increases when the crossflow velocity increases from 0.14 to 0.23 m/s, but declines if the crossflow velocity increases further to 0.34 m/s, when an electric field is present. The decline is also steeper the higher the electric field strength becomes. If no electric field is present only a small increase in the flux is observed at 0.34 m/s compared to 0.23 m/s indicating that no cake formation occurs beyond 0.23 m/s. The flux decline at 0.34 m/s compared to 0.23 m/s

when an electric field is present is explained by the authors as an increased back diffusion towards the membrane surface [13]. Henry *et al.* [14] also observed a decrease in the flux when the Reynolds number increased during filtration of an oil and water mixture. The decline was more pronounced when increasing the electric field strength. The same was observed when filtering solutions of clay. However, when the system was operated at an electric field strength below the critical an increase in the flux was reported when the crossflow velocity increased.

Wakeman *et al.* [93] found that the crossflow velocity only had a minor influence during EMF of BSA at 333 V/cm, while Rios *et al.* [17] found that the flux increased proportionally with the crossflow velocity over an electric field range from 0-2400 V/m during EUF of BSA. The difference is probably due to the significantly lower electric field strength used by Rios *et al.* [17], which probably is below the critical electric field strength.

Decreasing the crossflow velocity can have a positive effect if the ζ-potential is low. Filtration of anatase at $\zeta = -7\ mV$ by Wakeman *et al.* [92] showed an approximately 20% increase in the filtration rate when the crossflow velocity was decreased by one third. When the filtration experiment was operated at high crossflow velocity there was no effect of the electric field. A possible explanation is that a lower crossflow velocity will prolong the residence time of the particles in the filtration module; thereby increasing the effect of the electric field [92].

In electrofiltration the effect of the electric field increases at elevated TMP, since the concentration polarization layer increases. Houritari *et al.* [99] reported that the limiting flux increased to more than 350 L/(m^2h) at an electric field strength of 2400 V/m compared to 75 L/(m^2h) at 0 V/m during EMF of oily waste water. The result can be seen in figure 4.8. It also shows that the effect of the electric field is low at low pressure. However, if the TMP increases too much a decrease in the filtration rate has also been observed due to a compressed concentration polarization layer. This effect is reported by both Yang *et al.* [104] and Lazarova and Serro [13].

These examples show that the electrofiltration process can be operated at low crossflow velocity and higher TMP compared to conventional crossflow filtration. This is an advantage in industrial production, since the pressure loss in the filtration module decreases at low crossflow velocities. Hence a reduction of the pumping costs can be achieved. Less membrane area is also required if the flux can be increased by operating at a higher TMP.

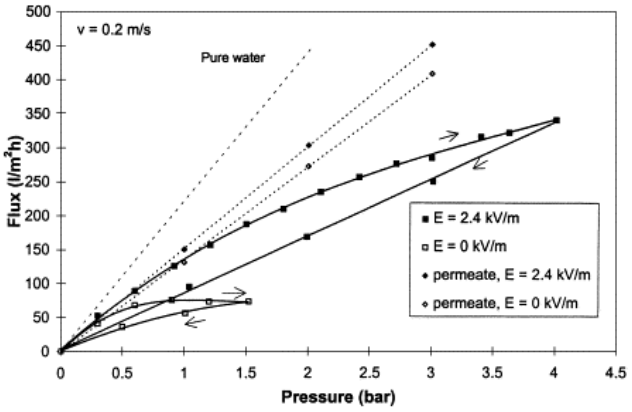

Figure 4.8: Flux versus pressure of the permeate and the pure water flux during filtration of oily waste water [99].

4.5 Retention

Electrofiltration may increase the retention of the membrane [93] [99] [103] [111] [112], and it is therefore possible to use a larger pore size without decreasing the retention. An example is EMF of 1 g/L BSA as shown in figure 4.9 where pore sizes in the range of 0.05-8.0 μm have been tested [93].

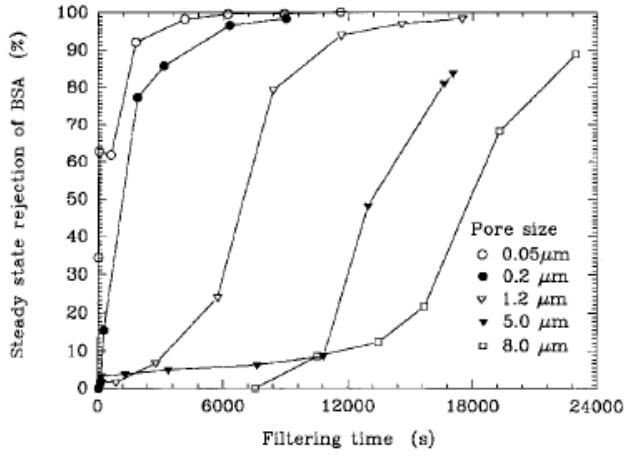

Figure 4.9: Steady state rejection of BSA using cellulose nitrate membranes with different pore sizes, $E = 267 V/m$, $TMP = 204$ kPa and $v = 1.5 m/s$ [93].

Membranes with pore sizes up to 1.2 μm all resulted in a retention of nearly 100%, although the occurrence of the steady state retention is delayed as the

pore size increases. The retention was in this example increased significantly compared to conventional MF at 0 V. The retention was also close to 100% for concentrations up to 10 g/L [93]. Rios *et al.* [17] also showed that the retention increased from 83% to 91% when applying an electric field of 2400 V/m to a 10 g/L gelatin solution. However, it is doubtful if a sufficiently high retention can be achieved by a membrane with a large pore size, if the solution is going to be concentrated to around 100 g/L, which is not unlikely in an industrial process.

4.6 Selectivity

It is also possible to enhance the separation of two different molecules by an electric field. The molecules must either have opposite charge, or one must be neutral while the other is charged [108] [113]. Lentsch *et al.* [106] showed that BSA (67 kDa) and polyethylene glycol (PEG) (20 kDa) can be separated by applying an electric field across an 100 kDa PS membrane. By using an electric field and setting the pH to 6.8 where BSA is negativity charged and PEG neutral, BSA was retained by the membrane while the transmission of PEG was enhanced. In conventional UF, such a separation is not possible due to fouling and concentration polarization of the membrane mainly by BSA. If UF is going to be used for separation the retained molecule must be at least 10 times larger than the molecule going through the membrane.

4.7 Process economy

Despite the good filtration performance in electrofiltration, the process is not yet (at least to my knowledge) used in large-scale production. One of the reasons could be the high energy consumption of the electric field. The conductivity of the feed solution is critical. According to Ohm's law a low conductivity is necessary if the energy consumed by the electric field is going to be kept low, since the current needed to maintain a certain voltage (hence the electric field strength) across the membrane increases if the conductivity increases [7] [105]. A high conductivity also increases the amount of heat and electrolyte gasses produced at the electrodes. If too much salt is present in the feed solution it could decrease the ζ-potential, and lead to a smaller effect of the electric field [1]. Weigert *et al.* [7] showed that if the conductivity of a cristobalit

solution exceeded 2 mS/cm, the advantage of using EMF disappeared, since the energy requirements of the electric field became too high. Huorari and Nyström [114] also concluded that electrofiltration of waste water is too expensive due to the high conductivity of the solution. On the other hand Wakeman and Sabri [90] found that the power consumption decreased during EMF of 1 w% TiO_2 compared to conventional MF, especially at a low crossflow velocity, a high TMP and a high electric field strength. However, TiO_2 was dissolved in double distilled water, which probably resulted in a low conductivity.

4.8 Electrical cleaning of membranes

The electric field can also be used to clean the membrane periodically during the filtration process. By applying the electric field for short time intervals after a period of filtration a reduction of the filtration time can be achieved [18] [115] [102]. Figure 4.10 shows the effect of applying 15 V to a solution of bovine plasma during UF [102].

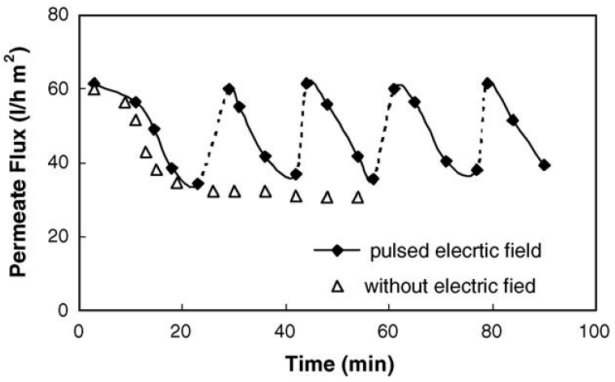

Figure 4.10: Permeate flux during filtration of bovine plasma (0.5 % & pH 7.8) with pulsed electrical cleaning. The dotted lines indicate the application time of the electric field [102].

By restoring the flux to its initial value after it has declined to nearly the same level as in conventional UF, it is possible to achieve a higher average flux. Similar results have been reported by Bowen *et al.* for periodically cleaning of membranes fouled with titanium oxide and bakers yeast [18] [91]. Webster *et al.* [115] reported on the other hand that *in situ* electrochemical cleaning of microporous silver membranes fouled with BSA and phosphate was relatively

inefficient. In contrary, *ex situ* electrochemical cleaning, where the protein solution was replaced with an acid or base solution was more efficient. SEM pictures showed that fouling occurred inside the membrane and not on the surface, which could be the reason for the low effect of the *in situ* cleaning.

The main reason for choosing a short duration of applying the electric field compared to applying it throughout the whole process is that it saves energy. The efficiency is dependent on the rate of the flux decline after the electric field has been turned off. If the flux decline is very fast, the advantage of electrical cleaning is small, and it would probably be beneficial to apply a constant electric field throughout the entire filtration process.

4.9 Dead-end electrofiltration

Electrofiltration can also be used in a dead-end separation processes [94] [95] [116] - [119]. One of the advantages of dead-end filtration compared to crossflow filtration is that it is possible to achieve a higher concentration in the concentrate [117]. Generally observations made in crossflow electrofiltration concerning feed properties can be transferred directly to the dead-end process.

The electrodes can be placed in different ways when using dead-end electrofiltration. Genç and Tosun [116] filtrated anatase particles (TiO_2) with 3 different electrode configurations, which is shown in figure 4.11.

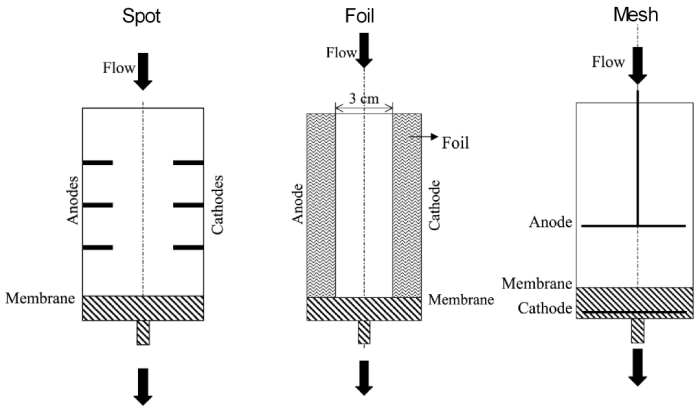

Figure 4.11: Spot, foil and Mesh configuration [116].

The electrodes are in all three cases placed inside a cylinder tube. The three configurations are called "spot", "foil" and "mesh". When the foil and spot configuration are used, the filter cake will build up along the electrode with

the opposite charge of the particles. All configurations resulted in an increased filtration rate. It was concluded that the mesh configuration gave the highest filtration rate, while the foil configuration used the smallest amount of energy [116].

The distance between the electrodes also influenced the filtration rate for the mesh configuration. It was reported that an increased separation distance between the electrodes resulted in an increased filtration rate, but only up to a distance of 5 cm, a further increase did not affect the filtration rate. According to the authors, the increased filtration rate was due to a larger number of particles being exposed to the electric field, even though the electric field strength decreases as the separation distance increased [116].

Hofmann and Posten [117] reported a decrease in the filtration time from 62.8 h to 1 h when filtering 135 cm^2 of xanthan solution using a foil electrode configuration. A decreasing filtration rate was observed when the ζ-potential was low, regardless of whether the value was changed by adding salt or by adjusting pH. In this case the filtration rate also increased when the pressure increased. Larue and Vorobiev [118] showed that the process time during filtration of kaolin solutions could be reduced by 50% when an electric field was applied for 37% of the total process time. Significant flux improvements have also been reported for dead-end electrofiltration of BSA [119], $CaCO_3$ and white clay slurry [95].

4.10 Acoustic and Electroacoustic

Sound waves with a frequency above 18 kHz are called ultrasonic waves and cannot be heard by the human ear. When ultrasound is propagated though a liquid medium, alternating rarefaction and compression cycles occur. Microbubbles can be formed during the rarefaction if the pressure is high enough to cause a fraction of the liquid. This phenomenon is called cavitation. Under the compression cycle the bubbles will grow and finally collapse causing shock waves to irradiate though the liquid, and can result in local temperatures up to 4000-6000 K and pressures of 100-200 MPa. If the collapse of the microbubbles occurs at the membrane surface they can release molecules from the fouling layer [120]. Figure 4.12[1] shows the formation and collapse of a microbubble.

[1]Picture from http://www.variclean.nl/Ultrasoon/theorie.php

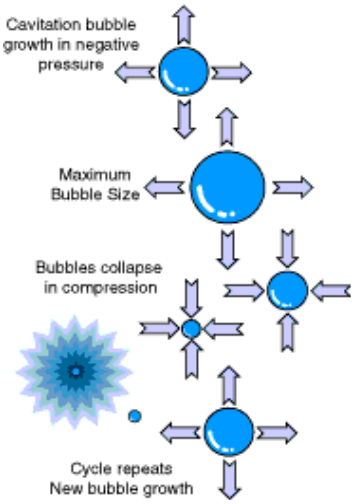

Figure 4.12: Cavitation and collapse of bubbles.

The violence of the cavitation collapse depends on the frequency. Low frequencies (20 kHz) result in a more violent collapse of the bubble compared to high frequencies (500 kHz), since the resonant bubble size is inversely proportional to the frequency of the sound wave [121].

Ultrasonic fields can be used in filtration to enhance the flux [122] - [126], cleaning of the membrane [127] [128], dewatering of filter cakes [129] or in combination with an electric field [89] [92].

Kobayashi and Fujii [124] showed an increase in the permeate flux when ultrasound was applied in crossflow ultrafiltration of dextran, which is shown in figure 4.13.

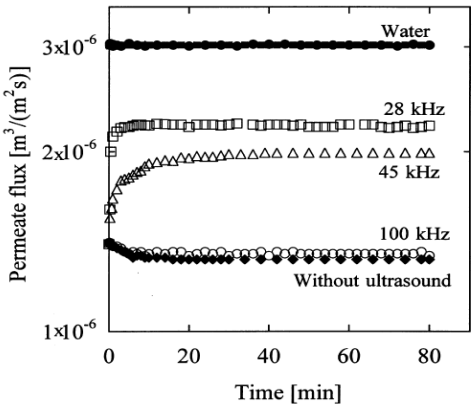

Figure 4.13: Permeate flux as a function of time for 1 %w dextran during irradiation of ultrasound with different frequencies [124].

The effect was highest at 28 kHz and decreased as the frequency increased. A frequency of 100 kHz had no effect, due to less cavitation. The experiments also showed that the direction of the propagated waves influenced the permeate flux. The highest flux enhancement was achieved when the sound waves was irradiated perpendicular on the feed side of the membrane, and lowest on the permeate side [124]. Ultrasound also increased the filtration rate 4-6 times in crossflow microfiltration of baker's yeast and BSA. Ultrasonic waves efficiently removed the filter cake deposit on the membrane surface, and prevented plugging of the membrane pores [122]. It is also possible to use a combined electric and ultrasonic field, which, due to a synergy between the fields can be more efficient than application of the two fields separately. A significantly reduction in the filtration time was observed by Wakeman and Smythe during dead-end filtration of rutile solutions, when a electroacoustic field was applied. The power consumption of the acoustic field was however too high to make the process economical sustainable [89] [129]. Flux enhancements above an order of magnitude have also been reported from crossflow MF experiments of anatase, calcite and china clay when ultrasonic and\or electric fields were applied [92].

4.10.1 Ultrasonic cleaning of membranes

It is also possible to use ultrasound to clean fouled membranes. Lamminen *et al.* [128] found that ceramic membranes fouled with sulfate polystyrene latex particles may be cleaned using ultrasound with frequencies from 70 kHz to 620 kHz. The cleaning was most efficient at low frequency and high power intensity. The flux recovery was dependent of the time the membrane was exposed to the ultrasonic field. A full recovery was observed when the membrane was irradiated for more that 30 sec. Muthukumaran *et al.* [127] reported a 80% flux improvement when PS UF membranes fouled with whey proteins were cleaned with ultrasound. The most efficient cleaning was obtained when surfactants was used in combination with an ultrasonic field.

4.11 Summary

- Application of an electric field across the membrane can reduce concentration polarization and membrane fouling. Flux improvements in the range

of 2-10 times have been gained for biological and mineral solutions.

- Pulsed dc electric fields have resulted in large flux enhancements in filtration of biological solutions, compared to constant electric fields. The contrary is the case for mineral slurries.

- Low conductivities and high ζ-potentials are necessary to achieve large flux improvements in electrofiltration, and to reduce the energy consumption.

- A low crossflow velocity and TMP can be used in electrofiltration compared to conventional crossflow filtration. The membrane selectivity also improves i.e. a larger pore size can be used.

- Applying an electroacoustic field can in some cases increase the flux even further due to synergistic effects, than if the electric field was used alone.

Chapter 5

Experimental

This chapter contains information about the experimental set-ups and procedures used to study EUF of enzyme solutions from Novozymes A/S. Two different filtration modules are described; an EUF module and an UF module. The UF module is used to collect flux data under different crossflow velocities and to compare the energy consumption during UF and EUF. The properties of the enzyme solutions are described together with the method used for determination of the enzyme concentration.

5.1 Enzymes

Five different enzymes have been tested; two amylases, two proteases and one lipase. The amylases are produced by fungi while the other enzymes are produced by bacteria. The solutions have been taken directly out of the production line after UF. The enzyme solutions are not completely pure, but contain impurities, which are produced during fermentation or added during the recovery process. Depending on the enzyme product the impurities can be carbonates, remaining amino acids, flocculation chemicals or other proteins formed during fermentation. The most common flocculation chemical is $CaCl_2$, which is present in all the enzyme solutions in large quantities. Other flocculation chemicals consist of large anionic or cationic polymers, which may be used during the recovery of the bacteria enzymes. For the protease-S solution antifoam is also added during fermentation.

To remove salt added previously in the process, the enzyme concentrates are dia-

filtrated with demineralized water until the conductivity in the permeate is below 0.5 mS/cm. After the diafiltration the solutions are concentrated until the enzyme concentration is between 50-150 g/L. The final concentration depends on the enzyme. The initial and final conductivity before and after diafiltration for the concentrated solutions can be seen in table 5.1. The conductivities in the experiments are a bit higher due to the pH adjustment. The amylase-F and amylase-S solutions have also been both polish and germ filtered after diafiltration, primarily to remove aggregates formed during the diafiltration process especially for the amylase-F solution. This procedure is also necessary for the amylase-S solution where the main purpose is to remove antifoam, which foul the membrane especially when the conductivity is low. This have been done by conducting the polish and germ filtration at 30°C. The solutions are stored frozen and thawed at 5°C before use. The size, isoelectric point (pI) of the enzymes and the pH used in the EUF and UF experiments can be seen in table 5.1.

Enzyme	size (kDa)	pI	pH_{EUF}	μ_e (pH 7.6)	μ_e (pH 5.0)	$\kappa_{initial}$	κ_{dia}
Protease-A	27	8.4	5.5	1.2	1.3	-	2
Amylase-F	55	3.5	7.0	3.0	2.0	4	2
Lipase	14	6.0	8.0	0.6	0.5	-	0.3
Protease-S	27	10	5.0	2.2	1.9	>7	0.7
Amylase-S	80	3.5	5.5	2.6	1.7	>7	0.5

$[\mu_e]$ 10^{-9} $m^2/(Vs)$, $[\kappa]$ mS/cm

Table 5.1: Enzyme properties.

The pH is adjusted to a value where a high surface charge of the enzyme is expected without violating the stability. Table 5.1 also shows the electrophoretic mobility of the enzymes. These mobilities have been measured by gel electrophoresis experiments (see appendix E), and are therefore most likely smaller than the mobilities in water due to a higher viscosity of the gel as seen from equation 2.18. Usually the ζ-potential is used as a measurement of the charge. Attempts to measure this parameter have however failed mainly due to the small size of the enzymes.

The EUF experiments have been carried out with 3 different batches for the amylase-F enzyme. A 4th batch is used for the UF experiments. The results reported, are unless stated otherwise, made using enzymes from the same batch to minimize the batch to batch variations.

5.2 Determination of the enzyme concentration

The concentration of the enzymes is measure with a Bradford reagent [130]. The method utilizes that proteins bind to Coomasssie Brilliant Blue G-250 dye. The dye exists in three forms: cationic (red), neutral (green), and anionic (blue).

$$Cation \overset{H^+}{\longleftrightarrow} Neutral\ form \overset{H^+}{\longleftrightarrow} Anion$$
$$470\ nm\ \ (red) \longleftrightarrow 650\ nm\ \ (green) \longleftrightarrow 595\ nm\ \ (blue)$$

Under acidic conditions, the dye is predominantly in the doubly protonated red cationic form ($A_{max} = 470\ nm$). However, when the dye binds to the proteins, it is converted to a stable unprotonated blue form ($A_{max} = 595\ nm$). This blue protein-dye can be detected at 595 nm in the assay by using a spectrophotometer (Perkin Elmer 320). Coomassie Brilliant Blue G-250 dye binds primarily to basic (especially arginine) and aromatic amino acid residues. Interference from non-protein compounds arises from their ability to shift the equilibrium levels of the dye among the three colored species. Known sources of interference, such as some detergents, flavonoids, and basic protein buffers, stabilize the green neutral dye species by direct binding or by shifting the pH [131].

The experiments are made by mixing 1 part of the Bradford reagent (Bio-Rad Protein assay cat.no: 500-006) with 4 parts of demineralized water and letting the dilute run through a filter paper. A standard curve is made from 5-6 enzyme solutions in the concentration range of 0.1-3 g/L depending on the enzyme. 100 μm of each enzyme solution is transferred with a pipette to tubes, and 5.0 ml of the diluted reagent is added. The solutions are mixed with a vortex mixer and incubated around 5 min at room temperature. A reference sample containing 100 μm of demineralized water is also made. The solutions are then poured into cuvettes, and the spectrophotometer is reset with the reference sample at a wavelength of 595 nm. The absorbance of the enzyme solutions can now be measured. A standard curve is made by plotting the absorbance against the enzyme concentration, and fitting a straight line in the linear area as seen in figure 5.1 for the amylase solutions.

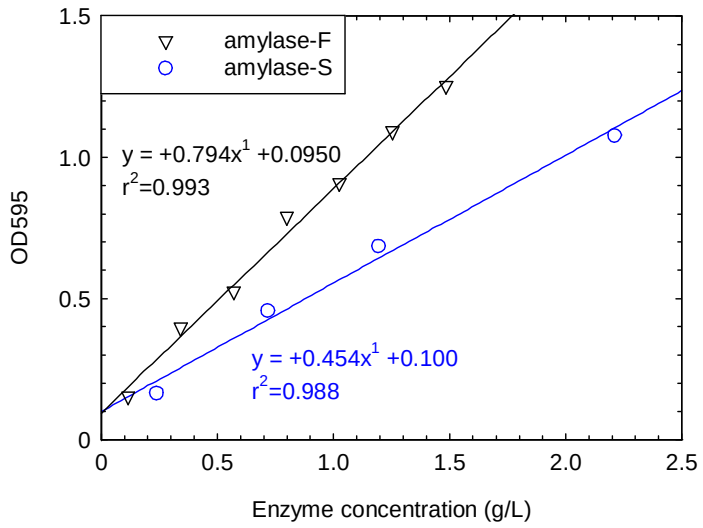

Figure 5.1: Standard curves for amylase-F and amylase-S. Data shown for the linear area.

From the fits the concentration of any enzyme solution can be determined by measuring the absorbance.

The activity of the enzyme samples were determined by sending the enzyme samples to the laboratory at Novozymes A/S.

5.3 EUF module

Three different modules have been used for EUF; the two which have been tested initially resulted in problems like electrocoagulation of the enzymes and large pH and conductivity changes in the feed solution. These modules and the results obtained are described in appendix A. The EUF module used for the results described in the next chapter is based on a commercial electrodialysis module. The enzymes are shielded from the electrodes by two cation-exchange (CIX) membranes according to figure 5.2.

The UF membrane are placed between the CIX membranes, and retains the enzymes due to the low pore size of the UF membrane compared to the size of the enzymes. Flow spacers are used to enable the different streams. A sodium sulfate solution is recirculated in the electrode chambers. By using CIX membranes in front of both the anode and cathode it is possible to prevent an accumulation of salt ions in the feed stream. They also prevent formation of $Cl_{2(g)}$ at the

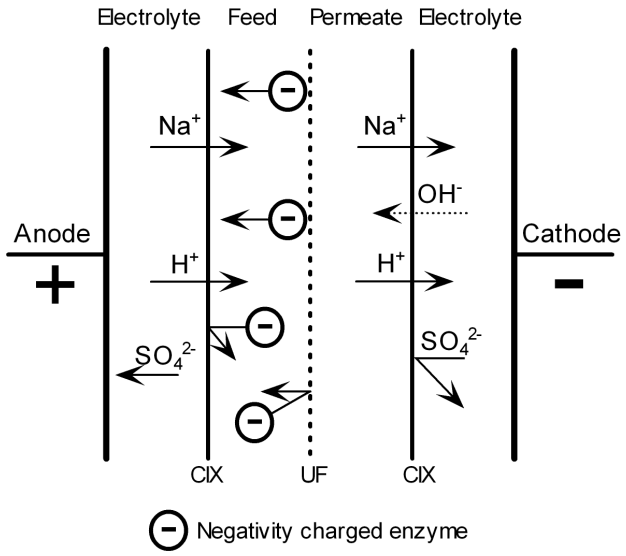

Figure 5.2: EUF module with an ultrafiltration membrane placed between two cation-exchange membranes.

anode, since any remaining Cl^--ions in the feed solution are rejected at the surface of the CIX membrane. This is important if EUF is going to be used in industrial production, where the solutions may not be diafiltrated, since $Cl_{2(g)}$ is an environmental work hazard.

Nettings are used as support for the UF and CIX membranes. The nettings consist of non-conductive material and is placed in the electrolyte, feed and permeate chambers to avoid damage to the membranes when the cell is under pressure. In the permeate chamber conductive nettings cut out of CIX material have been tested. The CIX nettings were used to minimize the limiting current effect, which is described below. Especially for the amylase-S solution it is an advantage because the conductivity of the solution and thereby the permeate is low. The flux is not affected by the type of nettings, but the current consumption and the appearance of the limiting current are due to the different resistances of the nettings. Non-conducting nettings have been used to filter all the enzyme solutions except for the amylase-S solution where both types have been tested.

The channel height of the electrolyte, feed and permeate chambers are 6, 5 and 5 mm, respectively. It is possible to expand the module to contain several cells.

The two main disadvantages with the configuration of the EUF module is pH changes in the permeate solution and the presence of a limiting current.

As shown in figure 5.2, the current is mainly carried by sodium ions, which are able to pass the CIX membranes, whereas the enzymes and sulfate ions are rejected. However, CIX membranes are not 100 % selective towards anions. At high current densities, transport of hydroxide ions from the catholyte to the permeate takes place due to the small size and high mobility of the hydroxide ion, which increases the pH in the permeate.

The limiting current effect is caused by concentration polarization of mainly sodium ions at the surface of the CIX membranes as illustrated in figure 5.3.

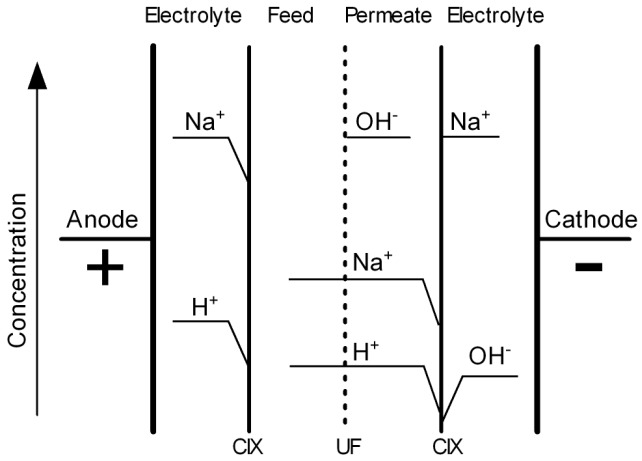

Figure 5.3: Concentration polarization in the EUF module.

The effect appears when the current density reaches a level, where the transport of sodium ions to the surface of the CIX membrane is slower than the transport of sodium ions through the membrane. In that case the concentration of sodium ions at the surface of the CIX membrane drops, and it is no longer possible to increase the current density any further.

5.3.1 Calculation of E over the feed chamber

The electric field strength E is defined as voltage U per distance (channel height h) [8]:

$$E = \frac{U}{h} \tag{5.1}$$

However, since the module contains four chambers with different conductivities it is not possible to use the applied voltage U_a in equation 5.1 directly. The module can instead be considered as a series of resistances, where the applied

voltage U_a is a sum of the electrical potentials over the different chambers:

$$U_a = U_e + U_{feed} + U_p + U^* \tag{5.2}$$

$$= (r_e + r_{feed} + r_p + r^*)I \tag{5.3}$$

where I is the current and r_e, r_{feed}, and r_p is the specific resistance of the electrolyte, feed and permeate chambers. r^* is the specific resistance of the other items (ion exchange membranes, electrodes etc.). The resistance of the feed chamber r_{feed} can be replaced by:

$$r_{feed} = \frac{h_{feed}}{\kappa_{feed} A_e} \tag{5.4}$$

where A_e is the electrode area (equal to the area of one membrane) and κ_{feed} is the conductivity. The electric field strength across the each chamber can therefore be calculated by [7]:

$$E_{feed} = \frac{I}{A_e \kappa_{feed}} \tag{5.5}$$

Equivalent equations can be derived for the electric field across the electrolyte and permeate chambers. The electric field strength across the feed chamber, which is reported in the next chapter is calculated by equation 5.5 from measured values of I and κ_{feed}. It is not possible to measure U_{feed} directly during the experiments due to the configuration of the EUF module.

5.3.2 EUF-rig

The experimental set-up of the EUF-rig is shown in figure 5.4.

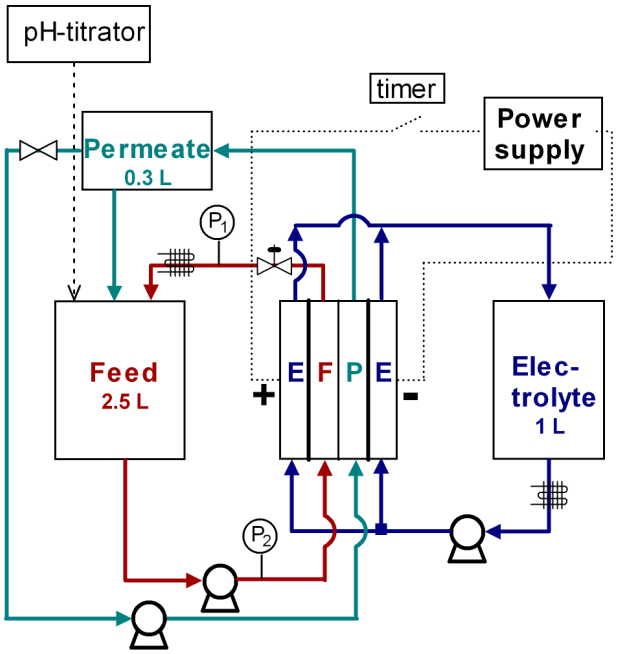

Figure 5.4: EUF rig.

The experiments are operated in full recycle mode by returning the concentrate and permeate back to the feed tank. Before the permeate is returned it is collected in a separate tank, where it is lead back into the permeate chamber via a pump. Recycling of the permeate stream is necessary in order to keep a relatively high salt concentration in the permeate chamber, and thereby reduce problems related to the limiting current effect. The permeate stream is kept at a constant volume by an overflow pipe from the permeate tank, which returns the excess amount of permeate back to the feed tank. This increases the pH of the feed solution, since the permeate becomes basic by the mechanisms described previously. A pH titrator is therefore connected to the feed chamber to maintain a constant pH. If EUF is going to be used in industrial production a pH titrator is probably not necessary, since the permeate will not be returned to the feed solution. The flux is measured manually as the mass of permeate from the overflow pipe during a certain time interval. Since H^+ is evolved at the anode and OH^- at the cathode the electrolyte streams are mixed to neutralize the pH changes.

The recirculation flow rate of the permeate stream is 22 L/h. It must be kept low to avoid pressure on the permeate side of the membrane, but high enough to avoid desalination. The flow rate of the electrolyte stream is 80 L/h, which is sufficient to remove the hydrogen and oxygen gasses formed by electrolysis at the electrodes. The total volume of the electrolyte, feed and permeate cycles are 1 L, 2.5 L and 0.3 L, respectively. The TMP is set by adjusting a valve on the retentate side. The module can be operated at a maximum pressure of 3 bar at the feed side, and a corresponding crossflow velocity of 0.15 m/s, which is low compared to the crossflow velocity used in industrial production.

The feed and electrolyte streams are connected to a cooler and the temperature is kept constant at 12°C in every experiment. The electrodes consist of a platinized titanium mesh (anode) and a stainless steel (cathode) plate. Later two platinized titanium mesh electrodes have been used to make the switching of the current direction easier. However it had no impact on the results wether the stainless steel or the platinized electrodes were used. The electric field is generated by a power supply from Xantrex (XHR 150-7), which can deliver up to 150 V and 7 A. Pulsed electric fields are generated by inserting a universal digital timer UDT (Tempatron) between the electrodes and the power supply. The timer can be set to switch the electric field on and off with time intervals between 0 and 9.00 seconds.

The electrolyte consists of 0.1 M Na_2SO_4 with a conductivity of 17 mS/cm. The cation-exchange membrane is a RELAX-CMH membrane from Mega (Czech Republic). The membrane area is 10×10 cm^2. The UF membrane is a 10 kDa low protein fouling surface-modified PVDF ETNA10PP membrane from Alfa Laval. A detailed description of the properties of the UF membrane can be found in appendix G, where the adsorption of amylase-F on the ETNA membrane has been studied and compared to a PES membrane.

5.3.3 Experimental procedure

The experiments are carried out at constant concentration. The concentration it set by diluting the enzyme concentrates with demineralized water. For the amylase-F the experiments have been carried out in a concentration range from 12 to 80 g/L and for the amylase-S the range is 12-120 g/L. The protease-S and the lipase have been tested at a concentration of 12 g/L. Since the filtration performance of the protease-A solution deteriorates if the conductivity is too low;

a higher concentration of 20 g/L is chosen. The majority of the experiments have been carried out at least twice and could be repeated with a deviation of less than 5%, when the same batch was used. The deviation is slightly larger between the batches, but this will be discussed in the next chapter.

Before the experiment starts, the pH of the feed solution is adjusted to the values given in table 5.1, and kept constant by titrating with either 0.1 M HCl or 0.1 M NaOH. The titrator starts automatically if the pH changes more than 0.3 from the initial value. The anode is placed on the feed side when the enzymes are negatively charged, and on the permeate side when they are positively charged. Before the electric field can be applied, permeate is collected at 0 V to fill up the permeate recycle loop. The voltage is then increased stepwise between 0 V and 50-100 V when steady state is reached at each voltage. A sample of the feed solution is collected in the beginning and end of the experiment and the concentration and activity is determined. A permeate sample is also collected, and the retention of the enzymes are determined based on both activity and concentration measurements. By comparing the activity in the beginning and in the end of the experiment any decrease in activity can be determined. The crossflow velocity is, unless stated otherwise, 0.07 m/s and the TMP 1.5 bar, which corresponds to an pressure on the feed side of 1.7 bar.

5.3.4 Cleaning

After each experiment the membrane is cleaned by the following procedure:

- Rinsing with demineralized water.
- Cleaning with 0.04 % NaOH at 50^{o}C for 30 min.
- Rinsing with demineralized water.

The water permeability is checked before the experiment starts to ensure that the membrane is cleaned properly. With this cleaning procedure it is possible to restore the water permeability to the same level as for a virgin membrane. The water permeability has been measured to 65 $\pm$ 5 L/(m^{2}h bar) at 12^{o}C.

5.4 Ultrafiltration experiments

Ideally the EUF equipment should have been used for the UF experiments as well. However, due to limitations of the EUF module regarding the crossflow velocity and TMP a different module have been used.

The UF experiments are carried out in a crossflow module made of two round Plexiglas plates with the membrane placed in between as shown on the right in figure 5.5. The module is kept tight with O-rings. The feed and retentate is let in and out of the module by tubes placed perpendicular to the module. The membrane is oval shaped with a length of 10 cm and a width of 4 cm. The channel height is 1 mm. The ETNA membrane is also used for the UF experiments. The design of the module has also been described previously by Jonsson and Boesen [132]. The setup is shown in figure 5.5 to the left.

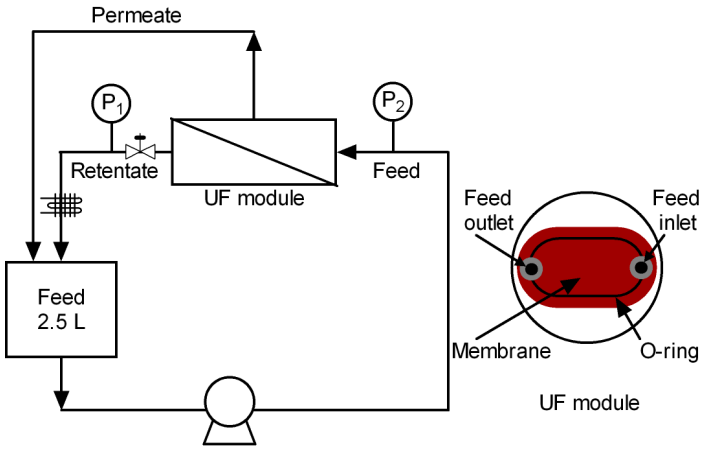

Figure 5.5: Skematic drawing of the UF-rig and the module.

The enzyme solution is recycled by a pump, and the pressure is measured on the feed and retentate side of the module by manometers (P_1 & P_2). The TMP can be set by adjusting a valve placed on the retentate side of the module. The total feed volume is 2.5 L. The feed tank is connected to a cooler, which keeps the solution at a constant temperature of 12°C. The experiments are operated in full recycle mode by returning the permeate and retentate back to the feed tank. UF experiments have been carried out with amylase-F and amylase-S enzymes.

To determined the crossflow velocity dependency on the mass transport coefficient, the flux is measured for the amylase-F solutions under the following conditions:

- The TMP is subsequently increased and decreased up to 3-4 bar at v = 1.0 m/s.
- The crossflow is increased to 2.0 m/s, and the TMP first increased then decreased.
- The crossflow is decreased to 1.5 m/s and the TMP increased.
- The crossflow is decreased to 0.5 m/s followed by an increase and decrease in the TMP.
- The crossflow is decreased to 0.3 m/s and the TMP increased.
- Finally the crossflow is set to 1.0 m/s, and the flux is measured again to compare the flux with the values obtained in the beginning of the experiment.

For the amylase-S the flux is only measured at 2.0, 1.0, and 0.5 m/s. The TMP is increased to around 2 bar, where the limiting flux is reached.

Four concentrations in the range of 15-140 g/L for amylase-F and 12-125 g/L for amylase-S have been studied. The series of experiments have been carried out once for each concentration except for a concentration of 56 g/L for amylase-F and 52 g/L for amylase-S, which is carried out twice, to check reproducibility. The deviation is less than 5%. For the amylase-S the same batch is used as in the EUF experiment, while a different batch is used for amylase-F.

Samples of the feed solution are collected at the beginning and at the end of the experiments and the concentration and activity are determined. A permeate sample is also collected, and the retention is determined based on both activity and concentration measurements.

5.5 Summary

- Enzyme solutions of amylases, proteases and lipase is used for the experiments. The concentration is determined with the Bradford reagent and the activity at the laboratories at Novozymes. The solutions are not completely pure but contains impurities of different nature depending on the enzyme. The solutions are diafiltrated before use, since $CaCl_2$ is present in all the solutions.

- An module based on an electrodialysis module is used for the EUF experiments. It consists of an UF membrane placed between two CIX membranes; which prevents direct contact between the enzymes and the electrodes. The experiments are conducted at constant concentration by returning the permeate and retentate back to the feed tank. The voltage is increased stepwise when steady state is reach.

- The effect of crossflow velocity and TMP is studied using an UF module. The experiments are also made at constant concentration. In both the EUF and UF experiments a 10 kDa ETNA membrane is used.

Chapter 6

Results and discussion

In this chapter the experimental results for the EUF and UF experiments are presented. Some of the results are already available in the paper "*Electro-ultrafiltration of industrial enzyme solutions*", which can be found in appendix E, and "*Electro-ultrafiltration of amylase enzymes: Process economy and design*" in appendix F. The focus in these two papers are mainly on the results obtained with amylase-S. This chapter will therefore present some additional results for amylase-F, but also include results from appendix E & F.

The membrane which have been used in the EUF and UF experiments have been examined in a separate study and the results are presented in appendix G.

6.1 Electro-ultrafiltration

Figure 6.1 shows the effect of the applied voltage during filtration of a 23 g/L amylase-F solution. The voltage is increased in four steps from 0-100 V after which it is decreased back to 0 V in two steps. The flux increases from 25 to 90 L/(m^2h) as the voltage increases from 0 to 100 V, which corresponds to an enhancement of a factor 3.6. The initial flux decline at 0 V is minor, and the steady state flux is reached after approximately 20 min for each step. However, the flux at 100 V decreases slowly with time, this is due to a limiting current effect, which causes desalination of the permeate stream. This results in a lower current and thereby a lower electric field strength as shown in equation 5.5. Figure 6.1 also shows that the system is reversible since the flux at 0 V and 50 V returns to the same level when the voltage is decreased as when it is increased. A similar plot for an amylase-S solution can be found in appendix E, where the

same trends are seen.

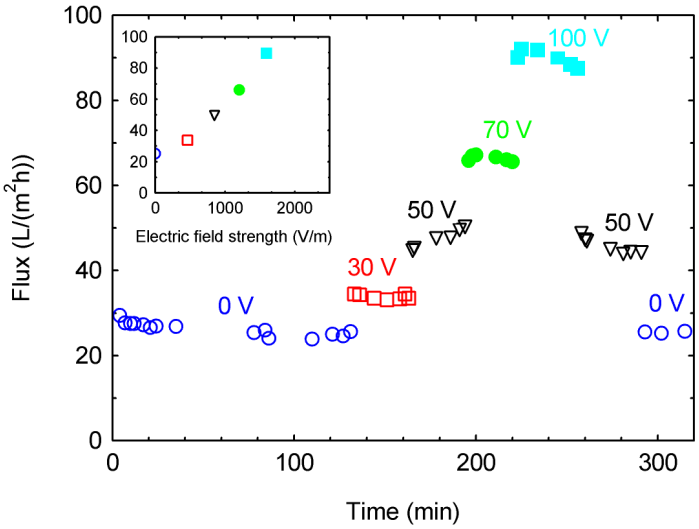

Figure 6.1: Example of the experimental procedure for a 23 g/L amylase-F solution. Stepwise increase in the flux with time under the influence of an increasing applied voltage. In the top left corner the flux data are plotted as a function of the electric field strength (calculated by eq. 5.5), which corresponds to the applied voltage. TMP=1.5 bar and v=0.07 m/s.

In the top left corner of figure 6.1 the data are plotted as a function of the electric field strength (calculated by eq. 5.5). The flux improvement for amylase-F is in the same range as the flux improvements found by Rios *et al.*, [17] and Radovich *et al.* [16] during EUF of a 10 g/L gelatin solution and BSA solutions of 1-4 g/L, respectively. The flux development for amylase-F as a function of the electric field strength have a non-linear appearance. The modified gel layer model in equation 2.23 is therefore not directly applicable for this system. This will be discussed further later in this chapter.

6.1.1 Enzymes

Figure 6.2 shows the effect of the electric field when applied during filtration of the enzymes presented in table 5.1. The results are here plotted as the relative flux improvement where the flux for the different enzymes are divided with their respective flux at 0 V.

As for the amylase-F, the flux also improves significantly for the amylase-S solution. At 1600 V/m the relative improvement is a factor of 2.5 for the

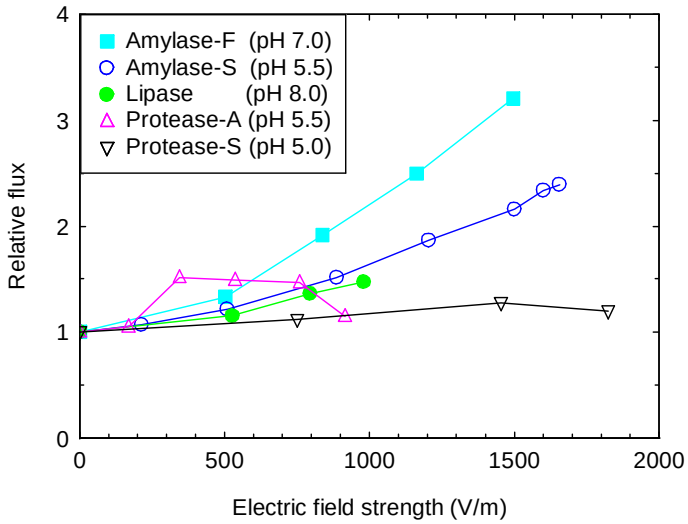

Figure 6.2: Relative flux improvement for the different enzymes tested. The concentration is 12 g/L except for the protease-A where it is 20 g/L.

amylase-S compared to 3.5 for the amylase-F. This is consistent with the higher mobility of amylase-F as seen in table 5.1.

The flux did not improve for the protease-A, which is expected due to the lower mobility of this enzyme compared to the amylases. The mobility of the protease-S is on the other hand in the same range as the amylases and the flux is therefore expected to increase as a function of the electric field strength. This is however not observed. Changing the pH from 5.0 to 7.0, where a slightly higher electrophoretic mobility is expected according to table 5.1, did not affect the results. A possible explanation could be the presence of other compounds in the solution. If there are other proteins with an opposite charge of the enzymes present in the solution they can foul the membrane considerably when the electric field is applied. As the enzyme is produced by bacteria, anionic and cationic polymers from flocculation may be present, which also contribute to the fouling of the membrane. Remaining antifoam in the solution might also adsorb to the membrane and decrease the effect of the electric field. With proteases there is also always the problem with auto-proteolysis, where the enzymes gets broken-down into smaller components, which can block the membrane pores. Further studies are needed to clarify the role of impurities in the solution and the steps necessary in order to remove them.

Some flux improvements are observed during EUF of the lipase solution, which could be due to the slightly higher pH used in the EUF experiment compared to the value at which the mobilities were measured. An increase in the ζ-potential and thereby the mobility is expected with increasing pH. Carrying out the experiment at pH 4.5 (where the lipase is positively charged) did not show any flux improvement. Overall there is good agreement between the mobilities in table 5.1, and the flux improvements measured in EUF, except for protease-S. Thus gel electrophoresis is a useful screening tool to identify the optimal pH, and to identify which enzyme solutions that with advantage may be concentrated by EUF. All of the enzyme solutions are tested for enzyme activity, and no loss is observed during EUF, due to the module configuration which prevents direct contact between the enzymes and the electrodes.

6.1.2 Effect of concentration

Due to the relatively high flux improvement for the two amylases they where chosen for further studies of the effect of the electric field at different concentrations. To test the effect of the enzyme concentration, amylase-F is studied in a concentration range of 12-80 g/L, and amylase-S in a range of 12-120 g/L. Figure 6.3 and 6.4 shows the relative flux improvement when applying an electric field to the amylase-F and amylase-S solutions, respectively. The retention is around 98 % at 0 V for both amylases.

The flux improves 3-7 times at 1600 V/m for both enzymes. The critical electric field strength is not reached for either of the amylases in figure 6.3 and 6.4. If the critical electric field strength had been reached a defection of the curves is expected as the electric field strength increases due to complete removal of the gel layer as described in section 4.2. It was not possible to reach the critical electric field strength, since the voltage could not be increased any further due to the limiting current effect. At high concentrations the flux improves relatively more compared to the lower concentrations, especially above 40 g/L (although the absolute flux decreases with increasing concentration as expected). Application of an electric field will therefore be more efficient for ultrafiltration of highly concentrated solutions.

This result is in agreement with studies done by Lazarova *et al.* [13] and Oussedik *et al.* [96] whom also showed that the relative flux improvement is greatest at high concentration when applying an electric field during filtration of

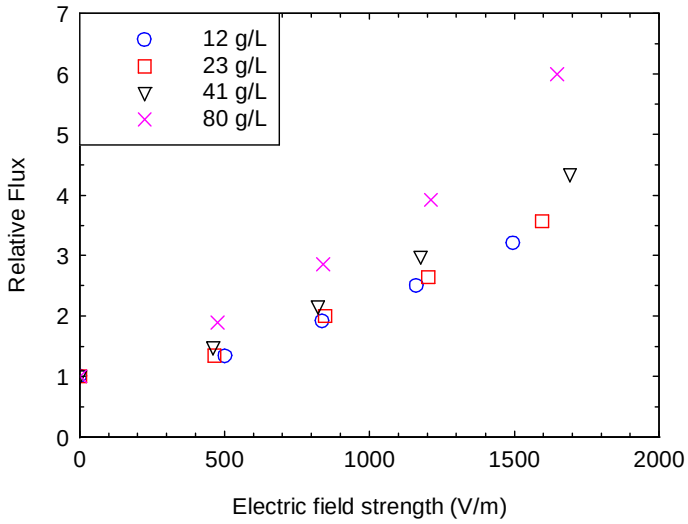

Figure 6.3: Relative flux improvement for amylase-F solutions at different concentration.

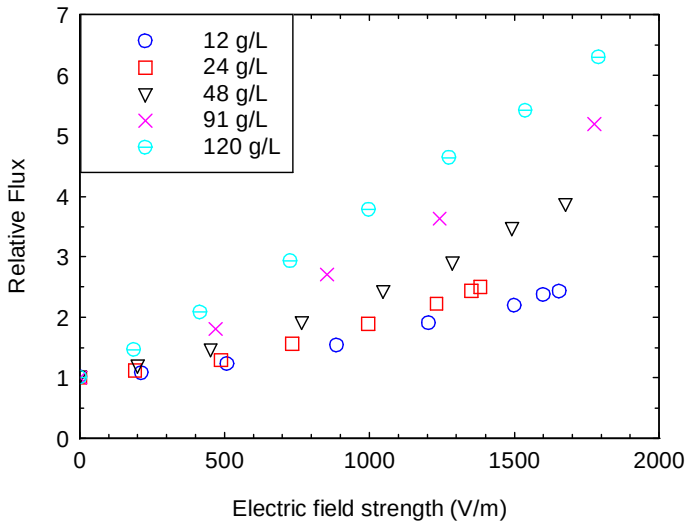

Figure 6.4: Relative flux improvement for amylase-S solutions at different concentration.

silicium oxide particles and BSA solutions, respectively. The increased effect of the electric field at high concentrations is probably due to the increased thickness of the concentration polarization layer, which means that the relative amount of enzymes removed from the membrane surface increases when the electric field is applied. Hence the impact on the flux is relatively larger with increasing concentration. See also the literature review in chapter 4.

Current consumption

Figure 6.5 and 6.6 shows the current as a function of the applied voltage during the EUF experiments of amylase-F and amylase-S as presented in figure 6.3 and 6.4. The voltage, which is expected from the measured values of the conductivity in the feed, permeate and electrolyte solutions are calculated from equation 5.2 and represented by the solid lines. The current is linear dependent of the applied voltage, which means that Ohm's low is valid for the EUF module, as expected. The current obtain in the experiments are in all cases lower than expected according to equation 5.2. This means that the resistance of the EUF module is higher than expected. A reason could be the low conductivity in the permeate, since the concentration of ions on the surface of the ion-exchange membrane is smaller than in the bulk solution, which makes the resistance of this chamber larger. A better design of the module with a smaller channel height of the permeate chamber may result in a substantial reduction in the overall resistance of the module. This can be seen for the amylase-S solution where two different nettings have been used on the permeate side as described in the chapter 5. The effect of these nettings on the current consumption can be seen for two concentrations in figure 6.7.

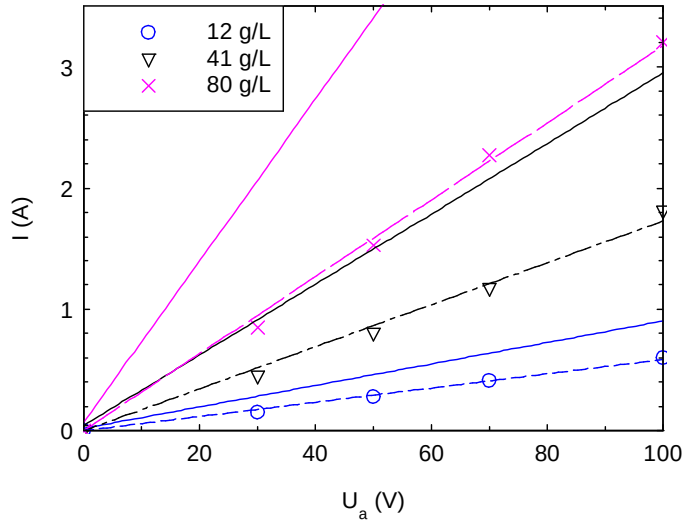

Figure 6.5: Current as a function of the applied voltage for different concentrations of amylase-F. The experimental values are given by the solid lines and the calculated by the solid lines.

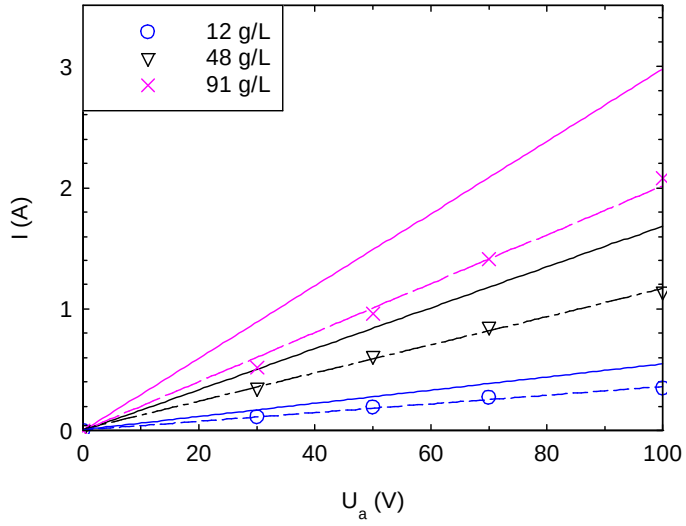

Figure 6.6: Current as a function of the applied voltage for different concentrations of amylase-S. The experimental values are given by the solid lines and the calculated by the solid lines.

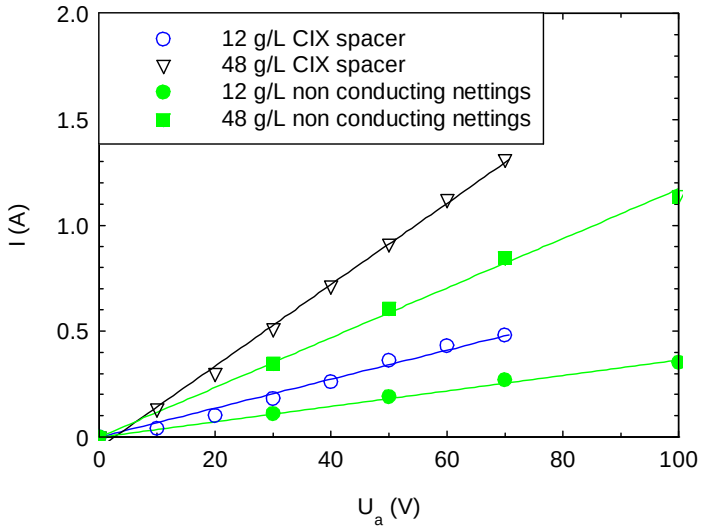

Figure 6.7: Current as a function of the applied voltage during filtration of amylase-S. The results are shown for two type of nettings.

The use of CIX nettings clearly decreases the resistance of the permeate chamber, this means that the electric field strength which is required for a certain flux improvement can be obtained at a lower voltage, which reduces the energy consumption.

6.1.3 Batch variations

In figure 6.8 and 6.9 the absolute flux for the 23 g/L and 41 g/L amylase-F solution from figure 6.3 are plotted with results from other batches. The experiments are reproducible within 5 % for batch 1 and 2, but there are some batch to batch variations between batch 2 and batch 1&3, especially at high electric field strengths. This is seen for both concentrations and is probably caused by variations during the production.

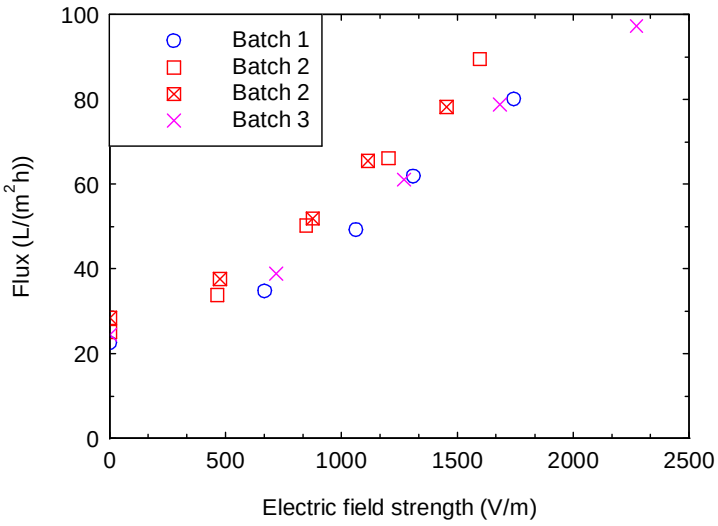

Figure 6.8: Increase in permeate flux as a function of the applied voltage for 3 different amylase-F batches. The concentration is around 23 g/L in all the experiments.

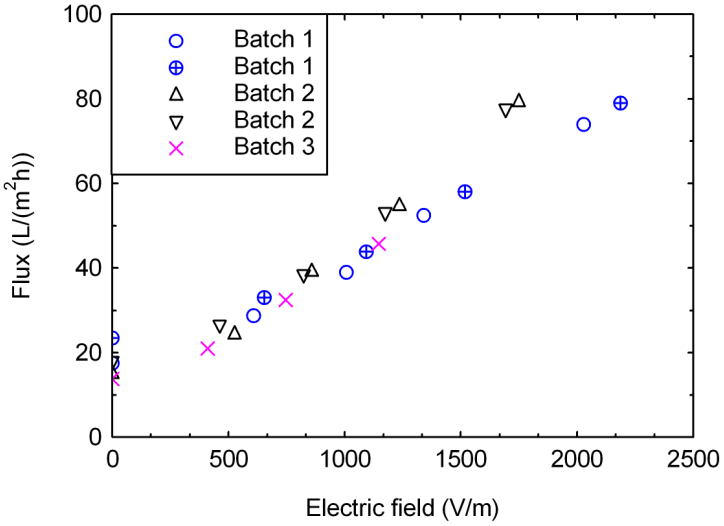

Figure 6.9: Increase in permeate flux as a function of the applied voltage for 3 different amylase-F batches. The concentration is around 41 g/L in all the experiments.

6.1.4 Effect of TMP and crossflow velocity

Figure 6.10 shows the effect of increasing the crossflow velocity from 0.07 m/s to 0.13 m/s at a TMP of 1.5 and 2.4 bar when filtering a 41 g/L amylase-F solution.

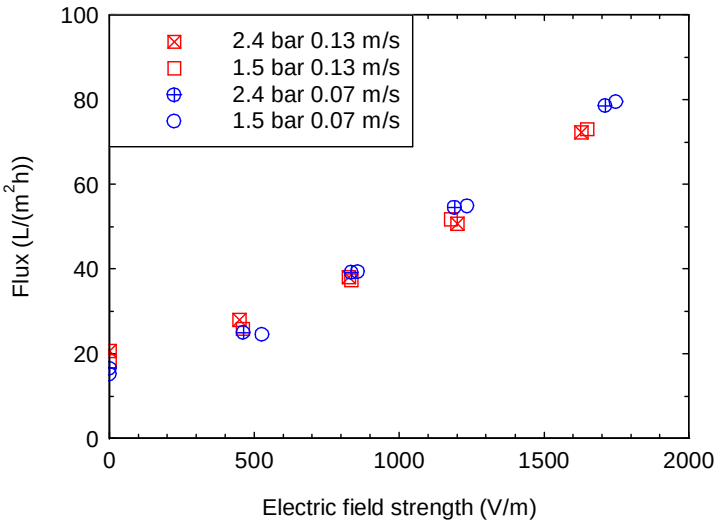

Figure 6.10: Effect of TMP and crossflow velocity for a 41 g/L amylase-F solution.

The effect of increasing the TMP is very small in the investigated range, probably since the limiting flux is already reached at this concentration. Other authors have also shown that an increased TMP is not beneficial. During electromicrofiltration of waste water and silicon oxide particles a decrease in the flux was observed if the TMP became too high [13] [104], this was however not observed for the amylases. See also section 4.4.

The effect of increasing the crossflow velocity in the investigated range is also limited. Only a small enhancement is seen when increasing the crossflow velocity from 0.07 to 0.13 m/s. As the electric field strength increases, the difference between the two crossflow velocities becomes smaller, and after 500 V/m it is no longer possible to distinguish between the curves. The same effect is seen for amylase-S, which is shown in appendix F. Since the electric field strength is expected to be below the critical electric field strength, an increase in the flux is expected when the crossflow velocity increases as described in the litterateur review section 4.4. A reason could be the low crossflow velocity in the module. Increasing the crossflow velocity from 0.07 to 0.13 m/s will not reduce the concentration polarization layer considerable as evident from the small enhancement

in the flux at 0 V. The electric field strength therefore controls the flux enhancement in the investigated crossflow range. Due to limitations of the EUF module the crossflow velocity could not be increased any further. However, if the crossflow velocity could be increased 5-10 times to obtain velocities used in industrial UF units an effect of the crossflow velocity would be expected. However, these results indicate that it is possible to replace the effect of a high crossflow velocity with an electric field. Whether or not EUF should replace UF depends on the energy consumption of the pump at high crossflow velocities, and the electric field, which is discussed in the next chapter.

6.1.5 Effect of a pulsed electric field

The effect of a pulsed electric field has been investigated as well. This was tried for solutions of amylase-S and presented in appendix E. However there are no advantages in using a pulsed electric field, since the concentration polarization layer is restored immediately when the electric field is turned off probably due the relatively small size of the enzyme. The same is expected to be the case for amylase-F. A pulsed electric field is usually only an advantage for large particles like baker's yeast as described in the literature review section 4.2.

6.1.6 Model development of the data

The flux data at 0 V are collected in figure 6.11 for both the amylase-F and the amylase-S enzyme to test if the gel layer model in equation 2.6 can be used to describe the flux development.

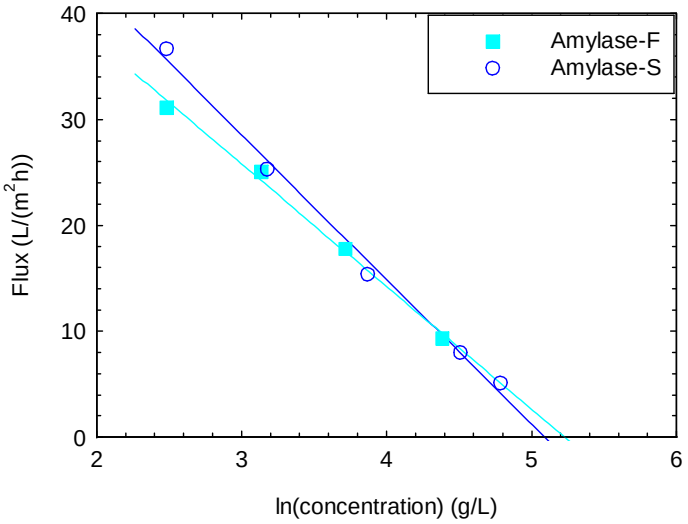

Figure 6.11: Flux data at 0 V, which corresponds to the values found in the experiments presented in figure 6.3 and 6.4.

The flux levels are almost identical for both enzymes and can be represented by a linear fit, which means that the gel layer model is applicable. The mass transport coefficient and the gel layer concentration can be found in table 6.1.

The modified gel layer model in equation 2.23 predicts a linear dependency of J as a function of E. An attempt to use this model on the amylase-F and amylase-S system is shown in figure 6.12 and 6.13, respectively, for a low, middle and high concentration and represented by the solid curves. The flux is here given in absolute values.

In both cases the data only fit a straight line at low fluxes. When the electric field strength becomes too high, the data deviate from a straight line, and the deviation increases as the concentration decreases. The appearance of the curves for both amylase-F and amylase-S is similar to the results reported by Radovich and Chao for EUF of cationic electrodeposition paint [12], which can be found in figure 2.7 in section 2.2. The non-linear dependency is caused by a disturbance in the gel layer when the electric field becomes sufficiently high. This is supported by the fact that the non-linearity is more pronounced at low concen-

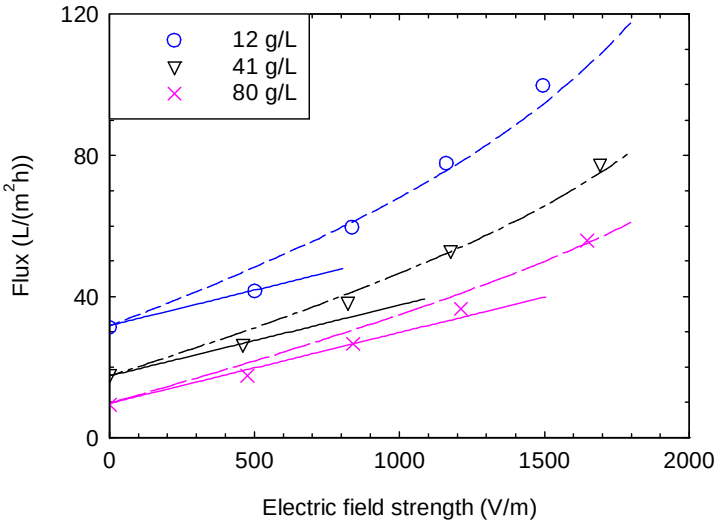

Figure 6.12: The flux as a function of the electric field strength for amylase-F. The modified gel layer model in equation 2.23 is given by the solid curve and the empirical model from equation 6.3 by the dotted lines.

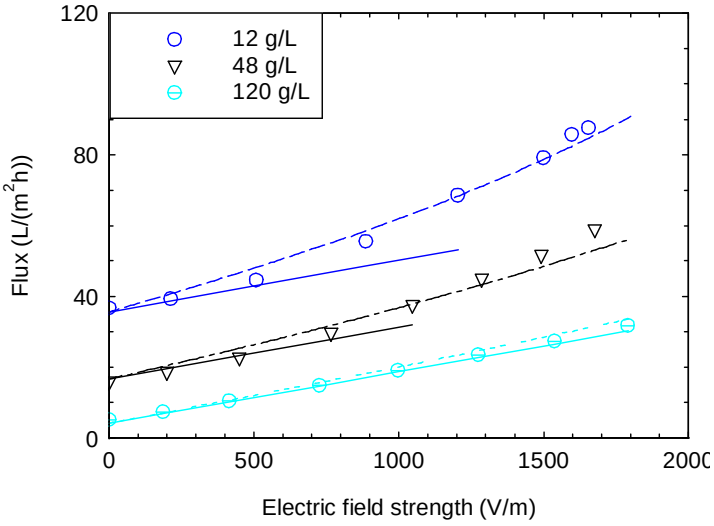

Figure 6.13: The flux as a function of the electric field strength for amylase-S. The modified gel layer model in equation 2.23 is given by the solid curve and the empirical model from equation 6.3 by the dotted lines.

trations where the thickness of the gel layer is smaller and easily disturbed. If the gel layer is disturbed, the mass transport coefficient and the gel layer concentration is no longer independent of E, which is assumed in the modified gel layer model. It is also assumed that the electrophoretic mobility is independent of the viscosity of the solution, which is not the case since it increases with the concentration. This might also contribute to the different slopes of the curves at different concentrations.

To describe the data it is therefore necessary to alter equation 2.23 and introduce a non-linear dependency of one of the constants. A possibility is to introduce a concentration dependency of the electrophoretic mobility so that μ_e increases when the concentration increases. This will however still lead to a linear dependency of the flux versus the electric field strength. The non-linearity must therefore be due to a non-constant behavior in first term in equation 2.23, which means that the gel layer concentration or the mass transports coefficient changes as the electric field strength increases. The gel layer concentration is represented by $\ln(c_g)$ in equation 2.23, which means that any change in c_g only has a small effect and cannot explain the non-linear slope. Instead the mass transport coefficient is considered. In conventional crossflow UF the mass transport coefficient increases when the crossflow velocity increases due to a reduced thickness of the concentration polarization layer. Since the thickness of the concentration polarization layer is also reduced during EUF it is possible that the mass transport coefficient is not independent of the electric field strength, but increases as the electric field strength increases. If the decrease in thickness of the concentration polarization layer with increasing electric field strength is described by:

$$\delta(E) = \delta_0(1 - a^{\dagger}E) \tag{6.1}$$

where $a^{\dagger}$ is a constant and δ the thickness of the concentration polarization layer at 0 V, k will have the following dependency of E:

$$k(E) = \frac{D}{\delta_0(1 - a^{\dagger}E)} = \frac{k_0}{1 - a^{\dagger}E} \tag{6.2}$$

if equation 6.2 is combined with equation 2.23, the flux can be expressed by the following empirical model:

$$J = \frac{k_0}{1 - a^{\dagger}E} \ln(\frac{c_g}{c_b}) + \mu_e E \tag{6.3}$$

This model is shown in figure 6.12 and 6.13 as dotted lines and seems to describe the data in the tested range. The parameters are given in table 6.1.

enzyme	k_0 (m/s)	c_g (g/L)	μ_e (10^{-9} m^2/(Vs))	$a^\dagger$ (m/V)
Amylase-F	3.2 10^{-6}	186	5.6	3.5 10^{-4}
Amylase-S	3.8 10^{-6}	163	4.0	2.5 10^{-4}

Table 6.1: Model parameters.

k_0 and c_g are determined from figure 6.11, and μ_e is determined from the modified gel layer model in equation 2.23, as an average of the slopes at low fluxes at the different concentrations; shown by the solid lines in figure 6.12 and 6.13. The constant $a^\dagger$ is determined as an average of the values found when fitting equation 6.3 to the different concentration.

The model is only valid as long as $E < 1/a^\dagger$ and $E < E_c$. If $E > 1/a^\dagger$ the first term in equation 6.3 would become negative, and if $E > E_c$ the flux exceeds the solvent flux for the membrane. When E approaches E_c, the effect of the electric field becomes smaller, and the flux will probably level off and approach $J_{\max}$ asymptotically. The mobilities determined from the modified gel layer model are higher than the mobilities found in the gel electrophoresis experiments given in table 5.1. This is expected since the viscosity of the gel is higher than the aqueous feed solutions. The relative difference between the mobilities is on the other hand comparable. The mobility of amylase-F is 1.4 times higher than amylase-S when comparing the values found in EUF, compared to 1.8 when comparing the values in table 5.1 at corresponding pH values. Thus gel electrophoresis can be used as a predictive tool.

6.2 Ultrafiltration

In this section the flux as a function of TMP and crossflow velocity is studied for conventional UF. These data will be used in the next chapter to compare UF and EUF economically.

The flux as a function of TMP is shown in figure 6.14 at different crossflow velocities for a 30 g/L amylase-F solution.

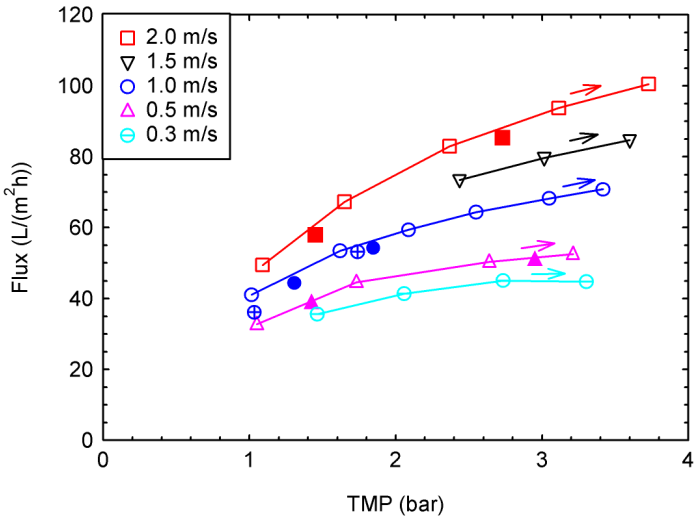

Figure 6.14: Flux versus TMP at different crossflow velocities for a 30 g/L amylase-F solution. The open symbols are date collected when the TMP is increased and the filled symbols are data collected when the TMP is decreased. The data represented by ⊕ is the data collected in the end of the experiment at 1.0 m/s.

As expected the flux increases with TMP until a limiting flux is reached, where after further increase in TMP do not result in a higher flux. The limiting flux appears at a lower TMP when the crossflow velocity is reduced as expected. Figure 6.14 also shows that the system is reversible, since the flux obtained when decreasing the TMP is almost the same as when increasing the TMP. Thus the flux at 1.0 m/s has decreased less than 5 % at the end of the experiment compared to its initial value. The retention is between $95 - 99$ % depending on the concentration, and no loss in enzyme activity is observed. The flux data at 3.5 bar from figure 6.14 is plotted in figure 6.15 together with data for other concentrations, which can be found in appendix B.

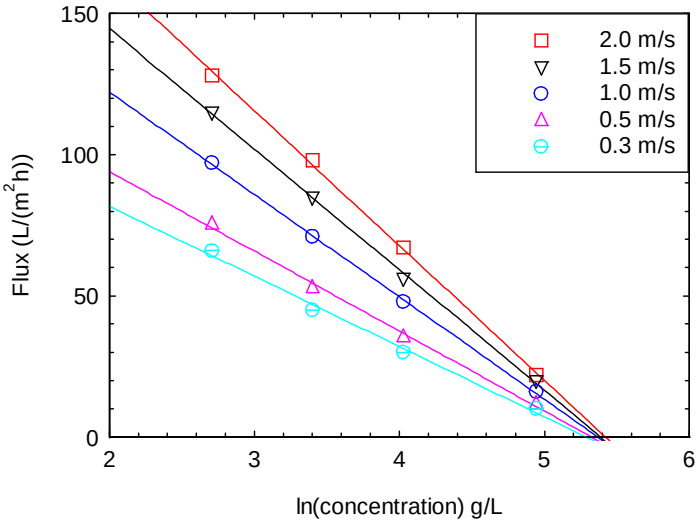

Figure 6.15: Flux versus concentration for amylase-F at different crossflow velocities.

The data gives a linear fit, which means that the gel layer model can be used to describe the data. The slope is therefore equal to $-k_0$, which increases with increasing crossflow velocity. c_g -given by the intercept with the x-axis -should according to the gel layer model be independent of the crossflow velocity. This is however not the case; the gel layer concentration increases as the crossflow velocity increases and is in the range of $200 - 225$ g/L. A non constant gel layer concentration is often seen experimentally and shows the limitations of the gel layer model. A similar set of experiments have been made for amylase-S, which also can be described by the gel layer model. The results can be seen in appendix F. In this case the limiting pressure is reached at a TMP of 2 bar at 2 m/s, and the gel layer concentration is between $210 - 250$ g/L. The UF flux for the amylase-S solutions are around 50% lower than the UF flux for amylase-F. A possible explanation could be the lower ζ-potential of the amylase-S enzymes compared to the amylase-F enzymes. This means that the electrostatic repulsing between the amylase-S enzymes are lower and allows for a closer packing of the gel layer, hence a lower flux is obtained.

6.2.1 Model of UF data

Figure 6.16 shows the mass transport coefficients, which is expected for the UF module according to the equations given in table 2.1 together with the experimental values. Neither of the equations fit the data, but the shape is closest to the shape of the laminar equation. This is also seen by plotting $\ln k_0$ as a function of ln(v), which is shown in figure 6.17.

The data can be described by a straight line with a slope of 0.36 and 0.31 for amylase-F and amylase-S, respectively. This is close to the value of 0.33, which is predicted by the laminar Sherwood equation in table 2.1, and means that k_0 can be described by:

$$k_0 = a\frac{D}{d_h}\left(\mathrm{Re}\, Sc\frac{d_h}{l}\right)^{0.33} \tag{6.4}$$

The a-value can be calculated from the intercept with the y-axis, and is found (setting $b = 0.33$ and the viscosity equal the value of water at 12^0C in equation 2.12) to be 4.68 and 3.26 for amylase-F and amylase-S, respectively. The experimentally determined a-values are higher than the value of 1.85 which is expected according to table 2.1. A reason could be the turbulent conditions at the inlet and outlet of the module. Since the UF module only has a short length, the inlet and outlet effects will have a relatively large impact on the flux [132]. In the calculations in the next chapter the a-value of 1.85 is therefore used, since a larger module will be considered. Thus the inlet and outlet effects is considered negligible. Using the a-value of 1.85 for both enzymes will, however, decrease the difference between the mass transport coefficients of the enzymes as seen in figure 6.16, where the mass transport coefficients are almost identical for the two enzymes.

The laminar model in equation 6.4 does not fit the mass transport coefficients found previously for the EUF model in table 6.1, but underestimates it. The mass transport coefficient is about 4-8 times lower for the amylase-F data and 2-4 times lower depending whether the a-value of 1.85 or the experimental value is used. The reason is most likely that the feed channel is filled with spacer nettings, which makes the flow turbulent instead of laminar. However none of the equations given in table 2.1 fits the data from the EUF module. Thus for further calculations the mass transport coefficient calculated by equation 6.4 is also used for the EUF module.

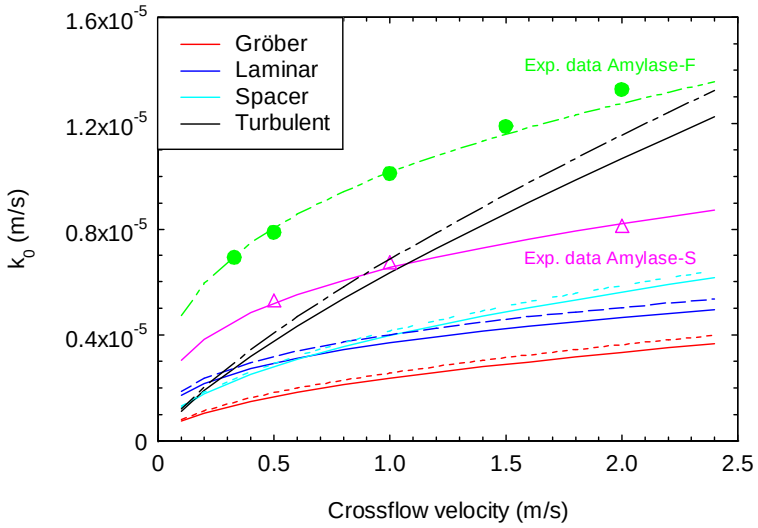

Figure 6.16: Experimental mass transport coefficients calculated from the equations in table 2.1 and the experimental values as a function of the crossflow velocity. The dashed lines represents the values for amylase-F, while the solid lines represents the values for amylase-S.

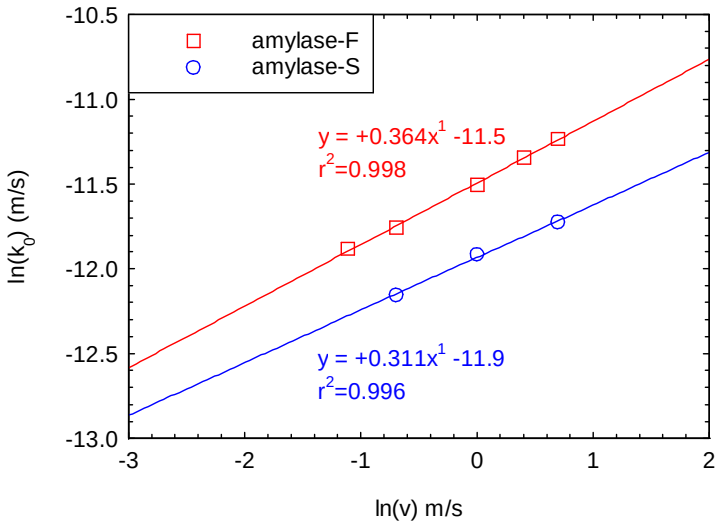

Figure 6.17: The logarithm to the mass transport coefficient as a function of the logarithm to the crossflow velocity for amylase-F and amylase-S. The flux versus TMP data for amylase-S can be seen in appendix B.

6.3 Summary

- EUF of amylase enzymes results in flux enhancements between 3-7 times depending on the concentration. The greatest relative enhancement is achieved at high concentration, which makes EUF feasible as a final concentration step in a continuous production line consisting of several concentration steps.

- EUF can only be described by the modified gel layer model at low electric field strengths, since the data have a non-linear appearance due to a disturbance of the gel layer at higher electric field strength. At high electric field strengths an empirical equation is found, which accounted for a higher mass transport coefficient when the electric field is applied.

- The proteases and the lipase solution did not result in any significant flux enhancements during EUF mainly due to low electrophoretic mobilities and impurities in the solutions.

- Increasing TMP had no influence at the flux regardless of the electric field strength. A higher crossflow velocity only had a small impact on the flux at low electric field strengths in the studied range. This means that the electric field is the main driving force, and that a higher crossflow velocity can be replaced by an electric field for the studied enzymes and the used EUF unit.

- The UF data could be described by a laminar Sherwood approximation. The data found in the experiments exceeds the values predicted by the laminar Sherwood approximation due to turbulent conditions at the inlet and outlet channels.

Chapter 7

Process design & economy

In this chapter the economy of EUF will be compared with conventional UF. The calculations are based on a plate-and-frame module operated as a feed-and-bleed system. A schematic drawing of the cell is shown in figure 7.1.

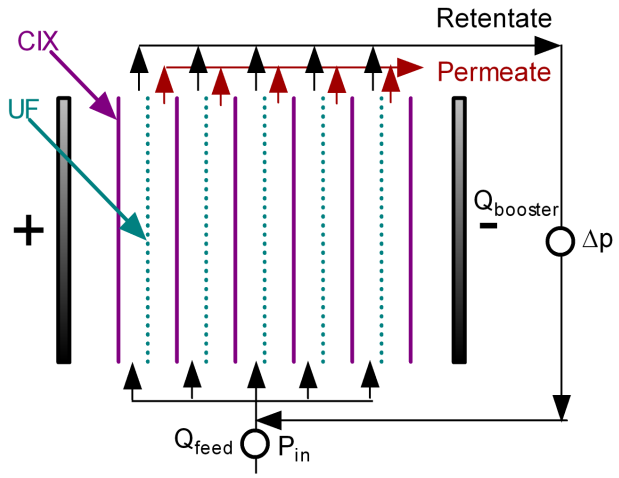

Figure 7.1: Schematic drawing of a EUF cell containing 5 cell pairs.

The stack is build of alternating CIX and UF membranes. In figure 7.1 the number of cell pairs is 5, but it is assumed that the stack can be expanded to any number of n pairs each with a membrane area of A_e, which is equal to the electrode area. In practice the number of cell pairs has a limit. As the number of cell pairs increases, the stack becomes bigger, and a higher voltage must be applied to achieve the required electric field strength across each cell pair. A total stack length of more than 0.5 m is probably not realistic, since it would require at least 1000 V across the entire stack. Depending on the design of the

stack, mainly the thickness of the flow-spacers, the number of cell pairs is limited to around 100-200.

A feed-and-bleed system consists of a feed pump that transports the feed into the filtration module at an inlet pressure of P_{in}, and a booster pump that recirculates the retentate back into the module until the desired final concentration is reached. The feed, retentate and permeate flow can be separated by flow spacers like in electrodialysis (ED), as shown in figure 7.2.

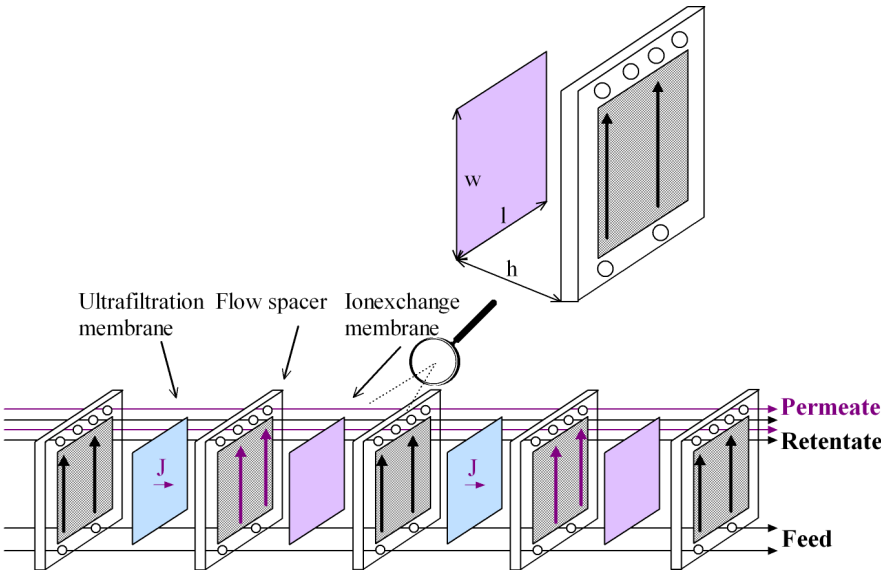

Figure 7.2: Schematic drawing of the flow in a EUF cell using flow spacers. The cell dimensions are specified at the top.

Contrary to ED, the TMP is high in EUF, which means that the demands for the packing of the module is bigger if leakage is to be avoided. These problems must be dealt with before EUF can be used in large scale.

7.1 Energy consumption and membrane area

The economy in the EUF process depends not only on the energy used by the electric field and the pumps. It also depends on the membrane area needed to ensure a reasonable permeate flow. Depending on the price of the membrane and the price of electricity the optimal operating conditions can be found.

7.1.1 Membrane area

The total membrane area A_T needed to concentrate a feed flow of Q_{feed} from c_{feed} to c_r may be calculated from the average flux J_{av} by considering the mass balance:

$$\begin{aligned} Q_{feed} &= Q_r + Q_p \\ &= Q_r + J_{av}A_T \end{aligned} \tag{7.1}$$

where Q_r and Q_p is the flow rate of the permeate and retentate, respectively. By introducing the relation:

$$\frac{Q_r}{Q_{feed}} = \frac{c_{feed}}{c_r} \tag{7.2}$$

under the assumptions that the enzyme concentration in the permeate is negligible, the following equation is obtained:

$$\frac{A_T}{Q_{feed}} = \frac{1 - \frac{c_{feed}}{c_r}}{J_{av}} \tag{7.3}$$

Equation 7.3 shows that the membrane area is inversely proportional to the average flux.

7.2 Energy calculations

The energy W used during EUF is a sum of the energy consumed by the pumps W_{pump}, and the energy consumed by the electric field W_E:

$$W = W_{pump} + W_E \tag{7.4}$$

In the next sections equations for calculating W_{pump} and W_E are derived.

7.2.1 Pump energy

In a feed and bleed system the energy consumed by the pumps can be calculated as a sum of the energy used by the booster pump $W_{booster}$ and the energy used by the feed pump W_{feed} [3]:

$$W_{pump} = W_{booster} + W_{feed} \tag{7.5a}$$

which can be calculated from the power used by the booster pump $P_{booster}$ and the feed pump P_{feed}:

$$W_{pump} = (P_{booster} + P_{feed}) / Q_{feed} \tag{7.6}$$

$$= \left(\frac{\Delta p Q_{booster}}{\eta_{pump}} + \frac{p_{in} Q_{feed}}{\eta_{pump}} \right) / Q_{feed} \tag{7.7}$$

where $Q_{booster}$ is the flow rate of the booster pump. Δp is the pressure-drop across the feed channel, and η_{pump} is the pump efficiency. $Q_{booster}$ can be expressed in terms of the crossflow velocity v:

$$Q_{booster} = n \alpha \mathrm{v} \tag{7.8}$$

where α is the area of the cross-section. Combining equation 7.6 and 7.8 with equation 7.3, gives the following equation for the energy consumed by the booster pump for a given Q_{feed}:

$$W_{booster} = \frac{P_{booster}}{Q_{feed}} = \frac{\Delta p n \alpha \mathrm{v}}{\eta_{pump}} \frac{\left(1 - \frac{c_{feed}}{c_r}\right)}{J_{av} A_T} \tag{7.9}$$

By introducing the cell dimensions (see figure 7.2):

$$A_T = n A_e = n w l \tag{7.10a}$$

$$\alpha = w h \tag{7.10b}$$

in equation 7.9, equation 7.11 is obtained.

$$W_{booster} = \frac{\Delta p h \mathrm{v}}{\eta_{pump} J_{av} l} \left(1 - \frac{c_{feed}}{c_r}\right) \tag{7.11}$$

Which gives the energy consumption for the booster pump with respect to the feed flow during concentration from c_{feed} to c_r. The pressure-drop across the channel is calculated by [3]:

$$\Delta p = 2 f l \rho \mathrm{v}^2 / d_h \tag{7.12}$$

where the friction factor f is equal to:

$$f = 24 / \mathrm{Re} \quad (laminar) \tag{7.13}$$

$$f = 0.133\, \mathrm{Re}^{-0.25} \quad (turbulent) \tag{7.14}$$

To analyse the influence of the dimensions of the feed channel on k_0, A_T, $W_{booster}$ and Δp, the effect of the length (l), width (w) and height (h) in equation 6.4, 7.3 7.11 and 7.12, is studied. Table 7.1 summarizes the effect of the dimensions of the module. The exponent of each parameter is given together with the percentage increase or decrease (represented by a ($-$)) when the value of the parameter is increased by a factor of 2.

parameter	Δp	k_0/J_{UF}	$W_{booster}$	A_T
channel height (laminar)	h^{-2}	$h^{-0.34}$	$h^{-0.66}$	$h^{0.34}$
$2 \times$ *channel height (laminar)*	-75%	-20%	-40%	25%
channel height (turbulent)	$h^{-1.25}$	$h^{-0.34}$	$h^{0.09}$	$h^{0.34}$
$2 \times$ *channel height (turbulent)*	-60%	-20%	6%	25%
length	l	$l^{-0.33}$	$l^{0.33}$	$l^{0.33}$
$2 \times$ *length*	100%	-20%	25%	25%

Table 7.1: Design parameters.

The pressure-drop depends of the height of the channel by h^{-2} in the laminar flow regime and $h^{-1.25}$ for the turbulent flow regime. Since the mass transport coefficient depends of the height by $h^{-0.34}$ for all flow regimes, the energy consumption is affected by $h^{-0.66}$ for laminar flow regimes and $h^{0.09}$ for turbulent flow regimes. Hence when the height is doubled the pressure drop is decreased by 75% and 60% for laminar and turbulent flow, respectively. The mass transport coefficient decreases by 20%, and the energy consumption decreases by 40% for the laminar flow and increases 6% for the turbulent flow. Even though the energy consumption is reduced by increasing the channel height in the laminar flow regime it is not necessarily an advantage to used a large channel height, since the membrane area is increases by 25% due to the lower mass transport coefficient. The Reynolds number is also increased by a factor of 2 when the height is doubled, which means that the maximum crossflow velocity that can be applied before the flow becomes turbulent decreases by a factor of 2. A large channel height can however be necessary if the feed is highly viscous. The optimal channel height therefore depends on the price of the membrane and the energy costs. The same conclusions can be made if the flow is turbulent.

Table 7.1 shows that the mass transport coefficient decreases by 20% when the length of the module is increased by a factor of 2, hence the energy consumption and membrane area increases by 25%. The width of the membrane does not influence k_0, Δp, $W_{booster}$ and A_T significantly, since it is only represented through

the hydraulic diameter in equation 2.9, which is independent of w if $w >> h$. This is usually the case in an UF module, where the width normally is a factor 10^2 larger than the channel height.

7.2.2 Energy used by the electric field

The power consumed by the electric field P_E is given by:

$$P_E = \frac{U_a I}{\eta_E} \tag{7.15}$$

where η_E the efficiency of the power supply. By combining equation 7.15 with equation 5.2 an 5.4, U_a can be expressed in terms of the resistance of the different chambers as:

$$U_a = \frac{I}{A_e}\left(n\frac{h}{\kappa_{feed}} + nr_p + 2r_e + nr^*\right) \tag{7.16}$$

Combining equation 7.15 and 7.16 with equation 5.5 the following equation is obtained:

$$\begin{aligned} P_E &= \frac{I^2}{\eta_E A_e}\left(n\frac{h}{\kappa_{feed}} + nr_p + 2r_e + nr^*\right) \\ &= \frac{E_{feed}^2 \kappa_{feed}^2 A_e}{\eta_E}\left(n\frac{h}{\kappa_{feed}} + nr_p + 2r_e + nr^*\right) \end{aligned} \tag{7.17}$$

Inserting equation 7.3 in equation 7.17 and replacing A_e with A_T/n, the energy input during concentration from c_{feed} to c_r can be calculated by:

$$W_E = \frac{P_E}{Q_{feed}} = \frac{E_{feed}^2 \kappa_{feed}^2}{J_{av}\eta_E}\left(1 - \frac{c_{feed}}{c_r}\right)\left(\frac{h}{\kappa_{feed}} + r_p + r^*\right) \tag{7.18}$$

assuming that r_e is negligible compared to the other resistances. This approximation is valid when a stack consisting of many cells is used, since the voltage across the two electrode chambers is small compared to the voltage across the entire stack.

The height of the feed channel is the design parameter that influence the energy used by the electric field mostly. It is proportional to the height considering only the energy used in the feed chamber (thus neglecting the influence of the height on the flux since the mass transport coefficient in EUF is low due to the low crossflow velocity), this means that h should be as small as possible. This is also the case for the height of the permeate and buffer chambers; the narrower the channel distance becomes the less energy is used.

In equation 7.3, 7.11 and 7.18 the average flux is required. It is therefore necessary to integrate equation 6.3 with respect to the concentration. However, the term $\ln(c_g/c_{feed})$ do not have an analytical solution. The energy consumption and membrane area is therefore calculated in small steps of $\Delta c = 1.0$ g/L and summarized. Matlab is used for this purpose. The program can be found in appendix C.

7.3 Energy considerations

The process economy for EUF should be compared to the energy requirements for conventional UF. It is therefore necessary to determine the optimal operating conditions for UF. For these calculations an UF/EUF module with the dimensions $l = 0.5$ m and $w = 0.2$ m is used, since it is a common dimension of both UF and ion-exchange membranes. The channel height h is set to 1.0 mm unless stated otherwise. Examples of the flux estimated in this module under both UF and EUF conditions are shown in figure 7.3 and 7.4 for amylase-F and amylase-S, respectively. The curves are made by using the expression for the mass transport coefficient found in equation 6.4 together with the empirical expression for EUF in equation 6.3.

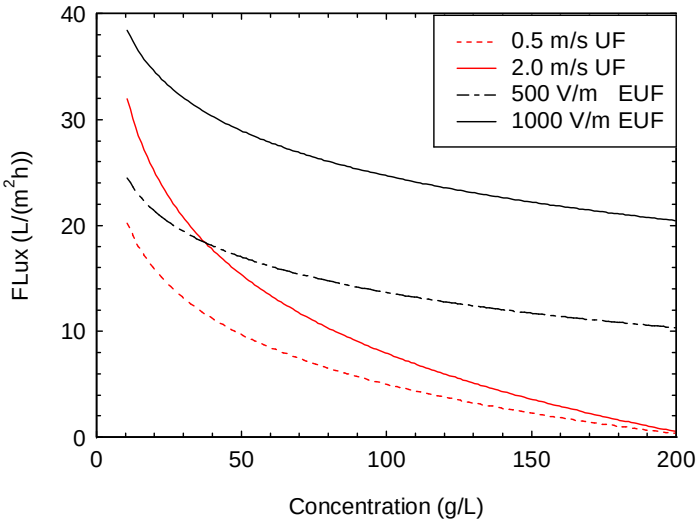

Figure 7.3: Expected limiting flux for amylase-F on a module with $h = 1$ mm, $l = 0.5$ m and $w = 0.2$ m. A crossflow velocity of 0.1 m/s is used for the calculations of the EUF curves.

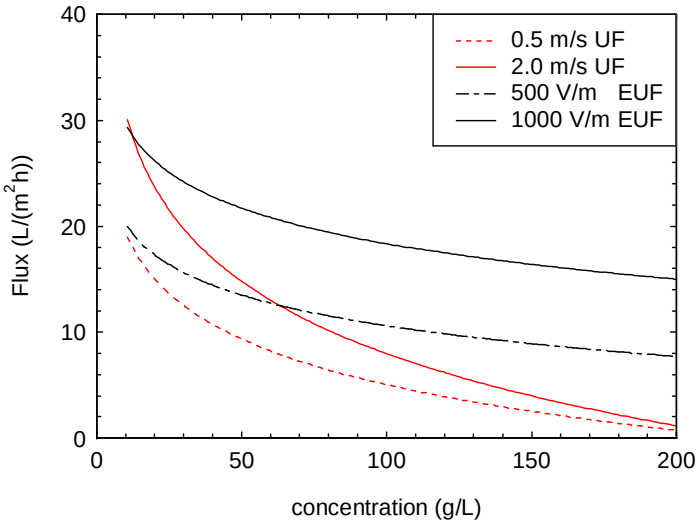

Figure 7.4: Expected flux for amylase-S on a module with $h = 1$ mm, $l = 0.5$ m and $w = 0.2$ m. A crossflow velocity of 0.1 m/s is used for the calculations of the EUF curves.

As expected from the experimental EUF data, the greatest relative flux improvement is obtained in the high concentration area. The flux in the low concentration area is more or less in the same range for both UF and EUF.

The calculations assume that the parameter $a^{\dagger}$ and the electrophoretic mobilities found in table 6.1 are independent of the dimensions of the module. Hence the relative effect of the electric field increases when the dimensions of the cells increases, since the mass transport coefficient decreases.

The calculations are based on a feed flow of $Q_{feed} = 1.0$ m^3/h, and a pump and power supply efficiency of $\eta_{pump} = \eta_E = 0.6$. The gel layer concentration is set to 210 g/L for amylase-F and 225 g/L for amylase-S. The viscosity and density of the feed solution is assumed to be equal to the viscosity and density of water at 12^{o}C, since it is the temperature of the solutions in the EUF and UF experiments. Only the energy requirements of the booster pump will be considered, since the energy used by the feed pump is negligible. Furthermore, the modules in a production line will be placed continuously so that the retentate from the first concentration step will be the inlet concentration for the second module and so forth as shown in figure 7.5.

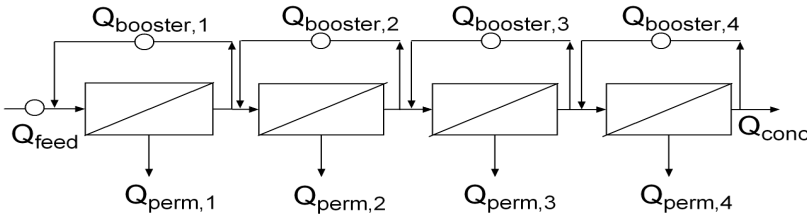

Figure 7.5: Sequence of UF/EUF modules in a production line.

The energy used by the feed pump is therefore only relevant for the first step. The calculations are divided into four steps with an overall concentration range from $10-200$ g/L. The calculations are made at a higher final concentration than the experiments were conducted to fully cover the potential of EUF. Equation 6.3 is assumed to be valid in the entire concentration range. The calculations are based on the resistance of the feed solution only unless stated otherwise. Hence r_p and r^* are set to zero. If the calculations show that EUF consumes more energy than UF under these conditions, EUF will not be an economical advantage in practice where r_p and r^* will have a value higher than zero. Only the figures representing the energy used when filtering amylase-F are shown. The corresponding figures for amylase-S can be found in appendix F.

7.3.1 Energy used in UF

In figure 7.6 the energy calculations for the UF process is shown for the amylase-F solutions. The energy consumption has been calculated for 4 different concentration ranges covering the concentration from 10 to 200 g/L. The highest concentration range from $150-200$ g/L has been included to cover a range relevant for industrial production, even though no experiments have been carried out in that range. The calculations are carried out for a crossflow range of $0.2-2.4$ m/s in steps of 0.2 m/s. The energy used by the booster pump (equation 7.11) is depicted on the abscissa, and the corresponding reciprocal total membrane area (Q_{feed}/A_T) calculated by equation 7.3 on the ordinate. From equation 7.3 it can be seen that $1/A_T$ is proportional to the average flux, which means that a high value of Q_{feed}/A_T and a low energy consumption is desired.

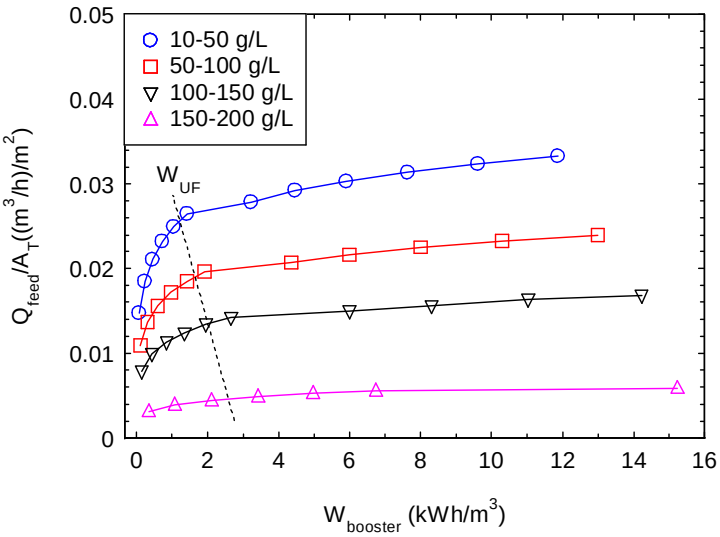

Figure 7.6: The reciprocal membrane area as a function of the energy consumption during conventional UF for different concentration ranges of amylase-F. The optimal conditions are marked by the dotted line.

Figure 7.6 shows that there exist an optimal combination of the energy consumption (and hence the crossflow velocity) and the membrane area. This is seen as a deflection in the curves around $2-3$ kWh/m^3, more pronounced for low concentrations due to higher influence of the crossflow velocity on the flux at these concentrations. Since the curves have a steep slope before the deflection point it is feasible to increase the crossflow velocity because it reduces the total membrane area considerably. After the deflection point a further increase in the crossflow velocity will not reduce the membrane area substantially. This means that it is too expensive to operate beyond this point. The optimal operating conditions for the different concentration intervals are indicated by the dotted line in figure 7.6, and corresponds to crossflow velocities between 0.7-1.0 m/s, which is in the laminar area. The results for UF of amylase-S are very similar to amylase-F and the optimal operating conditions are within the same range.

7.3.2 Energy used in EUF

In figure 7.7 the energy calculations for the EUF process is shown for the amylase-F solution for the same concentration ranges as in figure 7.6. The energy is a sum of the energy used by the electric field and the booster pump. However, the

energy used by the booster pump accounts for less than 5 % of the total energy consumption in EUF due to the low crossflow velocity. The calculations are carried out at different electric field strengths in the range of $0 - 2000$ V/m (in steps of 200 V/m) and a crossflow velocity of 0.1 m/s. The conductivity of the feed solution is set to 1.0 mS/cm, which corresponds to a diafiltrated solution.

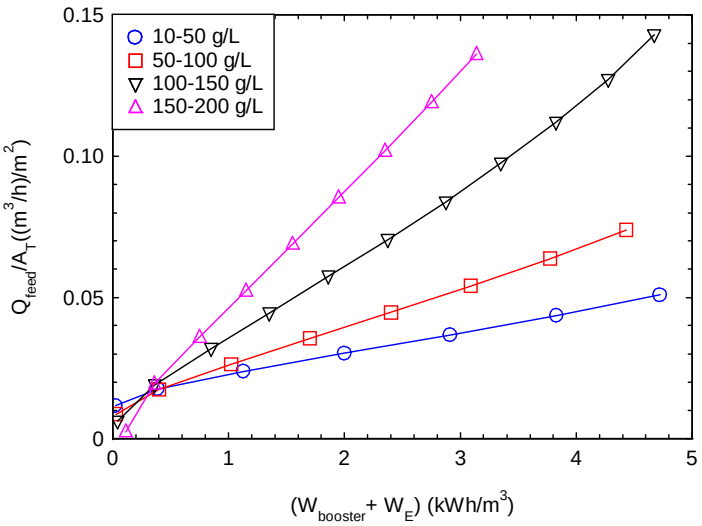

Figure 7.7: The reciprocal membrane area as a function of the energy consumption during EUF for different concentration ranges of amylase-F. $\kappa_{feed} = 1.0$ mS/cm.

Unlike the UF process shown in figure 7.6, the curves representing the EUF process do not show any deflection. The membrane area decreases with increasing energy consumption (higher electric field strength). The optimum electric field strength therefore depends on the price of the membrane and the costs of energy.

Energy comparison between UF & EUF

To compare the energy consumption in the UF and EUF processes for the different concentration ranges, the deflection points from figure 7.6, which corresponds to the optimal operating conditions for the UF process is inserted, and illustrated by the filled symbols on figure 7.8. The reduction in the membrane area which can be obtained by using the energy required for the UF in EUF instead is illustrated by the dotted lines.

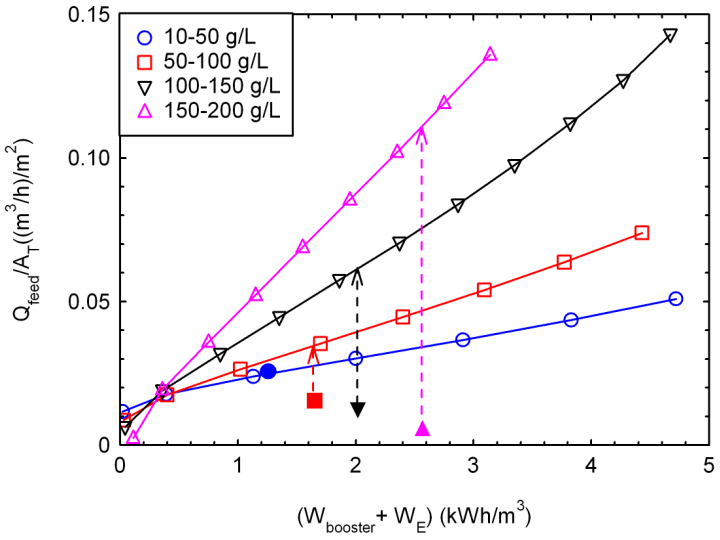

Figure 7.8: The reciprocal membrane area as a function of the energy consumption during EUF for different concentration ranges of amylase-F. The optimal operating conditions for UF form figure 7.6 is shown by the filled symbols.

When comparing the two processes it can be seen that the membrane area can be reduced when filtering the highly concentrated solutions if the energy used for UF is used for EUF instead. This is on the other hand not the case for the dilute solutions where the benefit of EUF is small or non existing. The membrane area reduction and the electric field which can be applied to utilize the same amount of energy in EUF as in UF can be seen in table 7.2.

Concentration range (g/L)	10-50	50-100	100-150	150-200
Electric field (V/m)	425	590	860	1300
membrane area reduction	1	2	5	24

Table 7.2: Electric field strength need to consume the same amount of energy in EUF as in UF, and the corresponding reduction in the membrane.

For the low concentration range ($10 - 50$ g/L) there is no advantage in using EUF, since the membrane area needed in EUF is almost equal the membrane area needed in UF when the same amount of energy is used. In the concentration range of $50 - 100$ g/L the calculations show a small advantage in favor of EUF, since the membrane area can be reduced by a factor of 2 if 590 V/m is applied. The advantage of EUF becomes more evident at high feed concentration. In

the concentration range of $150 - 200$ g/L a clear advantage in favour of EUF is seen. If an electric field strength of 1300 V/m is applied the energy requirements for EUF are the same as for UF. However, the membrane area can be reduced around 24 times. A considerable membrane reduction can also be achieved for the $100 - 150$ g/L concentration range. Therefore it is beneficial to use EUF as a final concentration step during production where the first steps are conventional UF modules.

Effect of conductivity

To further investigate the possibilities of using EUF for filtering high concentrated solutions the influence of the conductivity must be investigated, since diafiltration may not be possible in industrial production. The calculations from figure 7.7 is therefore repeated for the high concentration range ($150 - 200$ g/L) at conductivities up to 8.0 mS/cm for amylase-F and shown in figure 7.9. The optimal condition during UF is shown as the filled pink triangle. It is assumed that the flux is independent of the conductivity in the studied range, which have been tested for amylase-S solutions up to about 3 mS/cm (see appendix F) and also expected to be the case for amylase-F.

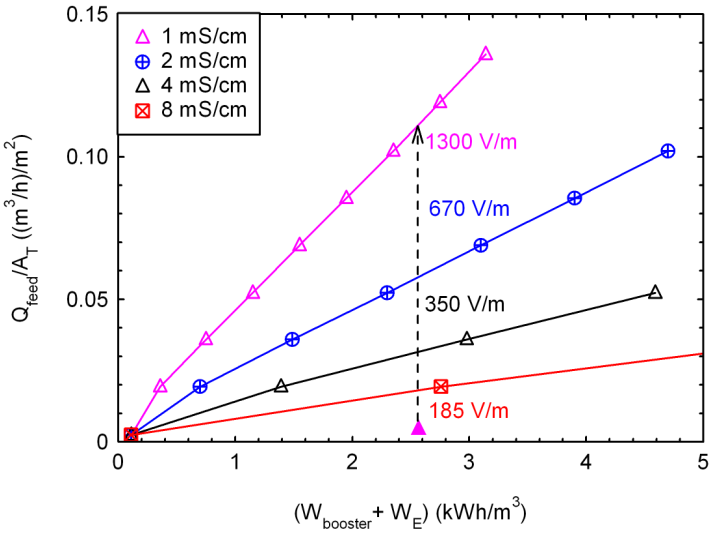

Figure 7.9: The reciprocal membrane area as a function of the energy consumption during EUF for amylase-F in the concentration range of 150-200 g/L for different conductivities. The optimal operating conditions for UF form figure 7.6 is shown by the filled triangle.

The effect of the conductivity is evident; the advantage of using EUF decreases almost inversely proportional to the feed conductivity. At 1 mS/cm an electric field strength of 1300 V/m can be applied before the energy used in EUF is the same as in UF, if the conductivity increases to 2 m/S only 670 V/m can be applied. When the conductivity is 8 mS/cm, the electric field strength has been reduced to 185 V/m. The reduction in the membrane area has also been decreased. Thus at 1 mS/cm a reduction of the membrane area of a factor of 24 can be obtained, while at 8 mS/cm it is only a factor of 4.

Effect of the channel height and resistance in the cell

The results from figure 7.9 are summarized in table 7.3, where the electric field strength needed to utilize the same amount of energy in EUF as in UF is shown together with the corresponding membrane area reduction. Two different channel heights of 1 mm and 0.5 mm are used, and the calculations are made in the conductivity range of $1.0 - 8.0$ mS/cm. In a real system there will be additional energy loses due to the resistance of the ion-exchange membranes and the permeate chambers. The calculations are therefore repeated by setting the specific resistance of the permeate chamber equal the specific resistance of the ion-exchange membrane, since it is probably not realistic to obtain a lower conductivity for the permeate chamber in practice. The specific resistance of the CIX membrane is given by the manufacture to 0.001 m^2/S.

$h,\ r^* = r_p$ κ_{feed}	$h = 1$ mm, 0 m^2/S	$h =$ 0.5 mm, 0 m^2/S	$h = 1$ mm, 0.001 m^2/S	$h = 0.5$ mm, 0.001 m^2/S
1.0 mS/cm	1300 (24)	$>$ 2000 ($>$25)	1100 (20)	1850 (30)
2.0 mS/cm	670 (12)	1300 (16)	490 (9)	710 (12)
4.0 mS/cm	350 (7)	670 (8)	205 (4)	280 (5)
8.0 mS/cm	185 (4)	250 (5)	70 (2)	90 (2)

Table 7.3: Electric field strength need to utilize the same amount of energy in EUF as in UF when concentrating 150 g/L amylase-F up to 200 g/L. The corresponding reduction in the membrane area (round off to the nearest integer value) is shown in parenthesis.

There is an advantage by decreasing the height of the feed channel from 1 mm to 0.5 mm also when accounting for the resistance of the permeate chamber and ion-exchange membranes. The electric field strength which can be applied before the same amount of energy is utilized in EUF as in UF increases and the mem-

brane area can be further reduced. e.g. at a conductivity of 2.0 mS/cm a channel height of 1.0 mm and $r^* = r_p = 0$ the membrane area can be reduced 12 times if the energy is used in a EUF process instead of a UF process. This requires an electric field of strength of 670 V/m. If the channel height is 0.5 mm instead, the membrane area can be reduced 16 times if 1300 V/m is used. Even if the resistance of the permeate chamber and the ion-exchange membranes are taken into account a substantial reduction in the membrane area of a factor 9 or 12 can be achieved depending of the channel height. However, as the conductivity increases the advantages of EUF decreases, and it is probably not economically feasible to use EUF when the conductivity is above 4.0 mS/cm, which might even be too high. The limit of 4.0 mS/cm are of course depending on wether the resistance of the permeate chamber can be reduced to the same level as for the ion-exchange membrane. Otherwise the conductivity limit at which EUF is profitable with respect to UF decreases even further.

In table 7.4 the same results are shown for amylase-S.

$h,\ r^* = r_p$	$h = 1$ mm,	$h = 0.5$ mm,	$h = 1$ mm,	$h = 0.5$ mm,
κ_{feed}	0 m$^2/S$	0 m$^2/S$	0.001 m$^2/S$	0.001 m$^2/S$
1.0 mS/cm	900 (8)	1770 (14)	760 (7)	1280 (10)
2.0 mS/cm	470 (4)	910 (7)	350 (3)	540 (5)
4.0 mS/cm	260 (3)	490 (4)	150 (2)	210 (2)
8.0 mS/cm	140 (2)	270 (3)	50 (1)	60 (1)

Table 7.4: Electric field strength need to utilize the same amount of energy in EUF as in UF when concentrating 150 g/L amylase-S up to 200 g/L. The corresponding reduction in the membrane area (round off to the nearest integer value) is shown in parenthesis.

In general the advantage of using EUF instead of UF is lower when considering amylase-S, due to the lower electrophoretic mobility of this enzyme. When comparing the numbers it can be seen that the membrane area reduction is lower for the amylase-S system, and the electric field strength which can be applied before the same amount of energy is used in EUF as in UF is smaller. The same conclusions concerning channel height and conductivity can however be made for amylase-S as for amylase-F.

A low channel height and a low feed conductivity is therefore of utmost importance if EUF is going to be applied successfully in industrial production. Also the design of the module is important, especially to minimize the energy

losses in the permeate chamber. A solution could be to fill the permeate chamber with a conducting ion-exchange resin or make the flow spacers and nettings of conducting material to reduce the resistance.

In table 5.1 the conductivities of the amylase-F and amylase-S solutions before diafiltration are given to 4 and >7 mS/cm, respectively. Table 7.3 shows that a membrane area reduction of around 4-5 times (depending on the channel height) is possible at a conductivity of 4 mS/cm when filtering amylase-F, if the resistance of the permeate chamber can be reduced to 0.001 m^2/S. Table 7.4 shows that no membrane area reduction can be achieved for amylase-S at 8 mS/cm when using EUF instead of UF, if the resistance of the permeate chamber is equal 0.001 m^2/S.

Since most of the enzymes solutions produced by Novozymes have conductivities >7 mS/cm, EUF can only be used to filter a few products and it therefore not at this point a useful technology. If EUF is going to be used in the future it requires that the production is changed, especially the flocculation process. If the amount of salt used during pretreatment could be reduced then EUF could be considered.

7.4 Summary

- The optimal operating conditions for UF is between 0.7-1.0 m/s, which corresponds to laminar flow conditions. This applies for both amylase-F and amylase-S.
- EUF is profitable in the high concentration area, where the relative flux improvement is the highest. Hence the membrane area can be reduced up to 24 times for amylase-F, and 8 times for amylase-S when using EUF instead of UF to concentrate a solution from 150 to 200 g/L.
- The advantage of EUF decreases as the conductivity of the feed increases. Above a conductivity of 4.0 mS/cm for amylase-F and 2.0 mS/cm for amylase-S the advantage of EUF disappears.
- Whether or not EUF should replace UF depends on the conductivity of the solution and the design of the module. It is important that the resistance of the cell is low, especially the resistance of the permeate chamber in order to avoid additional costs.

Chapter 8

Conclusion

Experiments with electro-ultrafiltration of enzymes solutions have shown that a large flux increase is obtained when filtering amylase solutions; whereas protease and lipase solutions did not result in any significant flux increase, mainly due to low electrophoretic mobilities and impurities in the solutions. Especially in the protease-S solution flocculation chemicals and antifoam were able to foul the membrane.

Flux improvements of a factor 3-7 is obtained when using EUF to filter the amylases. The greatest increase is achieved at high concentration, which makes EUF superior as a final concentration step in a production line.

To describe the EUF data obtained for the amylases, the modified gel layer model, which predicts a straight line of the flux as a function of the electric field strength, has been tested. The flux dependency is however only linear at low electric field strengths. At high electric field strengths the data deviates from a straight line and the deviation increases as the concentration decreases. The non-linear appearance is due to a disturbance of the gel layer, which decreases the concentration polarization layer and thereby increases the mass transport coefficient. An empirical equation have been developed, which accounts for a higher mass transport coefficient at high electric field strengths.

The TMP did not have any influence on the flux, probably since the limiting flux is already reached. The crossflow velocity has a small impact, but only at low electric field strengths where a small increase in the flux is observed. The small influence of the crossflow velocity is probably due to the low crossflow velocities (0.07-0.13 m/s), which are used in the experiments. This means that the electric field is the main driving force and that a high crossflow velocity can

be replaced by an electric field.

UF experiments of the amylase solutions have also been carried out. The UF data followed a development described by the laminar Sherwood correlation as a function of the crossflow velocity. The absolute values found in the UF experiments exceeded however the values predicted by the laminar Sherwood approximation due to turbulent conditions on the feed and retentate side of the UF module. These data are used to compared the flux, which can be obtained in conventional UF, where a high crossflow velocity is used, with the flux obtained in EUF at low crossflow velocity, but with the application of an electric field. The flux data are then used to compare the energy requirements in EUF with UF.

The energy consumption and membrane area in UF and EUF have been calculated and show that under certain conditions EUF is profitable compared to UF. In the high concentration area, where the flux increase is greatest it is attractive to used EUF. This is mainly due to a large reduction in the membrane area, which can be reduced up to 24 times depending on the resistance of the EUF module. However the advantage of EUF decreases as the conductivity (caused by salt ions) of the feed solutions increases. Above 4.0 mS/cm for amylase-F and 2.0 mS/cm for amylase-S the advantage of EUF almost disappears.

The used of EUF instead of UF is very much depended on the feed solution. If the electrophoretic mobility is high and the salt concentration low, it is possible to achieve large membrane area reductions when using EUF. Since EUF is most efficient at high concentrations a production line consisting of UF modules with one or two EUF modules as final concentration steps is an economical advantage.

Chapter 9

Future of the project in Novozymes

Despite the limited economical advantage of using EUF for concentration of Novozymes products, the project is going to continue as a new PhD project in collaboration between Novozymes and DTU, but with a different perspective. In table 5.1 it can seen that enzymes carry different charges, which can be adjusted by changing the pH value of the solution. It is therefore not unlikely that EUF or EMF can be used for separation of two enzymes with opposite sign of charge as briefly described in the literature review part in section 4.5. Another possibility is to separate the enzyme product from impurities in the solution by dragging the charged enzymes though the membrane. This could improve the purity of the enzyme product, which is desirable as Novozymes is moving into new business areas like the pharmaceutical industry; where a high purity of the enzyme product is required.

The conductivity of the enzyme solutions are of course still an issue. However, if EUF or EMF works for separation not only the energy consumption is important, but the quality of the product must also be taken into account. This is a significant difference between using EUF for separation instead of concentration, where the quality of the product is assumed to be the same whether UF or EUF is used. When used for separation, the economy in the EUF or EMF process is going to be compared to e.g. chromatography, which is a more expensive method than UF. Hence, the conductivity may not be the cost driver for EUF or EMF, but other issues like the equipment cost and the product quality may be more important.

Appendix A

Other EUF modules

Two other EUF modules have been tested before the one described in chapter 5 was successfully applied. The modules and the experimental set-up will be briefly described in the next section. In the following sections the results obtained on these modules together with the problems related to their design are discussed.

A.1 Description of the modules

A.1.1 Module containing one UF membrane

In the first module the electrodes were directly inserted into the feed and permeate solutions as shown in figure 2.4. The set-up of the rig is shown in figure A.1.

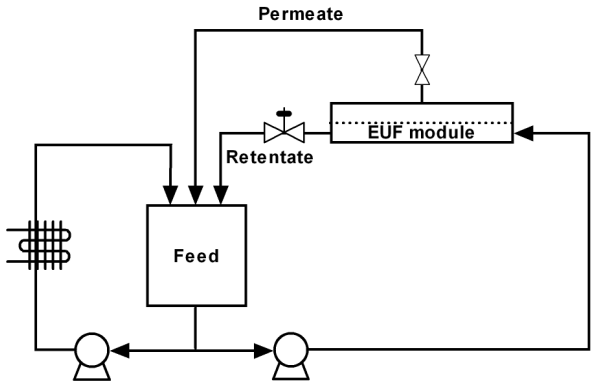

Figure A.1: Set-up of electrofiltration rig, where the electrodes were directly immersed in the feed and permeate solutions.

The feed was transferred from the tank into the module via a pump. Both the

retentate and permeate were recirculated to the feed tank. The electrodes were made of stainless steel, and the separation distance between the electrodes was 3 mm. The membrane was a 10 kDa PES membrane, with an area of 6x4 cm^2. A new membrane was used for each experiment. The volume of the feed solution was approximately 20 L. The temperature of the solution was kept constant at 20°C (lowest temperature possible) by an automatic temperature controller. The TMP was set by adjusting the back pressure. The permeate flux was measured manually with a measuring cylinder. The enzyme concentrate was diluted with twice distilled water and stirred 5-10 min before the experiment was started. Samples of the feed solution were collected at the beginning and at the end of the experiment and the enzyme activity and concentration were measured. Permeate samples were also collected with appropriate time intervals to monitor the retention. Amylase-F solutions were filtered on this equipment at a pH of 6.7, hence the anode was placed on the feed side and the cathode on the permeate side.

A.1.2 Module containing one UF and one IEX membrane

The second module which have been tested is shown in figure A.2.

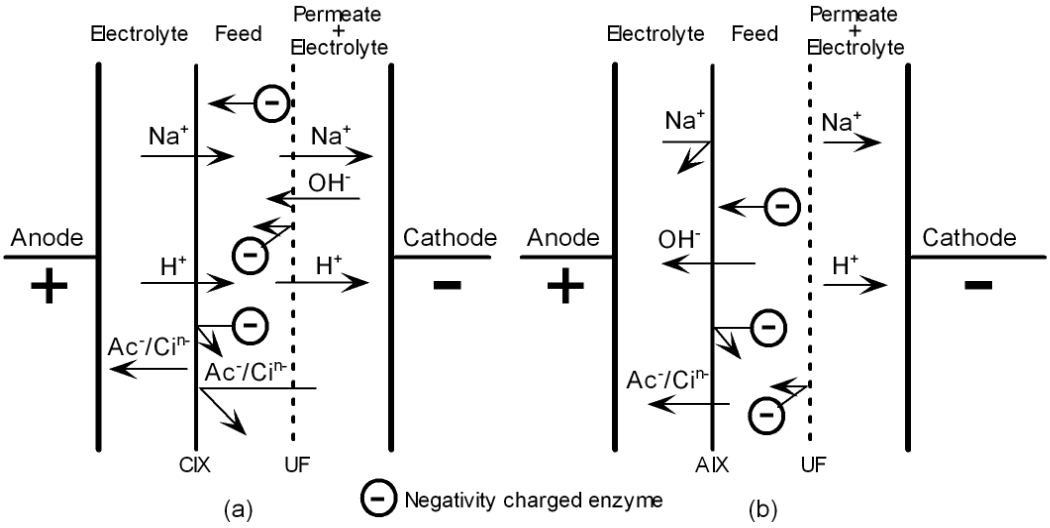

Figure A.2: EUF module with one ultrafiltration membrane and a cation or anion-axchange membrane between the feed and the electrode.

It consisted of 3 chambers separated with an IEX membrane and a UF membrane. The IEX membrane was placed between the feed solution and the anode.

The UF membrane was placed between the feed and the cathode. The IEX membrane was either a CIX membrane (figure A.2a) or an AIX membrane (figure A.2b). If a CIX membrane was used the conductivity increased in the feed chamber while it became desalinated if an AIX membrane was used, as illustrated in figure A.2. The experimental set-up is shown in figure A.3.

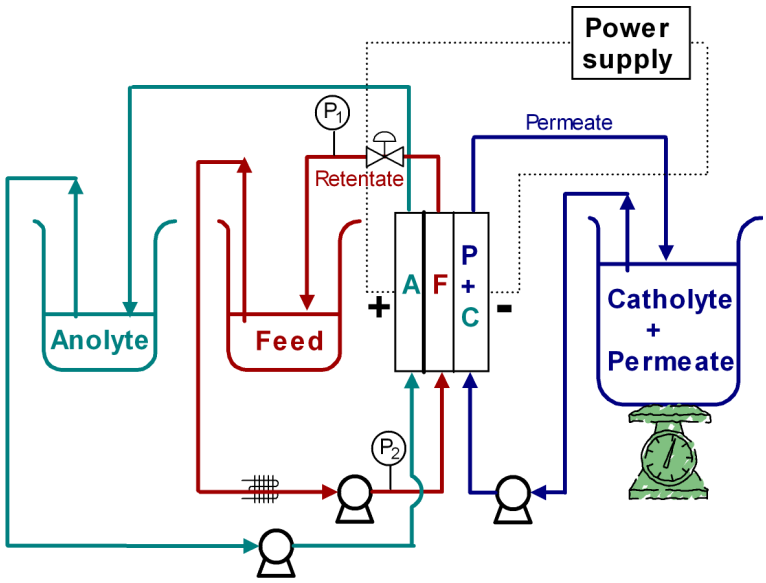

Figure A.3: Experimental set-up with the 3 compartment EUF module.

The anolyte and catholyte consisted of an sodium acetate-citric acid buffer at pH 4.6. The buffer solution was used to minimize an increase in pH from the H^+-ions generated at the anode. Likewise, the permeate was dissolved in a buffer solution to minimize a change in pH from the OH^--ions generated at the cathode. The anolyte and the retentate were recirculated. The permeate solution was mixed with the catholyte and recirculated in the cathode chamber. The flow rate was measured with a balance, as the increase in mass during a certain time interval. Since it was not possible to return the permeate back to the feed tank, the concentration in the feed container increased with time. A 10 kDa ETNA membrane was used, which had an area of 6x6 cm^2. The membrane was cleaned after each experiment as described in chapter 4. The flow rate of the anolyte and catholyte was 48 L/h and 22 L/h, respectively. A lower flow rate in the cathode chamber was chose to minimize the disturbance of the balance. The distance between the electrodes was 6 mm. The TMP was set to 1 bar, by adjusting the valve on the retentate side, and the crossflow velocity was 0.07 m/s. The feed

stream was connected to a cooler and the temperature kept between 13-16°C. The feed volume was about 1 L, and was concentrated to about 0.5 L. The concentration was therefore increased by a factor of 2 during the experiment. The start volume of the catholyte was about 0.5 L and the final volume was therefore about 1 L.

The set-up was tested with the amylase-F solution. The retention was tested on samples collected from the permeate + catholyte solution in the end of the experiment.

A.2 Results and problems related to the modules

A.2.1 Module containing one UF membrane

Figure A.4 shows the permeate flux as a function of time during filtration of a 2 g/L amylase-F solution at 0 and 100 V.[1]

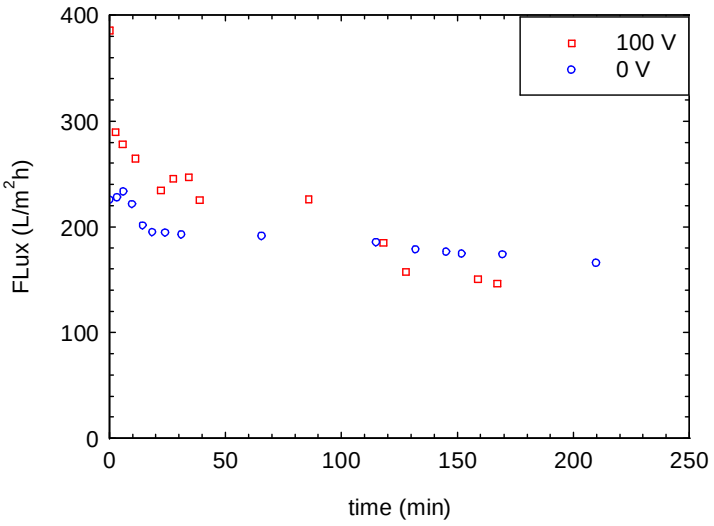

Figure A.4: Flux development for 2 g/L amylase-F solution filtered at 0 and 100 V. TMP = 2 bar, v=1.2 m/s, pH = 6.7.

Application of 100 V resulted in an approximately 25% flux enhancement during

[1] During the experiment a substantial amount of gas was developed at the electrodes. The development of gas made the flux measurements difficult, since the gas had to pass through the permeate tube, which resulted in scattered flux data. Hence figure A.4 only show some of the measured data points.

the first 90 min of the filtration. After 115 min the flux dropped to a level below the 0 V curve. After the EUF experiment a sticky brown substance on the anode (electrode on the feed side) and on the membrane surface was observed. This was most likely enzymes, which had been degraded by contact with the anode. Similar observations have been reported by Wakeman [93]. He reported that extensive degradation of proteins took place during electrofiltration of ovalbumin, lactalbumin and BSA as described in chapter 4. The degradation resulted in a brown deposit on the membrane and caused the flux to drop to zero [93].

To understand the chemical processes occurring at the electrodes, experiments with two identical stainless steel electrodes immersed in a glass beaker containing a solution of amylase-F was carried out. When an electric field was applied an extensive amount of gas was produced. At the anode a substantial amount of foam was developed, which caused the current to drop by a factor of 3. After 45 min the anode was covered with a brown substance, whereas the cathode stayed relatively clean. Several experiments were made at different concentrations and pH, and the result remained the same although the deposit layer at the anode increased with pH and the enzyme concentration. Also different temperatures were tested and the deposit amount increased as the temperature increased.

The glass beaker experiments with amylase-F confirmed the problem observed in the EUF experiments. The electric field caused a coagulation of the enzymes at the anode, which resulted in a brown deposit on the electrode. This reduced the current efficiency, and since the membrane was only placed about 3 mm from the anode some of the brown substance was also deposited on the membrane and caused a blockage of the pores.

A.2.2 Module containing one UF and one IEX membrane

Figure A.5 shows an example of the flux development with time during concentration of 5 g/L amylase-F to 10 g/L. The retention was close to 100 %. The experiment was made with both CIX and AIX membranes.

The flux increased 15-20 % when 30 V was applied compared to 0 V, at the same time the filtration time decreased from around 190 min to 130 min. The flux enhancement did not depend on the type of IEX membrane. Increasing the voltage to 45 V did not increase the flux any further. Figure A.6 shows the corresponding conductivity and pH, which illustrates the problems related to this design. During the experiment with the CIX membrane the conductivity increased from about 0.1 to 0.5 mS/cm in the feed, mainly due to accumulation of acetate and citric acid, which were not able to pass the CIX membrane as shown in figure A.2a. The pH remained on the other hand constant, since the transport of H^+ from the anolyte to the feed was counter balanced by the transport of OH^- from the catholyte solution. When an AIX membrane was used the pH decreased in the feed solution due to the transport of OH^--ions from the feed to the anolyte. It was therefore necessary to add NaOH to the feed to avoid a drop in pH. The pH adjustment was carried out manually, and can be seen as the saw-toothed appearance of the curve. It was expected that the feed solution would become desalinated when an AIX membrane was used. This was however not the case, the conductivity increased during the experiment due to the addition of NaOH to the feed to control the pH. The Na^+-ions cannot pass the AIX membrane, and was therefore accumulated in the feed. A small tendency to a decrease in the conductivity can however be seen when looking closely at the curve. The conductivity appears to decrease slightly between each pH adjustment.

The configuration of this module was not optimal, since the conductivity increased during the experiment, which according to equation 5.5 implies that the electric field strength decreased when the voltage was kept constant. Increasing the voltage was not beneficial, since the transport of ions increased at increasing current intensity. The pH was also difficult to control. However, degradation of the enzymes were not observed, which means that it is only a problem when the enzymes are in direct contact with the electrodes.

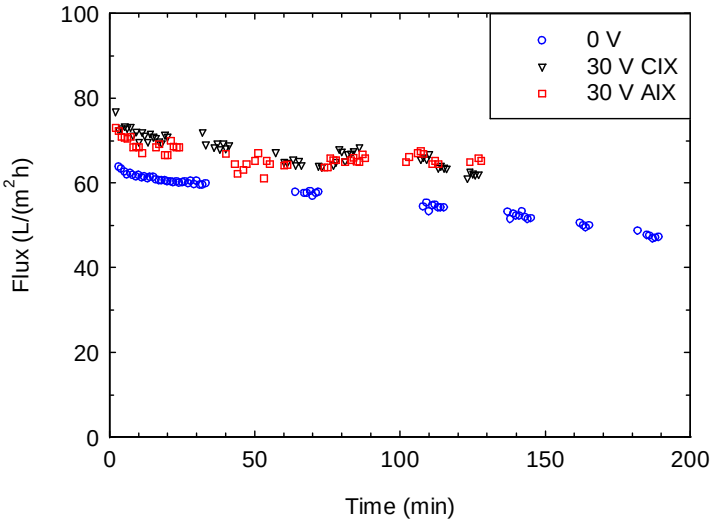

Figure A.5: Permeate flux as a function of time. Concentration of 1 L 5 g/L amylase-F to 10 g/L.

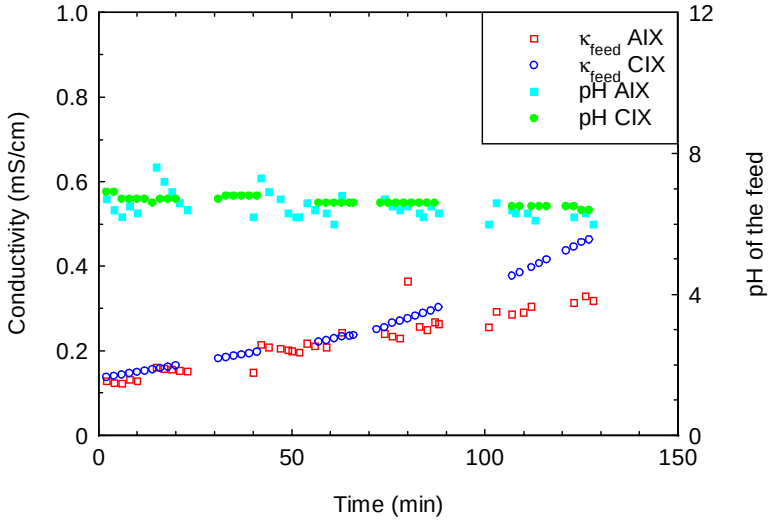

Figure A.6: pH and conductivity development in the feed during the EUF experiment shown on figure A.5. The squares represents the result when a CIX membrane was used, whereas the circles represents the AIX membrane.

Appendix B

UF data

Measured flux data as a function of TMP for different concentrations of amylase-F and amylase-S solutions. The data have been used to make figure 6.15 and 6.17.

B.1 Amylase-F

Figure B.1, B.2 and B.3 shows the flux versus TMP for amylase-F solutions for concentrations of 15, 56 and 140 g/L, respectively.

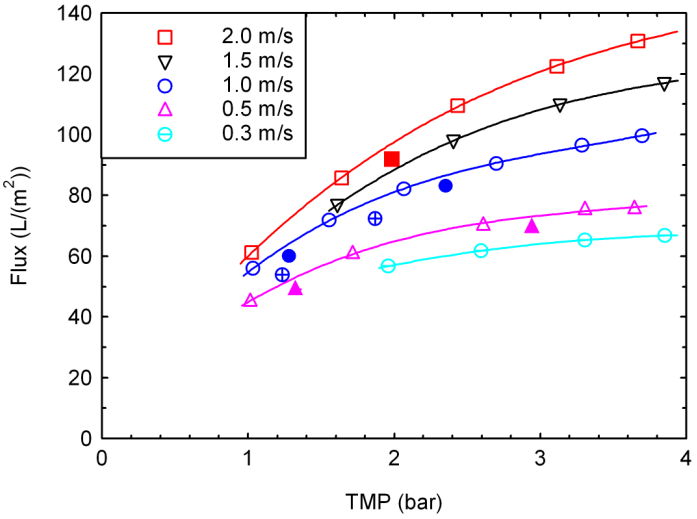

Figure B.1: Flux versus TMP at different crossflow velocities for a 15 g/L amylase-F solution. The open symbols are date collected when the TMP is increased, and the filled symbols are data collected when the TMP is decreased. The data represented by $\oplus$ is the data collected in the end of the experiment at 1.0 m/s.

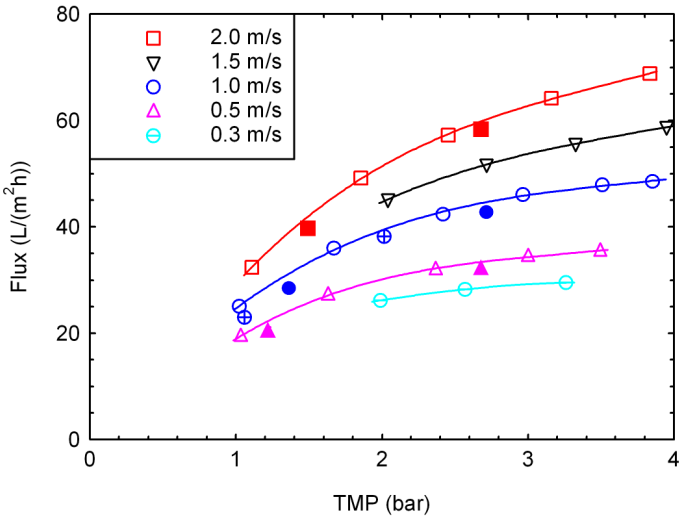

Figure B.2: Flux versus TMP at different crossflow velocities for a 56 g/L amylase-F solution. The open symbols are date collected when the TMP is increased, and the filled symbols are data collected when the TMP is decreased. The data represented by ⊕ is the data collected in the end of the experiment at 1.0 m/s.

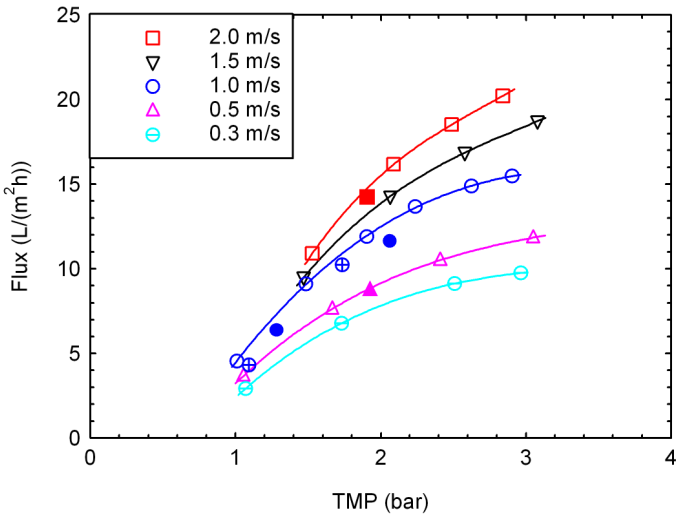

Figure B.3: Flux versus TMP at different crossflow velocities for a 140 g/L amylase-F solution. The open symbols are date collected when the TMP is increased, and the filled symbols are data collected when the TMP is decreased. The data represented by ⊕ is the data collected in the end of the experiment at 1.0 m/s.

B.2 Amylase-S

Figure B.4, B.5, B.6 and B.7 shows the flux versus TMP for amylase-S solutions for concentrations of 12, 24, 52, and 125 g/L, respectively.

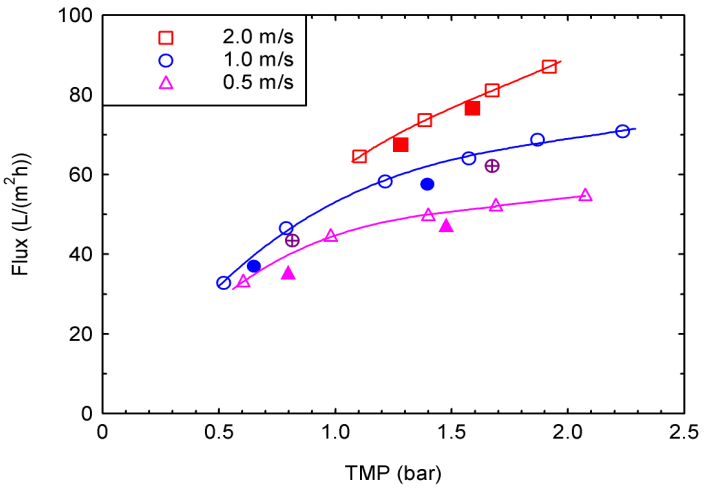

Figure B.4: Flux versus TMP at different crossflow velocities for a 12 g/L amylase-S solution. The open symbols are date collected when the TMP is increased, and the filled symbols are data collected when the TMP is decreased. The data represented by ⊕ is the data collected in the end of the experiment at 1.0 m/s.

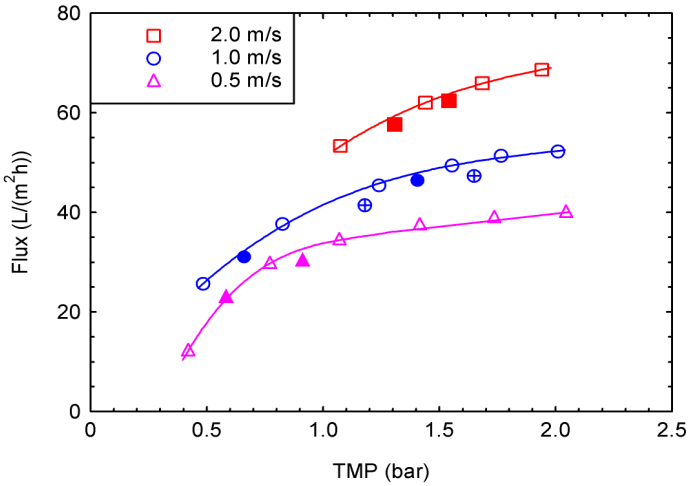

Figure B.5: Flux versus TMP at different crossflow velocities for a 24 g/L amylase-S solution. The open symbols are date collected when the TMP is increased, and the filled symbols are data collected when the TMP is decreased. The data represented by ⊕ is the data collected in the end of the experiment at 1.0 m/s.

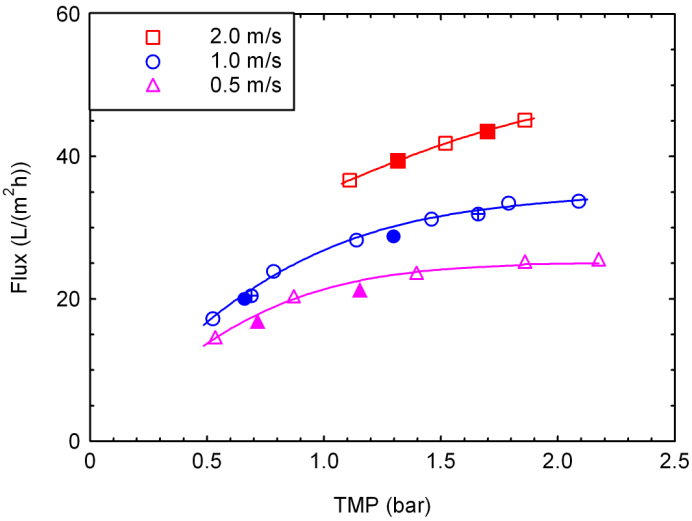

Figure B.6: Flux versus TMP at different crossflow velocities for a 52 g/L amylase-S solution. The open symbols are date collected when the TMP is increased, and the filled symbols are data collected when the TMP is decreased. The data represented by ⊕ is the data collected in the end of the experiment at 1.0 m/s.

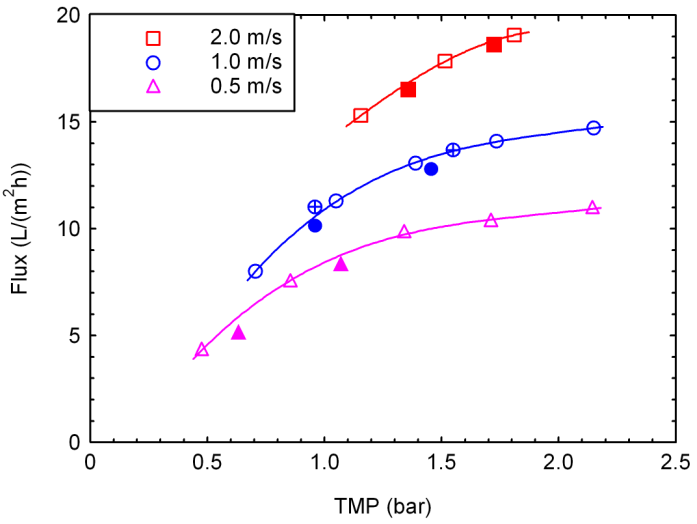

Figure B.7: Flux versus TMP at different crossflow velocities for a 125 g/L amylase-S solution. The open symbols are date collected when the TMP is increased, and the filled symbols are data collected when the TMP is decreased. The data represented by ⊕ is the data collected in the end of the experiment at 1.0 m/s.

Appendix C

Energy calculations -Matlab code

Example of the input file for energy calculations of amylase-S, when concentrating a solution from 150 g/L to 200 g/L at a conductivity of 1 mS/cm. The specific resistances of the permeate chamber and the specific resistance of the other items are in this example zero.

Amylase-S		
Enzyme concentration. c_{Feed}	150	g/L
Enzyme concentration. c_{conc}	200	g/L
Size:	80000	Da
conductivity	0.1	S/m
Feed volume: Q_{feed}	1	m^3/h
mass transport parameter UF *a*	1.85	
mass transport parameter UF *b*	0.33	
Gel layer concentration c_{gel}	225	g/L
electrophoretic mobility μ_e	4E-09	$m^2/V*s$
constant in modified gel layer model: a	0.00025	m/V
Specific resistance in permeate channel r_p	0	S/m^2
Specific resistance in other items r*	0	S/m^2
Height of feed channel h	0.001	m
Width of feed channel w	0.2	m
Length of feed channel l	0.5	m
pump efficiency η_p	0.6	
efficiency of power supply η_p	0.6	
Inlet pressure	0	Pa
Temperature	285.15	K

Example of the input variables, which are the electric field strength across the feed chamber and the crossflow velocity.

E_{feed} [V/m]	crossflow [m/s]	number of calculations	22	max 100
0	0.2			
0	0.4			
0	0.6			
0	0.8			
0	1			
0	1.2			
0	1.4			
0	1.6			
0	1.8			
0	2			
0	2.2			
0	2.4			
200	0.1			
400	0.1			
600	0.1			
800	0.1			
1000	0.1			
1200	0.1			
1400	0.1			
1600	0.1			
1800	0.1			
2000	0.1			

Output file for the chosen parameters.

Electric field V/m	Cross flow m/s	Energy/Qfeed kWh/m3 feed	Area m2/(m3/h)
0.00	0.20	0.24	227.65
0.00	0.40	0.76	181.10
0.00	0.60	1.50	158.42
0.00	0.80	2.42	144.08
0.00	1.00	3.51	133.85
0.00	1.20	4.77	126.03
0.00	1.40	10.76	119.78
0.00	1.60	14.87	114.62
0.00	1.80	19.77	110.25
0.00	2.00	25.51	106.48
0.00	2.20	32.13	103.18
0.00	2.40	39.66	100.26
200.00	0.10	0.45	64.36
400.00	0.10	0.99	36.60
600.00	0.10	1.54	25.56
800.00	0.10	2.10	19.63
1000.00	0.10	2.66	15.93
1200.00	0.10	3.22	13.39
1400.00	0.10	3.77	11.54
1600.00	0.10	4.33	10.14
1800.00	0.10	4.88	9.03
2000.00	0.10	5.42	8.13

Matlab code used for the calculations.


```
 1 global Wpump Welec cin cout Qfeed Atotal
 2
 3 M=[];
 4 V=[];
 5 %read the constant parameters
 6 M = xlsread('EUFprocess1.xls', 'constants', 'B2:B37');
 7 %read the variables parameters
 8 V = xlsread('EUFprocess1.xls', 'variables', 'A2:B100');
 9 Num = xlsread('EUFprocess1.xls', 'variables', 'D1');
10 %calculate the electric energy
11
12 %feed conditions!
13 cin=M(1); %g/L
14 cout = M(2); %g/L
15 size =M(3);
16 q1 =M(4); %
17 %*************************
18
19 %feed rate
20 Qfeed = M(5); %m3/h
21 %*************************
22
23 %Empirical gel layer model parameters
24 z1=M(6);
25 z2=M(7);
26 cgel1 =M(8); %g/L
27 my=M(9);   %m2/Vs
28 a=M(10);    %m/V
29 %*************************
30
31 %Resistance in the module
32 Rperm =M(11); %ohm
33 Rother=M(12); %ohm
34 %*************************
35
36 %Module dimensions
37 hfeed = M(13); %m
38 wfeed = M(14); %m
39 lfeed = M(15); %m
40 S=2*(hfeed+wfeed); %Circumference
41 Acs=hfeed*wfeed;   % cross-section
42 dh=4*Acs/S;      %hydraulic diameter
43 %*************************
44
45 %efficiency parameters
46 eta_pump =M(16);
47 eta_elec =M(17);
48 %*****************************
49
50
```

```
57
58 %Inlet pressure and Temperature
59 Pin=M(18);
60 Temperature=M(19);
61 %*****************************
62
63 %Density and viscosity
64 rho = 1000; %kg/m3 water
65 dynavis = 1.3*10^-3; %Ns/m2 value for water at 10 C
66 kappafeed=q1;
67 cgel=cgel1;
68 %*****************************
69
70 %Calculates the total energy and the area for each set of input parameters
71 Wtotal=[];
72 Area=[];
73 for l=1:Num
74     Efeed=V(l,1);
75     cf=V(l,2);
76     %call
77     pump_elec;
78     Wtotal(l) = (Wpump+Welec)/(Qfeed*3600000); %kWh/m3
79     Area(l)=Atotal/(Qfeed);                    %m2/(m3/h)
80 end
81 %*********************************
82
83 %Writes the output to EUFprocess.xls
84 xlswrite('H:\mat\EUFprocess1.xls',{'Electric field'},'result','A2')
85 xlswrite('H:\mat\EUFprocess1.xls',{'Cross flow'},'result','B2')
86 xlswrite('H:\mat\EUFprocess1.xls',{'Energy/Qfeed'},'result','C2')
87 xlswrite('H:\mat\EUFprocess1.xls',{'Area'},'result','D2')
88 xlswrite('H:\mat\EUFprocess1.xls',{'V/m'},'result','A3')
89 xlswrite('H:\mat\EUFprocess1.xls',{'m/s'},'result','B3')
90 xlswrite('H:\mat\EUFprocess1.xls',{'kWh/m3 feed'},'result','C3')
91 xlswrite('H:\mat\EUFprocess1.xls',{'m2/(m3/h)'},'result','D3')
92 xlswrite('H:\mat\EUFprocess1.xls',V,'result','A4')
93 xlswrite('H:\mat\EUFprocess1.xls',Wtotal','result','C4')
94 xlswrite('H:\mat\EUFprocess1.xls',Area','result','D4')
```

```
 1     Wp=0;
 2     We=0;
 3     A=0;
 4 %************************************************************
 5     nstep=ceil(cout-cin);  %| Number of integration steps
 6
 7 %************************************************************
 8     for j=1:nstep
 9         if ((cin+j)>cout);           %| Calculates the
10             cm=((cin+j-1+cout)/2); %| average concentration
11             vcf=1/((cin+j-1)/cout);  %| and volumetric
12         else                                    %| concentration
13             cm=((2*cin+2*j-1)/2);  %| factor for each
14             vcf=1/((cin+j-1)/(cin+j));     %| integration step
15         end
16 %*********************************************************************
17         Re=rho*cf*dh/dynavis;
18         if Re<=2100           %laminar flow
19             f=24/Re;
20         else
21             f=0.133*Re^(-0.25);  %turbulent flow
22         end
23 %*********************************************************************
24         Diff=8.34*10^(-12)*Temperature/(dynavis*1000*size^(1/3));
25         Sc=dynavis/(rho*Diff);
26         Sh=z1*(Re*Sc*dh/lfeed)^z2;
27         k=Sh*Diff/dh;
28         dP=f*S*lfeed*0.5*rho*cf^2/Acs;
29         R=((hfeed/kappafeed+Rperm+Rother)); %|Sum of Resistances
30         J=(k/(1-a*Efeed)*log(cgel/cm)+my*Efeed);       % flux
31
32         Q=(Qfeed*cin/(cin+j-1));            % start volume
33         wp=dP*hfeed*cf*(1-1/vcf)*Q/(J*lfeed*eta_pump); % Energy per step
34         we=Efeed^2*kappafeed^2*R*(1-1/vcf)*Q/(J*eta_elec); %|Energy for the↙
specific step
35         area=(1-1/vcf)*Q/(J*3600);                    % Area for each step
36
37         A=A+area;
38         We=(We+we);
39         Wp=(Wp+wp);
40
41     end
42 Wpump=Wp;
43 Welec=We;
44 Atotal=A;
45
46 Win=Pin*Qfeed/(eta_pump); %Calculates the energy from the feed pump
47 Wpump=Wpump+Win;          %Adds the energy from the feed pump to the energy from↙
the modules
48
49
```

Appendix D

Publications and presentations

D.1 Publications

A.D. Enevoldsen, E.B. Hansen and G. Jonsson, "Electro-ultrafiltration of industrial enzyme solutions," *Journal of Membrane Science* **299**, pp. 28-37, 2007.

A.D. Enevoldsen, E.B. Hansen and G. Jonsson, "Electro-ultrafiltration of amylase enzymes: Process design and economy,"*Journal of Chemical Engineering Science*, 2007.

S.P. Beier, A.D. Enevoldsen, G.M. Kontogeorgis, E.B. Hansen and G. Jonsson, "Adsorption of amylase enzyme on ultrafiltration membranes," *Langmuir* **23**, pp. 9341-9351, 2007

D.2 Conference contributions

"Enzyme recovery by crossflow electro-ultrafiltration." Poster: *Dansk Kemiingeniør Konference*, 31 May-2 June 2006, Lyngby, Denmark.

A.D. Enevoldsen, E. Hansen and G. Jonsson, "Enzyme recovery by crossflow electro-ultrafiltration" *Desalination* **199**, pp. 55-56, 2006.
Oral presentation: *Euromembrane*, 24-28 September, Taormina (messina), Italy 2006.

"Electrically enhanced ultrafiltration of enzyme solutions." Oral presentation: *European Congress of Chemical Engineering (ECCE-6)*, Copenhagen, 16-20 September 2007.

Appendix E

Paper 1

A.D. Enevoldsen, E.B. Hansen and G. Jonsson, "Electro-ultrafiltration of industrial enzyme solutions," *Journal of Membrane Science* **299**, pp. 28-37, 2007.

Reprinted with permission from the publisher.

Available online at www.sciencedirect.com
ScienceDirect
Journal of Membrane Science 299 (2007) 28–37
journal of MEMBRANE SCIENCE
www.elsevier.com/locate/memsci

Electro-ultrafiltration of industrial enzyme solutions

A.D. Enevoldsen [a,b], E.B. Hansen [a], G. Jonsson [b,*]

[a] *Recovery Development, Novozymes A/S, Smoermosevej 9, 3AM, DK-2880 Bagsvaerd, Denmark*
[b] *Department of Chemical Engineering, The Technical University of Denmark, DK-2800 Lyngby, Denmark*

Received 31 January 2007; received in revised form 15 March 2007; accepted 15 April 2007
Available online 24 April 2007

Abstract

To reduce the problems with fouling and concentration polarization during crossflow ultrafiltration of industrial enzyme solutions an electric field is applied across the membrane. The filtration performance during electro-ultrafiltration (EUF) has been tested with several enzymes. Results show that EUF is an effective method to filter high concentrated solutions at low crossflow. The flux improved 3–7 times for enzymes with a significant surface charge at an electric field strength of 1600 V/m compared to conventional UF. The greatest improvement is observed at high concentration. Not all enzymes can be filtered with EUF, mainly due to a low surface charge and impurities in the feed solution. Using a pulsed electric field did not improve the flux compared to a constant field. Gel electrophoresis experiments of the enzymes appear to be a useful method for estimating the influence of the electric field.

Keywords: Crossflow filtration; Enzyme; Electrophoretic mobility; Electrophoresis; Electrofiltration; Electric field; Membrane fouling

1. Introduction

Fouling and concentration polarization are major problems in crossflow ultrafiltration of industrial enzyme solutions. At high concentration the flux has usually declined a factor of 10 from its initial value. Large membrane areas are therefore required to get the necessary production capacity. Enhancing the shear rate at the membrane surface by using a high crossflow can reduce concentration polarization. To maintain a high crossflow large pumping capacities are required, which are energy consuming. Besides using a high crossflow, other methods like insertion of turbulent promoters [1,2] and flow manipulation like back-pulsing and flow reversal (mostly used in microfiltration) [3,4], have been used to reduce fouling and concentration polarization. Pre-treatment of the feed solution, e.g. pH adjustment, and the choice of membrane are also important. Especially in ultrafiltration of proteins severe fouling often occurs when the pH of the solution is close to the isoelectric point (p*I*) of the protein [5,6]. Hydrophilic membranes are often chosen, since proteins tend to adsorb less to hydrophilic surfaces due to their large hydrophobic regions [7,8].

Application of an external dc (direct current) electric force field across the membrane is another promising method to reduce fouling and concentration polarization. A schematic drawing of a crossflow electro-ultrafiltration (EUF) module is shown in Fig. 1. The electric field imposes an electrophoretic effect on the charged molecules dragging them away from the membrane surface. The concentration polarization layer is thereby reduced and the flux increases. The solvent flow through the membrane might also be enhanced by the electroosmotic effect; but this effect is considered secondary.

Flux improvements of a factor 2–10 have been gained by this method. A three-fold flux increase was reported by Oussedik et al. when filtering bovine serum albumin (BSA) solutions [9]. Weigert et al. obtained a six-fold increase in the filtration rate for bakers yeast, and a 10-fold increase for a cristobalit solution [10]. It is also possible to improve the filtration rate and purity of wastewater [11,12], and increase the selectivity when separating, e.g. amino acids and peptides [13]. Usually a direct current is applied, however, Zumbusch et al. showed that it is also possible to use an alternating current (ac) to improve the flux during filtration of BSA [14].

* Corresponding author. Tel.: +45 4525 2946; fax: +45 45932906.
E-mail address: gj@kt.dtu.dk (G. Jonsson).

0376-7388/$ – see front matter © 2007 Elsevier B.V. All rights reserved.
doi:10.1016/j.memsci.2007.04.021

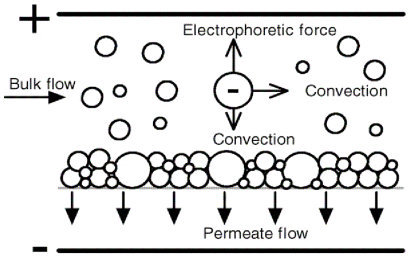

Fig. 1. Principle of electro-ultrafiltration. Inspired from ref. [10].

Instead of a constant field a pulsed electric field can also be used. A pulsed electric field consumes less energy than a constant field, and for some systems a pulsed electric field results in an even higher flux compared to a constant field [9,10]. The flux increased from 34 to 102 L/(m^2 h) when applying a constant electric field of 150 V/cm to a solution consisting of bakers yeast; a further increase to 136 L/(m^2 h) was reported when using a pulsed electric field [10]. However, for mineral solutions the flux generally decreases when using pulses compared to a constant field, which is reported by Weigert et al. and Wakeman et al. when filtering solutions of cristobalit and titanium dioxide, respectively [10,15]. Robinson et al. reported that the solute related resistance was lowest when using a constant electric field instead of a pulsed to filter BSA [16].

In a crossflow electrofiltration module the electrodes are generally placed on each side of the membrane; in some cases the membrane function as an electrode itself, usually the cathode [11]. Results have been reported for both tubular [17–19] and flat sheet modules [9,15]. In the plate module, the electrodes are usually configured like in Fig. 1, where the electrodes are placed directly in the feed and permeate solutions. There are some disadvantages with this configuration. Harmful pH changes in the feed solution due to electrochemical reactions at the electrode surface can occur, together with fouling of the electrodes. If the feed solution contains fragile components they may be damaged by direct contact with the electrodes [10]. Protein degradation has been observed when applying an electric field to solutions of bovine serum albumin (BSA), ovalbumin and lactalbumin. Here the membrane was completely blocked by degraded BSA when the concentration was higher than 15 g/L [20]. To avoid degradation of feed components the electrodes must be shielded, e.g. by ion exchange membranes [10,21] or dialysis membranes [22].

In this work, crossflow electro-ultrafiltration (EUF) is carried out on industrial enzyme solutions from Novozymes A/S, Denmark. The aim is to investigate the use of EUF in industrial production. In this paper the influence of enzyme mobility, electric field strength (constant and pulsed) and enzyme concentration will be presented. Process design and optimization will be addressed separately.

1.1. Theory

The flux improvement depends on the electrophoretic velocity of the enzyme v_e:

$$v_e = \mu_e E \tag{1}$$

where E is the electric field strength and μ_e is the electrophoretic mobility, which depends on the ζ-potential of the enzyme, and the viscosity of the solution η:

$$\mu_e = \frac{\varepsilon_0 \varepsilon \zeta}{\eta} \tag{2}$$

ε_0 and ε are the permittivity in vacuum, and the dielectric constant of the solution. The ζ-potential is given by:

$$\zeta = \frac{\sigma d}{\varepsilon_0 \varepsilon} \tag{3}$$

where σ is the charge density, and d is the thickness of the diffuse double layer surrounding the enzyme. d can be calculated from the Debye-Hückel theory by the following equation:

$$d = \left(\frac{\varepsilon_0 \varepsilon k_B T}{e^2 \sum N_i z_i^2} \right)^{1/2} \tag{4}$$

where e is the elementary charge, T the temperature, N_i the number of ions per unit volume and z_i is the valence of the ith ion. From Eqs. (3) and (4) it can be seen that the ζ-potential is proportional to d, which decreases with the square root of the ionic strength of the solution. It is therefore important to have a low salt concentration in the solution to achieve a high ζ-potential, and thereby a high effect of the electric field.

A critical electric field strength E_c is defined in EUF as:

$$E_c = \frac{J_{max}}{\mu_e} \tag{5}$$

where J_{max} is the highest flux possible at a given TMP and crossflow. If $E < E_c$ the flux can be improved by increasing E; if $E \geq E_c$ increasing E will not improve the flux any further.

One of the side effects in EUF is the electrochemical reactions occurring at the electrodes. A typical reaction is splitting of water, where hydrogen gas together with hydroxide are formed at the cathode; and oxygen gas and hydrogen ions are formed at the anode. These reactions cause pH changes, which can be harmful to the membrane and fragile feed components. Due to the formation of gasses, it is important that the EUF module is designed to continuously lead the gasses out of the filtration cell. The effect of the electrochemical reactions depends on the rate of the reactions, which depends on the current intensity [11].

1.1.1. Models

There exists no general model to predict the influence of an electric field in crossflow membrane filtration. Different authors have developed different models [11]. Most of the models are modified expressions of the resistance-in-series model [23–25], and the gel layer model [18,26,27].

The simplest model to adapt is the modified gel layer model. The model is based on a mass balance and may be written as:

$$Jc + D\frac{dc}{dx} - v_e(c - c_p) = Jc_p \quad (6)$$

where Jc is the flow of molecules towards the membrane, and $D(dc/dx)$ is the diffusive back transport of molecules from the membrane surface to the solution. x is the distance from the membrane. If the retention is not 100%, there will be a flow of molecules through the membrane of Jc_p. The third term on the left hand side is the electrophoretic term. By integrating Eq. (6) between the boundary conditions $c = c_g$ at $x = 0$ and $c = c_b$ at $x = \delta$, the following equation is obtained [18]:

$$J = k \ln \frac{c_g - c_p}{c_b - c_p} + \mu_e E \quad (7)$$

where c_g is the concentration of molecules at the membrane surface, c_p the concentration of molecules in the permeate and c_b is the bulk concentration. δ is the thickness of the concentration polarization layer, and k is the mass transport coefficient equal to:

$$k = \frac{D}{\delta} \quad (8)$$

The first term on the right hand side in Eq. (7) is the well-known gel layer model; and the second term represents the flux increase when an electric field is applied. Eq. (7) predicts a linear relation between the flux and the electric field strength [11]. Radovich and Behnam found a linear dependency during crossflow EUF of BSA, but Eq. (7) could not be used directly, since k and c_g did not remain constant, but depended on E [26].

2. Experimental procedures and methods

The experiments consist of two parts. The first part describes the procedure for carrying out gel electrophoresis of enzymes. These experiments are made to determine the mobility of the enzymes, and will give an indication of what to expect when applying an electric field during ultrafiltration. The second part describes the crossflow EUF experiments.

2.1. Enzymes

Five different enzymes (all produced by Novozymes A/S) have been tested; two amylases, two proteases and one lipase. The amylases are produced by fungi while the others are produced by bacteria. The solutions have been taken directly out of the production line after ultrafiltration. The enzyme solutions are not completely pure, but contain impurities, which are produced during fermentation or added during the recovery process. Depending of the enzyme product the impurities can be polycarbonates, remaining amino acids, flocculation chemicals and other proteins formed during fermentation. The most common flocculation chemical used is $CaCl_2$, which is present in all the enzyme solutions. Other flocculation chemicals consist of large anionic or cationic polymers, which are used during recovery of the bacteria enzymes.

Table 1
Enzyme properties

Enzyme	Size (kDa)	pI	μ_e (pH 7.6)	μ_e (pH 5.0)	pH_{EUF}
Protease-A	27	8.4	1.2	1.3	5.5
Amylase-F	55	3.5	3.0	2.0	7.0
Lipase	14	6.0	0.6	0.5	8.0
Protease-S	27	10.0	2.2	1.9	5.0
Amylase-S	80	3.5	2.6	1.7	5.5
BSA	65	4.7	2.1	–	–

[μ_e], 10^{-9} m^2/(V s).

To remove salt added during the production, the enzyme concentrates are diafiltrated with demineralized water until the conductivity in the permeate is below 0.5 mS/cm. The solutions are stored frozen and thawed at 5 ° C before use. The size, isoelectric point (pI) and the pH used in the EUF experiments can be seen in Table 1. The pH is set at a value where a high surface charge of the enzyme is expected without violating the stability. The enzyme concentration is measured with the Bradford reagent (Bio-Rad) [28], and the activity is measured at Novozymes, laboratory according to their standard methods.

2.2. Gel layer electrophoresis

Gel electrophoresis has been carried out at pH 7.6 and pH 5.0. The buffer at pH 7.6 contains 0.04 M Tris buffer (TRIZMA BASE Sigma) adjusted with HCl. At pH 5, a citrate buffer containing 0.01 M citric acid and 0.015 M sodium citrate has been used. The gel is made by dissolving 1% agarose (LITEX Agarose type HSA from Cambrex Copenhagen, Denmark) in the buffer. The solution is heated in the microwave at low effect until the agarose is dissolved. The temperature of the agarose solution is then set to 70 ° C in a water bath. The gel is made by casting 23 mL agarose solution onto a 10 cm × 15 cm gelbond film (Fisher) placed on a horizontal glass plate. A gel puncher connected to a vacuum pump is used to make the sample wells.

The gel is placed on a cooling plate (10 °C), and buffer solution placed in the anode and cathode compartments; filter paper is used as electrode wicks. About 5 μg of enzyme sample is loaded in the sample wells and the power supply turned on. BSA is also tested as a reference. Bromophenol blue (MERCK) is used as a marker. The experiments are made by applying 200 V (28 mA) for 60 min.

After the experiment the gel is washed in demineralized water for 10 min, and pressed between two glass plates surrounded by filter paper for another 10 min. The gel is then dried at room temperature. When dry the gel is stained with 50 mL GelCode Blue Stain Reagent (Pierce) for 1 h, and subsequently washed with water for 1 h before the result is read [29,30]. The mobility of the enzymes can be calculated by:

$$\mu_e = \frac{a}{E\,t} \quad (9)$$

where a is the migrated distance and t is the time. The experiments are repeated twice and the deviation is less than 5%.

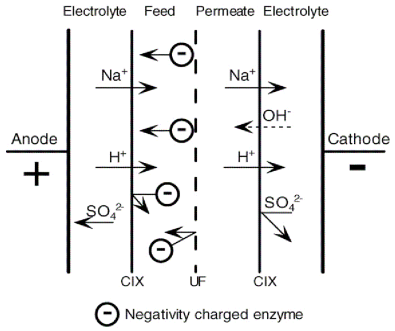

Fig. 2. Electro-ultrafiltration module.

2.3. Electro-ultrafiltration rig

The electro-ultrafiltration module is based on a commercial available electrodialysis module. To prevent direct contact between the enzymes and the electrodes, the crossflow EUF module is configured according to Fig. 2. The rig is shown in Fig. 3. The module consists of four chambers separated by an UF membrane surrounded by two cation exchange membranes. Flow spacers are used to enable the different streams. The channel height of the electrolyte, feed and permeate chambers are 6, 5 and 5 mm, respectively. It is possible to expand the module to contain several cells. It is necessary to shield the electrodes from the enzyme solution. If the enzymes are in contact with the electrodes foam is formed due to the gas formation at the electrodes. This causes fouling of the electrodes, and the membrane performance deteriorates due to degraded enzyme.

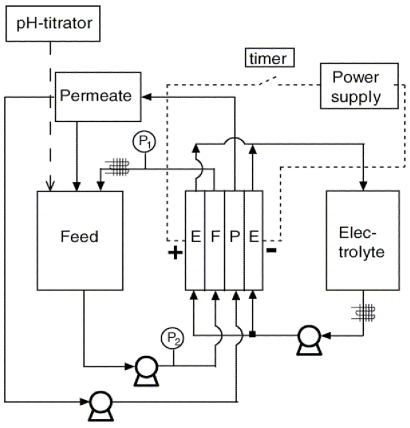

Fig. 3. Electro-ultrafiltration set-up.

By using cation exchange membranes in front of both the anode and cathode it is possible to prevent an accumulation of salt ions in the feed stream. They also prevent formation of $Cl_{2(g)}$at the anode, since any remaining Cl^--ions in the feed solution are rejected at the surface of the cation exchange membrane. This is important if electro-ultrafiltration is going to be used in industrial production, where the solutions may not be diafiltrated.

The experiments are operated by full recycle by returning the concentrate and permeate back to the feed container. Before the permeate is returned it is collected in a separate container, where it via a pump is lead back into the permeate chamber. The permeate stream is kept at a constant volume by an overflow pipe in the permeate container, which returns the excess amount of permeate back to the feed container. The flux is measured from the flow from the overflow pipe. Recycling of the permeate stream is necessary in order to keep a relatively high salt concentration in the permeate chamber, and thereby reduce problems related to a limiting current effect, which is described in the next paragraph. To equalize the pH changes in the anolyte and catholyte the two streams are mixed. The flow rate of the permeate stream is 22 L/h. It must be kept low to avoid pressure on the permeate side of the membrane, but high enough to avoid desalination of the permeate stream. The flow rate of the electrolyte stream is 80 L/h, which is sufficient to removed the electrolysis gasses formed. The total volume of the electrolyte, feed and permeate cycle are 1, 2.5 and 0.3 L, respectively. The module can be operated at a maximum pressure of 3×10^5 Pa at the feed side, and a corresponding crossflow velocity of 0.15 m/s.

The feed and electrolyte streams are connected to a cooler and the temperature is kept constant at 12 °C in every experiment. The anode consists of a platinized titanium mesh electrode and the cathode is made of stainless steel. The electric field is generated by a power supply from xantrex (XHR 150-7), which can deliver up to 150 V and 7 A. Pulsed electric fields are generated by inserting a universal digital timer UDT (Tempatron) between the electrodes and the power supply. The timer can be set to switch the electric field on and off with time intervals between 0 and 9.00 s.

The electrolyte consists of 0.1 M Na_2SO_4 with a conductivity of 17 mS/cm. The UF membrane is a 10 kDa surface-modified PVDF ETNA10PP membrane from Alfa Laval. See Wei et al. [31] for a detailed description of the UF membrane. The cation exchange membrane is a RELAX-CMH membrane from Mega (Czech Republic). The membrane area is 10 cm × 10 cm.

2.3.1. Limiting current effect

The two main disadvantages with the configuration of the EUF module is the presence of a limiting current effect, and pH changes in the feed solution. As shown in Fig. 2, the current is carried by sodium ions, which are able to pass the ion exchange membranes, whereas the enzymes and sulfate ions are rejected. However, cation exchange membranes are not a 100% selective towards anions. At high current densities, transport of hydroxide ions from the cathode to the permeate chamber takes place due to the small size and high mobility of the hydroxide ion. Because the permeate is returned to the feed tank the pH of the feed

solution increases. It is therefore necessary to have a pH titrator connected to the feed chamber to maintain a constant pH.

The limiting current effect appears when the current density reaches a level, where the transport of sodium ions to the surface of the cation exchange membrane is slower than the transport of sodium ions through the membrane. In that case the concentration of sodium ions at the surface of the cation exchange membrane drops, and it is no longer possible to increase the current density any further. This is mainly a problem in the permeate chamber due to the low conductivity in this chamber compared to the others. Recirculation of the permeate solution is therefore necessary to maintain a high concentration of sodium ions in the permeate solution as shown in Fig. 3.

2.3.2. Calculation of E over the feed chamber

The electric field strength E is defined as voltage U per distance (channel height h):

$$E = \frac{U}{h} \tag{10}$$

However, since the module contains four chambers with different conductivities it is not possible to use the applied voltage U_a in Eq. (10) directly. The module can instead be considered as a series of resistances, where the applied voltage U_a is a sum of the electrical potentials over the different chambers:

$$U_a = U_{electrolyte} + U_{feed} + U_{permeate} + U^* \tag{11}$$

$$= (R_{electrolyte} + R_{feed} + R_{permeate} + R^*)I \tag{12}$$

where I is the current and R^* is the resistance of the other items (ion exchange membranes, electrodes, etc.). The resistance of each chamber R_i can be replaced by:

$$R_i = \frac{h_i}{\kappa_i A} \tag{13}$$

where A is the electrode area (equal to the membrane area) and κ_i is the conductivity. The electric field strength across the feed chamber can therefore be calculated by [10]:

$$E_{feed} = \frac{I}{A\kappa_{feed}} \tag{14}$$

The electric field strength reported in this paper is calculated by Eq. (14) from measured values of I and κ_{feed}. It is not possible to measure U_{feed} directly during the experiments due to the configuration of the EUF module.

2.4. Experimental procedure

The experiments are carried out at constant concentration. The concentration it set by diluting the enzyme concentrates with demineralized water. For the amylases the experiments are carried out in a concentration range from 12 g/L to 80 g/L for the amylase-F and 12 g/L to 120 g/L for the amylase-S, which are the concentrations of the diafiltrated solutions. The 12 g/L is chosen since it is the concentration at the beginning of the ultrafiltration process during the production. Since the filtration performance of the protease-A solution deteriorates if the conductivity is too low; a higher concentration of 20 g/L is chosen.

Before the experiment starts the pH of the feed solution is adjusted to the values given in Table 1, and kept constant by titrating with either 0.1 M HCl or 0.1 M NaOH. The titrator starts automatically if the pH changes more than 0.3 from the initial value. The anode is placed on the feed side when the enzymes are negatively charged, and on the permeate side when the enzymes are positively charged. Before the electric field can be applied, permeate is collected at 0 V to fill up the permeate cycle. The voltage is then increased stepwise when steady state is reached. A sample of the feed solution is collected in the beginning and end of the experiment and the concentration and activity is determined. A permeate sample is also collected, and the retention (defined as $(1 - c_p/c_b)\,100\%$) is determined based on both activity and concentration measurements. By comparing the activity in the beginning and end of the experiment any decrease in activity can be determined.

After each experiment the membrane is cleaned by the following procedure: (1) Rinsing with demineralized water. (2) Cleaning with 0.04% NaOH at 50 °C for 30 min. (3) Rinsing with demineralized water. The water permeability is checked before the experiment starts to ensure that the membrane is cleaned properly. With this procedure it is possible to restore the water permeability to the same level as for a virgin membrane. The water permeability has been measured to $65 \pm 5 \times 10^{-5}$ L/(m^2 h Pa). The crossflow velocity is 0.07 m/s and TMP 1.5×10^5 Pa, which correspond to a pressure on the feed side of 1.7×10^5 Pa. The experiments are reproducible with a deviation of around 5%.

3. Results and discussion

3.1. Enzyme mobility

Fig. 4 shows the results of the gel electrophoresis experiments. Film (a) is made at pH 7.6 and film (b) at pH 5.0. The

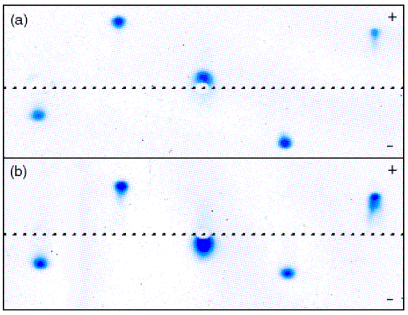

Fig. 4. Photos of gel electrophoresis plates. Film a is made at pH 7.6 and film b at pH 5.0. The dotted line indicates the application point. The enzymes are from the left: protease-A, amylase-F, lipase, protease-S and amylase-S.

anode is placed in the top of the film and the cathode in the bottom. The enzymes have been loaded in the middle along the dotted lines. The marks show the location of the enzymes after they have migrated for 60 min in a 2000 V/m electric field. The negatively charged enzymes have migrated towards the anode, whereas the positively charged enzymes have migrated towards the cathode. The mobilities are shown in Table 1. The mobility of BSA has also been measured for comparison, since several authors have obtained good results with BSA during EUF [9,14,23].

Generally the mobility is expected to decrease if the distance between the pH of the solution and the p*I* of the enzyme are reduced. This is also the case for protease-A, amylase-F and amylase-S. This is however not the case for protease-S. The mobility is a bit higher at pH 7.6 compared to pH 5.0, despite that the p*I* for protease-S is 10. A possible explanation is the different buffers used at the two pH values. At pH 7.6 a tris buffer is used and at pH 5.0 a citrate buffer. These buffers have different ionic strengths, which results in different thicknesses of the diffuse double layer around the enzyme, which according to Eqs. (3) and (4) effect the zeta potential of the enzyme.

The lipase migrates towards the anode at pH 7.6 and towards the cathode at pH 5.0, since the pH values lie on each side of the p*I*. The mobility is low in both cases.

The mobilities of amylase-F, amylase-S and protease-S are in the same range as BSA. It is therefore expected that the flux will increase during EUF of these enzymes. The mobilities of protease-A and the lipase are somewhat lower, and only small or no improvements in the flux is therefore expected.

3.2. Electro-ultrafiltration

An example of the flux enhancement during filtration of a 12 g/L amylase-S solution is shown in Fig. 5. The voltage is increased from 0 to 70 V in steps of 10 V. The flux decreases slightly at 0 V from an initial value at 40 L/(m^2 h) down to 36 L/(m^2 h) at steady state. When the electric field is applied the flux increases instantaneously and reaches steady state after approximately 20 min. At 70 V the flux has increased

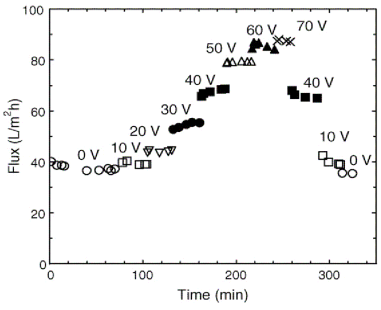

Fig. 5. Stepwise increase in the voltage for a 12 g/L amylase-S solution. The crossflow velocity is 0.07 m/s and TMP is 1.5 × 10^5 Pa.

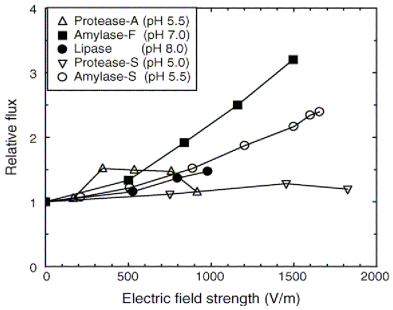

Fig. 6. The relative flux improvement for different enzyme solutions at a concentration of 12 g/L, except for the protease-A, where the concentration is 20 g/L.

to 87 L/(m^2 h). Fig. 5 also shows that the system is reversible, since the flux returns to the same level when the electric field is decreased. The limiting current effect appears above 60 V, where the flux is not increased any further when the voltage is increased to 70 V, since the current density is not increased.

The results from Fig. 5 is plotted in Fig. 6, where the relative flux improvement is shown as a function of the electric field strength. The relative flux from similar experiments with the other enzymes are also shown. As expected the flux is also improved significantly for the amylase-F solution. At 1600 V/m the relative improvement is a factor of 3.5 for the amylase-F compared to 2.5 for the amylase-S, which is consistent with the results found in the gel electrophoresis experiments, where the mobility of amylase-F is higher than amylase-S.

The flux did not improve for the protease-A, which is expected due to its low mobility. The flux is on the other hand expected to increase during EUF of protease-S due to the relatively high mobility measured in the gel electrophoresis experiments. This is however not the case. Changing the pH from 5.0 to 7.0 did not affect the result. A possible explanation could be the presence of other compounds in the solution. If there is an other protein with an opposite charge of the enzyme present in the solution, they can foul the membrane considerable when the electric field is applied. Since it is an enzyme produced by bacteria anionic and cationic polymers from flocculation is present, which also contribute to the fouling of the membrane. With proteases there is also always the problem with self-proteolysis, where the enzymes brakes each other into smaller pieces, which can block the membrane pores. Further studies are needed to clarify the role of impurities in the solution, and which steps are necessary in order to remove them.

Some flux improvements are observed during EUF of the lipase solution, which could be due to the slightly higher pH used in the EUF experiment compared to the gel electrophoresis experiments. Carrying out the experiment at pH 4.5 (where the lipase is positively charged) did not show any flux improvement. On an overall basis there is a good agreement between

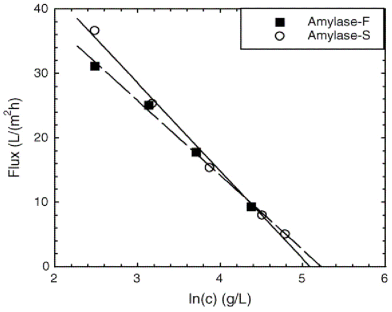

Fig. 7. Flux levels at 0 V for the amylases. The data points are fitted to the gel layer model assuming that c_p is 0 (first term in Eq. (7)). The parameters can be seen in Table 2.

the mobilities obtained by gel electrophoresis, and the flux improvements measured in EUF. This makes gel electrophoresis a useful screening method to find the optimal pH, and to find which enzyme solutions that can be filtered with EUF. All of the enzyme solutions are tested for enzyme activity, and no loss is observed.

3.2.1. Effect of enzyme concentration

Due to the relatively high flux improvement for the two amylases they where chosen for further studies of the effect of the electric field at different concentrations. To test the effect in a range relevant to the industrial production the amylase-F is studied in the concentration range 12–80 g/L, and the amylase-S in the range 12–120 g/L. The flux data at 0 V are collected in Fig. 7 for both the amylase-F and the amylase-S. As expected the flux decreases when the concentration increases, and the levels are almost identical for both enzymes. The retention is around 98% for both amylases at 0 V. Figs. 8 and 9 shows the relative flux improvement when applying an electric field to the amylase-F and amylase-S solutions, respectively. The flux improves 3–7 times at 1600 V/m for both enzymes, which is similar to the improvement obtained by other authors as described in the introduction.

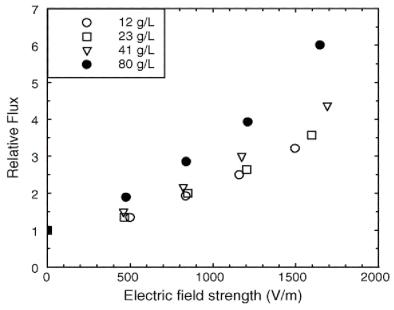

Fig. 8. Relative flux improvement for amylase-F solutions.

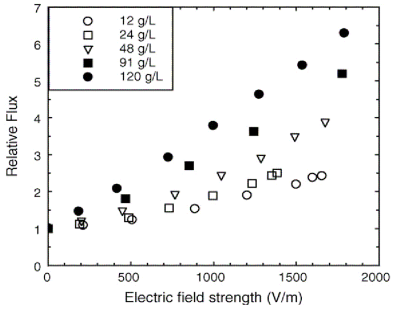

Fig. 9. Relative flux improvements for amylase-S solutions.

At high concentrations the flux improves relatively more compared to the lower concentrations. This is especially clear when the concentration is above 40 g/L. EUF will therefore be more efficient for ultrafiltration of high concentrated solutions. This result is in agreement with studies done by Lazarova and Serro where an electric field is applied during microfiltration of silicon oxide solutions. Here the relative flux improvement increased in the range 2–3.5 when the feed concentration increased from 10 to 50 g/L [24]. Oussedik et al. also showed that the relative flux improvement is greatest at high concentration when filtering BSA solutions [9].

3.2.2. Pulsed electric field

To test the effect of pulses, a pulsed electric field is applied during filtration of the amylase-S solution. Fig. 10 shows the effect of the pulse duration for a 12 g/L amylase-S solution for two electric field strengths. The ratio between the time the electric field is on (t_{on}) and the time it is off (t_{off}) is 1:1. The values at a pulse duration of 0 corresponds to a constant electric field.

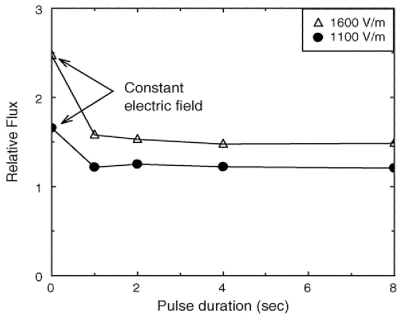

Fig. 10. Effect of pulse duration during filtration of a 12 g/L amylase-S solution. The pulse ratio is 1:1.

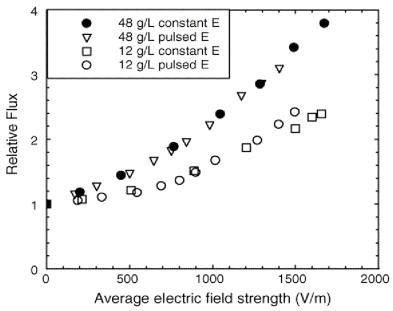

Fig. 11. Comparison between pulsed and constant electric fields for amylase-S solutions.

A decrease in the flux is observed when a pulsed electric field is used compared to a constant field. The flux decreases to the same level, regardless of the pulse duration. To compare the flux achieved with a pulsed electric field with a constant field, the pulse ratio is varied. First t_{on} is increased stepwise from 0 to 8 s while keeping t_{off} constant at 8 s. When the ratio is 1:1; t_{off} is decreased stepwise from 8 to 0 s, while keeping t_{on} constant at 8 s. An average electric field E_{av} during the pulse wave is then calculated from the t_{on}: t_{off} ratio by:

$$E_{av} = \frac{t_{on}}{t_{on} + t_{off}} E_{pulse}$$

where E_{pulse} is the electric field strength during t_{on}. The relative flux improvement is shown in Fig. 11, for a 12 g/L and a 48 g/L amylase-S solution, together with the results for a constant electric field. It clearly shows that there is no advantage in using a pulsed electric field. The results also show that concentration polarization is influenced by the electric field instantaneously, since there is no effect of the pulse duration. The main reason is probably the small size of the enzyme.

3.3. Modeling

The modified gel layer model in Eq. (7) predicts a linear dependency of J as a function of E. An attempt to use this model on the amylase-F and amylase-S system is shown in Figs. 12 and 13 for a low, middle and high concentration. The flux is here given in absolute values. In both cases the data only fits a straight line at low fluxes. When E becomes too high, the data at low concentration deviates from a straight line, and the deviation increases as the concentration decreases. A similar non-linear flux dependency has preciously been reported during EUF of cationic electrodeposition paint [23]. There could be several reasons for the non-linear dependency. The modified gel layer model assumes that c_g, k and μ_e is independent of E. Since the electrophoretic force removes enzymes from the membrane surface, it is not unlikely that the concentration at the membrane surface becomes smaller than c_g when E increases. Also the thickness of the concentration polarization layer could

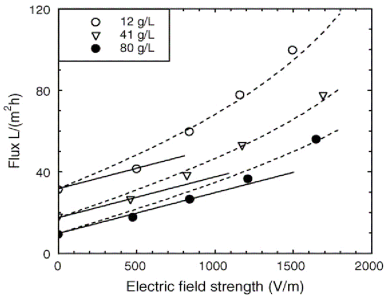

Fig. 12. Amylase-F data fitted to the modified gel layer model Eq. (7) (solid lines) and to the empirical model in Eq. (17) (dotted lines).

be affected by the electric field, which means that k is not constant. k and μ_e is also depended on the viscosity of the solution, which increases with increasing concentration. To describe the data it is therefore necessary to alter Eq. (7), and introduce a non-linear dependency of one of the constants. If the thickness of the concentration polarization layer is described by:

$$\delta(E) = \delta_0(1 - aE) \tag{15}$$

where a is a constant and δ_0 the thickness of the concentration polarization layer at $E = 0$ V/m, k will have the following dependency of E:

$$k(E) = \frac{D}{\delta_0(1 - aE)} = \frac{k_0}{1 - aE} \tag{16}$$

If Eq. (16) is combined with Eq. (7), the flux can be expressed by the following empirical model:

$$J = \frac{k_0}{1 - aE} \ln\left(\frac{c_g}{c_b}\right) + \mu_e E \tag{17}$$

This model is shown in Figs. 12 and 13 as the dotted lines and seems to describe the data in the tested window. The parameters

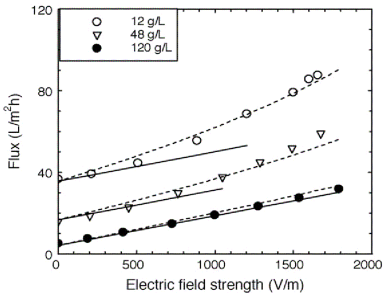

Fig. 13. Amylase-S data fitted to the modified gel layer model Eq. (7) (solid lines) and to the empirical model in Eq. (17) (dotted lines).

Table 2
Model parameters

Enzyme	k_0 (m/s)	c_g (g/L)	μ_e (10^{-9} m^2/(V s))	a (m/V)
Amylase-F	3.2×10^{-6}	186	5.6	3.5×10^{-4}
Amylase-S	3.8×10^{-6}	163	4.0	2.5×10^{-4}

are given in Table 2. k and c_g are determined from Fig. 7. μ_e is determined from the modified gel layer model in Eq. (7), as an average of the slopes at low fluxes at the different concentrations. Shown by the solid lines in Fig. 12 and 13. The constant a is also determined as an average of the values found when fitting Eq. (17) to the different concentrations.

The model is only valid as long as $E < 1/a$ and $E < E_c$. When E approaches E_c, the effect of the electric field becomes smaller, and the flux will probably level off and approach J_{max} asymptotically. The mobilities determined from the modified gel layer model is higher that the mobility found in the gel electrophoresis experiments; this is expected since the viscosity of the gel is higher than the water based feed solution. The relative difference between the mobilities is on the other hand comparative. The mobility of amylase-F is 1.4 times higher than amylase-S when comparing the values found in EUF, compared to 1.8 when comparing the values found in the gel electrophoresis experiments at corresponding pH values.

4. Conclusion

Crossflow electro-ultrafiltration experiments are carried out on five different industrial enzyme solutions. A 3–7 times flux increase is obtained compared to conventional crossflow UF for two amylase solutions; whereas only minor flux improvements are observed for the others, mainly due to a low surface charge and impurities in the solution. The greatest relative flux improvement is achieved at high concentration, which makes this process useful to as a final concentration step during UF of enzyme solutions. Using a pulsed electric field did not improve the flux compared to a constant field. The modified gel layer model could not describe the data since the flux showed a non-linear tendency, especially at low concentration. The data could be correlated by introducing a dependency of the gel layer thickness on E. Gel electrophoresis experiments of the enzymes proved to be a valid method to estimate the influence of the electric field during EUF.

Nomenclature

a	migrated distance during gel electrophoresis (m)
A	electrode area (m^2)
c	enzyme concentration (g/L)
d	thickness of the diffuse double layer (m)
D	diffusion coefficient (m^2/s)
e	elementary charge (C)
E	electric field strength (V/m)
h	channel height (m)
I	current (A)
J	flux (L/m^2 h), (m/s)
k	mass transport coefficient (m/s)
k_B	Boltzmann constant (J/K)
N_i	number of ions per unit volume
R	electrical resistance (Ω)
t	time (h), (s)
T	temperature (K)
U	voltage (V)
v_e	electrophoretic velocity (m/s)
x	distance from membrane surface (m)
z_i	valence of the ions of the ith type

Greek letters

δ	thickness of the concentration polarization layer (m)
ε	dielectric constant
ε_0	permittivity in vacuum (F/m)
η	viscosity (Pa s)
μ_e	electrophoretic mobility (m^2/V s)
σ	charge density (C/m^3)
ζ	zeta-potential (V)

References

[1] J. Schwinge, P.R. Neal, D.E. Wiley, D.F. Fletcher, A.G. Fane, Spiral wound modules and spacers: Review and analysis, J. Membr. Sci. 242 (2004) 129.
[2] N. Xu, W. Xing, N. Xu, J. Shi, Study on ceramic membrane bioreactor with turbulence promoter, Sep. Purif. Technol. 32 (2003) 403.
[3] S.C. Hargrove, H. Parthasarathy, S. Ilias, Flux enhancement in cross-flow membrane filtration by flow reversal: A case Study on ultrafiltration of BSA, Sep. Sci. Technol. 38 (2003) 3133.
[4] W.D. Mores, R.H. Davis, Direct observation of membrane cleaning via rapid backpulsing, Desalination 146 (2002) 135.
[5] I.H. Huisman, P. Prádanos, A. Hernández, The effect of protein–protein and protein–membrane interactions on membrane fouling in ultrafiltration, J. Membr. Sci. 179 (2000) 79.
[6] S. Kelly, A. Zydney, Protein fouling during microfiltration: comparative behavior of different model proteins, Biotechnol. Bioeng. 55 (1997) 91.
[7] G. Belfort, R.H. Davis, A.L. Zydney, The behavior of suspensions and macromolecular solutions in crossflow microfiltration, J. Membr. Sci. 96 (1994) 1.
[8] D.S. Wavhal, E.R. Fisher, Membrane surface modification by plasma-induced polymerization of acrylamide for improved surface properties and reduced protein fouling, Langmuir 19 (2003) 79.
[9] S. Oussedik, D. Belhocine, H. Grib, H. Lounici, D.L. Piron, N. Mameri, Enhanced ultrafiltration of bovine serum albumin with pulsed electric field and fluidized activated alumina, Desalination 127 (2000) 59.
[10] T. Weigert, J. Altmann, S. Ripperger, Crossflow electrofiltration in pilot scale, J. Membr. Sci. 159 (1999) 253.
[11] H.M. Huotari, G. Trägårdh, I.H. Huisman, Crossflow membrane filtration enhanced by an external dc electric field: A review, Trans. IChemE 77(A) (1999) 461.
[12] G.C.C. Yang, T.Y. Yang, Reclamation of high quality water from treating CMP wastewater by a novel crossflow electrofiltration/electrodialysis process, J. Membr. Sci. 233 (2004) 151.
[13] G. Bargeman, M. Dohmen-Speelmans, I. Recio, M. Timmer, C. van der Horst, Selective isolation of cationic amino acids and peptides by electromembrane filtration, Lait 80 (2000) 175.
[14] P.v. Zumbusch, W. Kulcke, G. Brunner, Use of alternating electrical fields as anti-fouling strategy in ultrafiltration of biological suspensions

-Introduction of a new experimental procedure for crossflow filtration, J. Membr. Sci. 142 (1998) 75.
[15] R.J. Wakeman, M.N. Sabri, Utilizing pulsed electric fields in crossflow microfiltration of titania suspensions, Trans. IChemE 73(A) (1995) 455.
[16] C.W. Robinson, M.H. Siegel, A. Condemine, C. Fee, T.Z. Fahidy, B.R. Glick, Pulsed-electric-field crossflow ultrafiltration of bovine serum albumin, J. Membr. Sci. 80 (1993) 209.
[17] H.M. Houtari, I.H. Huisman, G. Trägårdh, Electrically enhanced crossflow membrane filtration of oily waste water using the membrane as a cathode, J. Membr. Sci. 156 (1999) 49.
[18] H. Yukawa, K. Shimura, A. Suda, A. Maniwa, Cross flow electro-ultrafiltration for colloidal solution of protein, J. Chem. Eng. Jpn. 16 (1983) 305.
[19] C.C. Tarazaga, M.E. Campderrós, A.P. Padilla, Physical cleaning by means of electric field in the ultrafiltration of a biological solution, J. Membr. Sci. 278 (2006) 219.
[20] R.J. Wakeman, Electrically enhanced microfiltration of albumin suspensions, Trans. IChemE 76(C) (1998) 53.
[21] G. Bargeman, J. Houwing, I. Recio, R.H. Koops, C. van der Horst, Electro-Membrane filtration for the selective isolation of bioactive peptides from an α_{S2}-Casein hydrolysate, Biotechnol. Bioeng. 80 (2002) 608.
[22] J.M. Radovich, R.E. Sparks, Electrophoretic techniques for controlling concentration polarization in ultrafiltration, Polym. Sci. Technol. 13 (1980) 249.
[23] J.M. Radovich, I.M. Chao, Electroultrafiltration of a cationic electrodeposition paint, J. Coat. Technol. 54 (1982) 33.
[24] Z. Lazarova, W. Serro, Electromembrane separation of mineral suspensions: Influence of process parameters, Sep. Sci. Technol. 37 (3) (2002) 515.
[25] J.D. Henry, L.F. Lawler, C.H. Alex Kuo Jr., A solid/liquid separation process based on cross flow and electrofiltration, AIChE 23 (6) (1977) 851.
[26] J.M. Radovich, B. Behnam, Steady-state modeling of electroultrafiltration at constant concentration, Sep. Sci. Technol. 20 (4) (1985) 315.
[27] G.M. Rios, H. Rakotoarisoa, B. Tarodo de la Fuente, Basic transport mechanisms of ultrafiltration in the presence of an electric field, J. Membr. Sci. 38 (1988) 147.
[28] M.M. Bradford, A rapid and sensitive method for the quantitation of microgram quantities of protein utilizing the principle of protein-dye binding, Anal. Biochem. 72 (1976) 248.
[29] R. Westermeier, Electrophoresis in Practice, third ed., WILEY-VCH Verlag GmbH, D-69469 Weinheim, Germany 2001.
[30] R. Kim, H. Yokota, S.H. Kim, Electrophoresis of proteins and protein–protein complexes in a native agarose gel, Anal. Biochem. 282 (2000) 147.
[31] J. Wei, G.S. Helm, N. Corner-Walker, X. Hou, Characterization of a non-fouling ultrafiltration membrane, Desalination 192 (2006) 252.

Appendix F

Paper 2

A.D. Enevoldsen, E.B. Hansen and G. Jonsson, "Electro-ultrafiltration of amylase enzymes: Process design and economy,"*Journal of Chemical Engineering Science* **62**, pp. 6716-6725, 2007.

Reprinted with permission from the publisher.

ELSEVIER

Chemical Engineering Science 62 (2007) 6716–6725

Chemical Engineering Science

www.elsevier.com/locate/ces

Electro-ultrafiltration of amylase enzymes: Process design and economy

A.D. Enevoldsen[a,b], E.B. Hansen[a], G. Jonsson[b,*]

[a]*Recovery Development, Novozymes A/S, Smoermosevej 9, 3AM, DK-2880 Bagsvaerd, Denmark*
[b]*Department of Chemical Engineering, The Technical University of Denmark, DK-2800 Lyngby, Denmark*

Received 23 May 2007; received in revised form 31 July 2007; accepted 14 August 2007
Available online 22 August 2007

Abstract

Electro-ultrafiltration (EUF) has previously resulted in flux improvements in the order of 3–7 times during filtration of amylase enzymes [Enevoldsen, A.D., Hansen, E.B., Jonsson, G., 2007. Electro-ultrafiltration of industrial enzyme solutions. Journal of Membrane Science 299, 28–37]. To determine the energy balance for EUF, the influence of TMP, crossflow velocity and conductivity of the enzyme solution is studied and compared to conventional ultrafiltration (UF). EUF is favorable when filtering solutions of high concentration, while UF is favorable when filtering solutions of low concentration. The dimension of the feed channel, especially the height and the conductivity are crucial for the feasibility of the EUF process. The channel height should be below 1.0 mm and the conductivity less that 2 mS/cm before EUF is economically feasible.

Keywords: Crossflow filtration; Ultrafiltration; Enzyme; Electrofiltration; Electric field; Energy consumption

1. Introduction

To overcome problems with fouling and concentration polarization in crossflow ultrafiltration (UF) of proteins an electric field can be applied across the membrane. The electro-ultrafiltration (EUF) process utilizes an electrophoretic force that drags the charged proteins away from the membrane surface. The gel and concentration polarization layer are thereby reduced and the flux increases (Huotari et al., 1999a). Flux improvements in the range of 2–10 times have been reported for BSA (Radovich and Behnam, 1985; Radovich and Sparks, 1980; Oussedik et al., 2000; Zumbusch et al., 1998; Wakeman, 1998) and gelatin (Yukawa et al., 1983; Guizard et al., 1989). Another advantage with EUF is that it can be carried out at a low crossflow velocity, since the electric field replaces the need of a high shear rate at the membrane surface. A previous study of EUF, applied on enzyme solutions, showed a 3–7 time flux improvement for amylase enzymes, where the greatest flux enhancement was achieved at high concentrations (Enevoldsen et al., 2007). An example of the flux enhancement can be seen in Fig. 1, where the flux is plotted as a function of the applied electric field strength for amylase-S solutions.

Despite the good filtration performance in EUF, the process is not yet used in large-scale production. One of the reasons could be the high energy consumption of the electric field. The conductivity of the feed solution is critical. A low conductivity is preferred in EUF, since the energy consumption increases with increasing conductivity (Weigert et al., 1999; Bargeman et al., 2002). A high conductivity also increases the amount of heat and electrolyte gasses produced at the electrodes. If too much salt is present in the feed solution it could also decrease the ζ-potential of the proteins, and lead to a smaller effect of the electric field (Houtari et al., 1999b). Weigert et al. (1999) showed that if the conductivity of a cristobalit solution exceeded 2 mS/cm the advantage of using electro-microfiltration vanished, since the energy requirements of the electric field became too high.

In this work the economical aspects of EUF are considered when filtering industrial enzyme solutions produced by Novozymes A/S. The influence of the transmembrane pressure (TMP), crossflow velocity and conductivity is studied for both UF and EUF. The performance of EUF is compared to UF, and a model for calculating the energy requirements is presented.

* Corresponding author. Tel.: +45 261 13008.
E-mail address: gj@kt.dtu.dk (G. Jonsson).

0009-2509/$ - see front matter © 2007 Elsevier Ltd. All rights reserved.
doi:10.1016/j.ces.2007.08.040

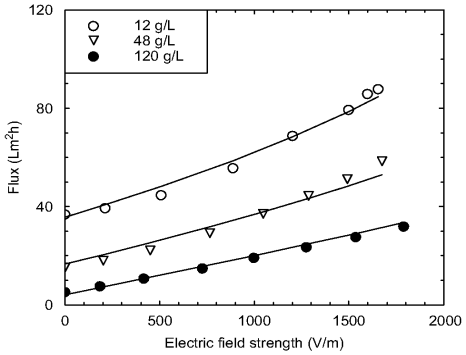

Fig. 1. Effect of the electric field for different concentrations of the amylase-S solution. The solid lines are the empirical model from Eq. (1). TMP = 1.5 bar and $v = 0.07$ m/s.

The optimal process design and the operating conditions for both UF and EUF are considered.

2. Theory

2.1. Flux

It has been previously shown that the flux obtained in EUF can be described by the following empirical equation (Enevoldsen et al., 2007):

$$J(c_{\text{feed}}, E_{\text{feed}}) = \frac{k_0}{1 - a^{\dagger} E_{\text{feed}}} \ln\left(\frac{c_g}{c_{\text{feed}}}\right) + \mu_e E_{\text{feed}}, \quad (1)$$

where k_0 is the mass transport coefficient at 0 V, c_g the gel layer concentration, c_{feed} the concentration of the feed solution, E_{feed} the electric field strength across the feed chamber and μ_e the electrophoretic mobility of the enzyme. The parameter $a^{\dagger}$ is used to correct the influence of the electric field strength on k_0 and accounts for the non-linear dependency of the flux as a function of E_{feed}. If $a^{\dagger}$ is set to zero, Eq. (1) reduces to the modified gel layer model, which is derived from the well-known gel layer model, which predicts a linear dependency of the flux versus the electric field strength (Huotari et al., 1999a). The gel layer model is obtained by setting E_{feed} to zero and is used in many cases to describe the flux in UF (Mulder, 2000). The empirical model is plotted in Fig. 1 as the solid lines and shows that the non-linear dependency is more pronounced at low concentrations. The non-linearity is due to a disturbance of the gel and concentration polarization layer (Radovich and Chao, 1982). When the electric field is applied the thickness of the concentration polarization layer is reduced and the concentration at the membrane surface decreased. The gel layer concentration and the mass transport coefficient are therefore not constant, which is assumed by the gel layer model. As a result the mass transport coefficient increases as the electric field increases, which is corrected by the $a^{\dagger}$ parameter (Enevoldsen et al., 2007). In a previous study of two enzymes called amylase-F and amylase-S, values of $a^{\dagger}$ are determined to 3.5×10^{-4} and 2.5×10^{-4} m/V and values of μ_e to 5.6×10^{-9} and 4.0×10^{-9} m^2/Vs, respectively (Enevoldsen et al., 2007). The model assumes that the influence of the electric field strength and the non-linear dependency of E_{feed} is independent of the dimensions of the filtration module.

The first term in Eq. (1) is dependent on the design of the filtration module through the mass transport coefficient. k_0 is expressed by the Sherwood number (Sh), the hydraulic diameter d_h, and the diffusion coefficient D by

$$Sh = \frac{k_0 d_h}{D}, \quad (2)$$

where the Sherwood number for laminar flow regimes can be calculated by

$$Sh = a\left(Re\, Sc \frac{d_h}{l}\right)^b \quad \text{(laminar)}, \quad (3)$$

where l is the length of the membrane and d_h the hydraulic diameter defined as

$$d_h = \frac{2wh}{w + h} \quad (4)$$

for a rectangular slit, w is the width and h the height of the slit. In general a is set to 1.85 and b to 0.33 (Mulder, 2000). The Reynolds and Schmidt's number is defined as $Re = \rho v d_h/\eta$ and $Sc = \eta/\rho D$ (Mulder, 2000). The diffusion coefficient can be calculated from an expression given by Young et al. (1980):

$$D(\text{m}^2/\text{s}) = \frac{8.34 \times 10^{-12} \times T}{\eta M^{1/3}}, \quad (5)$$

where M is the molecular size of the enzyme and η the viscosity of the feed solution. For turbulent flow regimes the Sherwood number can be calculated by

$$Sh = a\, Re^b\, Sc^d \quad \text{(turbulent)}, \quad (6)$$

where $a = 0.04$, $b = 0.75$ and $d = 0.33$.

The total membrane area A_T needed to concentrate a feed flow of Q_{feed} from c_{feed} to c_r may be calculated by considering the mass balance:

$$\begin{aligned} Q_{\text{feed}} &= Q_r + Q_{\text{perm}} \\ &= Q_r + J_{\text{av}} A_T, \end{aligned} \quad (7)$$

where Q_r and Q_{perm} are the flow rate of the permeate and retentate, respectively. J_{av} is the average permeate flux during the concentration interval. By introducing

$$\frac{Q_r}{Q_{\text{feed}}} = \frac{c_{\text{feed}}}{c_r} \quad (8)$$

under the assumption that the enzyme concentration in the permeate is negligible, the following equation is obtained:

$$\frac{A_T}{Q_{\text{feed}}} = \frac{1 - c_{\text{feed}}/c_r}{J_{\text{av}}} \quad (9)$$

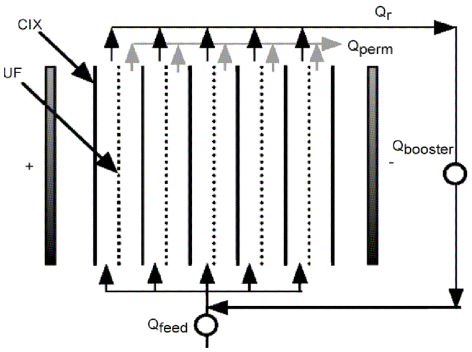

Fig. 2. Schematic drawing of the EUF module used for the energy calculations.

and shows that the area is inversely proportional to the average flux.

From Eqs. (2) and (3) it can be seen that k_0 depends on the length of the channel by $l^{-0.33}$, which means that k_0 decreases around 20% when l increases by a factor of 2. The width of the membrane does not influence k_0 remarkably, since the hydraulic diameter in Eq. (4) is independent of w if $w \gg h$. This is usually the case in a UF module, where the width normally is a factor 10^2 larger than the channel height. The height of the channel plays on the other hand a role. From Eq. (4) it can be seen that d_h is almost proportional to h, which means that the flux depends on the height by $h^{-0.34}$ for laminar flow regimes and $h^{-0.25}$ for turbulent flow regimes. Hence k_0 increases around 19–27% when the height is reduced by a factor of 2.

2.2. Energy calculations

The calculations are based on a plate-and-frame module operated as a feed-and-bleed system, which consists of a feed pump and a booster pump. The feed pump transports the feed into the filtration module at an inlet pressure of p_{in} and the booster pump recirculates the retentate back into the module until the desired final concentration is reached. The EUF system is assumed to be configured according to Fig. 2, where the stack is built of alternating ion-exchange and UF membranes. In Fig. 2 the number of cell pairs is 5, but it is assumed that the stack can be expanded to any number of n pairs each with a membrane area of A_e, which is equal to the electrode area.

The energy W used during EUF is a sum of the energy consumed by the pumps W_{pump} and the energy consumed by the electric field W_E:

$$W = W_{\text{pump}} + W_E. \tag{10}$$

2.2.1. Pump energy

In a feed-and-bleed system the energy consumed by the pumps W_{pump} are a sum of the energy used by the booster pump W_{booster} and the energy used by the feed pump W_{feed}:

$$W_{\text{pump}} = W_{\text{booster}} + W_{\text{feed}} \tag{11}$$

which can be calculated from the power used by the booster pump P_{booster} and the feed pump P_{feed}:

$$W_{\text{pump}} = (P_{\text{booster}} + P_{\text{feed}})/Q_{\text{feed}} \tag{12}$$

$$= \left(\frac{\Delta p Q_{\text{booster}}}{\eta_{\text{pump}}} + \frac{p_{\text{in}} Q_{\text{feed}}}{\eta_{\text{pump}}}\right) \Big/ Q_{\text{feed}}, \tag{13}$$

where Q_{booster} and Q_{feed} are the flow rate of the booster and feed pump, respectively. Δp is the pressure-drop across the feed channel, and η_{pump} is the pump efficiency. Q_{booster} can be expressed in terms of the crossflow velocity v:

$$Q_{\text{booster}} = n\alpha v, \tag{14}$$

where α is the area of the cross-section. Combining Eqs. (12) and (14) with Eq. (9), and by introducing the cell dimensions:

$$A_T = nA_e = nwl, \tag{15a}$$

$$\alpha = wh \tag{15b}$$

the energy consumed by the booster pump can be expressed as:

$$W_{\text{booster}} = \frac{P_{\text{booster}}}{Q_{\text{feed}}} = \frac{\Delta p h v}{\eta_{\text{pump}} J_{\text{av}} l}\left(1 - \frac{c_{\text{feed}}}{c_r}\right) \tag{16}$$

which gives the energy consumption for the booster pump with respect to the feed flow during concentration from c_{feed} to c_r. The pressure-drop across the channel is calculated by (Mulder, 2000):

$$\Delta p = 2 f l \rho v^2 / d_h, \tag{17}$$

where the friction factor f is equal to:

$$f = 24/Re \quad \text{(laminar)}, \tag{18}$$

$$f = 0.133 Re^{-0.25} \quad \text{(turbulent)}. \tag{19}$$

From Eqs. (16) and (17) it can be seen that the energy consumption only depends on the length of the module through the flux. Assuming that $E = 0\,\text{V/m}$ the flux is proportional to the mass transport coefficient, which in the laminar case depends on the length of the module by $l^{-0.33}$; hence the energy consumption increases 26% when l is doubled. In the turbulent case the energy consumption is independent of the length, since the Sherwood number in Eq. (6) does not depend on the length. The width of the module is only represented in the friction factor through the Reynolds number and do not influence the energy consumption, since the hydraulic diameter do not change significantly when the width is changed.

The pressure-drop in the laminar region depends on the hydraulic diameter by $1/d_h^2$, which means that it depends on the height of the feed channel by $1/h^2$. The energy consumption therefore depends on the height by $h^{-0.66}$ for laminar flow regimes, when the flux dependency of the height is taken into account through the mass transport coefficient in Eqs. (3) and (6). The energy consumption is therefore reduced 37% when h is increased by a factor of 2. In the turbulent flow regime

the energy consumption is independent of the height. It is not necessarily an advantage to use a large channel height. Eq. (9) shows that the membrane area increases with h, since the flux decreases. A large channel height can, however, be necessary if the feed is highly viscous. The optimal channel height depends therefore on the price of the membrane and the energy costs.

2.2.2. Energy used by the electric field

The power consumed by the electric field P_E is given by

$$P_E = \frac{U_a I}{\eta_E}, \tag{20}$$

where U_a is the applied voltage, I the current and η_E the efficiency of the power supply. The electric field strength is connected to I by (Weigert et al., 1999):

$$\frac{I}{A_e} = E_{\text{feed}}\kappa_{\text{feed}}, \tag{21}$$

where κ_{feed} is the conductivity of the feed solution. Eq. (21) shows that the conductivity of the feed should be low to ensure a high electric field strength at a given current density. U_a can be expressed in terms of the resistance of the different chambers (Enevoldsen et al., 2007):

$$U_a = \frac{I}{A_e}\left(n\frac{h}{\kappa_{\text{feed}}} + nr_{\text{perm}} + 2r_e + nr^*\right), \tag{22}$$

where r_{perm} and r_e are the specific resistance of the permeate and electrode chamber, and r^* is the specific resistance of the other items (ion-exchange membranes, electrodes, etc.). Combining Eqs. (20)–(22) and inserting Eq. (9), the energy input during concentration from c_{feed} to c_r can be calculated by

$$W_E = \frac{P_E}{Q_{\text{feed}}} = \frac{E_{\text{feed}}^2\kappa_{\text{feed}}^2}{J_{\text{av}}\eta_E}\left(1 - \frac{c_{\text{feed}}}{c_r}\right)\left(\frac{h_{\text{feed}}}{\kappa_{\text{feed}}} + r_{\text{perm}} + r^*\right) \tag{23}$$

assuming that r_e is negligible compared to the other resistances. This approximation is valid when a stack consisting of many cells is used, since the potential across the two electrode chambers is small compared to the potential across the entire stack.

The height of the feed channel is the design parameter that influences the energy used by the electric field mostly. It is proportional to the height if only the energy used in the feed chamber is considered (neglecting the influence of the height on the flux, since the mass transport coefficient in EUF is low due to the low crossflow velocity), this means that h should be as low as possible. This is also the case for the permeate and buffer chambers; the narrower the channels the less energy is used.

In Eqs. (9), (16) and (23) the average flux is required. It is therefore necessary to integrate Eq. (1) with respect to the concentration interval. However, the term $\ln(c_g/c_{\text{feed}})$ does not have an analytical solution. The energy consumption and membrane area is therefore calculated in small steps of $\Delta c = 1$ g/L and summarized. Matlab is used for this propose.

3. Experimental procedures

Two different enzyme solutions (both produced by Novozymes A/S) have been used; one amylase-F (55 kDa, pI = 3.5) and one amylase-S (80 kDa, pI = 3.5). The solutions have been diafiltrated with demineralized water until the conductivity of the permeate is below 0.5 mS/cm. The pH of the feed solution is adjusted with NaOH to 5.5 for the amylase-S solution and 7.0 for the amylase-F solution. The enzyme concentration is determined with the Bradford reagent (Bio-Rad) (Bradford, 1976) and the activity is measured at Novozymes laboratory according to their standard methods. The enzymes and their properties have been described in detail previously (Enevoldsen et al., 2007).

The EUF experiments have been described in detail elsewhere (Enevoldsen et al., 2007). In brief the EUF module is constructed according to Fig. 2 with just one UF membrane placed between two cation-exchange membranes (RELAX-CMH from Mega (Czech Republic)). The UF membrane is a 10 kDa low protein fouling surface-modified PVDF ETNA10PP membrane from *Alfa Laval*. The membrane area is 10×10 cm^2 and the channel height is 5 mm. The system is operated with full recycle by returning the permeate and retentate back to the feed container. In the electrode compartments a salt solution of 0.1 M Na_2SO_4 is recirculated. The experiments are made by stepwise increasing the flux from 0 to about 2000 V/m after steady state is reached.

A different module has been used for the crossflow UF experiments, since the EUF module cannot be operated at a crossflow velocity higher that 0.15 m/s. The UF experiments are carried out with the same type of membrane as for the EUF experiments. The membrane has an oval shape with a length of 10 cm and a width of 4 cm. The channel height is 1 mm. The design of the module has been described in detail previously by Jonsson and Boesen (1977). The enzyme solution is transported into the UF module by a pump and the pressure is measured on the in and outlet of the module by manometers. The TMP can be set by adjusting a valve placed on the outlet of the module. The total feed volume is 2.5 L. The feed tank is connected to a cooler, which keeps the solution at a constant temperature of 12 °C. The experiments are operated by full recycle by returning the permeate and retentate back to the feed container. The experimental procedure for amylase-S is as follows:

- The TMP is subsequently increased and decreased up to around 2 bar at $v = 1.0$ m/s.
- The crossflow is increased to 2.0 m/s and the TMP first increased then decreased.
- The crossflow is decreased to 0.5 m/s followed by an increase and decrease in the TMP.
- Finally the crossflow is set to 1.0 m/s and the flux is measured again to compare the flux with the values obtained in the beginning of the experiment.

For the amylase-F the TMP is increased to around 4 bar and some extra measurements are made at crossflow velocities of 1.5 and 0.3 m/s.

A sample of the feed solution is collected at the beginning and at the end of the experiment and the concentration and activity are determined. A permeate sample is also collected and the retention defined as $(1 - c_p/c_b)$ 100%) is determined based on both activity and concentration measurements. By comparing the activity at the beginning and at the end of the experiment any losses can be determined.

After each UF or EUF experiment the membrane is cleaned by the following procedure: (1) Rinsing with demineralized water. (2) Cleaning with 0.04% NaOH at 50 °C for 30 min. (3) Rinsing with demineralized water. The water permeability is checked before the experiment starts to ensure that the membrane is cleaned properly. With this procedure it is possible to restore the water permeability to the same level as for a virgin membrane. The water permeability has been measured to 65 ± 5 L/(m^{2}h bar).

4. Results and discussion

4.1. Effect of TMP and v in UF

The flux as a function of the TMP is shown in Fig. 3 for a 24 g/L amylase-S solution. As expected the flux increases with TMP until a limiting flux is reached. Here a further increase in TMP does not result in a higher flux. The limiting flux appears at a lower TMP when the crossflow velocity is reduced. Fig. 3 also shows that the system is reversible, since the flux obtained when decreasing the TMP is almost the same as when increasing the TMP. Thus the flux at 1 m/s has only decreased around 6% at the end of the experiment compared to its initial value. The retention is larger than 99% and no loss in enzyme activity is observed. The flux data at 2 bar from Fig. 3 is plotted in Fig. 4

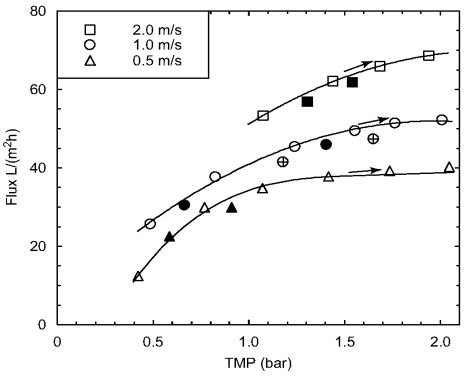

Fig. 3. Flux as a function of the TMP at different crossflow velocities for a 24 g/L amylase-S solution during UF. The open symbols (□ ○ △) are the flux measured when the TMP is increased ; while the filled symbols are the flux measured when decreasing the TMP. The symbol ⊕ gives the flux at the end of the experiment at 1 m/s.

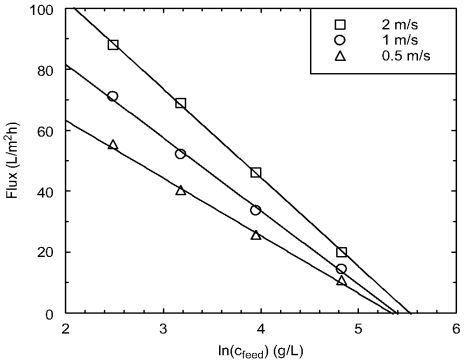

Fig. 4. Flux as a function of the feed concentration at different crossflow velocities during UF of amylase-S.

together with results from other concentrations. The data gives a linear fit, which means that the gel layer model can be used to describe the data. The slope is therefore equal to the mass transport coefficient, which increases with increasing crossflow velocity. The gel layer concentration given by the intercept with the x-axis should according to the gel layer model be independent of the crossflow velocity. This is, however, not the case; the gel layer concentration increases with increasing crossflow velocity. The gel layer concentration is in the range of 210–250 g/L. The same procedure is made for amylase-F, which also can be described by the gel layer model. In this case the limiting pressure is reached at a TMP of 4 bar at 200 m/s and the gel layer concentration is between 200 and 225 g/L. The retention is between 95% and 99% depending on the concentration.

The logarithm to the mass transport coefficients are plotted in Fig. 5 as a function of $\ln(v)$. The data for the UF experiments can be described by a straight line with a slope of 0.36 and 0.31 for amylase-F and amylase-S, respectively. This is close to the value of 0.33 in Eq. (3), which means that k_0 can be described by a laminar relationship. The a value can be calculated from the intercept with the y-axis, and is found (setting b=0.33) to be 4.68 and 3.26 for amylase-F and amylase-S, respectively. The experimentally determined a-values are higher than the value given in Eq. (3). A reason could be the turbulent conditions at the in and outlet of the module. Since the UF module only has a short length, the end effects will have a relatively large impact on the flux (Jonsson and Boesen, 1977). In the calculations in the next paragraph the a-value of 1.85 is therefore used, since a longer module will be considered.

The laminar model in Eq. (3) did not fit the mass transport coefficients found previously for the EUF model (Enevoldsen et al., 2007), but underestimated them. The reason is most likely that the feed channel in the EUF module is large (5 mm) and filled with spacer nettings, which makes the flow turbulent

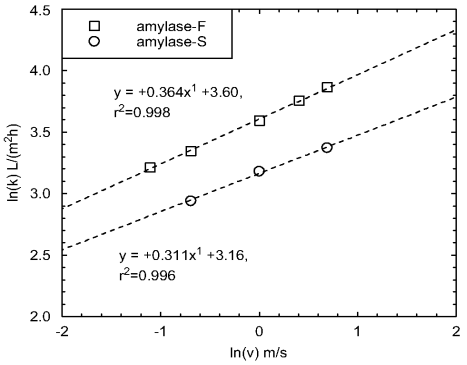

Fig. 5. The mass transport coefficient k_0 as a function of the crossflow velocity for amylase-F and amylase-S during UF.

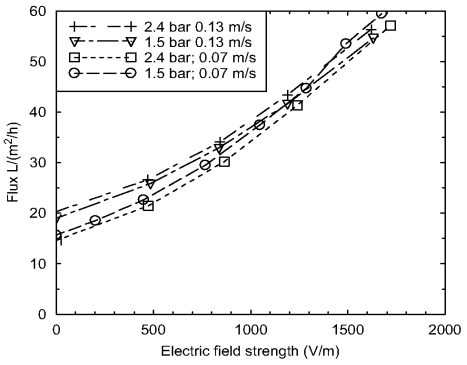

Fig. 6. Effect of TMP and crossflow for a 48 g/L amylase-S during EUF.

instead of laminar. However, for further calculations the mass transport coefficient calculated by Eq. (3) is also used for the EUF module, since a commercial EUF module probably will have a much narrower feed channel and the flow conditions closer to the flow conditions in a conventional UF module.

4.1.1. Effect of TMP and v in EUF

Fig. 6 shows the effect of increasing the crossflow velocity from 0.07 to 0.13 m/s at a TMP of 1.5 and 2.4 bar when filtering a 48 g/L amylase-S solution. The effect of increasing the TMP is very small. Similar observations have also been made for amylase-F. Increasing the TMP will in general increase the thickness of the concentration polarization layer, and will therefore make the effect of the electric field greater, since a large amount of enzymes will be removed from the membrane surface. However, if the TMP becomes too high a compression of the gel and concentration polarization layer might occur. In the experiments carried out in Fig. 6 the limiting flux is probably already reached at 1.5 bar, which is the reason for the small effect of the TMP; a further increase in the TMP could even lead to a decrease in the flux. This is seen during electromicrofiltration of wastewater and silicon oxide particles, where an increase in the flux with the TMP was followed by a decrease when the TMP became too high (Yang et al., 2003; Lazarova and Serro, 2002).

The effect of increasing the crossflow velocity is more pronounced, especially at 0 V. Here the flux increases from around 15 to 20 L/(m^{2}h). However, as the electric field strength increases, the difference between the two crossflow velocities becomes smaller, and at around 900 V/m it is no longer possible to distinguish between the curves. The same effect is seen for amylase-F. In general the flux is expected to increase when the crossflow velocity increases. However, in EUF the magnitude of the crossflow velocity and the electric field strength both influence the thickness of the concentration polarization layer. A higher flux can therefore only be expected by an increased crossflow velocity if the concentration polarization layer has not already been removed by the electric field (Huotari et al., 1999a). If the concentration polarization layer is removed by the electric field an increased crossflow velocity might even lead to a decrease in the flux, due to increased back diffusion towards the membrane surface (Huotari et al., 1999a). This is supported by findings of Lazarova and Serro (2002) and Henry et al. (1977). This could be the reason for the small effect of the increased crossflow velocity especially above 900 V/m. It is therefore not necessary to use a high crossflow in EUF, since the effect of the electric field is the dominating force.

4.1.2. Effect of conductivity in EUF

In the experiments shown in Figs. 1 and 6, the main contribution to the conductivity of the feed solutions came from the enzymes themselves, since the solutions have been diafiltrated. It is, however, important to know the influence of the conductivity in EUF, since diafiltration may not be an option in industrial production.

In Fig. 7 the effect of the conductivity is shown. Here 0.5, 1.0 and 2.5 g/L of $CaCl_2$ is added to a feed solution of 48 g/L amylase-S to gain the conductivities of 1.1, 1.8 and 2.9 mS/cm, compared to 0.7 mS/cm for the diafiltrated solution. $CaCl_2$ is chosen since it is a widely used flocculation chemical during production and therefore typically present in large quantities. At 0 V the flux decreases slightly with an increasing concentration of $CaCl_2$. A possible explanation is that the calcium and chloride ions decrease the repulsing electrostatic enzyme–enzyme and enzyme–membrane forces, which allows a closer packing of the enzymes. Hence the fouling layer becomes denser and the flux decreases. However, when the electric field is applied, the flux improvement is the same at similar electric field strengths, indicating that the ζ-potential of the enzymes in the solution has not been affected considerably by the calcium and chloride ions up to 2.9 mS/cm. This could indicate that the

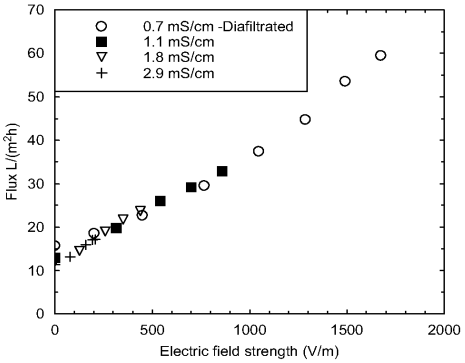

Fig. 7. Effect of added $CaCl_2$ to a 48 g/L amylase-S solution during EUF.

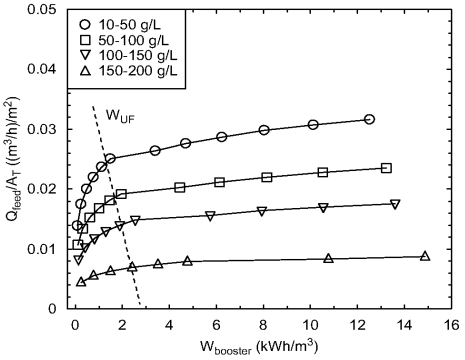

Fig. 8. The reciprocal total membrane area as a function of the energy used by the booster pump for four different concentration steps of amylase-S. The energy is calculated in the range of 0.2–2.4 m/s (not shown for all concentration ranges) in steps of $\Delta v = 0.2$ m/s, $Q_{\text{feed}} = 1.0\,\text{m}^3/\text{h}$, $\eta_{\text{pump}} = 0.6$, $l_{\text{feed}} = 0.5$ m, $w_{\text{feed}} = 0.2$ m and $h_{\text{heed}} = 1$ mm.

reason for the lower flux at 0 V, when salt is present, is mainly due to a reduction of the repulsing electrostatic membrane–enzyme forces. A reduction of the ζ-potential at conductivities higher that 2.9 mS/cm is, however, likely and will decrease the effect of the electric field. As can be seen in Fig. 7, the experiments at high conductivities are stopped at a lower E compared to the ones at lower conductivities. The end-point represents the maximum electric field strength possible at the given conductivity for this equipment. A better design of the EUF cell is therefore necessary if this technique is going to be used together with high conductivity solutions.

5. Energy consideration

The process economy in EUF should be compared to the energy requirements in conventional UF. It is therefore necessary to determine the optimal operating conditions in UF. For these calculations a UF/EUF module with the dimensions $l = 0.5$ m and $w = 0.2$ m is used; since it is a common dimension of UF and ion-exchange membranes. The channel height h is set to 1.0 mm unless stated otherwise. The calculations are based on a feed flow of $Q_{\text{feed}} = 1.0\,\text{m}^3/\text{h}$, and a pump and power supply efficiency of $\eta_{\text{pump}} = \eta_E = 0.6$. The gel layer concentration is set to 225 g/L for amylase-S and 210 g/L for amylase-F. The viscosity and density of the feed solution is assumed to be equal to the viscosity and density of water at 12 °C. Only the energy requirements of the booster pump will be considered, since the energy used by the feed pump is negligible. Furthermore, the modules will in a production line be placed sequential, so that the product from the first concentration step is the inlet concentration for the second module and so on. The energy used by the feed pump is therefore only relevant for the first step. The calculations are divided into four steps with an overall concentration range from 10 to 200 g/L. The calculations are made at a higher final concentration than the experiments were conducted to fully cover the potential of EUF. Eq. (1) is assumed to be valid in the entire concentration range. The calculations are based on the resistance of the feed solution only, unless stated otherwise. Hence, r_{perm} and r^* are set to zero.

5.1. Energy used in UF

In Fig. 8 the energy calculations for the UF process are shown for the amylase-S solutions. The energy used by the booster pump for crossflow velocities in the range 0.2–2.4 m/s (Eq. (16)) is depicted on the abscissa and the corresponding reciprocal total membrane area ($1/A_T$) calculated by Eq. (9) on the ordinate. From Eq. (9) it can be seen that $1/A_T$ is proportional to the flux, which means that a high value of $1/A_T$ and a low energy consumption is desired. Fig. 8 shows that there exist an optimal combination between the energy consumption (and hence the crossflow velocity) and the membrane area. This is seen as a deflection in the curves around $2\,\text{kWh}/\text{m}^3$, most pronounced for the low concentrations. Since the curves have a steep slope before the deflection point it is feasible to increase the crossflow velocity because it reduces the total membrane area considerably. After the deflection point a further increase in the crossflow will not decrease the membrane area substantially. This means that it is too expensive to operate beyond this point. The optimal operating conditions are marked as a dotted line in Fig. 8 and correspond to a crossflow velocity around 1.0 m/s. The results for UF of amylase-F are very similar to amylase-S, and the optimal operating conditions are also determined to 1.0 m/s.

5.2. Energy used in EUF

In Fig. 9 the energy calculations for the EUF process is shown for the amylase-S solution. The energy is here a sum of the energy used by the electric field and the booster pump.

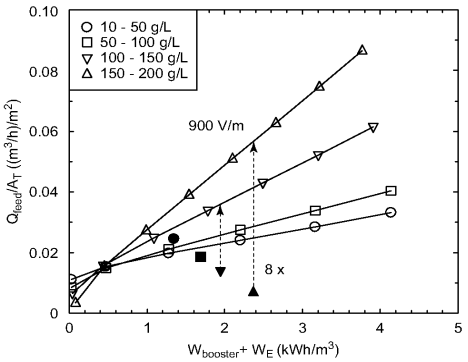

Fig. 9. The reciprocal total membrane area as a function of the energy used by the booster pump and the electric field for four different concentration steps of amylase-S. The energy is calculated in the range 0–2000 V/m (not shown for all concentration ranges) in steps of $\Delta E_{feed} = 200$ V/m. The filled symbols are the optimal operating conditions found in UF. $Q_{feed} = 1.0\,m^3/h$, $\eta_{pump} = \eta_E = 0.6$, $l_{feed} = 0.5$ m, $w_{feed} = 0.2$ m, $h_{heed} = 1$ mm, $v = 0.1$ m/s and $\kappa = 1.0$ mS/cm.

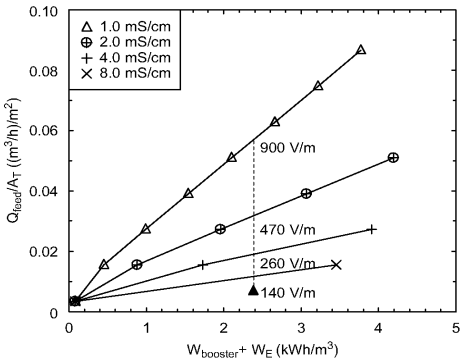

Fig. 10. The reciprocal total membrane area as a function of the energy used by the booster pump and the electric field for concentrating amylase-S from 150 to 200 g/L at different conductivities. The filled symbol is the optimal operating condition found in UF. $Q_{feed} = 1.0\,m^3/h$, $\eta_{pump} = \eta_E = 0.6$, $l_{feed} = 0.5$ m, $w_{feed} = 0.2$ m, $h_{heed} = 1$ mm and $v = 0.1$ m/s.

However, the energy used by the booster pump only accounts for less than 5% of the total energy consumption in EUF due to the low crossflow velocity. The calculations are carried out at different electric field strengths in the range of 0–2000 V/m and a crossflow velocity of 0.1 m/s. The conductivity of the feed solution is set to 1.0 mS/cm, which corresponds to a diafiltrated solution. The deflection points from Fig. 8 are illustrated by the filled symbols. Unlike the UF process shown in Fig. 8, the curves representing the EUF process do not show any deflection. The membrane area continues to decrease the more energy (higher electric field strength) that is consumed during the filtration process. The optimum electric field strength therefore depends on the price of the membrane and the cost of energy.

When comparing the two processes for the low concentration range (10–50 g/L) UF is more feasible compared to EUF, since a lower membrane area is required. In the concentrating from 50–100 g/L the calculations show a small advantage in favor of EUF, this becomes more evident the higher the initial feed concentration is. At the high concentration range (150–200 g/L) a clear advantage in favor of EUF is seen. If an electric field strength of 900 V/m is applied the energy requirements for EUF are the same as for UF at 1.0 m/s. However, the membrane area can be reduced around 8 times. For amylase-F the energy balance is even better with respect to EUF due to the higher mobility compared to amylase-S. EUF can therefore be used as a final concentration step during production where the first steps are conventional UF modules.

5.2.1. Effect of conductivity

To cover the possibilities of using EUF for filtering high concentrated solutions the influence of the conductivity must be illustrated. The calculations from Fig. 9 are therefore repeated for the high concentration range (150–200 g/L) at conductivities up to 8 mS/cm for amylase-S and shown in Fig. 10. The optimal condition during UF is shown as the filled triangle. It is assumed that the flux is independent of the conductivity in the studied range, as found in Fig. 7 for conductivities up to 2.9 mS/cm. The effect of the conductivity is clear; the advantage of using EUF decreases almost inversely proportional to the feed conductivity. Thus the electric field strength, which is needed to utilize the same amount of energy in EUF as in UF decreases correspondingly. If the conductivity exceeds around 4.0 mS/cm the advantage of using EUF instead of UF almost disappear.

5.2.2. Effect of the channel height

The influence of the height of the feed chamber is seen in Fig. 11, which shows results similar to Fig. 10, but with a channel height of 0.5 mm instead. Now 1770 V/m can be applied across the feed chamber instead of 900 V/m at 1.0 ms/cm before the energy consumption is the same for EUF and UF. This means that the advantage of EUF becomes greater. The feasibility of EUF is therefore strongly dependent on the height of feed channel.

5.2.3. Effect of the resistance in the cell

The results shown in Figs. 9–11 are based on the conductivity of the feed solution alone. In a real system there will be additional energy losses due to the resistances of the ion-exchange membranes and permeate chambers. The specific resistance of the ion-exchange membrane is given by the manufacturer to 0.001 m^2/S. Fig. 12 shows the energy balance for the concentration range 150–200 g/L at a channel height of 1 mm, under the assumption that the resistance of the permeate chamber is the same as for the ion-exchange membrane. The results can be

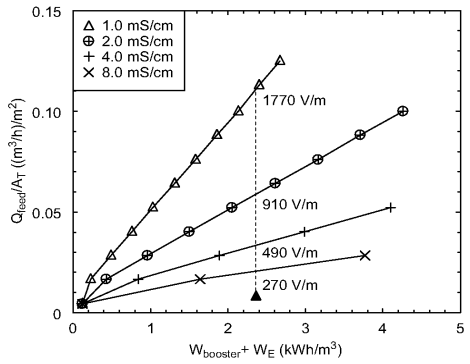

Fig. 11. The reciprocal total membrane area as a function of the energy used by the booster pump and the electric field for concentrating amylase-S from 150 to 200 g/L at different conductivities. The filled symbol is the optimal operating condition found in UF. $Q_{feed}=1.0\,m^3/h$, $\eta_{pump}=\eta_E=0.6$, $l_{feed}=0.5\,m$, $w_{feed}=0.2\,m$, $h_{heed}=0.5\,mm$ and $v=0.1\,m/s$.

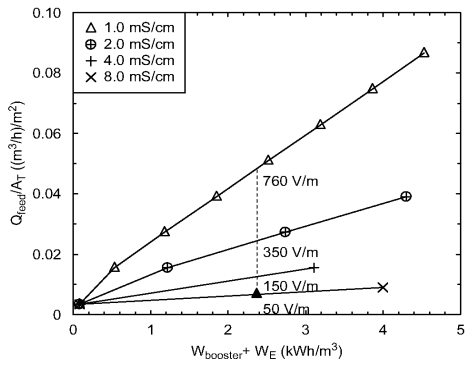

Fig. 12. The reciprocal total membrane area as a function of the energy used by the booster pump and the electric field for concentrating amylase-S from 150 to 200 g/L at different conductivities. The filled symbol is the optimal operating condition found in UF. $Q_{feed}=1.0\,m^3/h$, $\eta_{pump}=\eta_E=0.6$, $l_{feed}=0.5\,m$, $w_{feed}=0.2\,m$, $h_{heed}=1\,mm$, $v=0.1\,m/s$ and $r^*=r_{perm}=0.001\,m^2/S$.

compared to those in Fig. 10. The extra resistances mean that the conductivity of the feed solution must be lower to make EUF profitable. Depending on the height of the feed chamber a conductivity higher than around 2 mS/cm is probably not realistic if EUF is going to be economically feasible.

6. Conclusion

The influence of TMP, crossflow velocity, and conductivity have been determined in EUF and conventional UF for amylase enzymes, and used to determine the energy balance in the two processes. Increasing the TMP and conductivity did not affect the flux in EUF, while increasing the crossflow velocity only had an affect at low electric field strengths. In UF the mass transport coefficient was found to fit a laminar approximation of the Sherwood relation.

The UF process is found to be most feasible when using a crossflow velocity of around 1.0 m/s. An optimal electric field strength is not found in EUF. EUF is found to be favorable compared to UF when filtering high concentrated solutions, while the opposite is the case when filtering the low concentrated solutions. The conductivity of the feed solution is, however, of utmost importance for the feasibility of the EUF process. A low conductivity and a small channel height is important for the feasibility of the EUF process. If these requirements can be met, it would be an economical advantage to use EUF as a final concentration step in a production line, where the first steps are conventional UF.

Notation

$a^\dagger$	constant, m/V
a	constant parameter
A_e	electrode area equal the area of one membrane sheet, m^2
A_T	total membrane area, m^2
b	constant parameter
c_g	gel layer concentration, g/L
c_r	retentate concentration, g/L
c_{feed}	feed concentration, g/L
d	constant parameter
d_h	hydraulic diameter, m
D	diffusion coefficient, m^2/s
E	electric field, V/m
f	friction factor
h	channel height, m
I	current, A
J	permeate flux, L/m^2h, m/s
J_{av}	average permeate flux during concentration from c_{feed} to c_r, L/m^2h, m/s
k_0	mass transport coefficient, m/s
l	channel length, m
M	molecular size, Da
n	number of cells
p_{in}	inlet pressure, Pa, bar
Δp	pressure loss across the feed channel, Pa, bar
P	power, kW
Q	flow rate, m^3/h
r	resistance, m^2/S
Re	Reynolds number
Sh	Sherwood number
Sc	Schmidt number
T	temperature, K
TMP	transmembrane pressure, Pa
U_a	applied potential, V
v	crossflow velocity, m/s

w	channel width, m
W	energy consumption, kWh/m^3
z	constant parameter

Greek letters

α	cross-section area, m^2
η	viscosity of the feed solution, Ns/m^2
η_{pump}	efficient factor of the pumps
η_e	efficient factor of the power supply
κ	conductivity
μ_e	electrophoretic mobility, m^2/V
ρ	density of the feed solution, kg/m^3

References

Bargeman, G., Houwing, J., Recio, I., Koops, R.H., Horst, C.v.d., 2002. Electro-membrane filtration for the selective isolation of bioactive peptides from an α_{S2}-Casein hydrolysate. Biotechnology and Bioengineering 80, 599–608.

Bradford, M.M., 1976. A rapid and sensitive method for the quantitation of microgram quantities of protein utilizing the principle of protein-dye binding. Analytical Biochemistry 72, 248–254.

Enevoldsen, A.D., Hansen, E.B., Jonsson, G., 2007. Electro-ultrafiltration of industrial enzyme solutions. Journal of Membrane Science 299, 28–37.

Guizard, C., Legault, F., Idrissi, N., Larbot, A., Cot, L., Gavach, C., 1989. Electronically conductive mineral membranes designed for electro-ultrafiltration. Journal of Membrane Science 41, 127–142.

Henry Jr., J.D., Lawler, L.F., Kuo, C.H.A., 1977. Solid/liquid separation process based on cross flow and electrofiltration. A.I.Ch.E. Journal 23, 851–859.

Huotari, H.M., Trägårdh, G., Huisman, I.H., 1999a. Crossflow membrane filtration enhanced by an external dc electric field: a review. Transactions of the IChemE 77(A), 461–468.

Houtari, H.M., Huisman, I.H., Trägårdh, G., 1999b. Electrically enhanced crossflow membrane filtration of oily waste water using the membrane as a cathode. Journal of Membrane Science 156, 49–60.

Jonsson, G., Boesen, C.E., 1977. Concentration polarization in a reverse osmosis test cell. Desalination 21, 1–10.

Lazarova, Z., Serro, W., 2002. Electromembrane separation of mineral suspensions: influence of process parameters. Separation Science and Technology 37 (3), 515–534.

Mulder, M., 2000. Basic Principles of Membrane Technology. second ed.. Kluwer Academic Publishers, The Netherlands.

Oussedik, S., Belhocine, D., Grib, H., Lounici, H., Piron, D.L., Mameri, N., 2000. Enhanced ultrafiltration of bovine serum albumin with pulsed electric field and fluidized activated alumina. Desalination 127, 59–68.

Radovich, J.M., Behnam, B., 1985. Steady-state modeling of electroultrafiltration at constant concentration. Separation Science and Technology 20 (4), 315–329.

Radovich, J.M., Chao, I.M., 1982. Electroultrafiltration of a cationic electrodeposition paint. Journal of Coatings Technology 54, 33–40.

Radovich, J.M., Sparks, R.E., 1980. Electrophoretic techniques for controlling concentration polarization in ultrafiltration. Polymer Science and Technology 13, 249–268.

Wakeman, R.J., 1998. Electrically enhanced microfiltration of albumin suspensions. Transactions of the IChemE 76(C), 53–59.

Weigert, T., Altmann, J., Ripperger, S., 1999. Crossflow electrofiltration in pilot scale. Journal of Membrane Science 159, 253–262.

Yang, G.C.C., Yang, T.Y., Tsai, S.H., 2003. Crossflow electro-microfiltration of oxide-CMP wastewater. Water Research 37, 785–792.

Young, M.E., Carroad, P.A., Bell, R.L., 1980. Estimation of diffusion coefficients of proteins. Biotechnology and Bioengineering 22, 947–955.

Yukawa, H., Shimura, K., Suda, A., Maniwa, A., 1983. Cross flow electro-ultrafiltration for colloidal solution of protein. Journal of Chemical Engineering of Japan 16, 305–311.

Zumbusch, P.v., Kulcke, W., Brunner, G., 1998. Use of alternating electrical fields as anti-fouling strategy in ultrafiltration of biological suspensions—introduction of a new experimental procedure for crossflow filtration. Journal of Membrane Science 142, 75–86.

Appendix G

Paper 3

S.P. Beier, A.D. Enevoldsen, G.M. Kontogeorgis, E.B. Hansen and G. Jonsson, "Adsorption of amylase enzyme on ultrafiltration membranes," *Langmuir* **23**, pp. 9341-9351, 2007.

Langmuir **2007,** *23,* 9341−9351

Adsorption of Amylase Enzyme on Ultrafiltration Membranes

Søren Prip Beier,[†] Ann Dorrit Enevoldsen,[†] Georgios M. Kontogeorgis,[‡] Ernst B. Hansen,[§] and Gunnar Jonsson*,[†]

CAPEC, Department of Chemical Engineering, Technical University of Denmark, DK-2800 Kgs. Lyngby, Denmark, IVC-SEP, Department of Chemical Engineering, Technical University of Denmark, DK-2800 Kgs. Lyngby, Denmark, and Recovery Development, Novozymes A/S, Smørmosevej 9, 3AM, DK-2880 Bagsværd, Denmark

Received May 29, 2007. In Final Form: June 26, 2007

A method to measure the static adsorption on membrane surfaces has been developed and described. The static adsorption of amylase-F has been measured on two different ultrafiltration membranes, both with a cutoff value of 10 kDa (a PES membrane and the ETNA10PP membrane, which is a surface-modified PVDF membrane). The adsorption follows the Langmuir adsorption theory. Thus, the static adsorption consists of monolayer coverage and is expressed both as a permeability drop and an adsorption resistance. From the adsorption isotherms, the maximum static permeability drops and the maximum static adsorption resistances are determined. The maximum static permeability drop for the hydrophobic PES membrane is 75%, and the maximum static adsorption resistance is 0.014 m^2•h•bar/L. The maximum static permeability drop for the hydrophilic surface-modified PVDF membrane (ETNA10PP) is 23%, and the maximum static adsorption resistance is 0.0046 m^2•h•bar/L. The difference in maximum static adsorption, by a factor of around 3, affects the performance during the filtration of a 5 g/L amylase-F solution at 2 bar. The two membranes behave very similarly during filtration with almost equal fluxes and retentions even though the initial water permeability of the PES membrane is around 3 times larger than the initial water permeability of the ETNA10PP membrane. This is mainly attributed to the larger maximum static adsorption of the PES membrane. The permeability drop during filtration exceeds the maximum static permeability drop, indicating that the buildup layer on the membranes during filtration exceeds monolayer coverage, which is also seen by the increase in fouling resistance during filtration. The accumulated layer on the membrane surface can be described as a continually increasing cake-layer thickness, which is independent of the membrane type. At higher concentrations of enzyme, concentration polarization effects cannot be neglected. Therefore, stagnant film theory and the osmotic pressure model can describe the relationship between flux and bulk concentration.

1. Introduction

During ultrafiltration (UF) and microfiltration (MF) of macromolecular solutions, a severe flux decline is often observed after a short period of time. The decline is caused by concentration polarization and fouling on the membrane surface. In the literature, it is generally accepted that macromolecular content such as proteins, enzymes, and so forth in the feed solution highly contributes to the buildup of membrane fouling and thus has a great impact on the flux decline.[1,2] Ultrafiltration membranes are mainly fouled by macromolecules on the membrane surface, whereas microfiltration membranes are also fouled inside the porous structure. In general, membrane fouling consists of the following:

(i) A monolayer of macromolecules is adsorbed to the membrane surface (both UF and MF membranes) and to the pore walls inside the membrane (MF membranes).

(ii) Macromolecules and other feed stream components are deposited on the adsorbed monolayer. Denaturated and aggregated macromolecules may also stick to the membrane and act as sites for further fouling buildup.[1]

The adsorbed monolayer is often tightly bounded to the membrane and cannot be removed by rinsing with water but requires chemical cleaning to be removed. Therefore, such a monolayer is often referred to as being an irreversible adsorbed monolayer (chemical adsorption). The further deposition of macromolecules on the monolayer is often more loosely attached, which in some cases makes it possible to remove by cleaning with water. This layer is therefore referred to as being a reversible fouling layer (physical adsorption).[3]

Different investigations of the adsorption of proteins and biomolecules on different surfaces have been published.

The adsorption of proteins on membrane surfaces can be studied by various methods. The amount of protein adsorbed on membranes can be determined, for example, by streaming potential measurements,[4] radioactive measurements of isotopically labeled proteins,[5] contact angle determinations,[6] SEM pictures of the membrane surface,[7] or simply soaking the membrane in a protein solution and following the development of concentration.[1,2,8−10] In general, the adsorption in the above cases can be described by a Langmuir isotherm regardless of whether it is measured under static or dynamic conditions.

* Corresponding author. E-mail: gj@kt.dtu.dk. Tel: (+45) 4525 2946. Fax: (+45) 4588 2258.
† CAPEC, Department of Chemical Engineering, Technical University of Denmark.
‡ IVC-SEP, Department of Chemical Engineering, Technical University of Denmark.
§ Novozymes A/S.

(1) Marshall, A. D.; Munro, P. A.; Trägårdh, G. *Desalination* **1993**, *91*, 65−108.
(2) Belfort, G.; Davis, R. H.; Zydney, A. L. *J. Membr. Sci.* **1994**, *96*, 1−58.
(3) Shaw, D. J. *Introduction to Colloid and Surface Chemistry*, 4th ed.; Butterworth-Heinemann: Boston, 1992.
(4) Kontturi, K.; Vuoristo, M. *Desalination* **1996**, *104*, 99−105.
(5) Wei, J.; Helm, G. S.; Corner-Walker, N.; Hou, X. *Desalination* **2006**, *192*, 252−261.
(6) Bayramoğlu, G.; Yalçin, E.; Arica, M. Y. *Biochem. Eng. J.* **2005**, *26*, 12−21.
(7) Li, X.; Zhang, Y.; Fu, X. *Sep. Purif. Technol.* **2004**, *37*, 187−198.
(8) Cattoli, F.; Boi, C.; Sorci, M.; Sarti, G. C. *J. Membr. Sci.* **2006**, *273*, 2−11.
(9) Cattoli, F.; Sarti, G. C. *Desalination* **2002**, *149*, 465−470.
(10) Khokhlova, T. D.; Mchedlishvili, B. V. *Colloid J.* **1996**, *58*, 793−795.

10.1021/la701524x CCC: $37.00
Published on Web 08/04/2007

The adsorption of proteins can be a slow process especially if the experiment is carried out under static conditions. Bayramoğlu and co-workers have measured the adsorption of five different proteins on surface-modified track membranes.[6] The amount of adsorbed protein changes with time. Lysozyme, cytochrome, and γ-globulin adsorb to the membrane surface, and after approximately 2 days, the maximum adsorption level is reached. γ-Globulin has the highest adsorption level, followed by cytochrome and lysozyme. BSA and ferritin do not adsorb to the membrane surface at all.[6] However, adsorption is not always a slow process. Li and co-workers have measured the static adsorption of glutamicum onto a polysulphone ultrafiltration membrane at different ionic strengths and pH values.[7] In their work, the maximum adsorption is reached after just 1 h in all cases. Furthermore, they found a large influence of ionic strength and pH on adsorption. Generally, the highest amount of protein is adsorbed at a pH equal to the proteins' isoelectric point (pI), where the electrostatic repulsions between membrane−protein and protein−protein are at a minimum. If the protein has a net surface charge, then the amount of adsorbed protein depends on the charge of the membrane surface. Bayramoğlu and co-workers and Li and co-workers[6,7] both found that proteins with opposite surface charge compared to that of the membrane had the strongest adsorption.

The influence of hydrophilicity on surface adsorption was studied by Wei and co-workers.[5] They have shown that membranes made of hydrophobic materials such as polysulphone and polyethersulphone caused severe fouling during the filtration of BSA compared to UF membranes (ETNA01PP and ETNA10PP) made of more hydrophilic surfaces (e.g., surface-modified poly(vinylidene fluoride)). However, there are other considerations to take into account when choosing the proper membrane for a filtration process. When comparing a 10 kDa polysulphone membrane with a ETNA10PP membrane, the water permeability of the ETNA10PP membrane is easily restored just by rinsing with water after filtration with BSA. In contrast, the polysulphone membrane requires chemical cleaning before water permeability is restored. However, the filtration rate is higher using the polysulphone membrane than using the ETNA10PP membrane, probably because of the higher initial water permeability.[5] The retention (selectivity), lifetime, and cleaning needs are also important parameters to consider when choosing a membrane for a specific filtration purpose.

Thom et al. investigated how protein adsorption on membrane surfaces influences the biocompatibility of these surfaces. They also found that the amount of protein adsorption decreased with increasing hydrophilicity. However, the state of the adsorbed protein seemed to depend on the amphiphilic character of the surface, showing the lowest degree of protein denaturation when there was a large difference between the advancing and receding contact angles.[11]

The scope of this work is to investigate the adsorption of macromolecules (an amylase enzyme, 55 kDa) on two different UF membranes under static and pressure-forced conditions. One of the objectives is to show whether chemical (static) adsorption can be described by the well-known Langmuir adsorption theory. A method to measure the static adsorption is described. The relative adsorption is measured both as a membrane permeability drop based on the permeabilities before and after static adsorption and as an adsorption resistance. The effect of static adsorption is also investigated during the filtration (pressure-forced condition) of the amylase solution.

(11) Thom, V. H.; Altankov, G.; Groth, Th.; Jankova, K.; Jonsson, G.; Ulbricht, M. *Langmuir* **2000**, *16*, 2756−2765.

2. Theory

The adsorption of various components on different surfaces can be described by the Gibbs adsorption isotherm. The Gibbs adsorption isotherm is given below:

$$\Gamma_i = -\frac{C_i}{RT}\frac{\mathrm{d}\gamma}{\mathrm{d}C_i} \tag{1}$$

The adsorption of species i is denoted by Γ_i and is typically given in dimensions of mol/area. The concentration of species i in solution, from which the molecules are adsorbed, is denoted C_i. Equation 1 shows that, in order to determine the adsorption, knowledge of the surface tension γ as a function of concentration C_i is required. R is the gas constant, and T is the absolute temperature. The Gibbs equation has several applications:

- The surface concentration can be determined from the relationship between the surface tension and the concentration.
- The area occupied by each adsorbed molecule can be estimated.
- The molecular weight of the adsorbed macromolecules (proteins, enzymes, etc.) can be estimated, under the assumption that they form ideal films at low surface pressure.

The surface tension and adsorption phenomenon are linked, and at constant temperature, the adsorption can in many cases also be described by the Langmuir adsorption isotherm:

$$\Gamma_i = \frac{\Gamma_{i,\max} k C_i}{1 + k C_i} \tag{2}$$

The maximum adsorption of component i is denoted $\Gamma_{i,\max}$, and k is the adsorption equilibrium constant, which is related to the Gibbs adsorption energy. The Langmuir equation is often used in a linear form:

$$\frac{C_i}{\Gamma_i} = \frac{C_i}{\Gamma_{i,\max}} + \frac{1}{k\Gamma_{i,\max}} \tag{3}$$

Maximum adsorption corresponds to the surface being covered by a monolayer. In many cases, the adsorption of large molecules on solid surfaces follows Langmuir theory. The Langmuir adsorption equation is based on the following assumptions:

- The surface is homogeneous.
- Adsorption cannot occur beyond monolayer coverage.
- All adsorption sites are equivalent.
- There are no interactions between the adsorbed molecules and the molecules in the solution and no interactions between the solvent and the surface.

According to the last assumption, the Langmuir adsorption equation is only valid for dilute solutions. Although the last assumption can, in some contexts, seem unrealistic, the equation is still quite useful. The theory also assumes that the adsorption rate is proportional to the concentration in solution and the fraction of the free non-covered area of the adsorbent. Furthermore, the desorption rate is assumed to be proportional to the fraction of surface covered by adsorbed molecules. At equilibrium, the adsorption and desorption rates are equal. By plotting the adsorption and the concentration (eq 3), $\Gamma_{i,\max}$ can be determined. This value corresponds to the concentration at which the whole surface is covered by a monolayer of adsorbed molecules.

Adsorption is affected by many different parameters. The salt concentration in the solution can influence the geometric structure of the macromolecules, which in turn can influence the adsorption. Increased ionic strength decreases the thickness of the diffuse double layer around the macromolecule, and the electrostatic

Table 1. Membrane Data

name	producer	cutoff value	material	water permeability
ETNA10PP	Alfa Laval	10 kDa	PVDF (surface-modified poly(vinylidene fluoride))	63 ± 6 L/(m²·h·bar)
PES	Pall	10 kDa	PES (polyethersulfone)	207 ± 18 L/(m²·h·bar)

interactions between the proteins thus decrease. If the membrane and protein have opposite surface charge, then a higher ionic strength will, in general, decrease the adsorption due to weaker electrostatic interactions. A higher adsorption can, however, be achieved by increasing the ionic strength in the solution if the membrane and protein have the same surface charge because the repelling forces are reduced.[6,7]

The pH of the solution can also influence the adsorption because the charge of a macromolecule is highly dependent on the pH value. Equally charged molecules repeal each other, thus adsorption is assumed to be highest when the molecules have a low charge (close to the isoelectric point) or are uncharged.

The hydrophilic/hydrophobic nature of the surface also influences the adsorption. Hydrophobic surfaces tend to attract hydrophobic molecules more than hydrophilic molecules, and hydrophilic surfaces tend to attract hydrophilic molecules more than hydrophobic molecules. This is also the case for membrane surfaces. The membrane material and structure have an effect on the degree of adsorption and fouling, but the membrane material is not always crucial; its influence also depends on the filtration system. If cake buildup at the membrane surface is observed, then the filtration process will mostly depend on the cake properties.[1] The morphology and structure of the membrane also have an effect on fouling. Membranes with straight-through pores are more sensitive to fouling than isotropic membranes, where the membranes make up a network structure in which the fluid can pass the blocked pores.[12,13]

The chain length also influences the adsorption of, for example, hydrocarbons because of their hydrophobic nature. The temperature is also important because the surface tension depends on the temperature.[3]

Thus, the adsorption is affected by many parameters, which affects the maximum adsorption. In some cases, it is reached in a few hours, whereas in other cases, it takes several days before the maximum adsorption is reached.

In the evaluation of the adsorption, the permeabilities (l_p) of the membranes are determined. The permeability can be calculated according to Darcy's law from flux and pressure data.[14]

$$J_v = l_p \Delta P \tag{4}$$

The volumetric flux through the membrane is denoted J_v, and ΔP is the applied hydrostatic pressure across the membrane. In further analysis, the permeabilities can be interpreted as different subresistances. Thus, eq 4 can be rewritten into the following resistance-in-series model:[15]

$$J_v = \frac{1}{R_{tot}}\Delta P = \left(\frac{1}{R_m + R_a + R_f}\right)\Delta P \tag{5}$$

The total resistance toward transport through the membrane (R_{tot}) can be divided into different subresistances such as the membrane resistance (R_m), the adsorption resistance (R_a), and the fouling resistance (R_f). The membrane resistance is a membrane constant, whereas the adsorption resistance is a term that is used in the evaluation of the static adsorption. The fouling resistance is used in the evaluation of the pressure-forced adsorption. The fouling resistance can in some cases be thought of as a continuous growing cake on the membrane surface, similar to conventional filtration theory. In that case, the first layer of the cake corresponds to the adsorbed monolayer, and thus the adsorption resistance and the fouling resistance can be looked upon as one term. The resistance of such a cake is dependent on the specific cake resistance, which is a constant, and the thickness of the cake, which is a function of the mass of permeate, that passes the membrane.[15] In this case, the continually increasing cake layer (or fouling resistance) can be expressed as follows:

$$R_f = \alpha m_p \tag{6}$$

The fouling constant (α) depends on the specific cake resistance, the bulk concentration, and the concentration of solutes in the cake layer.[15] The mass of permeate is denoted m_p.

The fouling resistance is inserted into the resistance-in-series filtration model:

$$J_v = \left(\frac{1}{R_m + R_a + \alpha m_p}\right)\Delta P \tag{7}$$

This model can be rewritten as[15]

$$\frac{1}{J_v} = \left(\frac{R_m + R_a}{\Delta P}\right) + \frac{\alpha}{\Delta P}\cdot m_p \tag{8}$$

Thus, if the fouling on the membrane surface forms or can be described as a continually growing cake, one should get a straight line when plotting $1/J_v$ versus m_p because R_m, R_a, ΔP, and α are all constants.

At high macromolecular concentrations, the osmotic pressure difference across the membrane also has to be taken into account.[16] Because of concentration polarization on the feed side of the membrane, the concentration at the membrane surface will be larger than in the bulk solution. The enhanced concentration results in a lower solvent chemical potential on the feed of the membrane surface compared to the solvent chemical potential on the permeate side. This gives an osmotic "back suck effect" of solvent that has to be taken into account at high macromolecular concentrations on the feed side. This gradient of solvent chemical potential across the membrane can be expressed as an osmotic pressure difference ($\Delta\pi$) across the membrane. When the osmotic pressure difference is taken into account, eq 5 can be extended to an osmotic pressure model:

$$J_v = \frac{1}{R_{tot}}(\Delta P - \Delta\pi) \tag{9}$$

The flux in eq 9 is therefore determined by different subresistances in series (R_{tot}) and from an osmotic pressure difference that arises from concentration polarization on the feed side of the membrane. When the concentration polarization phenomenon is the domi-

(12) Ho, C.; Zydney, A. L. *J. Membr. Sci.* **1999**, *155*, 261−275.
(13) Ho, C.; Zydney, A. L. *Ind. Eng. Chem. Res.* **2001**, *40*, 1412−1421.
(14) Beier, S. P. *Pressure Driven Membrane Processes*; Ventus Publishing: Copenhagen, 2006.
(15) Mulder, M. *Basic Principles of Membrane Technology*, 2nd ed.; Kluwer Academic: Boston, 1996.
(16) Jonsson, G. *Desalination* **1984**, *51*, 61−77.

nating factor affecting the flux, stagnant film theory can be used to describe the flux dependency on the bulk concentration:[17]

$$J_v = K\left(\frac{C_m - C_p}{C_b - C_p}\right) \quad (10)$$

The mass transfer coefficient (K) is therefore a very important factor describing the level of back diffusion from the boundary layer on the feed side of the membrane. The concentration on the membrane surface (C_m) will be larger than the bulk concentration (C_b) due to concentration polarization. The permeate concentration (C_p) can be neglected if the retention of the membrane is close to 100%. The mass transfer coefficient can be determined from literature correlations. For a stirred cell (in the laminar region), the following correlation can be used:[18]

$$Sh = 0.285(Re)^{0.55}(Sc)^{0.33} \quad (11)$$

The Sherwood number is a dimensionless mass transfer coefficient ($Sh = Kr/D$), which is given by the mass transfer coefficient (K), cell radius (r), and diffusion coefficient of the solute/macromolecule in the solvent (D). The Reynolds number (Re) is calculated as $\omega r^2/\nu$, where ω is the stirring speed and ν is the kinematic viscosity. The Schmidt number is defined as the ratio between the kinematic viscosity and the diffusivity ($Sc = \nu/D$).

The initial and final water permeabilities of the membranes (before and after adsorption) are also used in the evaluation of the adsorption. The permeability drop is defined as follows:

$$\text{permeability drop} = \frac{(\overline{l_{p,initial}} - l_{p,final})}{\overline{l_{p,initial}}} \times 100\% \quad (12)$$

As a value of the initial water permeability, an average value is used that is given for the two investigated membranes in Table 1. The final permeability is measured (after adsorption) after rinsing the membrane with only water.

3. Material and Methods

In this section, the apparatus, solutions, and procedures used for the experimental work are described.

3.1. Apparatus, Materials, and Solutions. *3.1.1. Experimental Apparatus.* A dead-end batch cell is used for the adsorption experiments. The circular membrane area is 44 cm^2, and the pressure in the cell can be established by connecting the cell to a nitrogen gas flask. Permeate is collected in a beaker placed on a balance. A sketch of the system is given in Figure 1.

Pressure in the cell is established only when the water permeability of the membranes is measured, when the membrane before each adsorption experiment is chemically cleaned, and during the pressure-forced adsorption experiments. During the static adsorption experiments, no pressure is established in the cell, and the batch cell is stored in the refrigerator. Stirring in the cell is turned on only during the water flux measurements and during the pressure-forced experiments.

3.1.2. Membranes. Two commercial ultrafiltration membranes with different hydrophilicity have been tested. Relevant data for the two membranes are given in Table 1.

The PES membrane is more hydrophobic than the ETNA10PP. The difference in contact angles is visualized in Figure 2.

(17) Zeman, L. J.; Zydney, A. L. *Microfiltration and Ultrafiltration*; Marcel Dekker: New York, 1996.

(18) Blatt, W. F.; Dravid, A.; Michaels, A. S.; Nelson, L. Solute Polarization and Cake Formation in Membrane Ultrafiltration: Causes, Consequeneces, and Control Techniques; *Membrane Science and Technology - Industrial, Biological, and Waste Treatment Processes*, Columbus Laboratories of the Battelle Memorial Institute in Columbus, Ohio, Oct 21−22, 1969; pp 47−97.

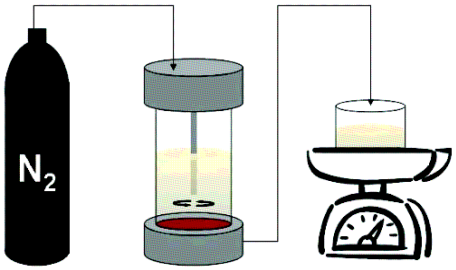

Figure 1. Sketch of the experimental apparatus.

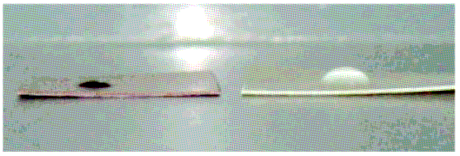

Figure 2. Two dry pieces of the membranes, ETNA10PP to the left and PES to the right. A 10 μL water droplet has been placed on each membrane.

In Figure 2, it is seen that the PES membrane is more hydrophobic than the ETNA10PP membrane because the contact angle is larger. The contact angle of the ETNA10PP membrane is around 40° whereas the contact angle of the PES membrane is around 85−90°. The contact angle of a polysulphone film that is very similar to the PES membrane surface had earlier been measured to be around 90°.[11] The ETNA10PP membrane is made hydrophilic by introducing a surface modification consisting of grafting a thin layer of hydrophilic polymer onto the PVDF surface. Because of the grafting, covalent bonds are formed between the PVDF membrane and the hydrophilic polymer layer. This ensures the stability of the surface-modified membrane.[5] The water permeability of the PES membrane is around 3 times higher than the water permeability of the ETNA10PP membrane. The water permeabilities of the two membranes are determined as an average from 10 and 7 measurements of the PES and the ETNA10PP membranes, respectively. The standard deviations of the water permeability measurements are also given in Table 1.

3.1.3. Membrane Water Permeability. The water permeability (l_p) is determined by measuring the water flux (J_v) at different pressures between 0 and 2 bar according to eq 4. The water permeability is measured in each experiment before and after the exposure to enzyme solution. The final water permeability is measured after the batch cell is emptied, and the rest of the enzyme solution is removed by rinsing with water.

3.1.4. Amylase Enzyme Solutions. Solutions of an amylase enzyme called amylase-F have been used. The concentrated enzyme solution is produced by Novozymes A/S. The molecular weight is 55 kDa, and the isoelectric point is around 3.5. The solutions were supplied by Novozymes A/S and were diafiltrated with demineralized water to remove salts and other minor components until the conductivity in the permeate is below 0.5 mS/cm. Beside the amylase enzymes, other compounds might be present (e.g., amino acids produced during fermentation or flocculation chemicals such as calcium chloride). However, a vast majority of these compounds are removed by diafiltration. A detailed description can be found elsewhere.[19] Adsorption has been measured in the concentration range from 0.1 to 100 g/L. The solubility of the amylase is above 200 g/L. The pH of the aqueous enzyme solutions is 5.5, which means that the enzymes are negatively charged. Concentration measurements are conducted by the Bradford reagent method.[20]

(19) Enevoldsen, A. D; Hansen, E. B.; Jonsson, G. *J. Membr. Sci.* **2007**, *299*, 28−37.

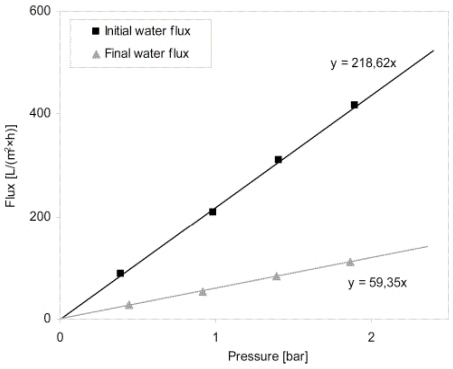

Figure 3. Water flux vs pressure for the PES membrane before and after static adsorption for 144 h at 5 °C. Amylase-F concentration = 50 g/L.

3.2. Adsorption Experiments. Two types of adsorption experiments were conducted: the static adsorption experiments and the pressure-forced adsorption experiments, which are defined as follows:

•Static adsorption is the adsorption of components from a solution that is in contact with a membrane under atmospheric pressure with no volumetric flux through the membrane.

•Pressure-forced adsorption is the adsorption of components that occurs during a membrane filtration experiment with volumetric flux through the membrane.

Both types of experiments are conducted in a batch cell. During static adsorption, the batch cell ensures that the adsorption takes place only on the skin layer of the membrane and not onto (and into) the support structure on the back side of the membrane. This would not have been the case if a piece of membrane was just immersed in the enzyme solution. However, some adsorption might take place on the pore walls inside the membrane, especially if the membrane has a broad pore size distribution, which seems to be the case for the ETNA10PP membrane (Figure 9).

3.2.1. Static Adsorption Experiments. In the static adsorption experiments, the batch cell is used only as a container. The membrane is placed in the bottom, and the solution is contained above the membrane. The permeate outlet of the cell is closed so that no volumetric flux occurs. No pressure above the membrane and no stirring are established. The batch cell with the membrane and the enzyme solution is kept in the refrigerator (to avoid decomposition of the enzymes) for 6 days. This rather long period of time is chosen to ensure that adsorption equilibrium is reached because adsorption can be a time-consuming process, as described earlier. Adsorption experiments have been carried out with different concentrations of the enzyme solution. The experimental procedure is the following:

•A virgin membrane is placed in the stirred cell.

•Cleaning is carried out with 300 mL of a 0.125% NaOH solution at 0.5 bar. Approximately 160−200 mL of permeate is collected. The cleaning temperature is 20 °C, and the cleaning time is ∼1 h.

•The membrane is rinsed with water. The remaining cleaning solution is removed as the cell is opened and separated. The different parts, including the membrane, are cleaned with demineralized water under a running tap.

•Initial water permeability is measured. Water (300 mL) is placed in the cell, and the flux is measured at approximately 0.5, 1.0, 1.5, and 2.0 bar. The temperature is 20 °C.

•Adsorption in the refrigerator is carried out for 144 h (6 days) at different enzyme concentrations between 0.1 and 100 g/L. The volume of enzyme solution is 30 mL with no stirring, and the temperature is 5 °C.

•Removal of enzyme solution followed by gently rinsing the membrane with water for 3 to 4 s under a running tap. The different parts of the batch cell are held under the running tap as well.

•The final water permeability is measured in a similar way as the initial water permeability.

From the initial and final water permeabilities, the permeability drop can be calculated according to eq 12. Furthermore, the adsorption resistance is calculated according to eq 5. The activity of a reference enzyme solution has been measured at Novozymes' laboratories before and after it has been placed in the refrigerator for 6 days. This is done to detect any loss in enzyme activity during the adsorption experiment.

3.2.2. Pressure-Forced Adsorption Experiments. In this case, the adsorption is conducted during concentration of the enzyme solution under a pressure of 2 bar. The flux is measured by collecting permeate in a beaker placed on the balance. The experimental procedure is as follows:

•Virgin membrane is placed in the batch cell.

•Cleaning is carried out with 300 mL of a 0.125% NaOH solution at 0.5 bar. Approximately 160−200 mL of permeate is collected. The cleaning temperature is 20 °C, and the cleaning time is ∼1 h.

•The membrane is rinsed with water. The remaining cleaning solution is removed, and the cell is opened and separated. The different parts, including the membrane, are cleaned with demineralized water under a running tap.

•Initial water permeability is measured. Water (300 mL) is placed in the cell, and the flux is measured at approximately 0.5, 1.0, 1.5, and 2.0 bar. The temperature is 20 °C.

•Enzyme solution (300 mL) is placed in the stirred cell (300 rpm), and the pressure is set to 2 bar. Filtration is continued until 150 g of permeate was collected. The enzyme concentrations are 5 and 50 g/L, and the filtration temperature is 20 °C.

•Removal of remaining enzyme solution followed by gently rinsing the membrane with water for 3 to 4 s under a running tap. The different parts of the batch cell are held under the running tap as well.

•The final water permeability is measured in a similar way as the initial water permeability.

In the pressure-forced adsorption experiments, the permeability drop is again calculated according to eq 12. From the static adsorption experiments, the adsorption resistance is known. Because the membrane resistance is also known, from the initial permeabilities given in Table 1, the fouling resistance can be calculated according to eq 5.

3.3. SEM Picture Analysis. Scanning electron microscopy (SEM) pictures have been made in the back-scattering mode of the two membrane types under different conditions:

•with clean surfaces (cleaned with 0.125% NaOH solution);

•with surfaces at which enzymes have been adsorbed for 144 h from a 100 g/L solution in the refrigerator (static adsorption); and

•with surfaces at which enzymes have been adsorbed during the concentration of enzyme solution from 50 to 100 g/L at 2 bar (pressure-forced adsorption).

These pictures have been taken as a supplement to the permeability data. The pictures are present in Figure 9.

3.4. Overview of Experimental Work. An overview of the different experiments and analysis is given in Table 2.

4. Results and Discussion

4.1. Permeability Drop and Adsorption Resistance. In Figure 3, the initial and final water permeabilities are depicted for one of the static adsorption experiments.

The membrane water permeability (l_p) corresponds to the slope of the fitted line according to Darcy's law.[14] In Figure 3, it is seen that for this amylase-F concentration the final water permeability is ∼59 L/(m²•h•bar). In this case, the initial water permeability is ∼219 L/(m²•h•bar), and according to Table 1, the average value of the PES membrane water permeability is 207 L/(m²•h•bar). According to eq 12, this gives a permeability

(20) Bradford, M. M. *Anal. Biochem.* **1976**, *72*, 248−254.

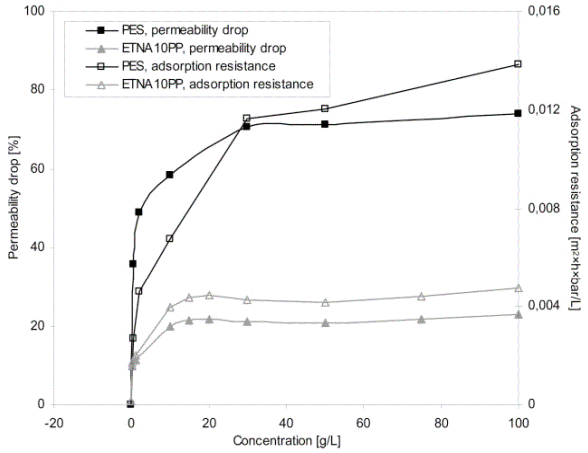

Figure 4. Adsorption isotherms. Permeability drop and adsorption resistance vs concentration for static adsorption experiments on the two membrane types at constant temperature (5 °C).

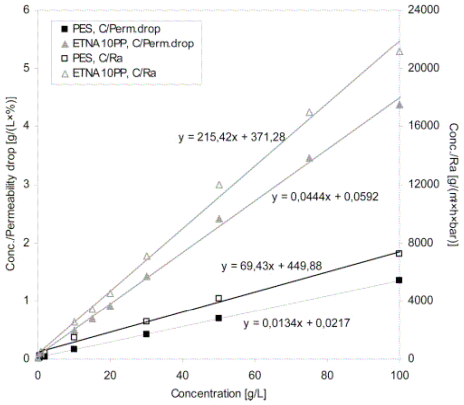

Figure 5. Linear plot of the static adsorption according to the Langmuir equation (eq 3). Concentration divided by permeability drop (Conc./Perm.drop) vs concentration and concentration divided by adsorption resistance (Conc./R_a) vs concentration at constant temperature (5 °C).

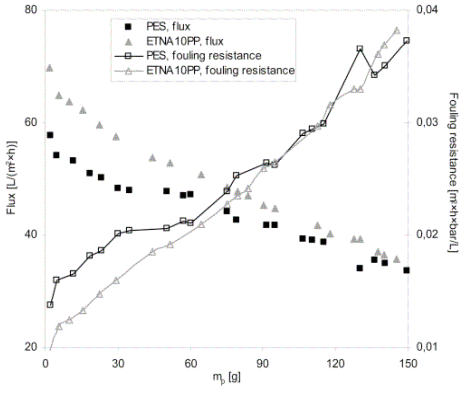

Figure 6. Flux and fouling resistance vs collected mass of permeate (m_p) during the pressure-forced adsorption experiments on the two different membranes at low enzyme concentration (5−10 g/L). Temperature = 20 °C, P = 2 bar.

drop of 71%. The permeability drop for all experiments listed in Table 2 are calculated according to eq 12.

Beside the permeability drop, the adsorption resistance (R_a) toward mass transport through the membrane can be determined by using eq 5. This adsorption resistance is also used to express the degree of adsorption. From the initial water permeability, the membrane resistance (R_m) is determined because at this stage the adsorption resistance and the fouling resistance (R_f) are both zero. The membrane resistance is calculated on the basis of the average water permeability value given in Table 1. The total resistance (R_{tot}) toward transport is determined on the basis of the final water permeability. In the static adsorption experiments, the fouling resistance is assumed to be zero. Thus, the adsorption resistance can be calculated as the difference between the total resistance and the membrane resistance. This has been done for all concentrations listed in Table 2 for both membrane types.

4.2. Static Adsorption. The permeability drop and the adsorption resistance can, as mentioned, be translated into a relative measurement of the adsorption. To determine if the static adsorption follows the Langmuir theory, these terms are plotted in Figure 4 at different concentrations.

The adsorption isotherms have the shape of a Langmuir isotherm. However, there is a clear difference in the level of permeability drop and adsorption resistance between the PES and the ETNA10PP membrane. The maximum permeability drop and adsorption resistance are around 3 times larger for the PES membrane compared to those for the ETNA10PP membrane. The adsorption for the PES membrane increases from around 40 to 60% when the concentration increases from 0.5 to 10 g/L. The curve levels out at a concentration of 30 g/L, where the permeability has dropped to around 70% from its initial value and the adsorption resistance has reached a value of ~0.013 m^2·h·bar/L. The permeability drop and adsorption resistance for

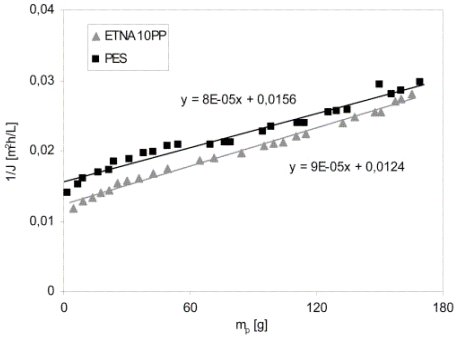

Figure 7. $1/J_v$ versus m_p during the pressure-forced adsorption experiments on the two different membranes at low enzyme concentration (5−10 g/L). Temperature = 20 °C, P = 2 bar.

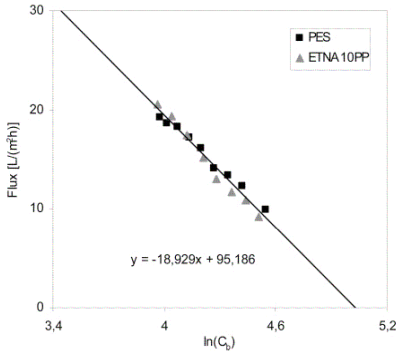

Figure 8. Flux vs ln(C_b) according to the stagnant film theory for the high-concentration pressure-forced experiments. Enzyme concentration = 50−100 g/L, P = 2 bar.

the ETNA10PP membrane are much smaller. At a concentration of 10 g/L, the permeability has dropped around 20% from the initial value, which is around the value of the maximum permeability drop. The adsorption resistance for the ETNA10PP membrane is also much smaller than for the PES membrane with a maximum value of around 0.004 m²•h•bar/L.

The activity analysis of the enzyme solution showed no change in activity during the 6 days in the refrigerator. Thus, the enzymes are not degraded during the adsorption experiments at 5 °C.

To determine whether the Langmuir theory (eq 2) actually describes the adsorption, the data in Figure 4 are plotted according to the linear form of the Langmuir adsorption theory (eq 3). In Figure 5, the concentrations divided by the permeability drop and the adsorption resistance are plotted as a function of the concentrations, respectively.

In Figure 5, it is seen that the linear form of the Langmuir isotherm fits the data for both membranes, regardless of whether the plots are based on the permeability drop or the adsorption resistance. This means that the Langmuir theory can indeed describe the adsorption over the entire concentration range, even though the membrane surfaces are not totally homogeneous as assumed in the derivation of the theory. Because the Langmuir theory describes the adsorption data well, we conclude that the static adsorption of amylase-F on the two different UF membranes consists of monolayer coverage. From the linear plots, the maximum static adsorption Γ_{max} (maximum static permeability drop or maximum static adsorption resistance) and the adsorption equilibrium constant k can be determined from eq 3. These terms are determined from the slopes and the intercepts of the linear plots in Figure 5, respectively. The results are given in Table 3.

The maximum static adsorption is around 3 times larger for the PES membrane compared to that for the ETNA10PP membrane. This shows that the degree of adsorption is significantly smaller on the ETNA10PP membrane than on the PES membrane, probably because of a more hydrophilic surface. This is in agreement with the results found by Wei and coworkers.[5] Because of the large adsorption on the PES membrane, the amylase-F molecules must be more closely packed on the PES surface than on the ETNA10PP surface. The adsorption equilibrium constants are determined from the intercepts with the y axis (Figure 5). The equilibrium constants, based on both the permeability drop and the adsorption resistance, have approximately the same value for the two different membranes except for one estimation, which is smaller. The Gibbs adsorption energy is related to the adsorption equilibrium constant;[3] therefore, the amylase-F must be attached to the adsorption sites on the PES membrane and on the ETNA10PP membrane, respectively, at approximately equal strength if the adsorption equilibrium constants are assumed to be at the same level. Thus, the number of adsorption sites on the ETNA10PP membrane seems to be less than on the PES membrane because the maximum static adsorption is 3 time larger for the PES membrane. This also supports the statement of the amylase-F molecules being more closely packed on the PES surface.

4.3. Pressure-Forced Adsorption. Pressure-forced adsorption experiments have been conducted for both membrane types during the collection of 150 g of permeate from an initial bulk volume of 300 mL, as seen in Table 2. The experiments are conducted at 20 °C. The permeability of the membranes is measured before and after each experiment similar to the static adsorption experiments, as described earlier. The permeability drop for the low concentration pressure-forced adsorption experiments is shown in Table 4.

It is seen in Table 4 that during filtration the maximum static adsorption is exceeded for both membranes, even at low enzyme concentrations. The static adsorption is measured at 5 °C, and the pressure-forced adsorption is measured at 20 °C. However, according to the Gibbs adsorption equation (eq 1), a higher temperature would result in a lower adsorption if the change in surface tension with concentration ($d\gamma/dC$) is assumed to be more or less constant at the two temperatures. Thus, the higher adsorption (permeability drop) for the pressure-forced adsorption measured at the higher temperature emphasizes that the maximum static adsorption is actually exceeded at the pressure-forced conditions. The higher permeability drop in the pressure-forced condition is likely due to a higher concentration on the membrane surface during filtration (concentration polarization), which leads to coverage of the surface beyond a monolayer. In this case, the Langmuir adsorption theory can no longer be applied, and permeability drops above the maximum static adsorption can be observed. The number of adsorbed macromolecules on membranes can be determined in many different ways, as extensively discussed in the literature.[4−10,21] The adsorption in these cases could be described by the Langmuir adsorption theory regardless of whether it is measured under static or dynamic conditions. In our case, this is in agreement only in the static case. The Langmuir

(21) Bowen, W. R.; Hughes, D. T. *J. Membr. Sci.* **1990**, *51*, 189−200.

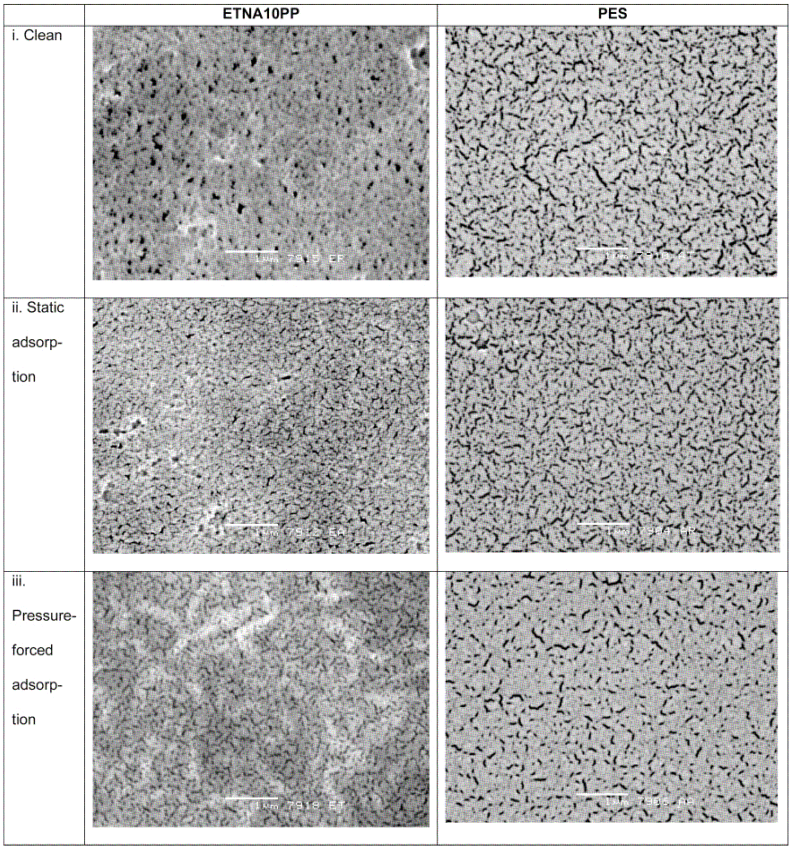

Figure 9. SEM pictures (backscattered mode) of the ETNA10PP and PES membranes. Magnification on the actual pictures is 20 000×. (i) Clean membrane surface, (ii) static adsorbed membrane surface (100 g/L enzyme solution at 5 °C for 144 h), and (iii) pressure-forced adsorbed membrane surface (50 g/L enzyme solution concentrated to 100 g/L at 20 °C). White lines corresponding to 1 μm are present at each SEM picture.

Table 2. Overview of Conducted Experiments and Analysis

membrane	static adsorption	pressure-forced adsorption	SEM pictures
ETNA10PP	enzyme concentration: 0, 0.1, 1, 10, 15, 20, 30, 50, 75, 100 g/L temperature: 5 °C pressure: atmospheric	enzyme concentration: 5, 50 g/L temperature: 20 °C pressure: 2 bar	clean static adsorbed pressure-forced adsorbed
PES	enzyme concentration: 0, 0.5, 2, 10, 30, 50, 100 g/L temperature: 5 °C pressure: atmospheric	enzyme concentration: 5, 50 g/L temperature: 20 °C pressure: 2 bar	clean static adsorbed pressure-forced adsorbed

adsorption theory is not able to describe the permeability drop during the pressure-forced experiments, in which a volumetric flux through the membrane exists.

It is interesting that because of the adsorption/fouling the two membranes behave similarly during filtration even though the initial water permeability of the PES membrane is around 3 times larger than for the ETNA10PP membrane even at low enzyme concentrations. The flux is depicted in Figure 6 at low enzyme concentration (concentration from 5 to 10 g/L) as a function of the collected mass of permeate for two of the pressure-forced experiments. The fouling resistance is depicted as well. The fouling resistance is calculated according to eq 5 in which the adsorption resistances (the maximum static adsorption resistance) and the membrane resistances are known from the static adsorption experiments. Thus, the level of maximum static adsorption resistance is assumed to be the same in the pressure-forced case, and thus the fouling resistance can be calculated according to eq 5.

Table 3. Results from Static Adsorption Experiments at Constant Temperature (5 °C), Maximum Static Adsorption (Maximum Static Permeability Drop or Maximum Static Adsorption Resistance), and Adsorption Equilibrium Constant

	membrane			
	ETNA10PP (perm. drop)	ETNA10PP (R_a)	PES (perm. drop)	PES (R_a)
maximum static adsorption Γ_{max} (1/slope)	23%	0.0046 m²·h·bar/L	75%	0.014 m²·h·bar/L
adsorption equilibrium constant k (1/(intercept·Γ_{max})	0.75 L/g	0.58 L/g	0.62 L/g	0.15 L/g

Table 4. Permeability Drop during Pressure-Forced Adsorption and Maximum Static Permeability Drop during Static Adsorption for the ETNA10PP and the PES Membranes[a]

membrane	permeability drop (%) (pressure-forced adsorption)	maximum static permeability drop (%) (static adsorption)[b]
ETNA10PP	63	23
PES	89	75

[a] Concentration from 5 to 10 g/L. [b] From Table 3.

It is seen in Figure 6 that even though the PES membrane has a high initial water permeability (Table 1), in practice this has no effect. Actually, the ETNA10PP membrane has a slightly larger flux. However, the flux during the amylase-F filtration is approximately the same for the two membranes at the end of the experiment, in spite of the initial difference in water permeability. It is also interesting that the fouling resistances during the experiments are almost the same for the two membranes. From the static adsorption experiments, we saw that the maximum static adsorption resistance is around 3 times larger for the PES membrane, which is attributed to a more dense adsorbed monolayer on the PES membrane. However, because the fouling resistance level and rate of increase are almost the same for the two membranes, the fouling layer on the adsorbed monolayer yields the same resistance whether it is on the PES or the ETNA10PP membrane. Because the increase in fouling resistances is almost identical for the two membranes, the fouling mechanisms on the adsorbed monolayer must be equal and independent of the membrane type. The fouling resistances versus mass of permeate increase more or less linearly, which is in agreement with the increasing resistance of a growing cake layer according to eq 6. This indicates that the fouling appears as cake-layer formation at the low enzyme concentration. This is further investigated in Figure 7, which shows a plot of $1/J_v$ versus m_p according to eq 8.

In Figure 7, it is seen that for both membranes almost straight lines with nearly equal slopes are obtained. Therefore, fouling during the pressure-forced experiments actually occur as or can be described by cake-layer formation. This is emphasized by the almost equal slopes, which shows that fouling parameter α is equal for both membranes and therefore independent of the membrane type. Thus, the increase in fouling resistance depends on the volume of permeate and is independent of the membrane itself. At these rather low enzyme concentrations (5−10 g/L), the osmotic pressure is neglected because it is assumed to be very low compared to the hydrostatic pressure. According to eq 8, the y-axis intercepts are related to the sum of the membrane resistance and the maximum static adsorption resistances. The two intercepts are almost equal, which is in agreement with results from the static adsorption experiments.

It has been shown that at low enzyme concentration the flux can be described by a resistance-in-series model (eq 7) with increasing fouling resistance that is dependent on the mass of permeate that passes the membrane. However, the osmotic pressure difference has to be taken into account at higher macromolecular concentrations at which the concentration polarization can play the role expressed as an osmotic pressure difference that has to be subtracted from the hydrostatic pressure difference (eq 9).[16] Therefore, when concentration polarization is the main factor determining the flux (when the osmotic pressure of the macromolecular solutions cannot be neglected), it can be shown that the flux is mainly determined by the bulk concentration. This can be shown for the pressure-forced experiments conducted with an initial bulk concentration of 50 g/L. Data for those high-concentration pressure-forced experiments are plotted according to stagnant film theory (eq 10).

Because straight lines for both membrane types are obtained (Figure 8) and because they are almost completely overlapping, it can be concluded that at these rather high enzyme concentrations, concentration polarization and thus the osmotic pressure difference determine the flux. Furthermore, the concentration polarization is independent of the membrane type. From the slope, the mass transfer coefficient is ∼19 L/(m²·h). With a stirring speed in the cell of 300 rpm, the flow in the cell is laminar, and from the flow and mass transfer literature correlation (eq 11), a mass transfer coefficient of ∼11 L/(m²·h) is obtained. This is rather close to the experimentally determined mass transfer coefficient, which emphasizes that at these concentrations the osmotic pressure difference caused by concentration polarization is the main term determining the flux. Using the osmotic pressure model combined with the stagnant film theory (eqs 9 and 10) and inserting $J_v = 0$, the concentration at which the osmotic pressure equals the hydrostatic pressure can be found.[16] From Figure 8, it can be seen that an enzyme concentration of around 150 g/L ($C = \exp(95/19)$) gives an osmotic pressure of 2 bar, which equals the hydrostatic pressure difference and thus gives zero flux.

Overall, it has been shown that when the immediate adsorbed monolayer has been established, a growing fouling layer is formed. The formation of this fouling layer can be described as a cake-layer formation. This cake-layer gives a subresistance that when added to the membrane resistance, and the adsorption resistance gives the total resistance toward transport through the membrane. Furthermore, it has been shown that at higher enzyme concentrations the concentration polarization results in osmotic pressure differences that cannot be neglected. Under these conditions, the flux is mainly determined by the bulk concentration and thus the concentration polarization. Cake-layer formation and concentration polarization are independent of the membrane type. The effect of static adsorption also affects cross-flow systems. Jonsson et al.[22] have reported flux decreases due to BSA adsorption in cross-flow ultrafiltration under both static and pressure-forced conditions.

The retention of amylase-F is also measured at the end of the pressure-forced experiments. For both membranes, the retention at the end is very close to 100%. This means that the two membranes act almost equally with the same retention and the

(22) Jonsson, G.; Johansen, P.; Li, W. Proceedings of The CEE-Brazil Workshop on Membrane Separation Processes, Rio de Janeiro, Brazil, May 3−8, 1992; pp 265−276.

same flux and indicates that the membrane properties of the two investigated UF membranes in our experiments are mainly determined by the (adsorbed) monolayer formed on the membrane surface (often referred to as a secondary membrane) rather than by the virgin membrane properties. It should be noted that the initial retention for the ETNA10PP membrane was measured to be approximately 97% whereas the initial retention for the PES membrane is measured to be close to 100%. The initial retentions were measured after 5 min of filtration (concentration 5−10 g/L), and after 20 min of filtration (concentration 5−10 g/L), the retention of the ETNA10PP membrane was close to 100%. The retentions are determined on the basis of enzyme concentration measurements of bulk and permeate samples, as described earlier. Thus, the retention of the ETNA10PP membrane increases relatively quickly to approximately 100% during filtration, resulting in a membrane with very similar properties compared to those of the PES membrane. This was also concluded by Wei and co-workers, who measured very similar BSA fluxes for the two UF membranes during filtration at 2 bar and a BSA concentration of 0.1 wt %, even though the initial water flux of the PES membrane is much larger than for the ETNA10PP membrane.[5]

Wei and co-workers[5] have described anti-fouling behavior during filtration for the ETNA10PP membrane. This is also seen in our data in Figure 6, where the fluxes are at the same level even though the initial water flux at 2 bar is around 3 times larger for the PES membrane. Thus, the maximum static adsorption (permeability drop and adsorption resistance), shown in Figure 4 and Table 3, gives an idea as to what extent the flux decreases during filtration from its initial water flux. The maximum static permeability drop of 23% and maximum static adsorption resistance of 0.0046 $m^2 \cdot h \cdot bar/L$ for the ETNA10PP membrane result in a relatively smaller flux decrease from the initial water flux during filtration (Figure 6) compared to that for the PES membrane with a maximum static permeability drop of 75% and a maximum static adsorption resistance of 0.014 $m^2 \cdot h \cdot bar/L$.

4.4. SEM Picture Analysis. SEM pictures have been taken for both membranes after they have been exposed to either static or pressure-forced adsorption. A picture of a chemically cleaned membrane was also taken. The pictures are shown in Figure 9.

The surfaces of the ETNA10PP and PES membranes are very different. The pictures of the clean surfaces show that the PES membrane has a more open structure compared to that of the ETNA10PP membrane. The pores are distributed more evenly on the clean PES membrane. The ETNA10PP membrane has a denser surface, which is consistent with the lower water permeability measured for that membrane compared to that for the PES membrane. The water permeability of the PES membrane is around 3 times larger than that of the ETNA10PP membrane, according to Table 1. Furthermore, the pores are not as evenly distributed for the ETNA10PP membrane. Some areas appear to be denser than others, and some large pores are present, which could be the reason for the lower initial retention (97%) measured for this membrane compared to the retention of almost 100% measured for both membranes after 20 min of the pressure-forced experiments. Also, the fact that the ETNA10PP membrane relatively quickly reached a retention of around 100% is in agreement with Jonsson et al.,[22] who reported relatively large pores to be blocked by protein adsorption, which therefore changed the retention of the membrane.

After static adsorption, the surface of the PES membrane appears to be denser than the clean membrane. The difference is clearer for the ETNA10PP membrane, where the surface has a denser appearance and the pore size has apparently decreased, which can explain the increase in retention after pressure-forced adsorption. The static adsorption gives monolayer coverage of the membrane surfaces. Whether the monolayer packing of molecules on the PES surface is denser than on the ETNA10PP surface is difficult to conclude from the SEM pictures. It shall be noted that denaturation is likely to occur for the vacuum under which the samples are prepared and coated with gold. Thus, the actual SEM pictures can be "disturbed" by this.

For both membranes, a change in the surface structure has taken place after pressure-forced adsorption. The membranes have a denser surface, and a large number of the pores have been blocked or narrowed by enzymes. The change in the surface structure is more pronounced for the ETNA10PP membrane than for the PES membrane after pressure-forced adsorption. There is a resemblance to the surface structure of the PES membrane regardless of whether it has been exposed to static or pressure-forced adsorption. There is a clear difference in the surface structure of the ETNA10PP membrane. The surface exposed to static adsorption has a granulated surface, whereas the pores have an oblong shape in the surface exposed to pressure-forced adsorption. The permeability drop after the pressure-forced experiments exceeds the maximum static permeability drop during static adsorption. This can be explained by the addition of a fouling resistance, which is seen in Figure 6. Therefore, it can be concluded that the adsorption (or rather fouling) during the pressure-forced experiments goes beyond monolayer coverage and the flux and mass of permeate data are in agreement with a cake filtration model. The SEM pictures seem to support this statement because the surfaces of the pressure-forced membranes seem to be denser and different in appearance than the surfaces of the static-adsorbed membranes. In particular, exceeding the monolayer coverage under the pressure-forced condition for the ETNA10PP membrane is visualized by the white "spaghetti areas", but the surface of the pressure-forced PES surface also seems to be much denser than under the static condition.

5. Conclusions

Static adsorption experiments were conducted with two different ultrafiltration membranes. The following can be stated:

- An easy method to measure static adsorption on a membrane surface in terms of a permeability drop or an adsorption resistance has been developed. The method ensures that the adsorption is facilitated only from the skin-layer side of the membrane and not from the support-layer side.
- It has been shown that the static adsorption of a 55 kDa amylase-F enzyme onto two different polymeric ultrafiltration membranes follows the Langmuir adsorption theory. Thus, static adsorption consists of monolayer coverage on the surface.
- From the adsorption isotherms, the maximum static adsorption (permeability drop and adsorption resistance) is determined. The maximum static adsorption is more than 3 times larger on the more hydrophobic surface (the PES membrane) compared to that on the more hydrophilic surface (the ETNA10PP membrane). On the basis of the maximum static permeability drops, the value is around 3 (75%/23%), and on the basis of the maximum static adsorption resistance, the value is also around 3 (0.014 $m^2 \cdot h \cdot bar/L$/0.0046 $m^2 \cdot h \cdot bar/L$). The amylase-F molecules must therefore be more closely arranged and packed in the monolayer on the PES surface than on the ETNA10PP surface.

In addition, some filtration experiments have been conducted to investigate the so-called pressure-forced adsorption. On the basis of these experiments, the following can be stated:

- The permeability drop during filtration exceeds the maximum static permeability drop, even at low enzyme concentration. Thus,

the surfaces are covered beyond a monolayer, which is also seen by the increasing fouling resistance during filtration. The fouling resistances are at the same level for the two membranes during filtration. Fouling onto the absorbed monolayer can be described as a cake-layer formation with a resistance that increases with the amount of permeate that passes the membrane. The exceeding of the monolayer coverage and cake/fouling formation are supported by SEM.

•The two membranes show almost equal properties during filtration, even at low enzyme concentration. Thus, the very high initial water flux for the PES membrane has no effect in practice because the flux during filtration and the final flux are almost equal to the flux of the ETNA10PP membrane that has a much lower initial permeability. This is attributed to the difference in static adsorption for the two membranes.

•At higher enzyme concentrations, concentration polarization has to be taken into account. High enzyme concentrations yield significant osmotic pressures; therefore, the flux can be described from stagnant film theory and the osmotic pressure model.

Overall, the static adsorption on the membrane contributes to the total resistance to transport through the membrane. The static adsorption is highly dependent on the membrane surface chemistry, but other factors such as cake-layer buildup and concentration polarization also have to be taken into account when the performance of a certain membrane is to be evaluated. The latter two phenomena are independent of the type and surface chemistry of the membrane.

List of Symbols

C	concentration (g/L)
D	diffusion coefficient (m^2/s)
J_v	volumetric flux ($L/(m^2 \cdot h)$)
k	adsorption equilibrium constant (L/g)
K	mass transfer coefficient ($L/(m^2 \cdot h)$)
l_p	membrane permeability ($L/(m^2 \cdot h \cdot bar)$)
m_p	mass of permeate (g)
P	pressure (bar)
r	cell radius (m)
R	gas constant ($J/(kg \cdot K)$)
$R_{m,a,f,tot}$	resistance ($m^2 \cdot h \cdot bar/L$)
T	absolute temperature (K)

Greek Symbols

α	fouling constant ($m^2 \cdot h \cdot bar/(L \cdot g)$)
Γ	adsorption (permeability drop) (%)
Γ_{max}	maximum static permeability drop (%)
Γ_{max}	maximum static adsorption resistance ($m^2 \cdot h \cdot bar/L$)
γ	surface tension (J/m^2)
ν	kinematic viscosity (m^2/s)
π	osmotic pressure (bar)
ω	stirring speed (rad/s)

LA701524X

Bibliography

[1] H. Huotari, G. Trägårdh, and I. Huisman, "Crossflow membrane filtration enhanced by an external dc electric field: A review," *Chemical engineering research and design* **77**, pp. 461–468, 1999.

[2] G. Belford, R. Davis, and A. Zydney, "The behavior of suspensions and macromolecular solutions in crossflow microfiltration," *Journal of Membrane Science* **96**, pp. 1–58, 1994.

[3] M. Mulder, *Basic Principles off membrane technology*, Kluwer Academic Publishers, London, UK, 2000.

[4] M. Young, P. Carroad, and R. Bell, "Estimation of diffusion coeffients of proteins," *Biotechnology and Bioengineering* **XXII**, pp. 947–955, 1980.

[5] G. Jonsson and C. E. Boesen, "Polarization phenomena in membrane processes.," *Synth Membr Processes, Fundam and Water Appl* , pp. 101–130, 1984.

[6] V. Vilker, C. Colton, and K. Smith, "The osmotic pressure of concentrated protein solutions: Effect of concentration and ph in saline solutions of bovine serum albumin," *Journal of Colloid and Interface Science* **79**(2), pp. 548–566, 1981.

[7] T. Weigert, J. Altmann, and S. Ripperger, "Crossflow electrofiltration in pilot scale," *Journal of membrane science* **159**, pp. 253–262, 1999.

[8] K. Laidler and J. Meiser, *Physical Chemistry*, Houghton Mifflin Company, Boston, New York, 1999.

[9] K. Mattison and M. Kaszuba, *Automated Protein Characterization*, American Biotechnology Laboratory, www.malvern.com, Dec. 2000.

[10] R. Srivastava and R. Rastogi, *Transport Mediated by Electrified Interfaces*, Elsevier, Amsterdam, Netherlands, 2003.

[11] A. Delgado, F. Gonzalez-Caballero, R. Hunter, L. Koopal, and J. Lyklema, "Measurement and interpretation of electrokinetic phenomena," *Journal of Colloid And Interface Science* **309**(2), pp. 194–224, 2007.

[12] J. M. Radovich and I. M. Chao, "Electroultrafiltration of a cationic electrodeposition paint.," *Journal of Coatings Technology* **54**(695), pp. 33–40, 1982.

[13] Z. Lazarova and W. Serro, "Electromembrane separation of mineral suspensions: Influence of process parameters," *Separation Science and Technology* **37**(3), pp. 515–534, 2002.

[14] J. D. J. Henry, L. F. Lawler, and C. H. A. Kuo, "Solid/liquid separation process based on cross flow and electrofiltration.," *AIChE J* **23**(6), pp. 851–859, 1977.

[15] H. Yukawa, K. Shimura, A. Suda, and A. Maniwa, "Characteristics of cross flow electro-ultrafiltration for colloidal solution of protein.," *Journal of Chemical Engineering of Japan* **16**(3), pp. 246–248, 1983.

[16] J. M. Radovich, B. Behnam, and C. Mullon, "Steady-state modeling of electroultrafiltration at constant concentration.," *Separation Science and Technology* **20**(4), pp. 315–329, 1985.

[17] G. Rios, H. Rakotoarisoa, and B. Tarodo de la Fuente, "Basic transport mechanisms of ultrafiltration in the presence of an electric field," *Journal of Membrane Science* **38**(2), pp. 147–159, 1988.

[18] W. Bowen and H. Sabuni, "Pulsed electrokinetic cleaning of cellulose nitrate microfiltration membranes," *Ind. Eng. Chem. Res.* **31**, pp. 515–523, 1992.

[19] Q. Gan, "Beer clarification by cross-flow microfiltration - effect of surface hydrodynamics and reversed membrane morphology," *Chemical Engineering and Processing* **40**(5), pp. 413 – 419, 2001.

[20] Q. Gan, J. Howell, R. Field, R. England, M. Bird, C. O'Shaughnessy, and M. MeKechinie, "Beer clarification by microfiltration - product quality control and fractionation of particles and macromolecules," *Journal of Membrane Science* **194**(2), pp. 185–196, 2001.

[21] A. Cassano, L. Donato, and E. Drioli, "Ultrafiltration of kiwifruit juice: Operating parameters, juice quality and membrane fouling," *Journal of Food Engineering* **79**(2), pp. 613–621, 2007.

[22] K. Narsaiah and G. Agarwal, "Transmission analysis in ultrafiltration of ternary protein mixture through a hydrophilic membrane," *Journal of Membrane Science* **287**(1), pp. 9–18, 2007.

[23] Y. Li, A. Shahbazi, and C. Kadzere, "Separation of cells and proteins from fermentation broth using ultrafiltration," *Journal of Food Engineering* **75**(4), pp. 574–580, 2006.

[24] S. Palecek and A. Zydney, "Intermolecular electrostatic interactions and their effect on flux and protein deposition during protein filtration," *Biotechnol. Prog* **10**, pp. 207–213, 1994.

[25] A. D. Marshall, P. Munro, and G. Trägårdh, "The effect of protein fouling in microfiltration and ultrafiltration on permeate flux, protein retention and selectivity: A literature review," *Desalination* **91**, pp. 65–108, 1993.

[26] L. Song, "A new model for the calculation of the limiting flux in ultrafiltration," *Journal of Membrane Science* **144**(1-2), pp. 173–185, 1998.

[27] V. Chen, A. Fane, S. Madaeni, and I. Wenten, "Particle deposition during membrane filtration of colloids transition between concentration polarization and cake formation," *Journal of Membrane Science* **125**, pp. 109–122, 1997.

[28] P. Priyananda and V. Chen, "Flux decline during ultrafiltration of protein-fatty acid mixtures," *Journal of Membrane Science* **273**(1-2), pp. 58–67, 2006.

[29] R. Chan and V. Chen, "Characterization of protein fouling on membranes: opportunities and challenges," *Journal of Membrane Science* **242**(1-2), pp. 169–188, 2004.

[30] I. Huisman, P. Prádanos, and A. Hernández, "The effect of protein-protein and protein-membrane interactions on membrane fouling in ultrafiltration," *Journal of Membrane Science* **179**, pp. 79–90, 2000.

[31] C. Duclos-Orsello, W. Li, and C. Ho, "A three mechanism model to describe fouling of microfiltration membranes," *Journal of Membrane Science* **280**(1-2), pp. 856–866, 2006.

[32] J. Li, R. Sanderson, G. Chai, and D. Hallbauer, "Development of an ultrasonic technique for in situ investigating the properties of deposited protein during crossflow ultrafiltration," *Journal of Colloid and Interface Science* **284**(1), pp. 228–238, 2005.

[33] D. J. Hughes, Z. Cui, R. W. Field, and U. K. Tirlapur, "In situ three-dimensional characterization of membrane fouling by protein suspensions using multiphoton microscopy," *Langmuir* **22**(14), pp. 6266–6272, 2006.

[34] K. L. Jones and C. R. Melia, "Ultrafiltration of protein and humic substances: effect of solution chemistry on fouling and flux decline," *Journal of Membrane Science* **193**(2), pp. 163–173, 2001.

[35] S. Kelly and A. Zydney, "Protein fouling during microfiltration: Comparative behavior of different model proteins," *Biotechnology and Bioengineering* **55**(1), pp. 91–100, 1997.

[36] G. Bayramoglu, E. Yalcin, and M. Arica, "Adsorption of serum albumin and @c-globulin from single and binary mixture and characterization of phema-based affinity membrane surface by contact angle measurements," *Biochemical Engineering Journal* **26**(1), pp. 12–21, 2005.

[37] X. Li, Y. Zhang, and X. Fu, "Adsorption of glutamicum onto polysulphone membrane," *Separation and Purification Technology* **37**(3), pp. 187–198, 2004.

[38] N. Lawrence, J. Perera, M. Iyer, M. Hickey, and G. Stevens, "The use of streaming potential measurements to study the fouling and cleaning of ultrafiltration membranes," *Separation and Purification Technology* **48**(2), pp. 106–112, 2006.

[39] A. Persson, A. Jönsson, and G. Zacchi, "Transmission of bsa during cross-flow microfiltration: influence of ph and salt concentration," *Journal of Membrane Science* **223**, pp. 11–21, 2003.

[40] T. Su, J. Lu, Z. Cui, B. Bellhouse, R. Thomas, and R. Heenan, "Identification of the location of protein fouling on ceramic membranes under dynamic filtration conditions," *Journal of Membrane Science* **163**, pp. 265–275, 1999.

[41] S. Palecek and A. Zydney, "Hydraulic permeability of protein deposits formed during microfiltration: effect of solution ph and ionic strength," *Journal of Membrane Science* **95**, pp. 71–81, 1994.

[42] S. Palecek, S. Mochizuki, and A. Zydney, "Effect of ionic enviroment on bsa filtration and the properties of bsa deposition," *Desalination* **90**, pp. 147–159, 1993.

[43] A. Marshall, P. Munro, and G. Trägårdh, "Influence of ionic calcium concentration on fouling during the cross-flow microfiltration of beta-lactoglobulin solutions," *Journal of Membrane Science* **217**, pp. 131–140, 2003.

[44] S. Yiantsios and A. Karabelas, "The effect of colloid stability on membrane fouling," *Desalination* **118**, pp. 143–152, 1998.

[45] T. Maruyama, S. Katoh, M. Nakajima, H. Nabetani, T. P. Abbott, A. Shono, and K. Satoh, "Ft-ir analysis of bsa fouled on ultrafiltration and microfiltration membranes," *Journal of Membrane Science* **192**(1-2), pp. 201–207, 2001.

[46] S. Kelly, W. Opong, and A. Zydney, "The influence of protein aggregates on the fouling of microfiltration membranes during stirred cell filtration," *Journal of Membrane Science* **80**, pp. 175–187, 1993.

[47] K. Kim, A. Fane, C. Fell, and D. Joy, "Fouling mechanisms of membrane during protein ultrafiltration," *Journal of Membrane Science* **68**, pp. 79–91, 1992.

[48] C. Güell and R. Davis, "Membrane fouling during microfiltration of protein mixtures," *Journal of Membrane Science* **119**, pp. 269–284, 1996.

[49] S. Kelly and A. Zydney, "Mechanisms for bsa fouling during microfiltration," *Journal of Membrane Science* **107**, pp. 115–127, 1995.

[50] L. Palacio, C.-C. Ho, P. Pradanos, A. Hernandez, and A. Zydney, "Fouling with protein mixtures in microfiltration: Bsa-lysozyme and bsa-pepsin," *Journal of Membrane Science* **222**(1-2), pp. 41–51, 2003.

[51] W. Richard Bowen and T. A. Doneva, "Atomic force microscopy studies of membranes: Effect of surface roughness on double-layer interactions and particle adhesion," *Journal of Colloid and Interface Science* **229**(2), pp. 544–549, 2000.

[52] C. Ho and A. L. Zydney, "Effect of membrane morphology on the initial rate of protein fouling during microfiltration," *Journal of Membrane Science* **155**, pp. 261–275, 1999.

[53] C. Ho and A. L. Zydney, "Protein fouling of asymmetric and composite microfiltration membranes," *Ind. Eng. Chem. Res.* **40**, pp. 1412–1421, 2001.

[54] M. Taniguchi and G. Belfort, "Low protein foulin synthetic membranes by uv-assisted surface grafting modification: varying monomer type," *Journal of Membrane Science* **231**, pp. 147–157, 2004.

[55] D. Wavhal and E. Fisher, "Membrane surface modification by plasma-induced polymerization of acrylamide for improved surface properties and reduced protein fouling," *Langmuir* **19**, pp. 79–85, 2003.

[56] L. Zhu, L. Xu, B. Zhu, Y. Feng, and Y. Xu, "Preparation and characterization of improved fouling-resistant ppesk ultrafiltration membranes with amphiphilic ppesk-graft-peg copolymers as additives," *Journal of Membrane Science* **294**(1-2), pp. 196–206, 2007.

[57] Y.-q. Wang, T. Wang, Y.-l. Su, F.-b. Peng, H. Wu, and Z.-y. Jiang, "Remarkable reduction of irreversible fouling and improvement of the permeation properties of poly(ether sulfone) ultrafiltration membranes by blending with pluronic f127," *Langmuir* **21**(25), pp. 11856–11862, 2005.

[58] D. Wavhal and E. Fisher, "Modification of polysulfone ultrafiltration membranes by co2 plasma treatment," *Desalination* **172**(2), pp. 189–205, 2005.

[59] J. Wei, G. Helm, and X. Hou, "Quantification of protein adsorption on membrane surfaces by radiolabeling technique," *Desalination* **199**(1-3), pp. 378–380, 2006.

[60] S. P. Beier, A. D. Enevoldsen, G. M. Kontogeorgis, E. B. Hansen, and G. Jonsson, "Adsorption of amylase enzyme on ultrafiltration membranes," *Langmuir* **23**(18), p. 9341, 2007.

[61] J. Wei, G. Helm, N. Corner-Walker, and X. Hou, "Characterization of a non-fouling ultrafiltration membrane," *Desalination* **192**(1-3), pp. 252–261, 2006.

[62] V. Kuberkar and R. Davis, "Effects of added yeast on protein transmissions and flux in cross-flow membrane microfiltration," *Biotechnol. Prog.* **15**, pp. 472–479, 1999.

[63] P. Nemade and R. Davis, "Secondary membranes for flux optimization in membrane filtration of biologic suspensions," *Applied Biochemistry and Biotechnology* **113-116**, pp. 417–432, 2004.

[64] M. Cheryan and B. H. Chiang, "Performance and fouling behaviour of hollow fibre and spiral wound ultrafiltration modules processing skimmilk.," *Ireland, Republic of, Institution of Engineers of Ireland, Agricultural Engineering Division [Engineering/Food Symposium]* , 1984.

[65] R. Chan and V. Chen, "The effects of electrolyte contentration and ph on protein aggregation and deposition: critical flux and constant flux membrane filtration," *Journal of Membrane Science* **185**, pp. 177–192, 2001.

[66] A. Marshall, P. Munro, and G. Trägårdh, "Influence of permeate flux on fouling during the microfiltration of beta-lactoglobulin solutions under cross-flow conditions," *Journal of Membrane Science* **130**, pp. 23–30, 1997.

[67] S. Metsamuuronen and M. Nystrom, "Critical flux in cross-flow ultrafiltration of protein solutions," *Desalination* **175**(1), pp. 37–47, 2005.

[68] M. Cheryan, *Ultrafiltration and Microfiltration Handbook*, Technomic Publishing Company, Inc., 851 New Holland Avenue, Box 3535, Lancaster, Pennsylvania 17604 U.S.A., 1998.

[69] S. Hargrove, H. Parthasarathy, and S. Ilias, "Flux enhancement in cross-flow membrane filtration by flow reversal: A case study on ultrafiltration of bsa," *Separation Science and Technology* **38**, pp. 3133–3144, 2003.

[70] V. Rodgers and R. Sparks, "Reduction of membrane fouling in the ultrafiltration of binary protein mixtures," *AIChE Journal* **37**(10), pp. 1517–1528, 1991.

[71] V. Rodgers and R. Sparks, "Effect of transmembrane pressure pulsing on concentration polarization," *Journal of Membrane Science* **68**(1-2), pp. 149–168, 1992.

[72] V. Rodgers and R. Sparks, "Effects of solution properties on polarization redevelopment and flux in pressure pulsed ultrafiltration," *Journal of Membrane Science* **78**(1-2), pp. 163–180, 1993.

[73] V. Kuberkar and R. Davis, "Microfiltration of protein-cell mixtures with crossflushing or backflushing," *Journal of Membrane Science* **183**, pp. 1–14, 2001.

[74] W. Mores and R. Davis, "Direct observation of membrane cleaning via rapid backpulsing," *Desalination* **146**, pp. 135–140, 2002.

[75] S. P. Beier, M. Guerra, A. Garde, and G. Jonsson, "Dynamic microfiltration with a vibrating hollow fiber membrane module: Filtration of yeast suspensions," *Journal of Membrane Science* **281**(1), pp. 281–287, 2006.

[76] S. Beier and G. Jonsson, "Separation of enzymes and yeast cells with a vibrating hollow fiber membrane module," *Separation and Purification Technology* **53**(1), pp. 111–118, 2007.

[77] P. Engler and M. Wiesner, "Particle fouling of a rotating membrane disk," *Water Research* **34**, pp. 557–565, 2000.

[78] J. Lipnizki, S. Casani, and G. Jonsson, "Optimisation of ultrafiltration of a highly viscous protein solution using spiral-wound modules," *Desalination* **180**(1-3), pp. 15–24, 2005.

[79] J. Schwinge, D. Wiley, A. Fane, and R. Guenther, "Characterization of a zigzag spacer for ultrafiltration," *Journal of Membrane Science* **172**(1-2), pp. 19–31, 2000.

[80] N. Krishna Kumar, M. Yea, and M. Cheryan, "Ultrafiltration of soy protein concentrate: performance and modelling of spiral and tubular polymeric modules," *Journal of Membrane Science* **244**(1-2), pp. 235–242, 2004.

[81] D. Krstić, M. Tekić, M. Carić, and S. Milanović, "Static turbulence promoter in cross-flow microfiltration of skim milk," *Desalination* **163**, pp. 297–309, 2004.

[82] D. Krstić, M. Antov, D. Pericin, W. Hoflinger, and M. Tekic, "The possibility for improvement of ceramic membrane ultrafiltration of an enzyme solution," *Biochemical Engineering Journal* **33**(1), pp. 10–15, 2007.

[83] V. Chen, R. Chan, H. Li, and M. Bucknall, "Spatial distribution of foulants on membranes during ultrafiltration of protein mixtures and the influence of spacers in the feed channel," *Journal of Membrane Science* **287**(1), pp. 79–87, 2007.

[84] J. Schwinge, P. Neal, D. Wiley, D. Fletcher, and A. Fane, "Spiral wound modules and spacers review and analysis," *Journal of Membrane Science* **242**, pp. 129–153, 2004.

[85] M. Cabero, F. Riera, and R. Álvarez, "Rinsing of ultrafiltration ceramic membranes fouled with whey proteins: effects on cleaning procedures," *Journal of Membrane Science* **154**, pp. 239–250, 1999.

[86] J. Baker and L. Dudley, "Biofouling in membrane systems- a review," *Desalination* **118**, pp. 81–90, 1998.

[87] P. Blanpain-Avet, J. Migdal, and T. Bénézech, "The effect of multiple fouling and cleaning cysles on a tubular ceramic microfiltration membrane fouled with a whey protein concentrate, membrane performance and cleaning efficiency," *Trans IChemE, Part C, Food and Bioproducts Processing* **82(C3)**, pp. 231–243, 2004.

[88] M. Argüello, S. Álvarez, F. Riera, and R. Álvarez, "Enzymatic cleaning of inorganic ultrafiltration membranes used for whey protein fractionation," *Journal of Membrane Science* **216**, pp. 121–134, 2003.

[89] R. Wakeman and M. Smythe, "Clarifying filtration of fine particle suspensions aided by electrical and acoustic fields," *Trans IChemE* **78**, pp. 125–135, 2000. Part A.

[90] R. Wakeman and M. Sabri, "Utilizing pulsed electric-fields in cross-flow microfiltration of titania suspensions," *Chemical engineering research and design* **73**, pp. 455–463, 1995.

[91] W. Bowen, R. Kingdon, and H. Sabuni, "Electrically enhanced separation processes: the basis of in situ intermittent electrolytic membrane cleaning (iiemc) and in situ electrolytic membrane restoration (iemr)," *Journal of Membrane Science* **40**(2), pp. 219–229, 1989.

[92] R. Wakeman and E. Tarleton, "An experimental study of electroacoustic crossflow microfiltration," *Trans IChemE* **69**, pp. 386–397, 1991. Part A.

[93] R. Wakeman, "Electrically enhanced microfiltration of albumin suspensions," *Trans IChemE* **76**, pp. 53–59, 1998.

[94] E. Iritani, Y. Mukai, and K. Y., "Effects of electric field on dynamic behaviors of dead-end inclined and downward ultrafiltration of protein solutions," *Journal of membrane science* **164**, pp. 51–57, 2000.

[95] E. Iritani, K. Ohashi, and T. Murase, "Analysis of filtration mechanism of dead-end electroultrafiltration for proteinaceous solutions," *Journal of chemical engineering of Japan* **25**, pp. 383–388, 1992.

[96] S. Oussedik, D. Belhocine, H. Grib, H. Lounici, D. Piron, and N. Mameri, "Enhanced ultrafiltration of bovine serum albumin with pulsed electric field and fluidized activated alumina," *Desalination* **127**, pp. 59–68, 2000.

[97] C. Robinson, M. Siegel, A. Condemine, C. Fee, Z. Fahidy, and B. Glick, "Pulsed-electric-field cross-flow ultrafiltration of bovine serum-albumin," *Journal of membrane science* **80**, pp. 209–220, 1993.

[98] C. Guizard, F. Legault, N. Idrissi, A. Larbot, L. Cot, and C. Gavach, "Electronically conductive mineral membranes designed for electro-ultrafiltration," *Journal of Membrane Science* **41**, pp. 127–142, 1989.

[99] H. M. Huotari, I. H. Huisman, and G. Trägårdh, "Electrically enhanced crossflow membrane filtration of oily waste water using the membrane as a cathode," *Journal of membrane science* **156**, pp. 49–60, 1999.

[100] G. Yang and T.-Y. Yang, "Reclamation of high quality water from treating cmp wastewater by a novel crossflow electrofiltration/electrodialysis process," *Journal of Membrane Science* **233**(1-2), pp. 151–159, 2004.

[101] P. Zumbusch, W. Kulcke, and G. Brunner, "Use of alternating electrical fields as anti-fouling strategy in ultrafiltration of biological suspensions - introduction of a new experimental procedure for crossflow filtration," *Journal of membrane science* **142**, pp. 75–86, 1998.

[102] C. Tarazaga, M. Campderros, and A. Padilla, "Physical cleaning by means of electric field in the ultrafiltration of a biological solution," *Journal of Membrane Science* **278**(1-2), pp. 219–224, 2006.

[103] Y.-H. Weng, K.-C. Li, L. Chaung-Hsieh, and C. Huang, "Removal of humic substances (hs) from water by electro-microfiltration (emf)," *Water Research* **40**(9), pp. 1783–1794, 2006.

[104] G. Yang, T. Yang, and S. Tsai, "Crossflow electro-microfiltration of oxide-cmp wastewater," *Water research* **37**, pp. 785–792, 2003.

[105] G. Bargeman, G.-H. Koops, J. Houwing, I. Breebaart, H. v. d. Horst, and M. Wessling, "The development of electro-membrane filtration for the isolation of bioactive peptides: the effect of membrane selection and operating parameters on the transport rate," *Desalination* **149**, pp. 369–374, 2002.

[106] S. Lentsch, P. Aimar, and J. Orozco, "Enhanced separation of albumin poly(ethylene glycol) by combination of ultrafiltration and electrophoresis," *Journal of membrane science* **80**, pp. 221–232, 1993.

[107] J. M. Radovich and R. E. Sparks, "Electrophoretic techniques for controlling concentration polarization in ultrafiltration.," *Polymer Science and Technology* **13**, pp. 249–268, 1980.

[108] G. Bargeman, J. Houwing, I. Recio, G. H. Koops, and C. v. d. Horst, "Electro-membrane filtration for the selective isolation of bioactive pep-

tides from an alpha s2-casein hydrolysate.," *Biotechnology and Bioengineering* **80**(6), pp. 599–609, 2002.

[109] R. Wakeman and C. Williams, "Additional techniques to improve microfiltration," *Separation and purification technology* **26**, pp. 3–18, 2002.

[110] R. Williams, C.and Wakeman, "Membrane fouling and alternative techniques for its alleviation," *Membrane Technology* **124**, pp. 4–10, 2000.

[111] G. Akay and R. Wakeman, "Electric field enhanced crossflow microfiltration of hydrophobically modified water soluble polymers," *Journal of Membrane Science* **131**, pp. 229–236, 1997.

[112] M. Sung, C. Huang, Y.-H. Weng, Y.-T. Lin, and K.-C. Li, "Enhancing the separation of nano-sized particles in low-salt suspensions by electrically assisted cross-flow filtration," *Separation and Purification Technology* **54**(2), pp. 170–177, 2007.

[113] G. Bargeman, M. Dohmen-Speelmans, I. Recio, M. Timmer, and C. v. d. Horst, "Selective isolation of cationic amino acids and peptides by electromembrane filtration.," *Lait* **80**(1), pp. 175–185, 2000.

[114] H. M. Huotari and M. Nyström, "Electrofiltration in industrial wastewater applications," *Trans. Filt. Soc.* **1**, pp. 17–22, 2000.

[115] R. Webster, S. Chilukuri, J. Levesley, and B. Webster, "Electrochemical cleaning of microporous metallic filters fouled with bovine serum albumin and phosphate under low cross-flow velocities," *Journal of Applied Electrochemistry* **30**, pp. 915–924, 2000.

[116] A. Genc, "Experimental studies on the effect of electrode configuration in electrofiltration," *Separation science and technology* **37**, pp. 3053–3064, 2002.

[117] R. Hofmann and C. Posten, "Improvement of dead-end filtration of biopolymers with pressure electrofiltration," *Chemical engineering science* **58**, pp. 3847–3858, 2003.

[118] O. Larue and E. Vorobiev, "Sedimentation and water electrolysis effects in electrofiltration of kaolin suspension," *AIChE Journal* **50**(12), pp. 3120–3133, 2004.

[119] H. Yukawa, K. Kobayashi, Y. Tsukui, and M. Yamano, "Analysis of batch electrokinetic filtration," *Journal of chemical engineering of Japan* **9**, p. 396, 1976.

[120] H. Kyllönen, P. Pirkonen, and M. Nystrom, "Membrane filtration enhanced by ultrasound: a review," *Desalination* **181**(1-3), pp. 319–335, 2005.

[121] J.-L. Laborde, C. Bouyer, J.-P. Caltagirone, and Gérard, "Acoustic bubble cavitation at low frequencies," *Ultrasonics* **36**, pp. 589–594, 1998.

[122] Y. Matsumoto, T. Miwa, S. Nakao, and S. Kimura, "Improvement of membrane permeation performance by ultrasonic microfiltration," *Journal of chemical engineering of Japan* **29**, pp. 561–567, 1996.

[123] X. Chai, T. Kobayashi, and N. Fujii, "Ultrasound effect on cross-flow filtration of polyacrylonitrile ultrafiltration membranes," *Journal of Membrane Science* **148**, pp. 129–135, 1998.

[124] T. Kobayashi, X. Chai, and N. Fujii, "Ultrasound enhanced cross-flow membrane filtration," *Separation and Purification Technology* **17**, pp. 31–40, 1999.

[125] R. Juang and K. H. Lin, "Flux recovery in the ultrafiltration of suspended solutions with ultrasound," *Journal of Membrane Science* **243**, pp. 115–124, 2004.

[126] H. Kyllönen, P. Pirkonen, M. Nystrom, J. Nuortila-Jokinen, and A. Gronroos, "Experimental aspects of ultrasonically enhanced cross-flow membrane filtration of industrial wastewater," *Ultrasonics - Sonochemistry* **13**(4), pp. 295–302, 2006.

[127] S. Muthukumaran, K. Yang, A. Seuren, S. Kentish, M. Ashokkumar, and F. Grieser, "The use of ultrasonic cleaning for ultrafiltration membranes in the dairy industry," *Separation and Puriication Technology* **39**, pp. 99–107, 2004.

[128] M. Lamminen, H. Walker, and L. Weavers, "Mechanisms and factors influencing the ultrasonic cleaning of particle-fouled ceramic membranes," *Journal of Membrane Science* **237**, pp. 213–223, 2004.

[129] M. Smythe and R. Wakeman, "The use of acoustic fields as a filtration and dewatering aid," *Ultrasonics* **38**, pp. 657–661, 2000.

[130] M. Bradford, "A rapid and sensitive method for the quantitation of microgram quantities of protein utilizing the principle of protein-dye binding," *Anal. Biochem.* **72**, p. 248, 1976.

[131] Biorad, *Quick Start Bradford Protein Assay*, 2000 Alfred Nobel Dr. Hercules, CA 94547 USA, http://www.bio-rad.com, Dec. 2000.

[132] G. Jonsson and C. Boesen, "Concentration polarization in a reverse osmosis test cell," *Desalination* **21**(1), pp. 1–10, 1977.